ORNL/TM--9783

DE86 001859

PROGRAM AND ABSTRACT BOOK

SECOND INTERNATIONAL CONFERENCE ON FUNDAMENTALS OF FRACTURE

Riverside Motor Lodge
Gatlinburg, Tennessee, U.S.A.

November 4–7, 1985

Sponsors

Oak Ridge National Laboratory

National Bureau of Standards

U. S. Army Research Office

Office of Naval Research

Date Published - October 1985

Organizing Committee

S. M. Ohr (Chairman)
Oak Ridge National Laboratory, Oak Ridge, Tennessee, U.S.A.
Robb Thomson
National Bureau of Standards, Washington, D.C., U.S.A.
Peter Neumann
Max-Planck-Institut für Eisenforschung, Düsseldorf, Germany
T. Suzuki
Science University of Tokyo, Tokyo, Japan

Local Committee

N. F. Callaham, S.-J. Chang, T. C. Estes, S. L. Evans, A. M. Keesee, C. G. Park, J. H. Schneibel, D. L. Slagle, C. L. White, M. H. Yoo

OAK RIDGE NATIONAL LABORATORY
Oak Ridge, Tennessee 37831
operated by
MARTIN MARIETTA ENERGY SYSTEMS, INC.
for the
U.S. DEPARTMENT OF ENERGY
under Contract No. DE-AC05-840R21400

LEGIBILITY NOTICE

A major purpose of the Technical Information Center is to provide the broadest dissemination possible of information contained in DOE's Research and Development Reports to business, industry, the academic community, and federal, state and local governments.

Although a small portion of this report is not reproducible, it is being made available to expedite the availability of information on the research discussed herein.

SECOND INTERNATIONAL CONFERENCE ON FUNDAMENTALS OF FRACTURE

Riverside Motor Lodge
Gatlinburg, Tennessee, U.S.A.

November 4–7, 1985

PROGRAM

Sunday, November 3: 7:00 p.m.–9:00 p.m. Registration and Reception, Riverside Motor Lodge

Monday, November 4:

8:00 a.m. Registration

(I) WELCOME AND OPENING LECTURE: S. M. Ohr, Chairman

8:30 Welcome: M. C. Wittels, U.S. Department of Energy

8:45 Opening Lecture: "Fracture Fundamentals: An Overview"
Robb Thomson, National Bureau of Standards

9:30 Break

(II) ATOMIC THEORY: Robb Thomson, Chairman

9:45 "Modern Atomistic Theories of Fracture" (Keynote)
M. S. Daw, Sandia National Laboratories

10:15 "Interatomic Potential Description of Atomic Processes in Metals"
A. E. Carlsson, Washington University

10:35 "Structural Prediction with the Tight Binding Bond Model"
D. G. Pettifor, Imperial College

10:55 "Electronic Theory for Hydrogen Embrittlement of BCC Transition Metals"
K. Masuda-Jindo, Tokyo Institute of Technology

11:15 "The Energetics of Structural Relaxations, Dynamics and Transport at Interfaces"
U. Landman, Georgia Institute of Technology

11:35 "Dependence of Crack Velocity on the Interatomic Potential"
G. J. Dienes, Brookhaven National Laboratory

11:55 "Atomic Computer Simulation of Fracture of Metals"
M. Doyama, University of Tokyo

12:15 p.m. "A Computer Simulation Study on the Propagation of a Surface Crack"
D. M. Cooper, NASA Ames Research Center

12:35 Lunch

(III) CONTINUUM THEORY I: A. S. Argon, Chairman

2:00 p.m. "Plasticity at Crack Tips: Dislocation and Continuum Scales" (Keynote)
J. R. Rice, Harvard University

2:30 "Crack Propagation Mechanisms and Local Crack Driving Force"
E. W. Hart, Cornell University

2:50 "The Analytical Solution of a Growing Steady-State Mode III Crack in an Elastic Perfectly-Plastic Solid through an Electrical Analogy"
J. Weertman, Northwestern University

3:10 "Finite DFZ Cracks: An Approximate Treatment"
N. Louat, Naval Research Laboratory

3:30 Break

(IV) CONTINUUM THEORY II: J. R. Rice, Chairman

3:45 "The Eigenstrain Method Applied to Fracture and Fatigue"
T. Mura, Northwestern University

4:05 "A Simple Method of Analysis of Crack Interactions"
M. Kachanov, Tufts University

4:25 "Dynamic Cleavage in Ductile Materials"
I.-H. Lin, National Bureau of Standards

4:45 "Universal Weight Functions for Loadings and Screenings of Cracks"
H. O. K. Kirchner, University of Vienna

5:05 "Response of a Dislocation to an External Stress"
F. Lund, University of Chile

5:25 Poster Session

6:30 Adjourn

Tuesday, November 5:

(V) EXPERIMENTAL STUDIES I: R. M. Latanision, Chairman

8:30 a.m.	"Experimental Studies of Crack Tip Processes" (Keynote) P. Neumann, Max-Planck-Institut für Eisenforschung
9:00	"Modeling of Ductile Fracture" A. W. Thompson, Carnegie-Mellon University
9:20	"Fracture of Amorphous Metals in Tensile Test and Fatigue Test" T. Imura, Nagoya University
9:40	"SXRF Studies of Bulk Crack-Tip Plastic Relaxation" J. C. Bilello, State University of New York at Stony Brook
10:00	"X-Ray Analysis of Prefracture Elastic and Plastic Strain Gradients" S. Weissmann, Rutgers University
10:20	"Influence of a Plastic Zone on the Static and Dynamic Toughness of Silicon" G. Champier, Institut National Polytechnique de Lorraine
10:40	Break

(VI) EXPERIMENTAL STUDIES II: A. W. Thompson, Chairman

10:55	"Crack Tip Shielding by Dislocation Deformation in Ionic and Diamond Cubic Solids" S. J. Burns, University of Rochester
11:15	"Dislocation Distribution around a Crack Tip and the Fracture Toughness in NcCl Crystals" N. Narita, Kyoto University
11:35	"On Fast Fracture and Crack Arrest" G. T. Hahn, Vanderbilt University
11:55	"Statics and Dynamics of Single Crystal Cleavage" W. W. Gerberich, University of Minnesota
12:15 p.m.	"Propagation of Cleavage Crack in Iron and LiF Single Crystals" K. Kitajima, Kyushu University
12:35	Buffet Lunch, Riverside Motor Lodge
2:00	Tour of the Great Smoky Mountains National Park

Wednesday, November 6:

(VII) Environmental Effects I: T. Suzuki, Chairman

8:30 a.m. "Environmental Cell HVEM Studies of Hydrogen Effects on Deformation and Fracture" (Keynote)
H. K. Birnbaum, University of Illinois

9:00 "Effects of Hydrogen on Deformation and Fracture of Iron"
M. Meshii, Northwestern University

9:20 "Hydrogen Assisted Crack Growth in Single and Bicrystals of FeSi and Ni"
H. Vehoff, Max-Planck-Institut für Eisenforschung

9:40 "Calculations of Two-Dimensional Transient Concentration Profiles during Hydrogen-Assisted Sustained-Load Cracking"
J. E. Hack, Los Alamos National Laboratory

10:00 "Chemistry and Fracture"
R. M. Latanision, Massachusetts Institute of Technology

10:20 Break

(VIII) ENVIRONMENTAL EFFECTS II: P. Neumann, Chairman

10:35 "Electrochemical Reactions and Corrosion Fatigue of Ferrous Alloys"
R. P. Wei, Lehigh University

10:55 "Stress Corrosion Cracking of High-Strength Steel under Mode III Loading"
W. Y. Chu, Beijing University

11:15 "Evidence for an Adsorption-Induced Localised-Slip Mechanism of Environmentally Assisted Cracking"
S. P. Lynch, Aeronautical Research Labs-Australia

11:35 "The Restraining Effect of Cleavage Ligaments in Transgranular Stress Corrosion Cracking of FCC Alloys"
E. N. Pugh, National Bureau of Standards

11:55 "Transgranular Stress-Corrosion Cracking"
K. Sieradzki, Brookhaven National Laboratory

12:15 p.m. Lunch

(IX) FATIGUE I: J. Weertman, Chairman

2:00 p.m.	"Mechanisms of Long-Life Fatigue" (Keynote) C. Laird, University of Pennsylvania
2:30	"A Mechanistic Model of Fatigue Crack Growth" J. E. Sinclair, AERE Harwell
2:50	"Crack Tip Shielding in Fracture and Fatigue: Intrinsic vs. Extrinsic Toughening" R. O. Ritchie, University of California
3:10	"Mechanisms of Fatigue Crack Growth through Aluminum Alloys" D. L. Davidson, Southwest Research Institute
3:30	Break

(X) FATIGUE II: W. W. Gerberich, Chairman

3:45	"Microstructure and Closure Related Growth Characteristics of Short Fatigue Crack Growth at Constant ΔK" M. E. Fine, Northwestern University
4:05	"High Temperature Fatigue Behavior of Ferritic Stainless Steels" J. R. Weertman, Northwestern University
4:25	"Low Cycle Fatigue Behavior of Alloy 800H at 800°C" V. Gerold, Max-Planck-Institut für Metallforschung
4:45	"The Growth of Persistent Slip Bands during Fatigue" W. J. Baxter, General Motors Research Laboratories
5:05	Poster Session Discussion
6:00	Adjourn
7:00	Banquet, Riverside Motor Lodge "Three Mile Island and Bhopal" A. W. Weinberg

Thursday, November 7:

(XI) CERAMICS: B. R. Lawn, Chairman

8:30 a.m.	"Chemistry of Fracture in Glass" (Keynote) S. M. Wiederhorn, National Bureau of Standards
9:00	"Transformation and Dispersion Toughening" J. C. M. Li, University of Rochester
9:20	"TEM Studies of the Formation of Microcracks in Zirconia-Containing Ceramics" M. Rühle, Max-Planck-Institut für Metallforschung
9:40	"On the Apparent Toughening at High Temperatures Exhibited by Ceramics Containing an Intergranular Glass Phase" D. R. Clarke, T. J. Watson Research Center, IBM
10:00	"The Role of Steric Hindrance in Stress Corrosion Fracture of Vitreous Silica" T. A. Michalske, Sandia National Laboratories
10:20	Break

(XII) HIGH TEMPERATURE PHENOMENA: J. R. Weertman, Chairman

10:35	"Micromechanical Modeling of Microstructural Damage in Creeping Alloys" (Keynote) A. S. Argon, Massachusetts Institute of Technology
11:05	"Nucleation of Intergranular Creep Cavities" M. H. Yoo, Oak Ridge National Laboratory
11:25	"Intergranular Cavitation at High Temperatures" H. Riedel, Max-Planck-Institut für Eisenforschung
11:45	"Creep Fracture of Polycrystalline Ceramics" R. A. Page, Southwest Research Institute
12:05 p.m.	"The Effects of Impurities on the Hot Tensile Ductility of Iron" D. P. Pope, University of Pennsylvania
12:25	Lunch

(XIII) INTERFACIAL FRACTURE: M. H. Yoo, Chairman

2:00 p.m.	"Intergranular Fracture due to Impurity Segregation in Iron" (Keynote) H. Kimura, Tohoku University
2:30	"Interfacial Forces and the Fundamental Nature of Brittle Cracks" B. R. Lawn, National Bureau of Standards
2:50	"Atomistic Studies of Segregation, Crack Initiation and Crack Propagation" J. K. Lee, Michigan Technological University
3:10	"Dislocation Pile-Up -- Grain Boundary Interaction at Elevated Temperature" A. A. Rubinstein, State University of New York at Stony Brook
3:30	"Structure-Dependent Intergranular Fracture Induced by Liquid Metal" T. Watanabe, Tohoku University
3:50	"Beneficial versus Harmful Grain Boundary Segregants: Boron and Sulfur in Ni_3Al" C. L. White, Oak Ridge National Laboratory
4:10	Conference Adjourn

(XIV) POSTER SESSION:

1. "Microcrack-Microdefect Interaction"
   A. A. Rubinstein

2. "Relativistic Dislocation Shielding of Cracks"
   I.-H. Lin and R. Thomson

3. "The Size Effect of Crack on Mode III Plastic Deformation"
   S. Lee and S. T. Shiue

4. "Elastic Solution of an Edge Dislocation near a Wedge Crack"
   S.-J. Chang, S. M. Ohr, and R. Thomson

5. "Dislocation-Free Zone Model of Fracture under Cyclic Loading"
   S.-J. Chang and S. M. Ohr

6. "The Stability of Cracks following Extensive Stable Growth"
   P. F. Thomason

7. "The Probablistic Physical Theory of Thermally Activated Fracture"
   A. S. Krausz and K. Krausz

8. "Stress Driven Migration of Point Defects around Crack-Tips"
   J. E. Sinclair and C. A. Hippsley

9. "Computer Simulation of Fracture in a Spatially Varying Anisotropic Glass"
   D. W. Berreman, S. Meiboom, J. A. Zasadzinski, and M. J. Sammon

10. "Effect of Surface Tension on the Toughness of Glass"
    T.-J. Chuang

11. "The Role of Plastic Work in the Cleavage of BCC Metals"
    J. E. Hack and D. F. Stein

12. "The Brittle-Ductile Transition in Silicon with Particular Regards to Doping"
    M. Brede and P. Haasen

13. "Mode I Crack Tip Shielding Applied to Warm Prestressing"
    B. S. Majumdar and S. J. Burns

14. "Direct Observation of Crack Tip Propagation in Brittle Materials"
    R. B. Tait and G. G. Garrett

15. "Dislocation Structures at Crack Tips"
    I. M. Robertson, G. M. Bond, and H. K. Birnbaum

16. "TEM Studies of Crack Tip Dislocations in BCC Metals"
C. G. Park and S. M. Ohr

17. "Modeling of Crack Growth and Fracture in Thin Specimens"
K. V. Jata, T. Hanamura, and W. A. Jesser

18. "Insights into the Fracture Toughness of Martensitic Stainless Steels using Stereoscopic Fractographic Measurements"
D. S. Gelles

19. "The Application of Statistical Model of Cleavage K_{1c} to Hot-Work Die Steel and Its Toughening by Double Quenching Treatment"
M. Zheng, B. Chen, and Q. Cai

20. "Delayed Fracture under Mode II Loading"
T. Y. Zhang, W. Y. Chu, Y. Li, and C. M. Hsiao

21. "Fracto-Emission: Particles from the Fracture of Solids"
J. T. Dickinson, L. C. Jensen, and M. R. McKay

22. "The Influence of Hydrogen on Deformation and Fracture Processes in High-Strength Aluminum Alloys"
G. M. Bond, I. M. Robertson, and H. K. Birnbaum

23. "Mechanism of Hydrogen Induced Softening"
T. Y. Zhang, W. Y. Chu, and C. M. Hsiao

24. "Hydrogen and Impurity Segregation Induced Subcritical Crack Growth of Fe and Ni"
R. H. Jones

25. "Stress Corrosion Cracking of an Aluminum Alloy under Compressive Stress"
W. Y. Chu, C. M. Hsiao, and J. W. Wang

26. "Observations of Creep Cavitation in Type 304 Stainless Steel"
T.-S. Liu, Y.-W. Wu, R. J. Fields, D. G. Harlow, and T. J. Delph

27. "The Effect of Sulphur Segregation and ALN Precipitation on the Hot Fracture of Ultra High Purity Iron Base Alloys"
M. Tacikowski, G. A. Dsinkolu, and A. Kobylanski

28. "Rare Earth Effects in Intergranular Fracture"
F. Cosandey

29. "Intergranular Cracking in Hydrogenated Alloy Steels"
J. Kameda

30. "Temperature Variations around the Crack Tip during a Fracture Test"
M. Beghi, C. E. Bottani, and G. Caglioti

OPENING LECTURE

FRACTURE FUNDAMENTALS: AN OVERVIEW

Robb Thomson
National Bureau of Standards
Gaithersburg, MD, 20899

The general theme of this conference is the attempt to understand and describe the basic events in a material which occur at the time of fracture. Much of the time, we shall be concerned with problems not easily viewed in terms of the continuum approximation. But since one cannot gain an adequate view of fracture without interpreting the average and collective properties of aggregates of atoms and even dislocations, one of the languages to be spoken extensively here will be that of continuum mechanics. Thus the subject matter will span the entire spectrum from the bonding of atoms in highly distorted crystals to continuum descriptions of plastic instability.

It is my purpose in this paper to preview a few of the new ideas and problems you have presented in your abstracts. It will not be possible or desirable to cover every interesting such idea or problem, but rather, a personal check list will be attempted which may help to identify important themes which will emerge over the next three days.

One of the important propositions a number of us have made, and which should get some "air time" here for discussion, is that the structure of the crack tip is crucial for determining the ultimate material behavior during failure. For this reason, the progress in theoretical physics to be reported here in providing insight into the bonding of metal atoms in the region of a crack tip is essential for further progress in atomic modeling of cracks. We will also hear a report of some early success in combining fundamental theory with actual structure modeling. In addition, we shall also hear examples of what one can do with simple force laws in suggesting some of the kinds of phenomena which might be taking place at a crack tip.

The simplest fractures occur in brittle materials like glass, and these materials provide convenient models where the chemistry taking place at cracks can be studied without the additional complexities caused by dislocations. It has been found that a whole class of molecules exists which act like water in the silicate glasses. On the one hand, it is possible to model how these molecules lead to slow crack growth in such materials. But on the other, it is also found that very interesting subtleties exist associated with the threshold region, where steric hindrance and long range molecular interactions appear to play a surprising role.

A number of papers will deal with both theoretical and experimental aspects of crack-dislocation effects. Most

theory and model experiments have suggested that not only are cracks in some cases sources of dislocations, but that the dislocations act to shield the crack from the external stress, and that in both cases, the idea of a dislocation free zone near the crack tip is important. A counterpart of these ideas has developed in ceramics where toughening due to stress induced martensite is described in terms of shielding. However, these general ideas are considered by some to be still controversial. In particular, it is not clear how to apply these ideas fruitfully to ductile fracture, where micro void formation and coalescence occur, and where current fracture criteria are based on the critical strain near the crack tip. For ductile fracture, the most successful modeling so far proceeds from a combination of metallurgical micro structure observations and continuum mechanics concepts.

A number of papers will deal with the classic problem of chemical effects on fracture in otherwise ductile materials. To some extent, the interpretation of these experiments is deeply entangled with the issues of the last two paragraphs. The case of hydrogen still resists full understanding, in part because of the complicating factors of dislocations, but also because of the ability of the hydrogen to penetrate the bulk, so it is still difficult to sort out the extent of the relative importance of the role of hydrogen at the crack tip (or an incipient internal crack tip), and at the internal dislocations. Some important new experimental studies will be reported in this field.

Descriptions of new stress corrosion experiments will lead us to entirely new ground, because it seems clear now from these experiments that cleavage can be induced into underlying ductile material by local corrosion embrittlement at the surface. (These experiments are only the most clear cut example of the ability of ductile materials to cleave under dynamic conditions.) Based on this early work, one gains the impression that some fundamental issues are here being raised in a new way which may lead ultimately new insight into a wide range of ductile/brittle phenomena in materials.

High temperature fracture, fatigue and intergranular effects are extensions of the forgoing subjects because of the additional variables introduced. A particular challange at this stage is see just how far one can go in incorporating the more basic ideas which may apply to simple model materials into the more complex situations. Generally also, in these areas, continuum mechanics concepts are the most useful theoretical tools used. In each case, it will be shown both what possibilities exist and what remains for the future.

How one builds an effective bridge across the disciplines comprising the field of fracture from continuum mechanics to atomic structure is a background issue which will be visible in many of our discussions. In part, we will see the direct involvement of the practitioners of one discipline in another, and in part we will see interdiscipinary collaboration. In whatever way these bridges are built, however, it is an essential activity because it provides a needed perspective which can highlight the crucial problems which most need solution.

MODERN ATOMISTIC THEORIES OF FRACTURE *

MURRAY S. DAW & MICHAEL I. BASKES
Sandia National Laboratories, Livermore, CA 94550

Two fundamental problems currently prevent atomistic calculations of fracture from becoming the powerful tool that it could be. The first difficulty is in describing the internal forces in a realistic way. The second lies with the boundary conditions imposed on the calculation.

In the past, the internal forces have been determined from two-body interatomic potentials. There are serious questions and also difficulties with the use of pair potentials, however. Pair potentials are on dubious theoretical grounds. One can derive pair potentials from pseudopotential theory in a perturbative way, leading to a succession of n-body terms (n=1,2,3,...). The 1-body term (or the so-called "volume-dependent term"), is *required* in addition to the 2-body interactions in order to describe the elastic properties of the solid. In practice, this requires a knowledge of the *volume* of an arrangement of atoms. How does one define the volume when the solid is plastically deforming, cracking, or forming internal voids? This volume dependent term is often ignored, thus leaving the serious question as to the elastic properties of the model; in a sense, such calculations are describing an unknown solid with unphysical elastic constants. Pair potential calculations by definition neglect all interactions among more than two bodies. These many-body interactions may in fact play an important role in such interesting processes as hydrogen embrittlement. In fact, fundamental cluster calculations show that hydrogen in metals *cannot be represented by simple pair interactions*. One does not want to berate pair potential calculations, because they have lead to significant understanding of atomistic processes. However, several weaknesses in such calculations are apparent.

The problem of realistic internal forces has been overcome largely by the recent development of the Embedded Atom Method (EAM). The EAM provides a new framework for calculating the energetics of transition metals. In this approach, the dominant energy of the metal is viewed as the energy to embed an atom into the local electron density as provided by the remaining atoms of the system. This is supplemented by a short-range core-core repulsion. The resulting approach combines the computational simplicity needed for defects and amorphous systems with a physical picture which includes many-body effects and avoids the ambiguities of the pair potential schemes. This method has been applied to such problems as phonons, liquid metals, defects, alloys, impurities, fracture, surface structure, surface

adsorbate ordering, and surface segregation. The required computer time is not significantly more than that required for pair potential calculations. The EAM should replace pair potentials in atomistic calculations.

The second fundamental difficulty facing atomistic calculations is that of boundary conditions for the calculation. Various schemes have been proposed for how to divide the real solid into an atomistic region surrounded by a boundary of some kind intended to simulate the properties of the extended crystal. Examples include the fixed boundary, the flexible boundary, and the fixed stress schemes. Even within these schemes, care must be taken as to how external stresses are applied; transients due to switching the external forces on too quickly may dominate the results. The schemes themselves of course do not model exactly the fully dynamical response of the extended crystal. (In fact, no *local* continuum can have the full dynamical properties of a real crystal!) The effects of boundary conditions and possible solutions to the problem should be at the focus of future efforts in improving atomistic simulations.

The two fundamental difficulties will be reviewed in depth. The EAM will be explored as an alternative to pair potentials. The effects of boundary conditions and possible solutions will be investigated.

*This work is supported by the U.S. Department of Energy.

INTERATOMIC POTENTIAL DESCRIPTIONS OF ATOMIC PROCESSES IN METALS*

A. E. Carlsson
Department of Physics, Washington University, St. Louis, Missouri 63130

Attempts to model the bonding energy in metallic media with interatomic potentials have led to the use of a bewildering variety of potentials, depending on both the type of *problem* under consideration and the properties of the local atomic *environment*. The talk will focus on the "problem" dependence of the potentials. The types of problems under consideration may be represented by two extreme varieties:

1) "Bond-Breaking" Problems. These problems include vacancy, void, and surface formation, and to a lesser extent, dislocation and grain boundary formation. The loss in bonding energy is associated with the reduced local bandwidth. Pair potentials for treating these types of problems can be generated[1-3] by analysis of the low-order moments[4] of the electronic density of states. These potentials (cf. Fig. 1) have a deep minimum and short range, and decay monotonically beyond the minimum. The relevant expansion parameter for use of the potentials is the change in coordination number. Thus vacancy and surface formation, which typically involve coordination number changes of 10-30%, can be well treated by this type of potential, while the whole cohesive energy of the crystal cannot. "Bond-breaking" potentials depend on the local density of atoms and coordination number through the local bandwidth. Empirical and semi-empirical realizations of the "bond-breaking" potential include a many-atom cluster formalism based on the cohesive energy,[5] the "embedded-atom" scheme,[6] and the "Johnson"-type potential.[7]

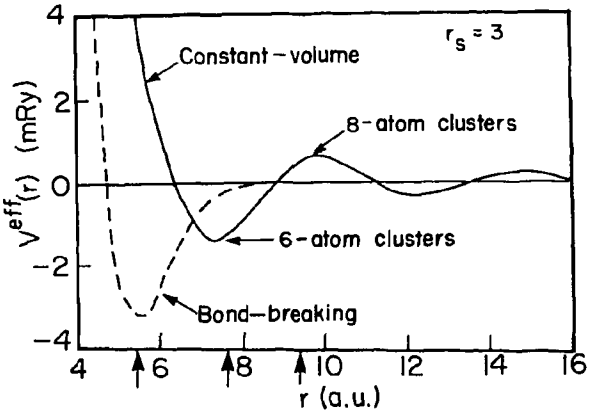

Figure 1
Effective pair potentials for model metal with Gaussian interatomic hopping terms. r_s is electron gas spacing parameter.

*Supported by the Department of Energy under grant No. DE-FG02-84ER45139.

2) "Constant-Volume" Problems. These include, for example, crystal structure energy differences, phonon dispersion curves, vacancy and grain boundary relaxation energies, and liquid structure factors. Little free volume is created on a local scale, although atoms may rearrange themselves around voids. The atomic rearrangements lead to a change in band-*shape* rather than band-*width*. The appropriate pair potentials for treating these problems are obtained by expansion[3,8,9] of the total energy in powers of the weak electron-ion pseudopotential. They generally have first minima shallower than in "bond-breaking" potentials and display long-ranged oscillations. (cf. Fig. 1) Their range of applicability excludes problems involving large changes in the long-wavelength part of the static structure factor, such as vacancy formation. On the other hand, *relaxation* around a vacancy can be treated fairly accurately. Like the "bond-breaking" potentials, the "constant-volume" potentials are sensitive to the local environment, through changes in the electron gas response function. Empirical "constant-volume" potentials can be obtained, for example, from measured phonon dispersion relations[10] and liquid structure factors.[11]

Although the limits described under 1) and 2) are physically quite distinct, they can be understood within a common theoretical framework[2] based on explicit many-atom cluster interactions. Provided the geometry of the system is well enough understood, the cluster terms can be resummed into an effective pair potential, valid for a restricted set of atomic configurations. In the constant-volume limit, for example, one assumes that all the atoms except one pair are uniformly distributed. Resumming the higher-order potentials on this assumption one obtains a potential very similar to the "constant-volume" potential described above. The oscillations in this potential are directly associated with the alternating signs of the cluster interactions, with oscillations at large distances arising from progressively larger clusters. (Cf. Fig. 1) It hoped that similar analyses can be used to generate a variety of potentials for problems which cannot at present be treated with pair potentials.

REFERENCES

1. A. E. Carlsson and N. W. Ashcroft, Phys. Rev. B 27, 2101 (1983).
2. A. E. Carlsson, Phys. Rev. B 32, xxxx (1985); R. H. Brown and A. E. Carlsson, Phys. Rev. B 32, xxxx (1985).
3. J. M. Wills and W. A. Harrison, Phys. Rev. B 28, 4363 (1983).
4. F. Cyrot-Lackmann, J. Phys. (Paris) 31, C1-67 (1970).
5. M. W. Finnis and J. E. Sinclair, Phil. Mag. A50, 45 (1984).
6. M. S. Daw and M. I. Baskes, Phys. Rev. B 29, 6443 (1984).
7. R. A. Johnson and W. D. Wilson, in *Interatomic Potentials and Simulation of Lattice, Defects*, edited by P. C. Gehlen, J. R. Beeler, and R. I. Jaffee (Plenum, New York, 1972), p. 301.
8. W. A. Harrison, *Pseudopotentials in The Theory of Metals* (W.A. Benjamin, New York, 1966), Chap. 2; N. W. Ashcroft, in Ref. 7, p. 91.
9. J. A. Moriarty, Int. J. Quant. Chem. Symp. 17, 541 (1983).
10. D. M. Esterling, in *Interatomic Potentials and Crystalline Defects*, edited by J. K. Lee (Metallurgical Society of AIME, Warrendale, Pennsylvania, 1981), p. 53.
11. C.C. Matthai, P.J. Grout, and N.H. March, Int. J. Quant. Chem. 12S, 443 (1978).

STRUCTURAL PREDICTION WITH THE TIGHT BINDING BOND MODEL

D. G. PETTIFOR
Department of Mathematics, Imperial College, London SW7 2BZ.

The atomic structure of a crack tip is crucial for determining whether a material is brittle or ductile and how the crack behaves in the presence of external chemical species [1]. Unfortunately, however, the computer simulation of structure is very sensitive to the particular choice of interatomic interaction, so that a theoretical model must be chosen which is compatible with the system under consideration. In this talk a microscopic, quantum-mechanical tight-binding model is presented which is accurate enough to predict trends in structural behaviour amongst the binary compounds of transition metals with metalloid elements, yet simple enough to offer the possibility of simulating defects and their interaction with impurity elements.

Recently all binary compounds with a given stoichiometry $A_m B_n$ have been separated successfully into different domains within a single two-dimensional structure map (χ_A, χ_B), where χ is a phenomenological chemical scale [2]. The upper panel of fig. 1 shows the structural domains of the seven most common pd bonded AB structure types, namely NaCl, CsCl, NiAs, MnP, FeB, CrB, and FeSi. The lower panel shows the predictions of tight-binding (TB) bond model [3] which writes the total energy as

$$U = U_{rep} + U_{bond} . \qquad (1)$$

The repulsive energy is represented by pair potentials, whereas the quantum mechanical bonding energy may be expressed [4] as a sum over the individual bonds, namely

$$U_{bond} = \sum_{\substack{ij \\ i \neq j}} h_{ij} \{ -\frac{1}{\pi} \mathrm{Im} \int^{\varepsilon_f} G_{ji}(\varepsilon)\, d\varepsilon \} \qquad (2)$$

where h_{ij} is the TB hopping integral between neighbouring atoms i and j, ε_f is the Fermi energy, G_{ij} is the inter-site Green function, and the expression inside the curly brackets is the bond order. We see from fig. 1 that the simple pd bonded TB theory predicts the broad topological features of the observed structure map, the main failure being the inability to predict the FeSi domain.

The preliminary results of extending this TB model to the structure of grain boundaries [5] are presented.

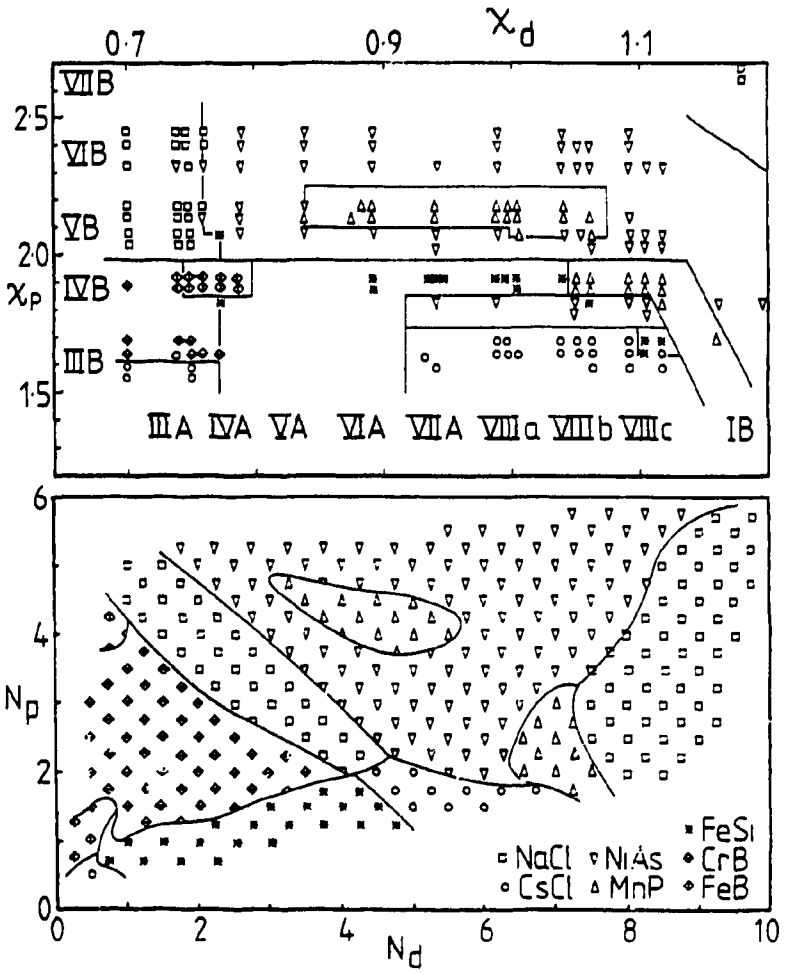

Fig. 1. Upper panel: The (χ_p,χ_d) structure map for 169 pd bonded AB compounds, where χ_p and χ_d are the values of the chemical scale for the metalloid and transition elements respectively. The 2p elements are not included in the present figure.
Lower panel: The theoretical structure map (N_p,N_d) where N_p and N_d are the number of p and d valence electrons respectively.

REFERENCES

1. R.M. Thomson in Physical Metallurgy R.W. Cahn and P. Haasen, eds. (North Holland, Amsterdam 1983), Ch. 23.
2. D.G. Pettifor, Sol. St. Commun. 51, 31 (1984); J. Phys. C. (1985).
3. D.G. Pettifor and R. Podloucky, Phys. Rev. Lett. 53, 1080 (1984); 55, 261(C) (1985).
4. M.W. Finnis and D.G. Pettifor in The Recursion Method and its Applications, D.G. Pettifor and D.L. Weaire, eds. (Springer, Berlin 1985), Springer Series in Sol. St. Sc., 58, 120.
5. Y. Ohta, M.W. Finnis, A.P. Sutton, and D.G. Pettifor (to be published).

ELECTRONIC THEORY FOR HYDROGEN EMBRITTLEMENT OF BCC TRANSITION METALS

K. MASUDA-JINDO

Department of Materials Science and Engineering, Tokyo Institute of Technology, Nagatsuta, Midori-ku, Yokohama 227, Japan

INTRODUCTION

The study of hydrogen enhanced fracture of metals and alloys has received a great deal of interest in recent years [1]. The purpose of the present paper is to investigate the interaction between the solute hydrogen and crack tips in bcc transition metals using a microscopic electronic theory. We will show that the electronic interaction energies E_{bin} between the hydrogen and the crack are quite important: E_{bin} depends strongly on the applied stress as well as on the geometry of the crack. We also estimate the energy E_{br} required to break the metallic bonding near the crack tips in the presence (and absence) of hydrogen atoms.

PRINCIPLE OF CALCULATIONS

We calculate the binding energies E_{bin} between the solute hydrogen and cracks in bcc transition metals taking into account three contributions, i.e., the d-band energy term which is treated in the tight-binding (TB) approximation, an electronic correlation contribution within the Hubbard model (second order perturbation theory) and a pairwise repulsive potential of the Born-Mayer type:

$$E_{bin} = \Delta E_{band} + \Delta E_{corr} + \Delta E_{rep} . \qquad (1)$$

The band energy term ΔE_{band} are evaluated by using the Gaussian density of states (DOS) fitted to the first and second moments μ_{1i} and μ_{2i}, and using the self-consistent Hartree approximation for the defect perturturbing potential [2].

The correlation terms can be calculated on each site i by assuming a rect-angular DOS of effective d-bandwidth W^i_{eff}, fitted to give the exact second moment on atom i [3]. For the solute hydrogen, we also use a second order perturbation theory for the Coulomb repulsion U_H (for simplicity, $U/W = U_H/W = 0.25$ are used in the present calculations, W (= 6.16 eV) being the d-bandwidth).

The short-range repulsive energies ΔE_{rep} between atomic sites i and j are calculated using a two-body potential of the Born-Mayer type: $C_0 \cdot \exp(-pR_{ij})$. The parameter values C_0 and p are determined, together with those for the d-band, so as to satisfy the equilibrium condition and so as to reproduce well the experimental bulk modulus and elastic constants. Specifically, $p = 5.157$ Å^{-1} and $C_0 = 9.243 \times 10^4$ eV are used for α-Fe.

The hopping matrix elements V_{da} between the solute hydrogen and host metal atoms are estimated from the atomic sphere approximation

$$|V_{da}|^2 = (2\sqrt{5})^2 \, \Delta_d \cdot \Delta_a \, |\vec{R}_d - \vec{R}_a|^{-6} \qquad (2)$$

where Δ_d and Δ_a are constants describing the d-states and hydrogen state, respectively. The atomic level ε_a of the solute hydrogen is determined using the condition of the local charge neutrality.

RESULTS

Using the above mentioned theoretical scheme and direct total energy minimization procedure [2], we have calculated atomic configurations around the cracks in bcc transition metals: To simulate the (micro) cracks, we introduced lines of vacancies (LOV) along <001> direction in the crystallite. In Fig.1, we present the calculated local DOS on atoms around a microcrack composed of three LOV in α-Fe. One can see that the detailed electronic structures around the microcrack are considerably different from those of the cleaved surfaces and of the bulk crystal. This indicates that crack behaviors in transition metals should be investigated using a microscopic electronic theory.

E_{bin} values for hydrogen solute in α-Fe are shown in Fig.2 (three LOV crack model). One can see in Fig.2 that E_{bin} depends strongly on the applied stress as well as on the geometry of the crack: In general, stronger (attractive) E_{bin} values are obtained for the higher tensile stresses.

Using the criterion for the decohesion proposed by Sayers [4], we have also calculated the changes in the metallic bonding near the crack tips. We have found that energy required to break the bond E_{br} in the presence of hydrogen becomes considerably smaller (~80%) than that of the hydrogen free crystal. We have also performed similar calculations for other types of cracks such as those introduced from cleaved surfaces, and obtained the similar results. In conclusion, the present theoretical findings are in good agreement with the experimental results on the hydrogen enhanced fracture of iron and high strength steels [5].

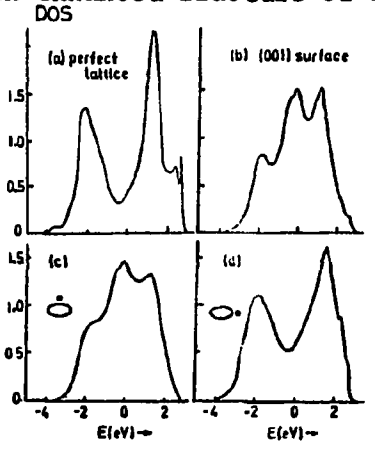

Fig.1 Local DOS for atoms around the microcrack in α-Fe.

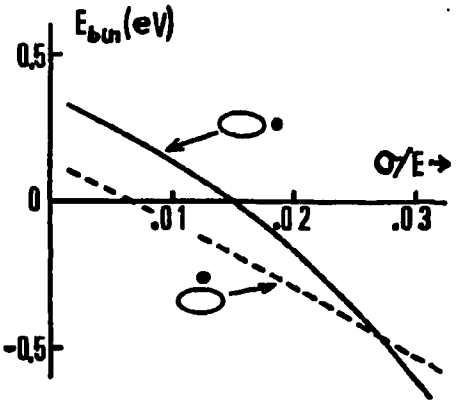

Fig.2 E_{bin} for H in α-Fe.

References

1. T. Tabata and H.K. Birnbaum, Scripta Met. 18, 231-236 (1984).
2. K. Masuda-Jindo, Materials. Lett. 3, 151-156 (1985).
3. G. Tréglia, F. Ducastelle and D. Spanjaard, J. Physique 41, 281 (1980).
4. C. M. Sayers, Phil. Mag. 50B, 635-640 (1984).
5. H. K. Birnbaum, "Mechanical Properties of BCC Metals" Edited by M. Meshii, The Metall. Soc. AIME (1981) P.153-169.

THE ENERGETICS OF STRUCTURAL RELAXATIONS, DYNAMICS AND TRANSPORT AT INTERFACES*

UZI LANDMAN
School of Physics, Georgia Institute of Technology, Atlanta, GA 30332

Extended defects such as external surfaces, grain boundaries, cracks and other interfaces modify electronic, crystallographical, dynamical and mechanical properties of solid materials. The energetics underlying structural relaxations, dynamical properties and transport at the vicinity of interfaces will be discussed in the light of recent theories based on total energy minimization methods and molecular dynamics simulations.

*Work supported by U. S. DOE contract No. EG-S-05-5489

DEPENDENCE OF CRACK VELOCITY ON THE INTERATOMIC POTENTIAL

G. J. DIENES*, A. PASKIN**, K. SIERADZKI*, B. MASSOUMZADEH**, AND K. SHUKLA**
*Brookhaven National Laboratory, Upton, New York 11973
**Queens College of C.U.N.Y., Flushing, New York 11367

The dynamic properties of moving cracks were studied by means of molecular dynamic simulations on two-dimensional triangular lattices.[1-2] The interatomic potential was found to be the most important factor in leading to ductility (dislocation generation) or to brittle crack propagation. Care was taken to compare the different potentials under similar initial conditions (e.g., rate of load application). Under carefully controlled conditions, the Johnson, J, empirical potential (originally designed for simulating iron) results in a considerably more brittle behavior than the 6-12 Lennard-Jones, L.-J., potential and reaches a higher limiting crack velocity.[3] Even in the J. solid there is evidence of dislocation generation after considerable crack growth.

"Covalent" potentials were also investigated. These potentials were constructed by adding an angular resistance term to the L.-J. and J. potentials. The lattice rigidity was varied over a very wide range by varying the intensity, a_0, of the angular resistance. For these potentials the crack propagation is brittle and the crack velocity increases very markedly with increasing a_0. The data are summarized in table I where the terminal crack velocities, v_{ct}, are given for a set of a_0 values normalized with respect to v_L, the longitudinal sound velocity. The crack velocity increases by a factor of two to four with increasing a_0 but this increase saturates at $v_{ct}/v_L \approx 0.42$. It is to be noted that while the longitudinal sound velocities have increased only by a factor of 1.5 the crack velocities changed by almost a factor of 6.

Table I. Crack velocity data as a function of a_0, the angular resistance amplitude.

	Lennard-Jones, L.-J. potential	Johnson, J. potential
a_0	v_{ct}/v_L	v_{ct}/v_L
0.00	0.12	0.24
0.30		0.28
0.50	0.28	
0.75		0.35
1.00	0.32	0.40
3.00	0.42	0.41
5.00	0.42	

ACKNOWLEDGEMENTS

This research was supported under the auspices of the U.S. Department of Energy, Division of Materials Sciences, Office of Basic Energy Sciences under Contract No. DE-AC02-76CH00016 and by the National Science Foundation under Grant No. DMR/8301775.

REFERENCES

1. A. Paskin, D. K. Som, and G. J. Dienes, Acta. Metall. 31, 1841 (1983); G. J. Dienes and A. Paskin, Computer modeling of cracks, in Atomistics of Fracture (edited by R. M. Latanision and J. R. Pickens), pp. 671-705, Plenum Press, New York (1983).
2. A. Paskin, D. K. Som, and G. J. Dienes, Acta Metall. 31, 1841-1848 (183).
3. G. J. Dienes, K. Sieradzki, A. Paskin, and B. Massoumzadeh, Bull. Am. Phys. Soc. 30, 617 (1985).

ATOMIC COMPUTER SIMULATION OF FRACTURE OF METALS

MASAO DOYAMA AND RYOICHI YAMAMOTO
Department of Metallurgy and Materials Science
Faculty of Engineering, The University of Tokyo
7-3-1 Hongo, Bunkyo-ku Tokyo 113 JAPAN

Body centered iron and face centered copper whiskers were pulled until broaken into two pieces in a super computer Hitachi M-200.

A needle shape whisker consisting of 2000 atoms was created by a computer. The axis was [001] direction. This axis is taken as z axis. The size was 8a x 8a x 14a atoms, where a is the lattice parameter. And truncated at the edges. This specimen is called Specimen A. Another needle shape whisker consisting of 2032 atoms were also created. The axis was [110] direction. The sides faces were (110) and (001). This specimen is called Specimen B.

The method of molecular dynamics was used. Two atomic layers at the both ends, "holder" region, were specially treated, extended and held at these positions. The tensile deformation of 0.004 was uniformly given in a tensile direction then the atoms were relaxed by the method of molecular dynamics. After each tension, atoms were relaxed by the molecular dynamics for 100 steps. Then uniform extension was again given. One hundred steps of relaxation was performed. This procedure was repeated. The atount of tension in each step was 0.004.

The interatomic potential between the i-th and j-th atoms was represented by

$$\phi(r_{ij}) = -0.188917(r_{ij} - 1.82709) + 1.70192(r_{ij} - 2.50000) + 0.$$

for iron which was determined by Pak and Doyama[1] and smoothly truncated at 3.44 A.

$$\phi(r_{ij}) = -1.5323\} (r_{ij} - 2.251664)(r_{ij} - 1.$$

for copper.

The total force in the axis direction of all the atoms in the "holder" region were calculated. This can be taken as the tensile stress. This tensile stress-strain curves for Specimen B is plotted in Fig.1. After the yield point, a phase transition was observed.

Specimen B was pulled in [111] direction. In the specimen, the resolved shear stress to [111] on 111 plane is the highest for one of the slip systems. A easier glide is expected. The slip started at the corner of the tip of the crack, i. e. the place where the crack ends at the surface. Slip started from the (001) surface. Up to 0.3, the specimen was very uniformly extended except very near the crack. After 0.3, the specimen was suddenly transformed. Inside the crystal six-fold symmetrical configuration was observed. This intermediate six fold symmetry

configuration suddenly changed to a twin at about 10% elongation. Twin region was expanded as the deformation progressed. The six fold symmetry region was also expanded. Above 17%, very severe deformation was observed.

The "necking" was started above 22% elongation [Fig. 2]. At 28% elongation, the specimen was brokgn into two pieces[Fig.3]. After fracture, the region of six-fold symmetry configuration decreased under no stress and the original body centred cubic lattice of alpha-iron was obtained.

The results of copper whiskers will be reported at the conference.

REFERENCES

1. H. M. Pak and M. Doyama, J. of the Faculty of Engineering, University of Tokyo (B) 30, 111 (1969).

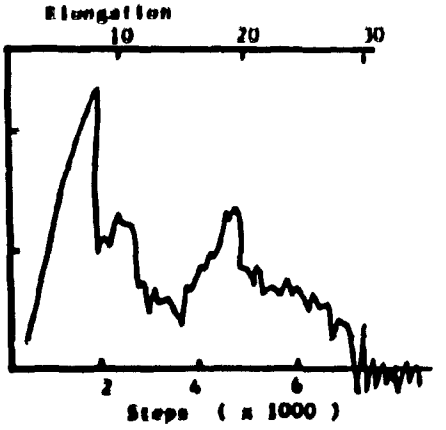

Fig. 1. Stress-strain curve for Specimen B pulled in [111] direction.

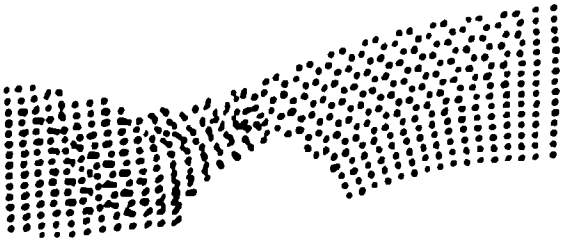

Fig. 2. Necking was observed at the elongation of 22% .

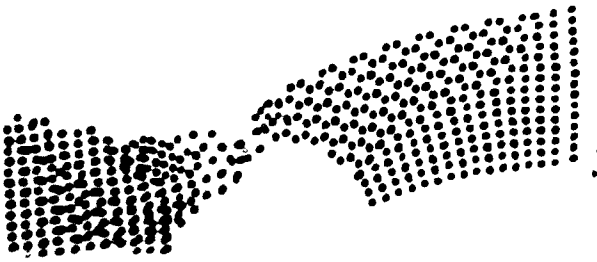

Fig.3. Specimen B is almost brocken into two pieces.

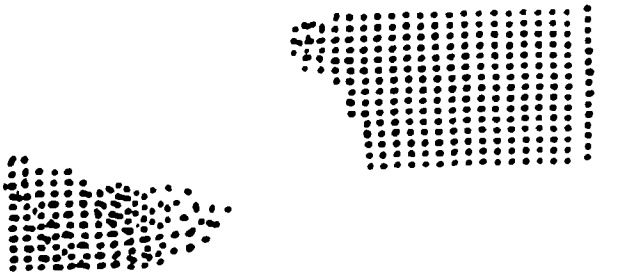

Fig.4. Specimen B is completely brocken into two pieces. Six-fold symmetrical structure is also disappeared.

A Computer Simulation Study on the Propagation of a Surface Crack

David M. Cooper* and Timur Halicioglu**
*Thermo- and Gas-Dynamics Division, NASA, Ames Research Center,
Moffett Field, California 94035
**Department of Materials Science and Engineering, Stanford University,
Stanford, California 94305

Introduction

A molecular dynamics technique based on a pair interaction model was employed to simulate the propagation of surface cracks in a two-dimensional triangular lattice. Calculations are aimed at investigating atomistic nature of the crack tip processes. Analyses include an investigation of the effect of the initial crack length as well as the distributions of the high stress regions in the system and their associations with the crack tip. The relationship between the stress distribution and the plastic deformation around the crack tip was also anlyzed. Calculated results were found to be consistent with existing continuum theories.

Method of Calculation

In this investigation simulation calculations were carried out by a molecular dynamics method using the fifth order Nordsieck-Gear algorithm [1]. This method is based on well established statistical mechanical considerations and, in general, employs a semiempirical potential function to estimate forces among the particles in the system. For instance, for particles interacting via pair interactions the total potential energy of a system of N particles can be expressed as:

$$\Phi = \frac{1}{2}\sum_{i}^{N} \phi_i \tag{1}$$

where, ϕ_i represents the potential energy of the i'th particle which is given by:

$$\phi_i = \sum_{j}^{M} u(r_{ij}) \tag{2}$$

where, M is the total number of neighbors of the atom i confined in a sphere of radius R_{cut} which is used as the cut-off radius in numerical evaluations. The distance between the particles i and j is denoted by r_{ij}. To represent pair interactions, $u(r_{ij})$, in this study, we employed the Lennard-Jones function. For each particle, stress components were also calculated considering Lagrange strain parameters.

In all energy, force and stress calculations the R_{cut} was assume to be equal to $3r_o$. Furthermore, in the calculations all values were normalized with respect to ϵ and r_o. In all cases, a dimensionless time step was taken to be equal to 0.0075 and the simulation calculations were performed under isothermal conditions. The model employed in this study consisted of a two-dimensional triangular lattice i.e., the basal plane of an hcp crystal containing 2400 - 5000 particles . First, the perfect lattice was brought to a static equilibrium condition. This system displays an almost elastic behavior and resists plastic deformations up to relatively high strain values (see reference [2]). Then, a surface crack in the $\{01\bar{1}\}$ direction (which was taken as the y-direction of the cartesian coordinates in this study) was created by removing several of atoms from the surface region. This system, now, bearing a surface crack was elongated in a stepwise fashion by imposing a uniaxial load in small increaments in the close-packed direction (i.e., the x-direction). A periodic boundary condition was applied in the x-direction to provide continuity. In the y-direction, however, two exposed surfaces, one bearing the initial crack, were left intact. After each incremental elongation, with $\Delta e = 0.005$ (where, Δe denotes the imposed incremental strain), the system was allowed to fully equilibrate under the molecular dynamics code.

Several separate tests were conducted on the model with an initial crack of varying lengths. In these tests, the system was prestressed to $e = 0.040$. The relaxation behavior of these prestressed systems was examined under the molecular dynamics code. All the calculated values for the energies, forces stresses and their fluctuations due to the thermal effect were monitored during the equilibration process.

Conclusions

A novelty introduced in the present simulation is the calculation of the individual stresses. As anticipated, in all cases, the high stress regions were found to be associated with the crack tip. Simulations also revealed the existence of dislocations radiating from the tip of the crack. In general, the present results agree well with other reported calculations, as well as with existing theories based on macroscopic approaches.

References

[1] C. W. Gear, in "Numerical Initial Value Problems in Ordinary Differential Equations", (Prentice-Hall, Princeton, NJ, 1971).

[2] T. Halicioglu and D. M. Cooper, Mater. Scie. Eng., **62**, 121 (1984).

PLASTICITY AT CRACK TIPS: DISLOCATION AND CONTINUUM SCALES

JAMES R. RICE
Division of Applied Sciences, Harvard University, Cambridge, MA 02138

SYNOPSIS

The presentation reviews various approaches to evaluating plasticity effects at crack tips.

One fundamental issue is that of whether an atomistically sharp crack remains so up to conditions for cleavage decohesion at its tip or whether, instead, a dislocation first nucleates from the tip and thereby makes impossible, or at least delays, the occurrence of cleavage. Recent extensions of the Rice-Thomson formulation for crack tip dislocation nucleation are reviewed and examined for consistency with the occurrence of cleavage in different materials and with dislocation emission observations by electron microscope studies of the Ohr type for cracks in thin films.

An important problem is that of if and how dislocation emission occurs in the dynamic situation when a rapidly moving crack leaves a brittle phase in which it nucleated and continues into a normally ductile lattice (e.g., crack nucleated in cementite inclusion continuing into ferrite grain).

To understand cracking processes in generality it is necessary to understand the kinematics and dynamics of large groups of dislocations near a crack tip. Such groups may include dislocations that have been nucleated from the tip or may instead be dominated by dislocations moving from non-tip sources activated by the crack stress concentration. Extensive dislocation activity is obviously necessary for operation of microscopically ductile (but, possibly, macroscopically brittle) fracture mechanisms involving cavity growth by flow processes, often terminated by localized shearing-off of ligaments between voids and a crack tip. However, surprisingly large amounts of plastic flow often accompany brittle, apparently cleavage-like fracture processes in metals, and there have been suggestions that environment or solute effects (e.g., hydrogen) may embrittle in a macroscopic sense by greatly increasing local plastic flow in the immediate vicinity of the crack tip. Cleavage decohesion and shear processes of fracture have been regarded traditionally as being mutually exclusive (although it is understood that both can operate simultaneously at different sites, e.g., by cavity nucleation at inclusions through cleavage or interface decohesion and growth to coalescence by plastic shear processes). Various observations suggest, however, the importance of determining if and in what circumstances decohesion and shear can act in unison at the same crack tip, thus allowing more-or-less continuous transitions from locally brittle to locally ductile crack opening modes with change of loading rate, temperature or environment.

There is now a vast literature on the treatment of multi-dislocation processes at crack tips by continuum plasticity. Most progress has been made with the classical Prandtl-Reuss-Mises type of theory which is intended to address response at a macroscopic scale, averaging over individual crystallites. This theory has had many successes, sometimes outside its expected range of validity. These include characterizing the overall crack tip stress field within which microscopic cleavage or rupture events nucleate at heterogeneities, explaining the effects of triaxial stress constraint and its loss in ductile-brittle transitions, describing crack tip opening and large strain development near the tip at onset of ductile rupture, and explaining the origins of potentially stable ductile crack growth and toughness increase with crack speed in dynamic fracturing. Recent extensions of such studies to modelling materials with nonlinear viscous response, representing elevated temperature creep, have provided a basis for understanding load history and hold-time effects on time dependent crack tip stressing, and suggested parameters for correlation of crack growth in the creep range. Also, extensions to modelling viscoplastic response at high strain rates show promise for explaining various aspects of ductile to brittle transitions in cleavable solids.

In the presentation I intend to focus on some recent continuum studies aimed at an intermediate scale between that for conventional macroplasticity and for discrete dislocations. These studies analyze crack tip stress and deformation fields according to the continuum plasticity of single crystals (limited set of crystal slip systems, critical shear stress to activate each) and interpret results in terms of dislocation processes necessary to accommodate the predicted deformations. The crystal plasticity solutions predict that, to the neglect of hardening, crack tip response is dominated by discontinuity surfaces emanating from the tip (discontinuity of stress and displacement for stationary cracks, but of particle velocity only for quasistatically growing cracks).

As an example, for cracks growing along [011] on a (100) plane in cubic lattices, the discontinuities coincide with {111} type slip planes for the f.c.c. case. However, for a hypothetical b.c.c. case in which (for illustration) slip occurs only on planes of {211} type, the predicted discontinuities are kink-like in that they lie perpendicular to the active {211} slip systems. Further, in examining the dislocation interpretation of deformations predicted for these two examples, plastic relaxation for the f.c.c. case can be effected by dislocations swept out from the crack tip, whereas for the hypothesized b.c.c. case (for which comparable plastic stress relaxation is predicted at the tip) none of the flow can be effected by dislocations swept out from the tip, but must involve pre-existing sources. These results have some experimental support and may have important implications for cleavage versus ductile response: They suggest that there is no requirement that dislocation emission from a crack tip accompany plastic relaxation of stresses, and also suggest that significant changes in crack tip stress fields will result, for certain crack orientations in crystals, when appropriate pre-existing sources are either not present or do not have time to operate.

CRACK PROPAGATION MECHANISMS AND LOCAL CRACK DRIVING FORCE

EDWARD W. HART
Cornell University, Ithaca, NY 14853

When a micro-mechanism for crack propagation is investigated, it is most commonly described as though the crack is embedded in a material medium that is otherwise elastic in its response to stress loading. The loading that is then acting on the crack is described in terms of the remote loading applied to the medium. In this "small scale yielding" description the loading can be characterized by an "apparent" stress intensity factor that we shall designate by K_A, where the mode of loading is understood to be that appropriate to the problem considered. In the context of the Barenblatt theory, any discrete cracking mechanics that is restricted to a single active plane extending from the actual crack tip can be fully characterized by the stress intensity factor K that would be operative at the sharp crack tip that would be present in the absence of the detailed cracking mechanism. If the material is otherwise linear elastic, the "local crack tip stress intensity factor" K is equal to K_A.

A theory has been developed [1,2] that extends this description to inelastic materials for which (a) the inelastic deformation is described by a real-time deformation rate, and (b) the crack tip is propagating at a steady, non-zero velocity v. For this case it has been shown that the local stress intensity factor K is well defined and that it differs from K_A by the amount of a term K_P that depends on the inelastic flow law and on v, and that describes the effect of the inelastic deformation in screening the crack tip.

The importance of this result for micro-mechanics is that comparison of micro-mechanical theory with experiment must also take account of the plastic effect K_P. New results extend the earlier work to all crack modes.

REFERENCES

1. E. W. Hart, Int. J. Solids Structures 16, 807 (1980).
2. E. W. Hart in: Elastic-Plastic Fracture: Second Symposium, Vol. I, ASTM STP 803, C. F. Shih and J. P. Gudas, eds. (American Society for Testing and Materials, 1983).

THE ANALYTICAL SOLUTION OF A GROWING STEADY-STATE MODE III CRACK IN AN ELASTIC PERFECTLY-PLASTIC SOLID THROUGH AN ELECTRICAL ANALOGY

J. WEERTMAN
Department of Materials Science & Engineering, Materials Research Center and Department of Geological Sciences, Northwestern University, Evanston, Illinois 60201

No analytical solution has been found up to now for the important theoretical problem of a growing crack in an elastic plastic solid. Only partial solutions have obtained for quasi-static growing steady state growth of mode III cracks in an elastic perfectly-plastic solid. Chitaley and McClintock [1] found the asymptotic analytical solution which is valid very close to the crack tip. Their (computer) solution at larger distances from the tip is not correct. The actual plastic zone, as shown with a computer calculation by Dean and Hutchinson [2], is much larger than the plastic zone which presumably is valid except very close to the crack tip. The DH computer solution did not approach the CM asymptotic solution at a distance from the crack tip equal to their smallest mesh length.

This paper presents an analytical solution of the growing, steady state mode III crack in an elastic perfectly-plastic solid which was started by the work of McClintock [3] and Chitaley and McClintock [1] and which was greatly enlightened by the computer calculations of Dean and Hutchinson [2]. This paper is built on the work of all of these investigators. The essential and new ingredient of the present work is the introduction of Eshelby's screw dislocation electrical line charge analogy. Attacking the problem through use of (non-redundant) dislocations enables the focus of the analysis to remain very physical. The physical picture leads the way and the mathematics tags along, rather than the other way around. Although the analysis is long the final answer is not too complicated.

Plastic strain is calculated from the motion of non-redundant infinitesimal screw dislocations. Calculation of the dislocation crack tip shielding can be used as an approximate check of the analysis. (For the stationary crack it is simple to show that the dislocations of the plastic zone shield the crack tip perfectly.) The solution contains the Chitaley and McClintock asymptotic solution near the crack tip, the Chitaley and McClintock plastic zone sector of a crack tip focused fan, and the Dean and Hutchinson unfocused fan plastic zone sector.

Dislocations can move when the magnitude of the stress vector equals the flow stress. Dislocations can only enter the solid from the crack tip. The stress trajectories are tangent to the direction of dislocation motion. In the secondary plastic zone the non-redundant dislocation density is zero. The non-redundant dislocation density at any place in a solid is equal to $\nabla.p/G$ where p is the stress vector and G is the shear modulus. At a crack tip the stress trajectories are a fan of radial stress trajectories. Dislocations enter the plastic zone in this fan. This is the CM plastic sector. If the fan is non-focused, dislocations cannot enter into it from a free surface because the trajectories neither converge to a point at a crack tip nor are they perpendicular to a free surface. However, if the crack moves, dislocations from a focused fan

region move into a non-focused region. This is the DH plastic sector. The straight trajectory, constant magnitude stress vectors p in the plastic zone satisfy the equations of static equilibrium which is $\nabla xp = 0$. But $\nabla.p \neq 0$ and dislocations must exist within the plastic sector.

In the plastic wake a mixed assortment of stress vectors describe the stress field. The stress vector introduced in the asymptotic crack tip region by Chitaely and McClintock is used. This stress vector by itself is satisfactory only in the limit of vanishingly small distance from the crack tip. The problem with the CM vector is "fixed" in this solution by introducing a displaced CM vector of opposite sign, making a dipole CM vector. When present as a dipole it is a dislocation source free stress suitable for any elastic region. One other stress in the wake is not dislocation source free and it carries the information about the dislocations that enter the wake. By the way it is defined it is automatically equal to zero at the elastic-wake boundary.

The plastic zone boundary was determined in the paper primarily, but not entirely, by setting the distance separating the two major CM stress vectors of opposite sign by an arbitrary distance and then attempting to calculate a boundary by finding where the magnitude of the total stress vector is equal to the yield stress. It turned out the success of such a calculation is very sensitive to the choice of the separation distance. The conservation of dislocation Burgers vectors is also used as a condition in determining the plastic wake boundary.

REFERENCES

1. A.D. Chitaley and F.A. McClintock, J. Mech. Phys. Solids 19, pp. 147-163 (1971).
2. R. H. Dean and J. W. Hutchinson, Fracture Mechanics, ASTM STP 700, pp. 383-405 (1980).
3. F.A. McClintock, Fracture of Solids (eds. D.C. Drucker and J.J. Gilman) Metallurgical Society of AIME Conferences, Vol. 20, New York: Interscience, pp. 65-102 (1963).

Finite D.F.Z. Cracks - An Approximate Treatment

N. Louat
Crystal Growth and Materials Testing Associates*
Lanham, MD 20801

Mathematical complexities make it improbable that analytical solutions for finite D.F.Z. cracks with plastic zones skewed to the main crack will be achieved in the near future. Furthermore, such solutions, if and when they are achieved, are likely to be in an indigestible form. Accordingly, it is germane to endeavour to develop approximations which are reasonably accurate and which can be represented in terms of simple functions.

Such an approach is considered here. To illustrate the method employed we first consider this, now familiar, case where crack and plastic zone are colinear and then successively skewed zones when the dislocations are of screw and edge type.

(1) Plastic Zones Colinear with Crack

We suppose a crack to lie in the range $-c<x<c$ and that each end of this region there are plastic zones $b\leq|x|\leq a$. To obviate the complexities involved in following Chang and Ohr and using Muskhelishvili's formulation we calculate:

(a) the dislocation distribution $g(x)$, which vanished at $|x|=b$ and a, and which is developed in the regions $b<|x|<a$ by a dislocation dipole with elements of strength $\pm f(\alpha)$ located at $x=\pm\alpha$.

(b) the magnitude of a uniform stress $\Delta\tau(\alpha)$ which must also be supposed present in order that the dislocation distributions exist;

*Work performed under contract N00014-84-C-2321 with the Naval Research Laboratory, Washington, DC 20375-5000

(c) The stresses developed in the region $-c<x<c$ by the distribution $g(x)$.

We then solve an approximation to the resulting singular integral equation for the dislocation distribution function $f(x)$ representing the crack, with the constraint that the implied sum over the elements $f(x)$ gives $\Sigma\Delta\tau(\alpha) = \tau$, where τ is the resistance to dislocation motion. The result is

$$f(x) = \frac{\sigma}{\pi A} \frac{x}{\sqrt{(c^2-x^2)}} \cdot F(a,b,c)$$

For F=1 this represents the familiar form for a crack of length 2c under a load τ. The effect of the foregoing calculations is to provide an expression for F(a,b,c), thus

$$F(a,b,c) \equiv \frac{B}{1+B},$$

where

$$B = \frac{1-k}{\pi} \int_{-c}^{c} \frac{\alpha^2 dx}{\sqrt{(c^2-\alpha^2)(a^2-\alpha^2)(b^2-\alpha^2)}}$$

$$= \frac{4\alpha}{\pi\sqrt{(a-c)b}} \{ K \sqrt{\frac{(a-b)c}{(a-c)b}} - \Pi \left(\frac{\pi}{2} \frac{-c}{a-c} \sqrt{\frac{(a-b)c}{(a-c)b}}\right)\}$$

and

$$k = \frac{ab-\sqrt{(a^2-c^2)(b^2-c^2)}}{c^2}.$$

Here K and Π are elliptic integrals of the first and third kinds. This result is subject to the constraint that

$$\tau = \sigma F \left(\frac{\sqrt{(a^2+b^2)}}{\sqrt{(a^2+b^2-2c^2)}} - 1\right).$$

(2) Plastic Zones Skew with the Crack

The analyses in these cases differ from that outlined above only through the additional complications which result from the form of the interactions between dislocations in the plastic zones and the main crack.

In the case of screw dislocations (mode 3) these are dealt with by using approximations such as

$$\frac{\zeta+y\ \cos\gamma}{y^2+\zeta^2+2y\zeta\ \cos\gamma} = \frac{\zeta+y\ \cos\gamma}{(y+\zeta)^2}$$

where γ is the angle between the skewed planes. This introduces an error certainly less than 25% provided $\gamma<60°$.

Similar approximations are involved for mode 1.

Results obtained using this method will be discussed.

THE EIGENSTRAIN METHOD APPLIED TO FRACTURE AND FATIGUE

T. Mura
Department of Civil Engineering and Materials Research Center
Northwestern University, Evanston, Illinois 60201

The eigenstrain method has been applied to several problems in fracture and fatigue mechanics. The eigenstrain ε^*_{ij} is a generic name given by the author to represent a class of nonelastic strains such as thermal expansion, phase transformation, initial strains, plastic, misfit strains. Eshelby (1957) referred to the eigenstrains as the stress-free transformation strains in his celebrated paper on inclusions and dislocations.

The eigenstrain method is a method to solve defect problems after defects in solids are simulated by a proper choice of eigenstrains in the homogeneous media. The defects include cracks, dislocations, inhomogeneities and inclusions, precipitates, vacancies, interstitials etc.

The first part of this paper is a summary of the fracture and fatigue problems and results which were obtained by the eigenstrain method. The second part of the paper is a new adventure aimed at extending the concept of eigenstrains to the atomic lattice theory and the quantum mechanical aspects of the defect theory.

The fundamental equations of the eigenstrain method are the equations of motion in elastic continua under a given distribution of eigenstrain ε^*_{ij}. They are

$$\rho \ddot{u}_i = C_{ijk\ell} (u_{k,\ell j} - \varepsilon^*_{\ell k,j}) , \tag{1}$$

where ρ is the density of material, $C_{ijk\ell}$ the elastic moduli, and u_i is the displacement.

For a stationary crack Σ under applied stress σ^o_{ij} at infinity, the total potential energy change ΔW caused by the introduction of Σ can be expressed by the following three equivalent equations,

$$\Delta W = \frac{1}{2} \int_\Sigma \sigma^o_{ij} n_j [u_i] \, ds \tag{2a}$$

$$= -\frac{1}{2} \int_\Omega \sigma^o_{ij} \varepsilon^*_{ij} \, dD \tag{2b}$$

$$= -\frac{1}{2} \int_\Omega \sigma_{ij} \varepsilon^*_{ij} \, dD - \int_\Omega \sigma^o_{ij} \varepsilon^*_{ij} \, dD, \tag{2c}$$

where $[u_i]$ is the displacement jump across Σ, n_i the normal to Σ, dS

the surface element of Σ, Ω the infinitesimally thin ellipsoid where the eigenstrain ε^*_{ij} is defined, and σ_{ij} is the eigenstress caused by ε^*_{ij}. For an elliptic plane crack, the volume element of Ω is

$$dD = 2h\, dS, \tag{3}$$

with

$$h = a_3 (1 - x_1^2/a_1^2 - x_2^2/a_2^2)^{1/2}, \tag{4}$$

where a_1 and a_2 are the two principal axes of the elliptic crack and a_3 is the third principal axis. In the above equation $a_3 \varepsilon^*_{ij}$ is kept finite while $a_3 \to 0$.

The crack opening displacement $[u_i]$ can be derived from the equation (2a) = (2b) with (3) and (4).

The stress field caused by σ^o_{ij} and Σ is $\sigma^o_{ij} + \sigma_{ij}$ in the matrix and $\sigma^o_{ij} + \sigma_{ij} = 0$ in Ω. The proper ε^*_{ij} to simulate the crack is obtained by the minimization condition of (2c) with respect to ε^*_{ij}, where σ_{ij} in Ω is a linear function of ε^*_{ij}. The minimization condition simply is $\sigma^o_{ij} + \sigma_{ij} = 0$.

The Griffith fracture criterion has the form $\partial(\Delta W + 2\pi a_1 a_2 \gamma)/\partial a_1 = 0$ or $\partial(\Delta W + 2\pi a_1 a_2 \gamma)/\partial a_2 = 0$, where (2b) is used for ΔW, and γ is the surface energy.

The stress intensity factor K along the boundary of Σ is calculated by applying the equation

$$[u_i] = 4K (1-\nu) (r/2\pi)^{1/2}/\mu \tag{5}$$

where r is the distance from the crack edge.

It will be shown that the crack stress intensity factor in a fiber composite material saturates and tends to a constant value with increasing crack size.

Under certain appropriate assumptions it can be shown that a smaller crack has a larger stress intensity factor.

In fatigue cyclic loading causes inhomogeneous deformation. The eigenstrain generated as a result of cyclic loading will be discussed in terms of numbers of cycles and applied strain amplitudes.

The stress corrosion and corrosion fatigue will be discussed. The area of discussion is limited to hydrogen atoms including interaction with a dislocation array.

Finally the eigenstrain method is extended to the atomic scales. The eigenstrain caused by hydrogen atoms in a cluster consisting of six F_e atoms will be evaluated by the first-principle Hartree-Fock-Slater

model. The discrete variational $X\alpha$ method is used. In this model, the one electron Hamiltonian is given by

$$H(r) = -(1/2)\nabla^2 + V(r) , \qquad (6)$$

where $V(r)$ is the cluster potential and it is the sum of the Coulomb term V_c and the exchange - correlation term V_{ex}. In a non-spin polarized calculation,

$$V_{ex} = -6\alpha \left(\frac{3}{8\pi}\rho(r)\right)^{1/3} \qquad (7)$$

where $\rho(r)$ is the electron density and α is a parameter. The eigenstrain is defined by the displacement of atoms caused by the hydrogen atoms in the cluster divided by the original lattice parameter. The atomic displacement will be determined by the minimum condition of the energy

$$E = \sum_{\lambda} \int \psi_\lambda^* H \psi_\lambda \, dD \Big/ \int \psi_\lambda^* \psi_\lambda dD \qquad (8)$$

where ψ_λ is the wave function of the Schrödinger equation. The hydrogen embrittlement may be explained by the bond order.

For the atomic lattice dynamics theory, the eigenstrain or eigendistortion β^*_{ij} becomes

$$M\ddot{u}_i(\ell) = -\sum_{\ell'} \phi_{ij}(\ell\ell') u_j(\ell') + \sum_{\ell'} \phi_{ij}(\ell\ell') \beta^*_{kj}(\ell\ell') x_k(\ell\ell') \qquad (9)$$

, where M is the mass of the atom, $u_i(\ell)$ the displacement component from the perfect lattice state of atom ℓ, $\phi_{ij}(\ell\ell')$ the force constants between ℓ and ℓ'atoms, and $x_k(\ell'\ell) = x_k(\ell') - x_k(\ell)$. $x_k(\ell)$ is the coordinate component of ℓ atom in the perfect lattice state.

The interaction of a hydrogen atom and a dislocation will be evaluated by this new lattice theory. As an application, the diffusion of hydrogen along the dislocation array is solved. The crack initiation under the environment of stress corrosion or corrosion fatigue will be discussed in terms of hydrogen content accumulated at the dislocation pile-up tip.

ACKNOWLEDGEMENT

This work was supported by NSF-MRL Grant DMR-8216972 and partially by U.S. Army Research Grant DAAG29-85-K-0134.

A SIMPLE METHOD OF ANALYSIS OF CRACK INTERACTIONS

Mark KACHANOV
Department of Mechanical Engineering
Tufts University, Medford, MA 02155, USA

It is well known that the problem of a linear elastic solid with N cracks can be represented as a superposition of N problems, each involving only one crack but loaded by unknown tractions. These tractions can be interrelated through a system of integral equations. Approximate methods of solution of the mentioned system constitute a possible approach to the crack problem. A simpler method of analysis is proposed. It is applicable to both 2-D and 3-D crack arrays of arbitrary geometry. The accuracy remains good even when the distances between cracks are one order of magnitude smaller than the crack sizes. In the case of weak interactions, the method becomes asymptotically exact.

The key idea is to take the tractions induced on a given crack line by the other cracks as "responses" of the latter to the uniform average tractions on them; the influence of traction non-uniformities having zero average is neglected. The averages are interrelated through "transmission factors" (characterizing attenuation of averages in transmission of stress from one crack onto the other crack lines). Thus, the traction averages are found from a system of linear algebraic equations, with the matrix ("crack interaction matrix") composed of transmission factors and reflecting the intrinsic geometry of the crack array; the right-hand parts of the equations reflect the external loading conditions. After the averages are found, the stress intensity factors (SIF's) on a given crack are readily found as generated by "responses" of the other cracks to average tractions on them and by the external loading.

Consider, as a test problem having exact solution [ ], the 2-D problem of two collinear cracks of equal length (-1, -k) and (k, 1), along the x-axis, loaded by uniform normal traction p_0; dimensionless parameter k characterizes the ratio of the distance between cracks to the crack length. By superposition, the problem reduces to two problems (identical, in this case) involving only one isolated crack each. Crack 1, (-1, -k) is loaded by a sum $p_0 + p_2$ where $p_2 = p_2(x)$ denotes the traction σ_{yy} generated by crack 2 (loaded by $p_0 + p_1$ where $p_1(x)$ is the crack 1 - generated traction). Simple calculation yields the value of a single transmission factor Λ (characterizing the average $\langle p_1 \rangle$ along the interval (k, 1), as generated by crack 1 loaded by uniform normal traction of unit intensity): $\Lambda = \sqrt{2(1+k)}/(1+\sqrt{k}) - 1$. Observing that $\langle p_1 \rangle = \Lambda (p_0 + \langle p_2 \rangle)$ and making use of symmetry of the configuration ($\langle p_1 \rangle = \langle p_2 \rangle$) we obtain $\langle p_1 \rangle = p_0/(1 - \Lambda)$. The SIF's at the crack 2 tips, 1 and k, are readily found now as induced by p_0 plus "response" of crack 1 to $\langle p_1 \rangle$; Table 1 compares them with the exact ones (normalized to $K_I^0 = p_0 \sqrt{\pi(1-k)/2}$). The agreement is very good; even at k = .05 (distance between cracks is one order of magnitude smaller than the crack length) the error is only 1.4% for $K_I(k)$ and .2% for $K_I(1)$. [Note that this simple configuration represents a difficult situation for the proposed method: at k = .05, actual traction along crack varies from 1.94 p_0 to 1.07 p_0 deviating considerably from the average $\langle p \rangle = 1.23\ p_0$].

Table 1. Comparison with the exact solution (two collinear cracks)

	$K_I(1)/K_I^0$		$K_I(k)/K_I^0$	
		Exact		Exact
k = .2	1.052	1.052	1.112	1.112
k = .1	1.086	1.087	1.251	1.255
k = .05	1.118	1.120	1.453	1.473

Comparison with the exact solutions for periodic crack arrays yields similar results: accuracy remains very good when distances between cracks are one order of magnitude smaller than the crack lengths.

In the general case, since normal (shear) traction on a crack generates both normal and shear tractions on the other crack lines, the transmission factors are second rank tensors. The average tractions on cracks are found from 2N linear algebraic equations (N is a number of cracks). Thus, the method operates with "standard" stress fields (generated by cracks loaded by uniform tractions) and requires integration of these fields along the other cracks and solving a system of linear algebraic equations.

The method is asymptotically exact in the case of weak crack interactions when the average tractions induced on a given crack by the other cracks are much smaller than the ones due to remote loading. This condition can be satisfied for relatively closely located cracks, particularly in 3-D. If the additional conditions (distances between cracks) >> (crack sizes) is assumed (approximation of remotely located cracks), major simplifications result: the "standard" stress fields can be taken as their remote asymptotics. Moreover, since the stress gradients attenuate faster than the stress themselves, the traction averages can be substituted by the values of the remote fields at the crack centers. In this case the first orders corrections to SIF's on a given crack S will depend on the other cracks' sizes but not on the size of S. In this approximation, solutions for various crack arrays (in both 2-D and 3-D) are obtained practically without any calculations.

More detailed presentation and examples are given in [2,3].

REFERENCES

1. I.N. Sneddon and M. Lowengrub, Crack Problems in the Classical Theory of Elasticity, John Wiley and Sons (1969).
2. M. Kachanov, International J. Fracture 28, R11-R19 (1985).
3. M. Kachanov, International J. Solids Struc. (submitted for publication)

DYNAMIC CLEAVAGE IN DUCTILE MATERIALS

I.-H. Lin and R. Thomson
National Bureau of Standards
Boulder, CO and Gaithersburg, MD, USA

Experiments in a variety of materials indicate that fully brittle cracks (in the atomic sense) are possible under dynamic conditions in normally completely ductile materials. Probably the most clear-cut evidence of this fact is found in the experiments described at this conference by Kaufman and Pugh[1]. This result poses a considerable problem to conventional treatments of the competition between dislocation emission and crack cleavage, which we believe is at the heart of the ductile or brittle response of the material. The reason is that if a dislocation is emitted from a fast moving crack, it creates a shielding K-field at the crack of the form

$$K_d = \frac{\mu b}{\sqrt{2\pi r}} \qquad (1)$$

μ is the shear modulus, b the Burgers vector and r is the distance from the dislocation to the crack tip. This shielding field is singular at the crack tip, and means that a strong impulse is given to the crack on emission. Current theories of cracks [2,3] have shown that cracks have zero inertia, and respond instantaneously to local stresses. Thus, the expectation is that the crack is stopped when the dislocation is emitted, and continuous emission can then take place, thereby blunting the crack.

In this paper, we investigate this paradox, and show that there is a critical velocity near that of sound above which the crack can propagate by cleavage. We shall do this in two different approximations. In the first, we assume the crack-dislocation system move at a constant uniform velocity with only small accelerations, and rederive the dislocation emission/cleavage crossover point. This approximation yields the result that both emission and cleavage critical K-values increase with velocity. In pure mode III, there is therefore no tendency to shift to more brittle behavior as the velocity is increased. However, in a mixed mode case, where the cleavage condition is set by the mode I loading, and emission is achieved in additional mode III loading, increasing the velocity decreases the emission capability. This result is shown by the equation for the critical K for emission, $K_e(v)$, in the forward direction,

$$k_e(v) = k_e(o)\sqrt{1+v/c} \qquad (2)$$

v is the velocity of the crack, and c is the velocity of sound.

The approximation of constant velocity is a poor one for the dislocation emission event for the reason mentioned that the interactions and accelerations are large. For this reason, we have estimated the shielding k on the crack during the emission, taking account of time retardation effects. It turns out that the crack experiences a maximum dislocation induced shielding k-field during emission. Thus a criterion can be written such that the crack is not stopped by the emission in terms of the external K-field which is required to drive the crack at the velocity, v. This criterion is

$$\left(\frac{1+v/c}{1-v/c}\right)^{1/4} - \frac{\sqrt{2}bc}{\sqrt{\pi r_o}\, v_d}\sqrt{\frac{\mu}{b}} > 1 \qquad (3)$$

A critical velocity is therefore predicted above which cleavage occurs, but the reader is reminded that (3) is a very rough estimate. v_d is the average dislocation velocity after emission and may simply be set to v=c for estimation purposes.

REFERENCES

1. M. Kaufman and E.N. Pugh, see this volume of abstracts.
2. J.D. Eshelby, Phys. of Strength and Plasticity, E. Orowan Anniversary Volume, ed. A. Argon, MIT Press, p.263 (1969).
3. L.B. Fruend, Mech. & Phys. of Sol. 20, 129 (1972).

UNIVERSAL WEIGHT FUNCTIONS FOR LOADINGS AND SCREENINGS OF CRACKS

H.O.K. KIRCHNER[+]
Laboratoire de Physique du Solide, Associé au CNRS n°155
Ecole des Mines, Parc de Saurupt, F-54042 NANCY Cedex, FRANCE
+ on leave of absence from Institut f. Festkoerperphysik,
University of Vienna, Boltzmanngasse 5, A-1090 VIENNA, AUSTRIA

The stress intensity vector K_i is defined as the limiting behaviour of stress or displacement near the tip of a crack, these being proportional to $r^{-1/2}$ and $r^{1/2}$, respectively, for any type of external loading. Internal stresses caused by dislocations show the same power dependence at the crack tip; the stress intensity associated with a loading can thus be screened (or amplified) by a plastic zone.

Since for any particular specimen or crack geometry the stress intensity vector must be a functional of the loading or screening which are of vectorial character, it is possible to define two tensorial weight functions, one for screenings, $D_{si}(x,a)$, and one for forces, $F_{si}(x,a)$, so that the stress intensity can be found by integration over the product of weight functions and dislocation or force density. With b_s being the Burgers vector of the dislocation and f_s being the strength of the line force,

$$K_i = \int \left[b_s D_{si}(x,a) + f_s F_{si}(x,a) \right] \, d^2x$$

where a is the crack length. The elastic energy of a distribution of dislocations and line forces is

$$G = \frac{1}{2} \int \left[b_s(x) \phi_s(x) + f_s(x) u_s(x) \right] \, d^2x$$

where ϕ_s is the vector Airy stress function and u_s is the displacement.

Even for elastically anisotropic media the energy release rate is a quadratic form in the stress intensity vector [1]

$$K_i (B^{-1})_{ij} K_j = -8\pi \, dG/da$$

If the cross terms between two elastic states under mixed mode loading or screening are considered, the product of the stress intensity vectors for the two states is related to the derivative of the interaction energy between the two states with respect to the crack length. With Betti's theorem for the interaction between two elastic states, the stress intensity for any state becomes proportional to the derivative of the Airy stress function or displacement field with respect to the crack length, the proportionality factor being the force and dislocation

densities. With the three stress intensity vectors for the three reference states z=1,2,3 written as a matrix K^z_j, and its inverse

$$(K^{-1})^z_j \, K^z_u = \delta_{ju}$$

the universal weight functions are, with B_{it} being known from dislocation theory [1]

$$F_{si}(x,a) = -8\pi \, B_{it}(K^{-1})^z_t \, du^z_s/da$$

$$D_{si}(x,a) = -8\pi \, B_{it}(K^{-1})^z_t \, d\phi^z_s/da$$

Although the displacements u^z_s and stress functions ϕ^z_s are taken for three specific reference states, the tensorial weight function constructed from their derivatives with respect to the crack length are universal; the particular choice being compensated for by the stress intensities for the reference configurations chosen. The universal weight functions depend only on the crack geometry, but are independent of loading or screening.

If the two states in the quadratic form for the energy release rate are chosen as loaded (and unscreened) and screened (but without loads) it is possible to find the stress intensity for a screening from the stress function of the loaded crack. Knowledge of the stress function or displacement field for the screened crack are not necessary. Vice versa, it is possible to find the stress intensity for a loading from the displacement field around a screened, but loadless crack by integration. Since the stress function of a loaded crack is essentially known once the displacement field is known, computation of the screening effect of a plastic zone is reduced to straightforward integration.

This work presents an extension of the scalar universal weight function defined by Bueckner [2] for loadings to plastic zones and elastic anisotropy.

REFERENCES

1. D.J. Bacon, D.M. Barnett, and R.O. Scattergood, Progress in Materials Science 23, 51 (1978).
2. H.F. Bueckner, Zeitschrift angew. Math. Mech. 50, 529 (1970).

RESPONSE OF A DISLOCATION TO AN EXTERNAL STRESS

FERNANDO LUND
Departamento de Física, Facultad de Ciencias Físicas y Matemáticas, Universidad de Chile, Casilla 5487, Santiago, Chile.

Dislocation dynamics in an elastic continuum is studied in the context of classical field theory. The idea is to have a theory of sources (dislocation loops) interacting with a field (particle displacement) in the same sense that classical electrodynamics is a theory of point charged particles interacting with the electromagnetic field.

Although the particle displacement generated by a moving dislocation involves an integration over the whole slip plane, it was shown by Mura |1| that both particle velocity and strain can be expressed in terms of line integrals along the dislocation loop. If $\vec{u}(\vec{x},t)$ is the displacement at point $\vec{x}$ at time t, the Mura expressions are

$$\frac{\partial u_m(\vec{x},t)}{\partial t} \int G_{mk}(\vec{x}-\vec{x}',t-t')f_k(\vec{x}',t')d\vec{x}'dt' \qquad (1)$$

$$\frac{\partial u_m(\vec{x},t)}{\partial x_n} \int G_{mk}(\vec{x}-\vec{x}',t-t')g_{kn}(\vec{x}',t')d\vec{x}'dt \ .$$

Namely, strain and velocity are given as convolutions of the elastodynamic Green function G_{mk} with functionals f_k and g_{kn} of the dislocation loop that vanish everywhere except along the loop itself. The slip plane does not appear. Since physical quantities carried by the field such as energy and momentum depend only on strain and velocity and not on displacement, this justifies the identification of the dislocation loop as the source of the field and (1) gives the value of the field for a prescribed motion of the source, analogously to what the Lienard-Wichert potentials do in electrodynamics.

We have a source, the dislocation loop, which can be mathematically described as a time-dependent curve $X_i(\sigma,t)$ with σ a parameter along the curve. Is it possible to determine the response of this source to a prescribed, externally applied, elastic field? Yes. To see this, consider the action integral whose extrema give the equations of classical dynamic elasticity:

$$S = \frac{1}{2} \int dtd\vec{x}(\rho(\frac{\partial\tilde{u}}{\partial t})^2 - c_{ijk\ell} \frac{\partial\tilde{u}_i}{\partial x_j} \frac{\partial\tilde{u}_k}{\partial x_\ell}) \ . \qquad (2)$$

Since the medium is linear, displacements at any point in the presence of a dislocation loop will be the sum $\tilde{u} = u + U$ of the displacements u due to the loop, given by (1) and a displacement U due to externally applied stresses, which may be time dependent. Substitution of this sum into (2) gives an action that depends functionally both on the external field $U(\vec{x},t)$ and the dislocation loop $X(\sigma,t)$. Extrema of this action with respect to variations of U give the displacements generated by the loop

$X(\sigma,t)$ undergoing prescribed motion, in the form of a differential equation whose solutions are (1). Extrema of S with respect to variations of the loop X select the trajectory that will be followed by the dislocation loop under prescribed external stresses. More precisely, the action (2) will become the sum of three terms:

$$S = S_e + S_m + S_s \quad , \tag{3}$$

an external action S_e that depends only on the external U, a mixed action S_m depending both on U and X, and a self action S_e involving only the loop X. The last one is divergent and must be regularized with a cut-off procedure.

The evolution of the loop will be governed in general by an integral (both in σ and t) equation. It is possible to get a differential equation in the following approximation: a) The work done on the dislocation by external stresses is much larger than the radiation emitted and b) The motion of any point on the loop is affected only by those other loop points in its immediate neighborhood. In the case of a screw dislocation of Burgers vector b moving with velocity v_a (a= 1,2) in a medium of density ρ, shear modulus μ and shear wave velocity β the differential equation is |2|

$$M \frac{d}{dt} \left(\frac{v_a}{(1-v^2/\beta^2)^{1/2}} \right) = \mu b \varepsilon_{ac} \frac{\partial U}{\partial x_c} + \rho b \varepsilon_{ac} v_c \frac{\partial U}{\partial t} \tag{4}$$

where $\varepsilon_{11} = \varepsilon_{22} = 0$, $\varepsilon_{12} = \varepsilon_{21} = 1$ and $M = (\rho b^2/4\pi) \ell n(\delta/\varepsilon)$, in which $\delta >> \varepsilon$ are two cut-offs. The first term on the right of (4) is the usual Peach-Koehler force while the second is a velocity dependent force proposed by Eshelby |3|.

It is hoped to apply these results to study the interaction of dislocations and cracks, a problem whose relevance to fracture has been particularly emphasized by Thomson |4|.

Part of this research was done at the ITP in Santa Barbara. Research there was supported in part by the National Science Foundation under Grant N° PHY82-17853, supplemented by funds from the National Aeronautics and Space Administration. The support of DIB Grant E 1963-8522 and Fondo Nacional de Ciencias Grant 1147-1984 is also gratefully acknowledged.

REFERENCES

1. Mura, Phil. Mag. 8, 843 (1963).
2. F. Lund, Phys. Rev. Lett. 54, 14 (1985).
3. J. D. Eshelby, Phys. Rev. 90, 248 (1953).
4. R. Thomson, "Physics of Fracture" (to be published in the Solid State Physics series).

EXPERIMENTAL STUDIES OF CRACK TIP PROCESSES

PETER NEUMANN
Max-Planck-Institut für Eisenforschung, Max-Planck-Str. 1,
4000 Düsseldorf, FRG

There are to different separation modes at crack tips by which the crack can grow: tearing bonds by over-stretching ("brittle fracture") or shearing bonds by dislocation egress or emission ("ductile fracture" or "rupture"). Both processes usually depend strongly on the gaseous environment in the crack and/or on layers on the crack surface. The experimental studies reviewed in the following are those, which allow local measurements of these processes.

Fracture mechanics characterises the external loading and the resulting driving force for the crack. These parameters should be measured whenever possible as part of the characterization of the experimental situation.

The environment at the crack tip can be readily characterized only under equlibrium conditions. Then the activities of relevant components (e.g.hydrogen), which are measured externally are a good approximation to the values at the crack tip. Therefore, K_{Ic} measured as a function of these activities yield valuable information without explicitly local measurements.

A more local crack tip quantity is the size of the plastic zone and the amount of strain in it. The knowledge of these parameters allows an estimate of the plasic work beeing done during fracture in the framework of a modified Griffith fracture criterion. There are various classical methods of measurements on the side faces of a cracking specimen: Distortion of surface grids (scratched or etched) and broadening of electron channeling patterns.

Higher sensitivity for small amounts of plasticity is obtained by etching of individual dislocations or by examination of the fracture surface. Two methods are used to determine the plastic strain underneath the fracture surfaces: broadening of electron channeling patterns and X-ray topography (mostly using synchrotron radiation). Both methods can be used to measure depth profiles by intermittent polishing.

Detailed information about the structure near crack tips is obtained by TEM studies. Foils containing crack tips were prepared from bulk specimens. In ductile metals very high dislocation densities are usually reported but also atomically sharp brittle crack with small dislocation densities were observed in ceramics. The measured quantities are the geometrical shape of the crack tip and the dislocation density in the vicinity.

In situ TEM observation of cracking foils is the most powerful tool to study the crack tip. Cracks in all three modes of loading were observed in such studies. The resulting crack geometry and the processes of dislocation emission can be followed in all details. The most important result is the observation of a dislocation free zone at the crack tip under these circumstances, which can be rationalized in terms of dislocation crack interactions. These results have led to an extension of the Dugdale model allowing for a dislocation free zone and non-zero local stress intensity at the crack tip. The differences between fracture experiments in foils and those in bulk material have been recognized and will be discussed.

Plasticity is often considered only as an energy consuming pertubation of brittle fracture as defined above. In ductile metals this is not always justified because slide off on two alternating slip planes may contribute significantly to the crack growth process. The best parameter to measure the relative abundance of both fracture processes is the crack tip angle, because slide off produces a characteristic crack tip angle of the order of 90^{o}. Thus intimate mixtures between slide off and brittle fracture (zero crack angle) produce intermediate angles depending on the relativ amounts of both processes. In monocrystals large amounts of plasticity can be accommodated if slip extends through the whole ligament. Thus crack tip plasticity can be studied in bulk specimens without the confinement of an elastic surrounding. Such experiments were performed to study the embrittlement due to temperature, strain rate, gaseous hydrogen and aqueous stress corrosion conditions.

The crack tip angle of intergranular cracks was studied in a corresponding way in bicrystals as a function of disorientation, segregation and SCC conditions. By deliberate changes in the loading, markings can be produced on the fracture surface which indicate the position of th crack tips at given intervals. In this way preferred crack front directions could be studied and correlated with the crystallography of slip intersecting various types of grain boundaries.

If inhomogeneities are absent, crack initiation is a highly undefined process. In fatigue cracks initiate over a period of many cycles in a rather well defined way at slip loalization ("persistemt slip bands"). Recently progress has been made in observing early crack nuclei by high resolution sections made at right angle with the surface thus revealing the surface profile.

MODELING OF DUCTILE FRACTURE

ANTHONY W. THOMPSON
Department of Metallurgy and Materials Science, Carnegie-Mellon University, Pittsburgh, PA 15213

The process of ductile fracture, which is well established to proceed by nucleation, growth and coalescence of microvoids, is a complex phenomenon from the perspective of physics, but is fairly well characterized in mechanics terms. Moreover, extensive metallurgical knowledge of microvoid nuclei and matrix plastic flow properties provides essential input to overall understanding of the fracture process. There is, however, no comprehensive mechanics analysis which encompasses all the important variables of stress state, strain localization tendency, and microvoid nucleation parameters, nor is there a complete metallurgical model which incorporates details of the micromechanical processes which accompany nucleation, growth and coalescence of the microvoids. Accordingly, it is not surprising that at present it is not possible to predict fracture strains accurately, using either mechanics or metallurgical approaches. These problems are perhaps most evident in considering ductile fracture events at sharp crack tips, although other mechanical conditions also pose challenges to existing viewpoints. Recent work from a materials perspective has addressed this problem by combining a general metallurgical model with current mechanics work which incorporates "microscale" parameters. This permits an integrated treatment of "micromechanisms", i.e. fracture processes which take place on the scale of the microstructure. Fractographic information appears essential to experimental testing of this approach, and has in fact been incorporated into the model directly. One outcome is that a direct experimental value of the local fracture strain can be obtained under any state of stress or strain, rather than obtaining such a value by back-calculation or estimation, as is otherwise the procedure. For this and other reasons, the present modeling approach appears to have promise in extending understanding of ductile fracture.

FRACTURE OF AMORPHOUS METALS IN TENSILE TEST AND FATIGUE TEST

T. IMURA*, M.DOI**, Y. MASUO*** AND H. TOKUDA*
* Department of Metallurgy, Faculty of Engineering, Nagoya University, Chikusa-ku, Nagoya 464; ** Department of Materials Engineering, Nagoya Institute of Technology, Showa-ku, Nagoya 466; *** Nagoya Muncipal Industrial Research Institute, Atsuta-ku, Nagoya 456, Japan

INTRODUCTION

A number of studies on mechanical properties of amorphous metals have been reported to date and the static strength of amorphous metals is found to be usually higher than that of ordinary metals. On fatigue behavior of amorphous metals, however, only a few studies have been reported so far[1-5]. Furthermore, in such cases, all the fatigue tests were conducted in tension-tension mode except ours[5]. In this study, a cyclic bending apparatus, which can alternately apply tension and compression to a ribbon specimen of 20-30 μm thick, was constructed. By using this apparatus, fractographic investigation and preparation of strain-lifetime diagram of amorphous ribbons as well as reference metal ribbons were made. In addition, fracture in tensile tests and compression tests of amorphous blocks prepared by the author's group was studied for comparison.

EXPERIMENTAL PROCEDURE

Amorphous ribbons and powders (Fe-B-Si, Co-B-Si, Ni-B-Si) were prepared by rapid quenching from the melt, using twin-roll method and modified in-rotating-liquid quenching method, respectively. Amorphous blocks of $Fe_{78}B_{13}Si_9$ alloy were prepared by explosive consolidation at about 10GPa and also by high-pressure-high-temperature sintering at 450°C in the pressure range of 1-5 GPa. A cyclic bending apparatus was newly designed and constructed for fatigue test of thin ribbons. Tensile test or compression test of amorphous blocks was conducted up to fracture by ordinary testing machine. X-ray diffraction and high resolution electron microscopy were used for identification of amorphous state. Observations of fracture surface were made by SEM and optical microscope.

RESULTS AND DISCUSSIONS

Fig.1 illustrates strain-lifetime diagrams; (a) for fatigue tests of different frequencies (1-8 Hz), and (b) for those in vacuum, Ar-gas and the air. Even in the case of amorphous metals which usually have high corrosion resistivity , effects of environment are conspicuous in room temperature fatigue tests. Fracture surface observations support this view as is illustrated in Fig.2 (a) and (b). Vein structure can be seen on the fracture surface of the specimen tested in Ar-gas and vacuum but not so for the specimen tested in the air. The specimen showed brittle material-like behavior in the latter case. Fig.3 indicates fracture

surfaces; (a) those of the amorphous block prepared by explosive consolidation and (b) those of the central part of the same block where high concentration of shock waves was expected. Effects of oxide film of the surface will be discussed.

REFERENCES

1. T. Ogura, T. Masumoto and K. Fukushima, Script. Met. 9 109 (1975)
2. T. Ogura, K. Fukushima and T. Masumoto, Script. Met. 9 979 (1975)
3. C.A. Davis, J. Mat. Sci. 11 711 (1976)
4. T. Imura, M. Doi and H. Kosaki, Sci. Rep. RITU A, suppl. June 47(1978)
5. M. Doi, K. Sugiyama, T. Tono and T. Imura, Jpn. J. Appl. Phys.20 1573 (1981)

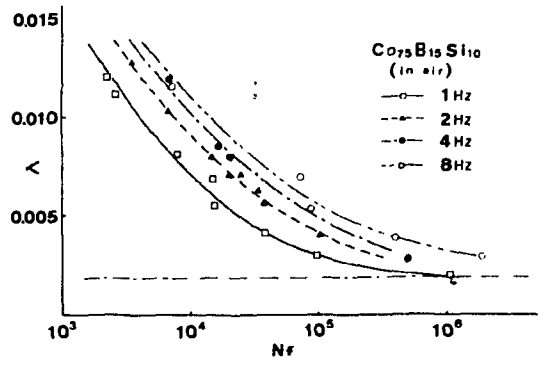

Fig.1 (a)

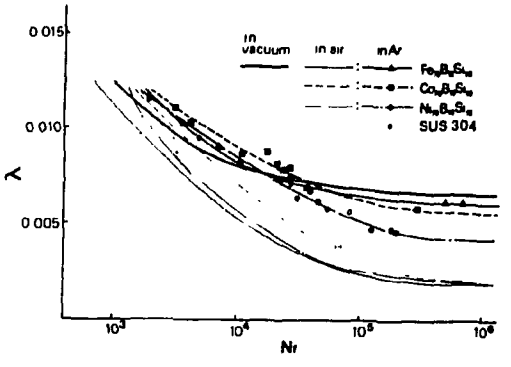

Fig.1 (b)

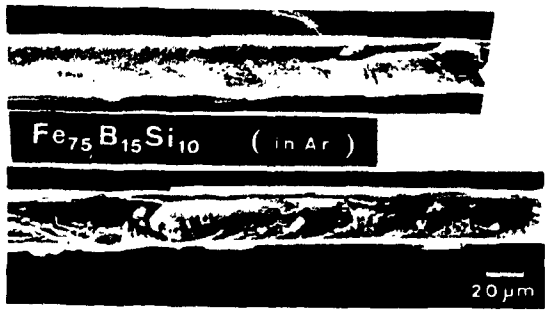

Fig.2 (a)

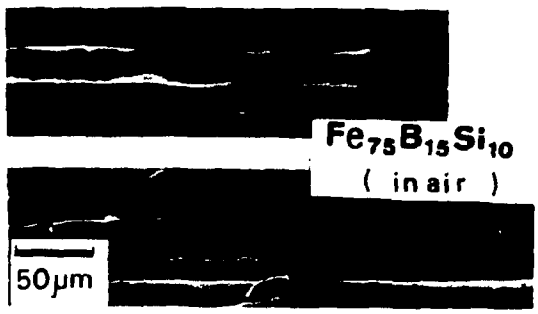

Fig.2 (b)

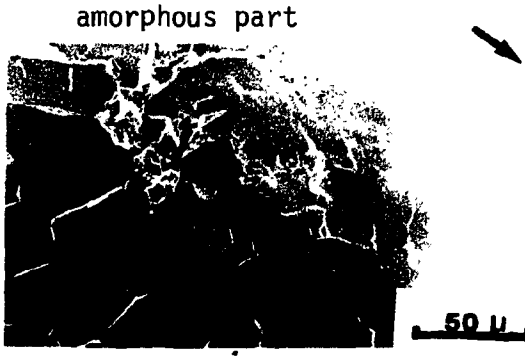

Fig.3 (a)

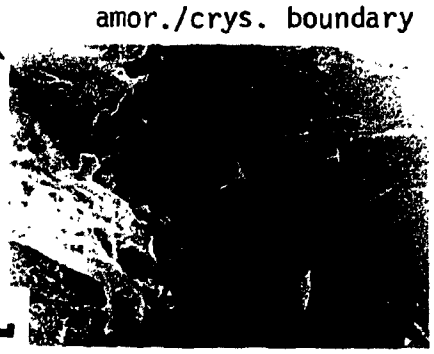

Fig.3 (b)

SXRF STUDIES OF BULK CRACK-TIP PLASTIC RELAXATION*

JOHN C. BILELLO
Department of Materials Science and Engineering, State University of New York at Stony Brook, Stony Brook, NY 11794

INTRODUCTION

Synchrotron x-ray fractography (SXRF) has been developed as a non-destructive probe of the plastic relaxation zone accompanying bulk fracture in semi-brittle crystals. [1] This method uses white beam synchrotron x-radiation impinging on the cleavage surface of a fractured sample at grazing angle incidence. Topographs are collected in the $2\theta = 90^{\circ}$ with information obtained about the bulk microstructure down to the first extinction depth, i.e. approximately 5-10 micrometers below the surface. In comparison with other fractography methods such as, Berg-Barrett topography, optical and Scanning Electron Microscopy, SXRF offers some unique advantages. These include the ability to assess the bulk microstructure associated with crack initiation and propagation coupled with extremely high data collection rates. SXRF data taken at Daresbury, U. K., Stanford SSRL and Brookhaven NSLS will be compared with the more conventional fractography methods.

RESULTS AND DISCUSSION

Investigations on crack-tip plasticity using SXRF have been performed on a wide variety of crystals including Mo, Nb, Mo-Nb alloys, Zn, and Zn-Cd solid solution alloys. [2, 3] The extent of the plastic zone can be mapped out using level polishing techniques. A Mo crystal, with a precursor crack having a radius of a few micrometers, had a measured plastic zone approximately 10 times larger. White beam radiation is also sensitive to local lattice rotations with the diffracted beam being broadened when reflected from such a region. Data for such a Mo crystal is shown in Table 1.

Table 1. Crack-tip lattice rotations in the plastic relaxation zone of a Mo crystal measured by SXRF.

Reflection (hkl)	Image Width (mm)	(2θ -90°) (degs.)	Lattice Rotation (rads)
051	0.246	67.38	0.0012
031	0.194	53.14	0.0023
042	0.144	36.88	0.0031
011	0.102	0.0	0.0034
024	0.208	36.88	0.0044

The nature of the local distortion can also be studied by taking advantage of the crystal symmetry properties. Figure 1 shows two SXRF topographs taken on a Mo crystal with the incident on vector S_o rotated 180° between each topograph as shown by arrows on the figure; the image contrast is not equivalent. The contrast is thus not due to the strain tensor, where of necessity ij components must equal ji, rather the contrast is attributed to the local rigid body rotation at the crack-tip given by the curvature tensor K_{ij}. This observation may be re-lated to the dislocation tensor described by Nye [4] to find that the excess density of edge dislocations segments at the crack-tip is of the order of 10^{11} cm^{-2}.

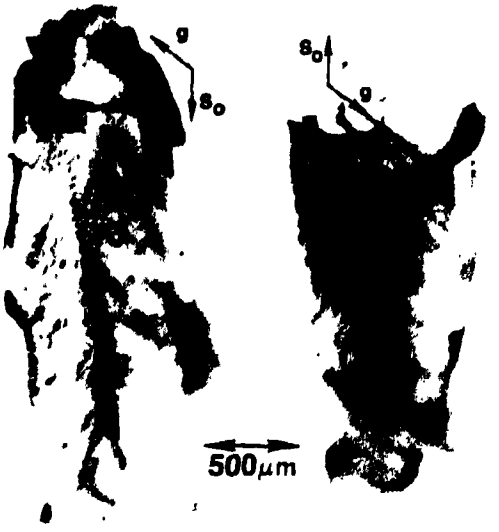

Fig. 1 SXRF for $S_o = -S_o$

SUMMARY

The dislocation density and plastic zone size has been determined for fine scale cracks in bulk crystals of a number of elastic-plastic cracks using a new non-destructive synchrotron x-radiation imaging technique.

REFERENCES

1. A. B. Hmelo, J. C. Bilello, S. T. Davies, and D. K. Bowen, Mater. Lett., 1, 6, (1983).
2. A. B. Hmelo, J. C. Bilello, S. T. Davies, and D. K. Bowen, in "Applications of X-ray Topographic Methods to Materials Science", eds. S. Weissmann, F. Balibar, and J-F. Petroff, Plenum Press, New York, (1984), pgs. 343-357.
3. H. A. Schmitz, Master's Thesis, SUNY Stony Brook, (1984).
4. J. F. Nye, Acta Metall., 1, 153, (1953).

*The author thanks the U. S. Department of Energy, Office of Basic Energy Sciences, Materials Science Division, for support, under grant No. DE-FG02-84ER45098.

X-RAY ANALYSIS OF PREFRACTURE ELASTIC AND PLASTIC STRAIN GRADIENTS

SIGMUND WEISSMANN
Department of Mechanics and Materials Science, College of Engineering, Rutgers University, Piscataway, NJ 08854, USA.

INTRODUCTION

To characterize and to determine quantitatively elastic strains and microplasticity in a material induced by deformation, it is most desirable that prior to deformation the material should contain none of them. Silicon crystals fulfill this requirement because they can be obtained free of elastic strains and of dislocations. At room temperature the fracture characteristics are those of an ideal brittle material and above 60% of T_m the crystals become ductile and behave like metal crystals [1]. Consequently, silicon crystals were used as model materials for the elucidation of the strain gradients.

ANALYSIS OF ELASTIC STRAINS

The integrated X-ray reflectivity of elastically bent, perfect Si crystals was calculated for Laue type of reflections covering the entire curvature range. Anomalous transmission and elastic anisotropy were taken into account, and it is shown that both these effects have a substantial influence on the reflected intensities of weakly and strongly bent crystals [2]. The validity of the reflectivity-versus-curvature relation thus obtained was experimentally confirmed for a number of reflections as shown in Fig. 1; the solid curves representing calculated values. The data acquisition from many (hkl) reflections leads directly to the construction of a strain ellipsoid for every deformation stage. If stress raisers are present such as notches, holes and inclusions, and if an external bending moment is applied, the lattice curvature associated with stress raisers become locally enhanced, manifested by local intensity enhancement. This enhancement was experimentally determined for a variety of stress raisers by measuring on X-ray topographs the reflected intensities from point-to-point along the path of the strain gradient. Good agreement was obtained between experiment and theoretical calculations based on continuum mechanics [3,4]. Elastic strain interactions emanating from several stress raisers have also been determined experimentally and the results are being compared to those of finite element analysis. It is well known that in anisotropic materials the triaxial, elastic strain distribution near a stress raiser cannot be calculated theoretically. The preliminary X-ray studies, however, indicate that such determination can be achieved by X-ray intensity measurements of several (hkl) reflections; the data acquisition being greatly facilitated by using a white beam synchrotron source.

ANALYSIS OF PLASTIC STRAIN DISTRIBUTION

A computer-aided X-ray double crystal diffractometer method (CARCA) was developed [5] to analyze the distribution of micro-plasticity induced in single and doubly-notched silicon crystals deformed in mode I under

plane-strain condition at 800°C. It was shown that at a very early deformation stage the direction of the maximum plastic strain trajectory in the plastic zone, manifested by maxima of measured lattice misalignment, outlined the future zigzag fracture path (Fig. 2). The results are complementary to the TEM studies of Gardner and Wilsdorf [6] and particularly to those of Ohr and Narayan [7] and Horton and Ohr [8], showing the assistance which cell and subgrain walls in the plastic zone offer to crack propagation.

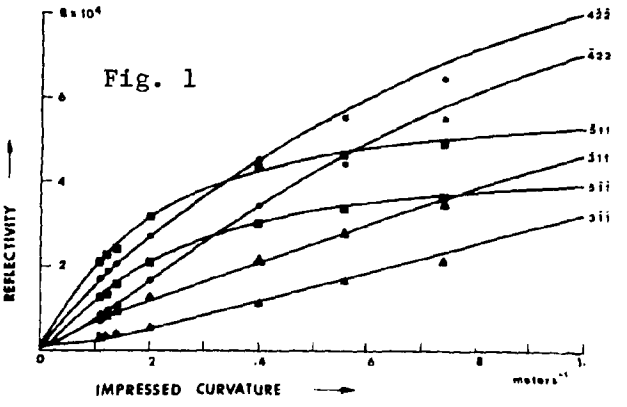

Fig. 1 Dependence of calculated and observed X-ray reflectivity on Impressed curvature

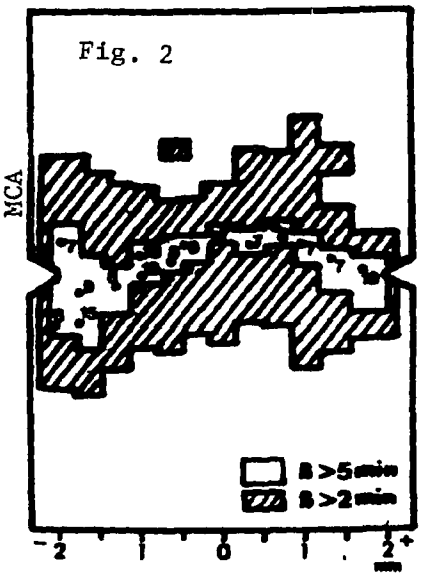

Fig. 2 CARCA mapping of lattice misalignment by plastic zone interaction; induced by tensile deformation of doubly-notched silicon crystal (σ=27.5 MPa, ε=1.04%; MCA, multichannel analyzer)

SUMMARY

Elastic strain gradients and strain interactions in Si crystals, induced by stress raisers, are determined by local measurements of reflected X-ray intensities. Microplastic strain gradients and interactions are determined by X-ray double crystal diffractometry.

REFERENCES

1. H. Alexander, Phys. Status Solidi. 26 pp. 725-741 (1968); ibid 27 pp. 391-741 (1968).
2. Z.H. Kalman and S. Weissmann, J. Appl. Cryst. 16, pp. 295-303 (1983).
3. Z.H. Kalman, J. Chauduri, G.J. Weng and S. Weissmann, J. Appl. Cryst. 13, pp. 290-296 (1980).
4. J. Chaudhuri, Z.H. Kalman, G.J. Weng and S. Weissmann, J. Appl. Cryst. 15, pp. 423-429 (1982).
5. H.Y. Liu, W.E. Mayo and S. Weissmann, Mat. Sci. and Eng. 63, pp. 81-90 (1984).
6. R.N. Gardner and H.G.F. Wilsdorf, Metall. Trans. A. 11, pp. 659-669 (1980).
7. S.M. Ohr and J. Narayan, Phil. Mag. 41, pp. 81-89 (1980).
8. J.A. Horton and S.M. Ohr, J. Mat. Sci. 17, pp. 3140-3148 (1982).

INFLUENCE OF A PLASTIC ZONE ON THE STATIC AND DYNAMIC TOUGHNESS OF SILICON

G. MICHOT, G. CHAMPIER
Institut National Polytechnique de Lorraine - ENSMIM - Parc de Saurupt
54042 NANCY Cedex - FRANCE

I - EXPERIMENTAL RESULTS

A limited {111} brittle cleavage crack has been introduced at 300 K in dislocation free single crystals. Creep tests at high temperature ($T > 900$ K) show a development of a plastic zone for a stress intensity factor K_I higher than $K_I^m = 0.25$ MPa$\sqrt{m}$. After freezing-in of the dislocations by cooling down, the toughness increase of the material has been measured via fracture tests carried out at 300 K (Fig.1) [1].

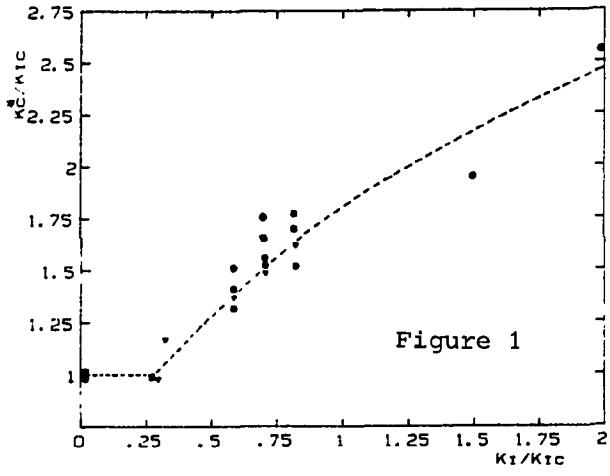

Figure 1

High temperature dynamic tests have been performed under a constant opening rate $\dot{\delta}$ on pure crystals (FZ) and crystals with oxygen (CZ). Under a critical temperature T_C, fracture occurs for a low stress level, upper T_C a strong plastic opening of the crack is observed (Fig.2). T_C is clearly higher for CZ crystals than for FZ crystals [2].

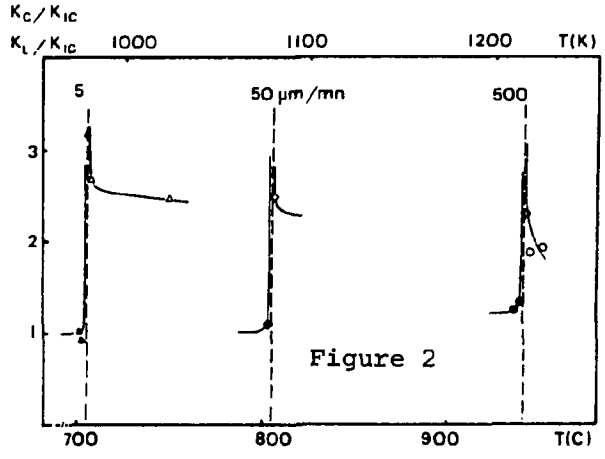

Figure 2

II - DISCUSSION

It can be shown that blunting is negligible [1,2,4]. The toughness increase must be related essentially to a shielding effect. During a

dynamic tensile test the applied stress field $\bar{\bar{\sigma}}_A$ ahead of the crack tip increases. The shielding of the developing plastic zone corresponds to an opposite stress field - $\bar{\bar{\sigma}}_p$ depending on the ductility of the material and limited by the nucleation rate and mobility of dislocations. The mobility beeing thermally activated, the higher the temperature, the more effective will be the shielding. For a critical temperature T_c a stationnary stress field can be obtained for $d\bar{\bar{\sigma}}_A/dt = d\bar{\bar{\sigma}}_p/dt$. The Arrhenius plot of the plastic opening rate $\dot{\delta}_p$ of the crack versus the brittle to ductile transition temperature T_c gives the same value of the activation energy for dislocation movement for FZ and CZ crystals as mentionned in the litterature [5]. This point could not be explained by a blunting model [6,2].

For this reason creep results have been interpreted with the help of a mode III model : the equilibrium of a dislocation distribution submitted to a $K/\sqrt{r}$ applied stress and $-A/r$ image stress is solved using singular integral equations methods [7]. Following Chang and Ohr [8] a DFZ has been introduced. A complete solution needs one more additionnal information than in the BCS model. This is obtained in our experiments in measuring the shielding $|\Delta K| = K_c^* - K_{IC}$ (Fig.1).

The threshold value K_I^{th} is related to a barrier for inhomogeneous nucleation. Numerical application of the model gives satisfying agreement with the measured extension of the plastic zone [9] and number of dislocations inside this plastic zone [4]. A reasonnable value of the friction stress is also obtained.

REFERENCES

1. G. Michot, A. George, G. Champier, Proceedings ECF4 - Leoben, Austria 2, 30-35 (1982).
2. G. Michot, A. George, Proceedings ICSMA 7 - Montreal, Canada (1985).
3. G. Michot, A. George, Phil. Mag. 42A, 195 (1980).
4. G. Michot, Thèse d'Etat INPL, Nancy (1982).
5. M. Imai, K. Sumino, Phil. Mag. 47A, 599 (1983).
6. C.F. St John, Phil. Mag. 32, 1193 (1975).
7. N.I. Muskhelishvili, Singular Equations (Noordhoff, Groningen 1953).
8. S.J. Chang, S.M. Ohr, J.A.P. 52, 7174 (1981).
9. G. Michot, A. George, Scripta Met. 16, 519-524 (1982).

CRACK TIP SHIELDING BY DISLOCATION DEFORMATION IN IONIC AND DIAMOND CUBIC SOLIDS

K.Y. CHIA AND S.J. BURNS
Materials Science Program
Department of Mechanical Engineering
University of Rochester
Rochester, New York 14627

INTRODUCTION

Dislocations when emitted by a crack relax the crack tip stresses and shield the true crack tip from the applied stress intensity factor, K. The shielding of cracks by dislocations [1,2] and dislocation dipole [3] arrangements, with the dislocation lines parallel to the crack front, have been analyzed and are in the literature (the above references are not intended to be complete).

Shielding and blunting phenomena have now been observed using etching techniques for mode I and mode II cracks introduced into {100} surfaces of LiF crystal slabs and {111} surfaces of Si crystals. Microhardness indents, crack the LiF crystals on {110} planes and subsequently on {100} planes. Both crack systems contain crack tip dislocations - the {110} plane cracks have dislocations with Burgers' vectors perpendicular to the crack plane when loaded in mode I. These cracks are very strongly shielded and blunted. When loaded in mode II the dislocations have Burgers' vectors that are parallel to the crack plane and the cracks are shielded but not blunted. The {100} plane cracks are jogged by unique crack tip dislocations structures and are only partially shielded. These cracks subsequently propagate and break the sample. Observations of additional deformation and crack propagation after unloading will be presented (see Figure 1).

Silicon crystals indented and cracked at elevated temperatures produce crack tip deformation as observed by etching when subsequently cooled, under load, to room temperature. The indents initially produce cracks on three {112} planes. These cracks are shielded and blunted by slip on {111} planes. At higher loads three additional {112} planes crack with little or no shielding dislocations.

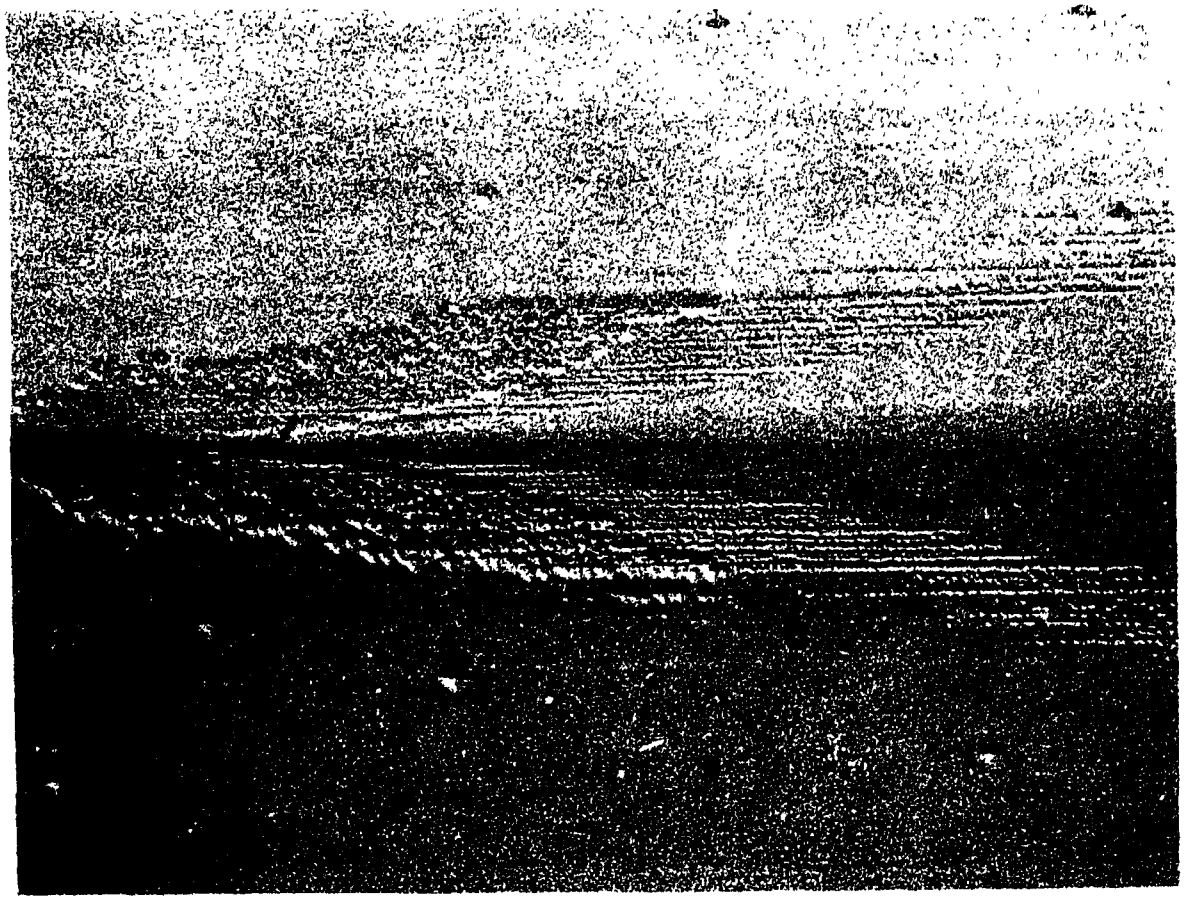

Figure 1 - A crack tip deformation zone in LiF for a [100] plane crack. The half dozen or so very large pits are from a pre-etch to show grown-in dislocations. The larger pits are from etching while held under load. The smallest pits are from etching after the load was removed. The crack is on the left side of the photo. Note the symmetry of each slip system about the crack plane.

ACKNOWLEDGEMENTS

This work has been supported by the U.S. Department of Energy under grant #DEFG02-84ER45051.

REFERENCES

1. J.R. Rice and R. Thomson, Phil. Mag., 29, 73 (1974).
2. B.S. Majumdar and S.J. Burns, Acta. Met., 29, 579 (1981).
3. R.J. Seyler, S. Lee and S.J. Burns, Adv. in Ceramics, Vol. 12, 213 (1984). American Ceramics Society.

DISLOCATION DISTRIBUTION AROUND A CRACK TIP AND THE FRACTURE TOUGHNESS IN NaCl CRYSTALS

N. NARITA,* K. HIGASHIDA,* S. KITANO* AND J. TAKAMURA**
*Department of Metallurgy, Kyoto University, Kyoto, Japan ; **Department of Metal Science and Technology, Kyoto University : Now, Professor Emeritus

INTRODUCTION

Modification of the stress intensity factor for a mode I crack by dislocations introduced at the crack tip has been theoretically treated in terms of crack tip shielding [1,2]. However, little observation has been made on the actual configuration of dislocations in connection with fracture toughness. The purpose of the present work is to obtain the quantitative evidence for the crack tip shielding due to dislocations by the observation of dislocation etch-pits and the fracture toughness.

EXPERIMENTAL PROCEDURE

Single crystals of NaCl (99.95% purity) grown by Bridgman technique were used. The crystals were cleaved along {100} plane into pieces for tensile and fracture toughness tests. The fracture toughness tests were made by using two kinds of loading methods, i.e., tensile loading on edge-cracked specimens (ECT) having the <100> axis, and wedge opening loading of double cantilever-beam type (DCB). The dimensions of tensile and ECT specimens are $3 \times 3 \times 40$ mm, and of DCB specimens are $6 \times 3 \times 50$ mm. To observe the dislocation distribution, etch-pit tests were made by using an etchant developed by Argon et al.[3]. The location of each dislocation etch-pit was read from the photograph by use of a graphic digitizer, in order to calculate the contribution to the local stress-intensity factor.

RESULTS AND DISCUSSION

NaCl crystals studied are easily deformed in tension at room temperature but are very brittle at 77 K. In specimens fractured at 77 K, the dislocation density near the crack surface was only about $10^6/cm^2$ or less. ECT and DCB specimens were deformed at room temperature to introduce dislocations of density about $10^7/cm^2$ near the crack tip. In ECT specimens, dislocations were observed mostly in front of the crack tip along oblique {110} slip planes. In DCB specimens, however, dislocation clusters tend to appear behind the crack tip. Such dislocation distribution in DCB specimens may not give a large effect to the stress intensity factor, as predicted from the theory[1]. A half of ECT and DCB specimens were directly subjected to fracture toughness tests at 77 K. The others were annealed for 1 hr at 1033 K to remove the dislocations, and subsequently subject to the fracture toughness test at 77 K. The results for ECT and DCB specimens

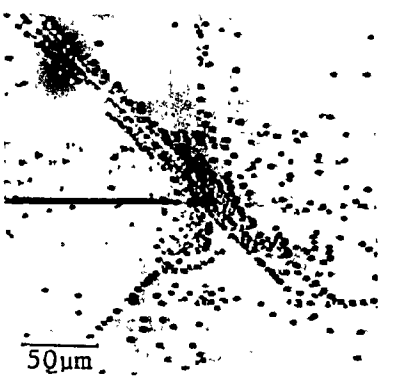

Fig.1 Dislocation distribution near crack tip in a DCB specimen deformed.

are listed in Table 1 ; the increase of K_{IC} value due to dislocations introduced is more pronounced for ECT specimens than that for DCB specimens. This implies that the method of loading affects the value of K_{IC} through the configuration of dislocations.

When a dislocation is located at (X,Y) on an oblique {110} slip plane near the tip of crack existing along the negative X-axis, the change of stress intensity factor due to dislocations, kd , can be expressed as [1],

$$kd = -\frac{\mu b}{4\sqrt{2\pi}(1-\nu)\rho^3}\sqrt{\rho+X}\{q|Y|(2X-\rho)+(3\rho-2X)(\rho+X)\}$$

where μ is the shear modulus, ν the Poisson's ratio, b the Burgers vector, ρ the distance between the dislocation and the crack tip ($=\sqrt{X^2+Y^2}$) and q the parameter relating to the direction of the Burgers vector. In the calculation, we assumed the parameter, q , to be 1 for ECT and -1 for DCB specimens by keeping in mind the slip direction of dislocation. The overall value of kd arisen from dislocations was computed by using the etch-pit data (Fig.2). The results show that the average kd va. es for ECT and DCB specimens are about -0.4 and -0.3 MPa$\sqrt{m}$, respectively ; the values of |kd| are somewhat larger than the actual increase of fracture toughness K_{IC} by the introduction of dislocations, but the tendency is similar. The discrepancy is ascribable to the presence of anti-shielding dislocations, i.e., dislocations having the opposite Burgers vector.

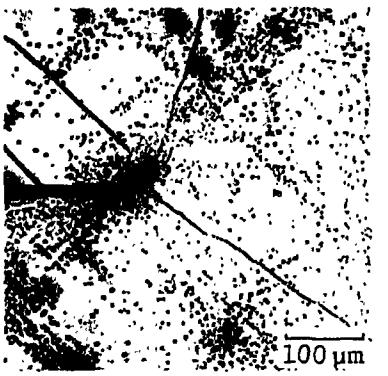

Fig.2 The distribution of dislocations introduced around a crack tip in a ECT specimen.

To sum up, dislocations introduced around a crack tip really raise the value of K_{IC} , and their configuration also has a substantial effect on the fracture toughness.

Table 1 Values of K_{IC} for NaCl crystals tested at 77 K.

Specimen	ECT type			DCB type		
	a/W	K_{IC} (MPa$\sqrt{m}$)	Average	a (mm)	K_{IC} (MPa$\sqrt{m}$)	Average
As deformed at R.T. (with dislocations)	0.257	0.211	0.224	17.32	0.245	0.205
	0.320	0.225		13.00	0.236	
	0.320	0.241		9.88	0.159	
	0.363	0.214		6.66	0.179	
	0.441	0.229				
Annealed after deform. (without dislocations)	0.330	0.166	0.168	18.44	0.182	0.170
	0.348	0.163		15.03	0.173	
	0.386	0.178		10.18	0.167	
	0.280	0.165		7.36	0.157	

W : Width of specimen a : Crack length

REFERENCES

1. R.M.Thomson, I.-H.Lin, S.M.Ohr and S.-J.Chang, Dislocation in Solids, Ed. by H.Suzuki, T.Ninomiya, K.Sumino and S.Takeuchi, (University of Tokyo Press, 1985), p.613.
2. N.Narita and J.Takamura, ibid., p.621.
3. A.S.Argon and G.E.Padawer, Phil. Mag., 25, 1073 (1972).

ON FAST FRACTURE AND CRACK ARREST

A. M. KUMAR*, N. XU**, G. T. HAHN***
*Graduate Student, Vanderbilt University, Nashville, TN; **Research Engineer, Ministry of Nuclear Industry, Beijing, Peoples Republic of China; ***Professor, Vanderbilt University, Nashville, TN

INTRODUCTION

The existing method for measuring crack arrest toughness, K_{Ia} [1], does not produce enough crack driving force and is not suitable for tough, arrester grade steels like HY-80, HY-100, and HY-130. Analytical methods based on LEFM are not applicable for these toughness levels [2]. There is need for increasing the measuring capacity and for newer approaches for characterizing arrest toughness. This paper describes a "fast fracture loading device" designed to increase the elastic strain energy release rate produced in conventional compact crack arrest test specimens, and early test results obtained with this device for tough aluminum and steel.

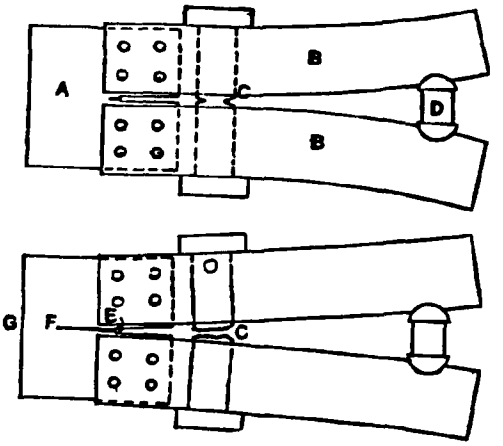

Figure 1.

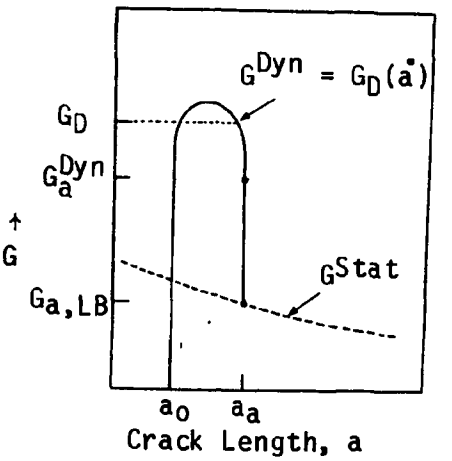

Figure 2.

Figure 1 schematically describes the operation of the device. The design provides more measuring capacity by attaching reusable, hardened steel arms (B) to a small, precracked, and deeply face grooved test specimen (A). The arms attached to the specimen are wedged open until the notched bolt (C) breaks. The system then behaves as if a very brittle crack were propagating from C to E. When this hypothetical crack arrives at E, the energy release rate, G^{Dyn}, increases rapidly as shown in Figure 2. The pre-existing crack extends when the propagating condition $G^{Dyn} = G_D(\dot{a})$ is satisfied and arrests when $G^{Dyn} < G_D$ $(\dot{a} = 0) \equiv G_a$. The remaining kinetic energy is dissipated and the system approaches the static configuration characterized by G^{Stat}, the static energy release rate.

The average value of the propagating crack fracture energy, $\overline{G}_D$, expressed as an equivalent stress intensity parameter, $\overline{K}_{ID}$, was esti-

mated assuming all the energy is conserved or converted to fracture energy. The energy values $U(a = a_o)$ and $U(a = a_1)$ were calculated from the compliance of the device, just before the rupture of the notched bolt and after crack arrest derived from a finite element model. A lower bound value of G_a, expressed as a strain intensity parameter, $K_{Ia,LB}$ was obtained from G^{Stat} evaluated at arrest. The above calculations are summarized in Table I.

RESULTS

Table I. Summary of compliance analysis using energy balance.

Specimen	B_n/B*	$U(a=a_o)$ (J)	$u(a=a_1)$ (J)	$\bar{G}_D$ (KJ/m^2)	$\bar{K}_{ID}$ (MPa$\sqrt{m}$)	K_{Ja}^{**} (MPa$\sqrt{m}$)	$K_{Ia,LB}$ (MPa$\sqrt{m}$)
HY-80 Steel	80%	712.8	416.0	5499	1099.3	259	>172
7075-Al	25%	808.0	357.0	2439	430.0	226	>156

*B_N = Notched thickness, B = Full thickness; **From Dantam [3].

It is to be observed that K_{ID} is very large due to the combined effect of rising R-Curve and further increase due to high crack velocity. K_{JR} values determined from ordinary J-test are for zero crack velocity, and due to the effect of velocity the K_{JR} values seem to approximately double. This observation is qualitatively consistent with the calculations of Hoff [4] and experimental measurements [5]. The value of K_{Ja}, an estimate of arrest toughness derived from the static J_R-curve: $K_{Ja} = K_{JR}$ (Δa = 1.5 mm), is consistent with $K_{Ia,LB}$, the lower bound estimate.

CONCLUSIONS

Tough materials are very resistant to rapidly propagating crack, and can absorb the kinetic energy released. J-resistance curve can provide an estimate of arrest capability.

REFERENCES

1. Rosenfield, A. R., et al., Fracture Mech: 15th Symp., ASTM STP 833, Sanford, R. j., Ed. (June 84, in press).
2. Dantam, V., and Hahn, G. T., Proc. of US-Japan Coop. Seminar, "Fracture Tolerance Evaluation", Honolulu, (1981).
3. Dantam, V., M.S. Thesis, Vanderbilt Univ., (1980).
4. Hoff, R., Rubin, C. A., and Hahn, G. T., Fracture Mech: 16th Symp., Ohio, (1983).
5. Joyce, J.A., No. NUREG/CR-2274, Washington, (1981).

STATICS AND DYNAMICS OF SINGLE CRYSTAL CLEAVAGE

WILLIAM W. GERBERICH
Chemical Engineering and Materials Science, University of Minnesota, Minneapolis, MN 55455

A combination of continuum fracture mechanics and dislocation-micromechanics is being applied to the understanding of cleavage fracture in Fe-4 at.% Si. For measured velocities up to 800 m/s, the surface plasticity is being measured with an electron channeling technique which will be described in some detail. The plasticity is shown to account for much of the energy dissipation at initiation. Is this fortuitous? Related to this question are some surprising features of the fracture surface, ligaments and ledges, which form at cleavage steps between parallel {100} fracture planes. The importance of these to the surface plasticity as well as to the effective stress intensity and hence the effective surface energy is given.

PROPAGATION OF CLEAVAGE CRACK IN IRON AND LIF SINGLE CRYSTALS

K. KITAJIMA
Research Institute for Applied Mechanics, Kyusyu University,
Kasuga-koen 6, Kasuga-shi, Fukuoka 816, Japan

Characteristic mechanisms of cleavage fracture of semi-brittle and brittle materials are discussed based on the experimental evidences obtained using iron and LiF single crystals.

The evidences of thermally activated nucleation of dislocation loops observed at the tip of fast propagating cleavage crack suggest the condition at the tip of the crack, $(\tau th/\sigma th) \gtrsim (\tau max/\sigma max)$, where τth and σth are the critical stresses of slip and separation of lattice, and τmax and σmax the maximum shear and tensile stresses operating at the tip of crack.

On the other hand, the evidences of athermal nucleation of dislocation loops produced by indentation in LiF suggest that some type of dislocation sources with various sizes present even in high purity crystals, and this explain the production of dislocation loops at the tip of propagating crack under condition of $(\tau th/\sigma th) > (\tau max/\sigma max)$ in the crystals.

Calculations are then presented for the plastic work depending on temperature and velocity of crack, and applied to the explanations for various experimental evidences observed.

An explanation was suggested on the increase or decrease of ductitily of iron by alloying of Ni or Si, which is known to be austenite stabilizing or destabilizing element respectively.

ENVIRONMENTAL CELL HVEM STUDIES OF HYDROGEN EFFECTS ON DEFORMATION AND FRACTURE

H.K. BIRNBAUM, I.M. ROBERTSON, D. SHIH, AND G.M. BOND
Department of Metallurgy and Mining Engineering and Materials Research Laboratory, University of Illinois, Urbana, IL 61801, USA

The deformation and fracture of a number of metallic systems have been studied using environmental cell techniques in the Argonne National Laboratory HVEM. In situ dynamic studies have been performed as the specimens were stressed in vacuum and in atmospheres of H_2 or H_2 saturated with H_2O. The responses of the materials were recorded dynamically using video techniques. While the pressures in the environmental cell were limited to about 300 torr by electron scattering from the gas, the fugacity of the hydrogen was very much greater. This fugacity was estimated from studies of the bubble formation under the aluminum oxide to be in excess of about 400 atmospheres. The high hydrogen fugacity probably results from dissociation and possibly ionization of the hydrogen under the electron beam.

The specimen behavior was studied during slow strain rate tensile deformation, during constant displacement relaxation and during constant load relaxations. In broad outline, the behavior of the material was consistent for these three modes of loading. The deformation mode was tension and the general fracture mode observed was primarily Mode I transgranular fracture. In a few cases, Mode II fracture was observed and a few cases of intergranular fracture were studied.

A number of systems have been examined with these techniques. These include hydride formers such as alpha and beta Ti, non-hydride formers such as Fe and Ni alloys, possible hydride formers such as Al and Al based alloys, and high strength alloys such as gamma prime strengthened Ni superalloys. These were chosen to illucidate the various mechanisms of hydrogen embrittlement which have been suggested in the literature.

While relatively "thick" specimens could be used in the HVEM, the stress state of the crack tips was still plane stress. The question of whether the behavior observed in the electron microscope was characteristic of thick specimens is of concern. This issue was addressed by a parallel series of experiment which used relatively thick specimens; the behavior of which was studied by in situ SEM deformation and fracture studies as well as slow strain rate deformation and fracture studies. It will be demonstrated that the results observed in the HVEM are characteristic of those observed in more macroscopic specimens and that while the details of some of the observations may be affected by the plane stress nature of the HVEM observations, the general conclusions drawn are not unique to thin specimens.

Two mechanisms of "hydrogen embrittlement" have been observed; stress induced hydride formation and fracture and hydrogen enhanced local

plasticity. The former mechanism had been well established in the group Vb metals and the present work extends these observations to alpha Ti alloys. Dynamic observations of the growth of the hydrides at the crack tips and the subsequent fracture of the hydrides have been made. The conditions for the growth of the hydrides will be discussed.

In the case of the non-hydride forming systems, "hydrogen embrittlement" was caused by hydrogen enhanced dislocation mobility and the localization of the deformation in the vicinity of the crack tips. Introduction of hydrogen into the specimens or into the environmental cell resulted in an increase of dislocation velocities for both screw and mixed dislocations. Crack propagation occurred as a result of the enhanced plastic deformation at the crack tip when hydrogen was added to the environment. Thus a crack which was stable in vacuum at constant stress could be started or stopped by the addition or removal of hydrogen from the environment. The fracture mechanism in vacuum and in hydrogen atmospheres were essentially the same; a failure due to local plastic processes. The significant differences were that these processes occurred at much lower stresses in hydrogen atmospheres and appeared to be more localized than in specimens stressed in vacuum. Hydrogen related fracture occurred along slip planes and appeared to be "brittle" when viewed at relatively low resolution, as the plasticity was localized to regions close the fracture surfaces. Careful observations of the fracture surfaces of macroscopic specimens revealed features which could be directly associated with the microscopic observations. These support our contention that the microscopic observations are not qualitatively different than those which characterize fracture of large sections.

This work was supported by the Department of Energy through contract DE AC02 76 ER01198.

EFFECTS OF HYDROGEN ON DEFORMATION AND FRACTURE OF IRON*

M. MESHII
Materials Research Center and Department of Materials Science and Engineering, Northwestern University, 2145 Sheridan Rd., Evanston, IL 60201, USA

The multiplicity of effects of hydrogen on mechanical properties of metals has been the difficulty in understanding hydrogen embrittlement, but can be rationalized by examining the states of hydrogen in metals and relating each state to various observations of mechanical effects. The state of hydrogen was examined by measuring hydrogen evolution in a UHV system during isochronal and isothermal annealing. It was found that the method of hydrogen charging into a specimen and the structure of the specimen strongly influenced the state of hydrogen. For example, the electro-chemical charging produces a large quantity of molecular hydrogen strongly trapped in micro-cavities, while the hydrogen introduced into a specimen by quenching from a high temperature in the hydrogen atmosphere is highly mobile and is thought to be in solution in iron. The presence of grain boundaries promotes the gaseous precipitation of hydrogen by forming microcracks at the boundaries.

A softening effect has been observed in iron single crystals to which hydrogen is introduced by the high temperature quenching technique in the temperature range between 77 and 200 K. Therefore, the softening effect must be caused by the interaction of solute hydrogen with dislocations, proving the presence of the intrinsic softening effect of hydrogen. The presence of hydrogen also lowers the twinning stress. The formation of micro-cavities due to the precipitation of gaseous hydrogen causes a hardening effect which persists after the complete evolution of hydrogen at elevated temperatures. It also has been shown that hydrogen-solute atom complexes also cause a hardening effect.

Hydrogen-induced fracture takes place in a number of different ways. The lowering of twinning stress promotes cleavage fracture in iron. Hydrogen also induces quasi-cleavage fracture; this mode of fracture is caused by the severe localization of plastic deformation. Therefore, the fracture is dominated by shear in spite of the implication of this terminology. The presence of hydrogen in a highly mobile form is required for this fracture mode to take place.

Hydrogen also promotes the intergranular fracture by two different mechanisms. The segregation of hydrogen as solutes onto grain boundaries lowers the cohesion across the boundaries. The magnitude of the reduction in the fracture stress per atomic fraction has been estimated for hydrogen and is significantly higher than those of other grain boundary weakening elements such as sulfur. Since this fracture is caused by hydrogen as solutes which are highly mobile, the effect can be complete-

*Based on research projects sponsored by the NSF-MRL program through the Northwestern University Materials Research Center and the Department of Energy.

ly removed by aging at room temperature when the supersaturation of hydrogen is relatively low. On the other hand, hydrogen preferentially precipitates along grain boundaries and forms microcracks when the supersaturation becomes high. These microcracks lower the intergranular fracture stress, thus, the intergranular fracture is promoted even after hydrogen diffuses out of a specimen. Since the sintering of the microcracks is considerably slower than the hydrogen evolution out of the specimen, the effect can be considered as permanent.

HYDROGEN ASSISTED CRACK GROWTH IN SINGLE AND BICRYSTALS OF FESI AND NI

Horst Vehoff
Permanent address: MPI fuer Eisenforschung, 4000 Duesseldorf 1, FRG
Current address: University of Pennsylvania, Department of Materials Science and Engineering, K1, 3231 Walnut Street, Philadelphia, Pa 19104

INTRODUCTION

Liquid metal embrittlement (LME), hydrogen embrittlement (HE) and temper embrittlement (TE), have many properties in common, which can be explained by similar mechanisms. The necessary requirements for environmental assisted brittle crack growth are a local stress concentration together with a local enrichment of the embrittling agent. On stressed interfaces, concentrations in the order of unity are needed to obtain a significant mean reduction of the cohesive forces. Therefore, interfaces which are sensitive to embrittlement must be effective sinks but not vice versa.

It is now assumed that the stressed bonds at the crack tip as well as the dense dislocation structure at the tip are effective traps. These traps are continuously produced during straining. The bonds break if a critical concentration and a critical stress is reached locally. A continuous transport of the environment to the stressed region is needed in order to fill the newly produced traps.

RESULTS AND DISCUSSION

In pure metallic single and bicrystals, bond breaking and dislocation emission must occur simultaneously, since the local stress amplitude at the tip of a sharp crack is large enough to activate dislocation sources. We now postulate that, for a given stress, the number of bonds which cleave per emitted dislocation is simply proportional to the atomic fraction of hydrogen in the defect field.

Crack growth tests in oriented single and bicrystals have shown that the crack tip opening angle decreases with increasing hydrogen pressure for cracks, which grow with a constant rate. For the typical V-shaped cracks obtained in these tests, a simple geometric consideration shows, that the increase in the cotangent of the crack tip opening angle, a_{nh}, is linearly related to the number of bonds which break per emitted dislocation. This angle change is measured as a function of the hydrogen pressure, p_{H2}, temperature, T and frequency. If a_{nh} is linearly related to x, the hydrogen coverage, as postulated above, a Langmuir-McLean plot of the pressure and temperature dependence of a_{nh} should give a straigth line.

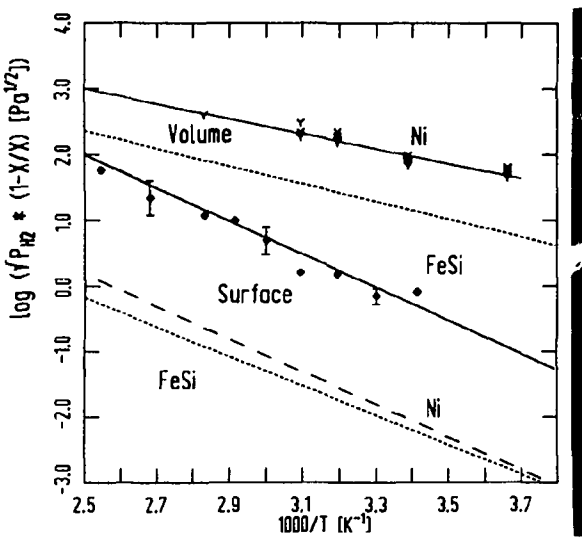

Fig. 1: McLean plot of $x = a_{nh}/kl$ vs. 1/T

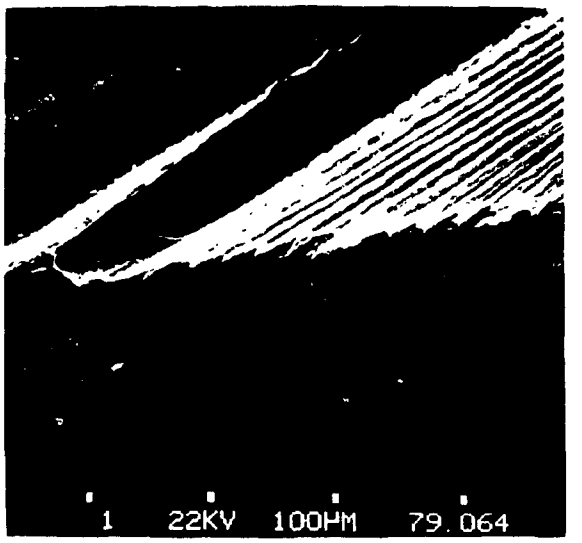

Fig. 2. Fracture and side surface of a Ni bicrystal after crack-growth in hydrogen and in vacuum.

Results obtained from tests on Ni and FeSi single crystals are shown in Fig.1 [1,2]. This plot supports the assumption that for a nearly constant stress state, which can be realized in fully plastic specimens, the number of bonds which break per emitted dislocation is simply proportional to the atomic fraction of hydrogen in the defect field. In addition, the strong frequency and temperature dependence of a_{nh}, observed in Ni single crystals, can be only explained if fracture occurs within a zone of less than 10 nm from the crack tip [2].

On the other hand, under otherwise identical conditions, Ni bicrystals show increasing embrittlement with increasing sulphur coverage on the grain boundary . For the severest heat treatment, clear Kikuchi patterns can be observed on the fracture surface. But, if the hydrogen pressure is reduced below 10^{-4} Pa, ductile crack growth is observed again as can be seen on Fig.2. FeSi bicrystals, however, which are found to be strongly sensitive to stress corrosion cracking, show no intergranular cracking in hydrogen gas. Therefore, HE strongly depends on the chemical nature of the stressed bonds. In order to understand the role of hydrogen and of impurities in reducing the cohesive strength, cluster calculations are needed, which simulate the actual conditions at the crack tip.

REFERENCES

1. H. Vehoff and W. Rothe, Acta Metal., 31, 1781, 1983
2. H. Vehoff and H. K. Klameth, Acta Metal., 33, 955, 1985

CALCULATIONS OF TWO-DIMENSIONAL TRANSIENT CONCENTRATION PROFILES DURING HYDROGEN-ASSISTED SUSTAINED-LOAD CRACKING

J. E. HACK[1], K. A. ROBBINS[2], A. NACHMAN[3], AND H. L. MARCUS[4]
1) Center for Materials Science, Los Alamos National Laboratory, Los Alamos, NM 87545; 2) Dept. of Math. and Computer Science, University of Texas at San Antonio, San Antonio, TX 78249; 3) Dept. of Math. and Computer Science, The Hampton Institute, Norfolk, VA 23668; 4) Dept. of Mat. Sci. and Engrg., University of Texas at Austin, Austin, TX 78712.

The tendency for solute atoms to redistribute due to a stress-induced chemical potential gradient has long been accepted. Such redistribution in the hydrostatic stress field at the tip of a loaded crack has been proposed as the rate controlling step in hydrogen-assisted sustained load cracking of metals in inert atmospheres, where the bulk hydrogen content is too low to cause embrittlement if randomly distributed. Calculation of the kinetics and degree of the redistribution of hydrogen about a loaded crack tip have been hindered by the lack of a suitable crack tip stress field.

In the present study, a closed-form crack tip hydrostatic stress field was developed based upon the approach of Barenblatt [1]. The solution is unique in that the stresses are finite and continuous at all points. Although an analytical solution to the governing partial differential equation was not possible, a numerical procedure was established, which incorporates the desired stress field. In the calculations, the maximum hydrostatic stress was assumed to occur at the elastic-plastic boundary directly ahead of the crack or notch. Calculated concentration profiles at observed incubation times for cracking in 4340 steel and Ti-6Al have been obtained. These profiles have been rationalized with respect to the various fracture mechanisms proposed for these materials.

Table I gives a comparison of calculated maximum concentration enhancement ratios for times equivalent to those observed by Page and Gerberich [2] in 4340 steel as a function of notch roof radius (and, therefore, maximum hydrostatic stress).

Table I. Maximum hydrogen concentration enhancement ratios calculated for 4340 steel.

Applied Stress Intensity (mPa $\sqrt{m}$)	Plastic Zone Length Ahead of Notch(μm)	Incubation Time (sec)	Calclulated Maximum Concentration Enhanacement Ratio at Incubation Time	Calculated Maximum Equilibrium Concentration Enhancement Ratio
54.9	175	120	1.74	14.34
54.9	325	370	1.59	6.86
54.9	475	920	1.70	4.82

As can be seen from the table, although the equilibrium concentration enhancement ratios at the elastic-plastic boundary ahead of the notch varied by a factor of 3 the maximum value achieved before fracture was essentially constant. The full two-dimensional distributions were also equivalent. Thus, in the case of 4340 steel, the results support the contentions of Troiano [1] that a critical distribution of hydrogen is required for embrittlement and that the distribution is not dependent on the stress level. The results are also qualitatively in agreement with general trends observed in crack velocity as a function of applied stress intensity and yield strength [3].

The results of calculations in Ti-6Al suggest that there is no correlation between cracking and solute redistribution due to stress-assisted diffusion. Cracking was not observed in specimens which were predicted to have significant enhancement of hydrogen above the stress-free solvus value. On the other hand, significant cracking was observed in specimens tested below room temperature where the predicted redistribution is trivial. The data in this case support the conclusions of Pardee and Paton [4] which suggest that the nucleation kinetics for hydride formation control sustained-load crack growth kinetics in titanium alloys.

REFERENCES

1. A. R. Troiano, Trans. ASM, 52, 54 (1960).
2. R. A. Page and W. W. Gerberich, Metall. Trans. A, 13A, 305 (1982).
3. W. W. Gerberich, Y. T. Chen and C. St. John, Metall. Trans. A, 6A, 1485 (1975).
4. W. J. Pardee and N. E. Paton, Metall. Trans. A., 11A, 1391 (1980).

CHEMISTRY AND FRACTURE

M. E. Eberhart and R. M. Latanision
Department of Materials Science and Engineering, Massachusetts Institute of Technology, Cambridge, Massachusetts 02139

INTRODUCTION

In the final analysis fracture, regardless of origin, is the macroscopic manifestation of the breaking of chemical bonds. Consequently, a complete view of fracture, and certainly an atomistic understanding, requires a description of what it means to break a chemical bond. Despite the fact that there has been much recent attention directed toward gaining a first principles understanding of the origin and mechanisms of environmentally induced intergranular embrittlement (1-5), an electronic description of a broken bond has not been forthcoming. This is almost certainly because the idea of a broken bond is treated as a fundamental concept, not requiring further definition, within the metallurgical community. However, an electronic understanding of bond breaking is fundamental to the study of chemical reaction theory. Here we exploit chemical reaction theory to describe the electronic process leading to bond breaking. It will be shown that a broken bond is characterized by a unique feature of the electronic structure which allows one to utilize molecular orbital theory to suggest possible mechanisms for embrittlement.

BOND FORMATION AND BOND BREAKING

In order to understand the electronic origins of bond breaking it is first necessary to describe the process of bond formation. Therefore, consider that the products of a cleavage process are to be brought together so as to form a single system (as if the fracture is to be healed). Each of the cleavage products is characterized by an electronic charge distribution which is fully determined by the wavefunction. The wavefunction derives its name from the fact that it behaves mathematically as a wave, that is, the tails of the wavefunctions corresponding to each of the cleavage products can interfere when they are brought near each other. Just as waves can interefere constructively or destructively, so too do the tails of the wavefunctions of the cleavage products. Therefore, when the cleavage products are brought together, two new wavefunctions will be formed; one in which the tails of the original wavefunctions add constructively, and another where they add destructively. The new wavefunction resulting from constructive interference generally is of lower energy than the wavefunction resulting from destructive interference. For a system which is to be bound all of the electrons will occupy the wavefunction of lowest energy (pictured in Fig. 1). The important point is that the process can be reversed, that a material can be strained and the wavefunction resulting from destructive interference will move down in energy, while the wavefunction corresponding to constructive interference will begin to move up in energy. When both of these wavefunctions are of equal energy, i.e. degenerate, the bond between the two products of the cleavage process is broken.

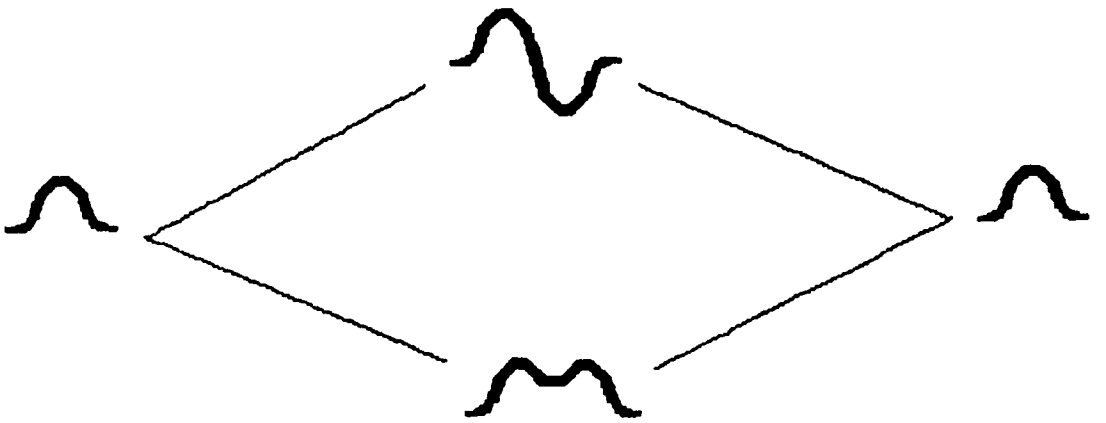

Figure 1. The process of bond formation. The two wavefunctions of the cleavage products are shown to the right and left. When brought together these wavefunctions overlap constructively and destructively to form the two new wavefunctions shown in the center. Fracture is just the reverse of this process and must be characterized by a degenerate pair of wavefunctions.

What we are suggesting is that a broken bond must be characterized by degenerate wavefunctions. There is a good deal of experimental support for this view. For example, an EPR experiment detects unpaired electrons, which can only be unpaired when a degeneracy of the type discussed above exists. EPR experiments performed on polymeric systems broken in tension reveal the existence of unpaired electrons that accompany the fracture of the system.

The simplifying point to the above comments is that degeneracies and the underlying causes of degeneracies are easily identifiable through first principle quantum mechanical calculations. While on the other hand, there is currently no feasible way to determine the energy differences that are responsible for brittle failure. As a result, it is possible to ascertain information regarding the mechanism of hydrogen embrittlement (6,7), for example, without the necessity to calculate thermodynamic data (as will be demonstrated in the oral presentation accompanying this extended abstract).

REFERENCES

1. S. Wakayama, M. Hashimoto, Y. Ishida, R. Yamamoto and M. Doyama, Acta Metall., 32, 21 (1984).
2. C. L. Briant and R. P. Messmer, Phil. Mag. B, 42, 569 (1980).
3. C. L. Briant and R. P. Messmer, Acta Metall., 30, 457 (1982).
4. C. L. Briant and R. P. Messmer, Acta Metall., 30, 1811 (1982).
5. M. E. Eberhart, K. H. Johnson and R. M. Latanision, Acta Metall., 32, 955 (1984).
6. M. E. Eberhart, Advances in the Mechanics and Physics of Surfaces Vol.3, ed. R. M. Latanision and T. E. Fischer, to be published.
7. M. E. Eberhart, R. M. Latanision and K. H. Johnson, Acta Metall., in press.

ELECTROCHEMICAL REACTIONS AND CORROSION FATIGUE OF FERROUS ALLOYS

R. P. Wei
Department of Mechanical Engineering and Mechanics,
Lehigh University, Bethlehem, PA 18015 USA

Corrosion fatigue crack growth of ferrous alloys in aqueous environments is an important technological problem in terms of the durability and reliability of engineering systems. Accumulating evidence now clearly shows a strong dependence of corrosion fatigue crack growth rate on the cyclic-load frequency and temperature. Crack growth rates tend to increase with decreases in frequency. The overall crack growth response tends to shift to higher frequencies (or shorter times per cycle) with increases in temperature, and exhibits "structure". The evidence strongly indicates electrochemical reaction rate control of corrosion fatigue crack growth, with the frequency dependent structure corresponding to specific electrochemical reactions with the environment. To provide a better understanding of the relationship between the kinetics of electrochemical reactions and corrosion fatigue crack growth response, coordinated electrochemical and fatigue crack growth experiments on high strength steels have been and are being carried out. A review of the background and the data is given to illustrate the current state of understanding. The need for cooperative research by chemists, solid-state physicists and materials scientists to further advance the understanding of this important problem is discussed.

Fatigue crack growth experiments have been and are being carried out, under prescribed mechanical driving force (constant stress intensity range), over a range of frequencies (0.03 to 10 Hz) and temperatures (275 to 363 K) on a number of steels in distilled water, and acetate buffer, carbonate-bicarbonate, sodium chloride and sodium sulfate solutions. The results show consistent increase of corrosion fatigue crack growth rate with decreasing frequency, and a shift in response to higher frequencies (or shorter exposure times per cycle) with increasing temperature. The dependence on frequency and temperature is consistent with electrochemical reaction control, and the presence of specific ions appears principally to moderate (or retard) the kinetics of the electrochemical reactions.

To establish the relationship between electrochemical reactions and corrosion fatigue crack growth in high strength steels, a special technique was developed to measure the galvanic current transient between a "clean" surface and a surface (of the same material) that had been "oxidized" in the electrolyte. The technique is intended to simulate reactions at the crack tip under freely corroding conditions, and the galvanic current transients are expected to provide information on the kinetics of these reactions. Based on experimental simplicity and on the rapid production of a relatively large area of fresh surfaces, the "clean" surface is obtained by in-situ fracture of a sharply notched round tension specimen. Counter electrodes made from the same material

are placed concentrically around the working electrode. The ratio of geometric surface areas between the counter electrodes and the fracture surfaces is greater than 250:1.

In the experiment, the counter electrodes are first "cathodically cleaned" in the electrolyte, and are allowed to equilibrate under open circuitconditions to establish a surface condition that would simulate that of the "oxidized" crack flank. The electrolyte is flushed out and is replaced with a fresh solution, and the test specimen (working electrode) is then loaded to failure to exposure new surfaces. The resulting galvanic current transient and the mixed potential are measured with a potentiostat operated as a zero-impedance ammeter, and are recorded digitally for further analyses. Although the technique is designed to measure the galvanic current transient, because of the large ratio between the surface areas of the counter and working electrodes, the measurements would correspond to those of a potentiostatic experiment at the free corrosion potential. It is expected that the technique can be adapted for measuring the kinetics of reactions under potentiostatic conditions.

Experiments have been carried out at several temperatures on high strength steels in several deaerated solutions used in the crack growth experiments. The current transients indicate the operation of several processes, and show clearly the influence of temperature. The very fast initial decay may be associated with the initial chemisorption of water or with the formation of the double layer. The slower portions are tentatively identified with anodic reactions that control corrosion fatigue crack growth response. Preliminary estimates of "time constants" and apparent activation energy associated with these reactions are consistent with that obtained from available fatigue crack growth data, and tend to confirm electrochemical reaction control of corrosion fatigue crack growth.

The need for more detailed studies of the mechanisms and kinetics of electrochemical reactions, however, is indicated and is discussed. The relevance of this finding to reliable service life prediction is considered.

STRERR CORROSION CRACKING OF HIGH-STRENGTH STEEL UNDER MODE III LOADING

Wu-Yang Chu, Chi-Mei Hsiao and Bai-Ji Xu*
Dept. of Metal Physics, Beijing Univ. of Iron and Steel Technology,
Beijing CHINA

The 30CrMnSiNi2 Steel with tensile strength 1760MPa was used. The circular notched specimen was of gauge diameter 14mm and the radius of the notch was about 0.3 mm. Hydrogen induced cracking under Mode III loading can occur during dynamic charging in 1N H_2SO_4 + 2.25g/L As_2O_3 solution and the cracks initiate and propagate intergranularly along the planes inclined at 45° to the original notch plane. For a precharged III type specimen loaded in air under constant toque, hydrogen induced cracking can also occur along the 45° planes. However, if the precharged III type specimen was twisted to failure immediately, a flat fracutre surface will be obtained, which is composed of torsional dimples (1,2) The threshold stress intensity of hydrogen induced fracture during dynamic charging under Mode III and Mode I loading were K_{IIIH}/K_{IIIX}=0.17 and K_{IH}/K_{IX}=0.045, respectively.

Stress corrosion cracking of the high-strength steel in 3.5% NaCl solution can also occur under Mode III loading. The stress corrosion cracking initiate and grow intergranularly along the planes inclined at 45°, similar to hydrogen induced cracking under Mode III loading. If 1g/L thiourea as a poison is added into the 3.5% NaCl solution, the similar result will be obtained. The threshold stress intensity of stress corrosion cracking under Mode III and Mode I loading were K_{IIISCC}/K_{IIIX}= 0.73 and K_{ISCC}/K_{IX}=0.42, respectively. If there was a poison in the solution, the corresponding values were K_{IIISCC}/K_{IIIX}=0.40 and K_{ISCC}/K_{IX}=0.12, respectively.

The strain field of hydrogen in α-Fe is non-spherical symmetry, i.e., $\varepsilon_{11} > \varepsilon_{22}=\varepsilon_{33}$ (3). Therefore, there is an interaction between hydrogen atoms and the torsional stress field and a minimum interactive energy on the planes inclined at 45°, i.e.,

$$U_{min} = -0.53\ a^3(\varepsilon_{11} - \varepsilon_{22})\tau \qquad (1)$$

where $\tau = K_{III}/(\pi\rho)^{\frac{1}{2}}$, which is a torsional stress at the notch tip in the III type specimen. Hydrogen will enrich toward these planes and the equilibrium hydrogen concentration on these planes is

$$C = C_o \exp(0.53\ a^3(\varepsilon_{11}-\varepsilon_{22})\ K_{III}/RT(\pi\rho)^{\frac{1}{2}}) \qquad (2)$$

when the hydrogen concentration reaches a critical value C_{th}, the hydrogen induced cracking will occur. In this case, $K_{III}=K_{IIIH}$. Therefore, we can get

$$K_{IIIH} = RT(\pi\rho)^{\frac{1}{2}} \ln \frac{C_{th}}{C_o} / 0.53\, a^3(\varepsilon_{11}-\varepsilon_{22}) \qquad (3)$$

For I type crack, we obtain similarly

$$K_{IH} = RT(\pi\rho)^{\frac{1}{2}} \ln \frac{C_{th}}{C_o} / a^3\,(1.48\varepsilon_{11} + 1.02\varepsilon_{22}) \qquad (4)$$

Our work showed that $\varepsilon_{11}=0.177$, $\varepsilon_{22}=\varepsilon_{33}=0.026$ (3). Therefore

$$K_{IIIH}/K_{IH} = (1.48\varepsilon_{11} + 1.06\varepsilon_{22})/\ 0.53(\varepsilon_{11}-\varepsilon_{22}) = 2.3$$

which is close to the experimental result, i.e., $K_{IIIH}/K_{IH}=3.2$.

Since K_{IIIH} is larger than K_{IH}, though K_{IIISCC} is larger then K_{ISCC}, we still consider that stress corrosion cracking of high-strength steel under Mode III loading is a kind of hydrogen induced cracking. The reasons are below.

1. Stress corrosion cracking under Mode III loading initiate and propagate along the planes inclined at 45°, similar to hydrogen induced cracking and both have the same fractograph.
2. The addition of a poison decreased the threshold value for stress corrosion cracking under Mode III and Mode I loading.
3. The influence of loading mode on stress corrosion cracking was consistent with that on hydrogen induced cracking.

(1) W.Y.Chu, C.M.Hsiao, S.Y.Ju and C.Wang, Corrosion 38 446-452(1982).
(2) W.Y.Chu, T.Y.Zhang, C.M.Hsiao, Corrosion 40 197-199(1984).
(3) T.Y.Zhang, W.Y.Chu, C.M.Hsiao, Scri. Metall. 19 271-274(1985).

EVIDENCE FOR AN ADSORPTION-INDUCED LOCALISED-SLIP MECHANISM OF ENVIRONMENTALLY ASSISTED CRACKING

S.P. LYNCH*
*Aeronautical Research Laboratories, Defence Science and Technology Organisation, Dept. of Defence, Melbourne, Australia

INTRODUCTION

Detailed metallographic and fractographic comparisons of hydrogen-assisted cracking (HAC) and stress-corrosion cracking (SCC) with adsorption-induced liquid-metal embrittlement (LME) in a number of materials suggest that HAC and SCC are commonly caused by adsorbed hydrogen rather than by dissolved hydrogen, hydrides, or dissolution [1-3]. These observations also suggest that crack growth is accomplished by localised slip rather than by decohesion. Results for single crystals of nickel (fcc), iron-silicon (bcc), and magnesium (cph) are outlined below.

RESULTS

Nickel Single Crystals [1,2]: Crack growth in specimens, with a <100> axis, in gaseous hydrogen and in liquid mercury at 25°C produced cleavage-like fractures approximately parallel to {100} planes (on a macroscopic scale) with crack fronts parallel to <110> directions; extensive slip was observed on {111} planes intersecting cracks. For crystal orientations such that {100} planes were at large angles to the specimen axis, deviations of fracture planes of up to 25° from {100} planes were often observed in both environments. The detailed appearance of fracture surfaces, e.g. numbers of serrated steps, tear ridges, dimples, slip lines, varied with crystal orientation but was the same in mercury and hydrogen for each orientation. Fracture surface characteristics were not markedly affected by strain rate and embrittlement was observed at crack velocities as high as 1mm/s in hydrogen and 10mm/s in mercury.

Fe 2.6% Si Single Crystals [3,4]: Slow crack growth (~0.002mm/s) in specimens, with a <100> axis, in gaseous hydrogen (at 25°C) and rapid crack growth (~10mm/s) in liquid lithium (at 220°C) produced cleavage-like fracture surfaces parallel to {100} planes with crack fronts parallel to <110> directions; significant slip was observed on {112} planes intersecting cracks. Fine details on fracture surfaces, e.g. river lines, tear ridges, were similar in both environments.

Magnesium Single Crystals [3]: Crack growth in specimens, with a wide variety of orientations, in an aqueous $NaCl+K_2CrO_4$ environment at 25°C, liquid sodium at 120°C, and dry air at 25°C-120°C produced fluted fracture surfaces which were macroscopically parallel to $\{1\bar{1}02\}$ planes; crack growth generally occurred in an overall $<1\bar{1}01>$ direction with slip predominantly on pyramidal planes intersecting cracks. Flutes produced in aqueous and sodium environments were much shallower than those

produced in dry air (Fig. 1). Fracture surface characteristics were not markedly affected by strain rate and embrittlement was observed at crack velocities as high as ~10mm/s in both sodium and aqueous environments.

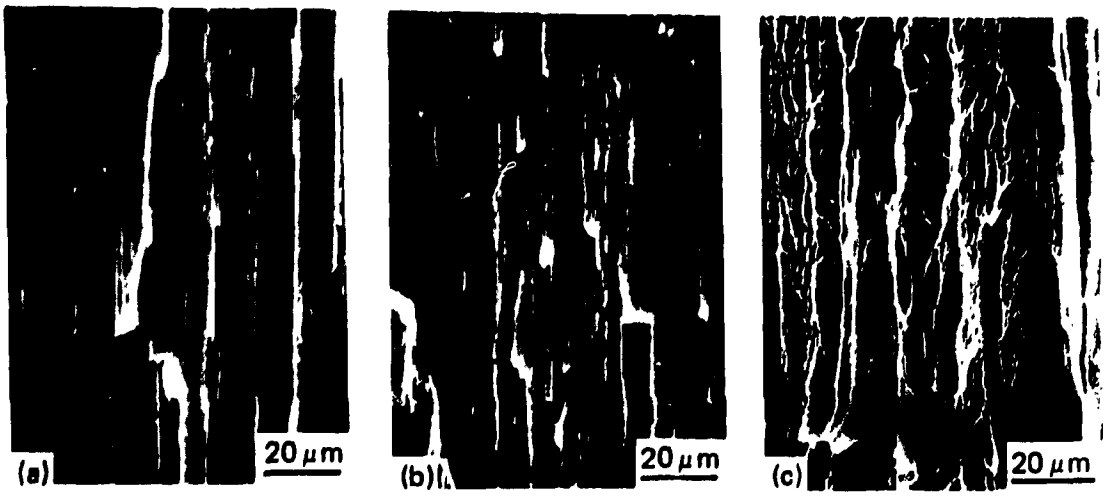

FIG. 1 SEM of fracture surfaces of magnesium produced by crack growth in (a) liquid sodium, (b) $NaCl+K_2CrO_4$, and (c) dry air environments.

DISCUSSION

The observations that fracture planes and directions, active slip planes, and fine details on fracture surfaces are the same for HAC/SCC fractures as for LME fractures strongly suggest that the mechanism of embrittlement is the same in all the environments. Observations of embrittlement under conditions where hydrogen does not have time to diffuse ahead of cracks, e.g. at high crack velocities for HAC of nickel and SCC of magnesium, HAC of nickel at 77K [5], support this suggestion.

The metallographic and fractographic observations, e.g. large localised strains beneath fractures, slip on planes intersecting cracks, dimples, flutes, tear ridges on fracture surfaces, suggest that HAC, SCC and LME occur by a plastic-flow/microvoid-coalescence process that is more localised than that which occurs in inert environments. Specifically, it has been proposed that adsorption reduces the strength of interatomic bonds at crack tips thereby facilitating the nucleation of dislocations and promoting the coalescence of cracks with small voids ahead of cracks, as described in detail elsewhere [1,2].

REFERENCES

1. S.P. Lynch in: Advances in the Mechanics and Physics of Surfaces, Vol. 2, R.M. Latanision and T.E. Fischer, eds. (Harwood Academic Press 1983) pp. 265-364.
2. S.P. Lynch, J. Mat. Sci., in press.
3. S.P. Lynch, unpublished results, 1985.
4. H. Vehoff and P. Neumann, Acta Metall., 28, 265-272 (1980).
5. W. Wei, Ph.D. Thesis, Metallurgy Dept., Univ. of Illinois (1983).

THE RESTRAINING EFFECT OF CLEAVAGE LIGAMENTS IN TRANSGRANULAR STRESS CORROSION CRACKING OF FCC ALLOYS

M. J. KAUFMAN,* E. N. PUGH,* AND A. J. FORTY **
*National Bureau of Standards, Gaithersburg, MD 20899, USA
**Dept. of Physics, University of Warwick, Coventry CV4 7AL, UK

It is characteristic of transgranular stress corrosion cracking (T-SCC) in FCC alloys that the fracture resembles cleavage of brittle solids although these metals are normally ductile. The crack surfaces show extensive faceting and cleavage steps [1]. Furthermore, measurements of the crack velocity obtained by periodically pulsing the load on a test piece have shown that the fracture proceeds by short steps of fast cleavage between periods of natural crack arrest [2]. It is supposed that re-initiation of the brittle cleavage after each arrest follows chemical embrittlement of the material at the tip of the crack by the corrosive environment [3]. This phenomenological description of the stress corrosion crack raises the important question of whether it is possible for a brittle crack to propagate in a ductile material, and the equally important question of why the cleavage occurs discontinuously. This paper is concerned only with the latter question.

It has been suggested [4] that the work done in forming cleavage steps may be an important contribution to the work of fracture in quasi-brittle cleavage. Cleavage steps may be considered to be formed by the breakdown of the ligaments arising from the overlap of neighboring cleavage facets as the fracture is propagated. If, as seems likely for a ductile metal, this breakdown occurs by shearing of the ligaments, which presumably occurs at a lower velocity than the overall cleavage, then the length of unfractured ligaments should increase during a crack propagation event and thereby increase in load bearing capacity. It is possible that crack arrest, and hence the discontinuous nature of T-SCC, is a direct consequence of this. This would explain why the propagation of T-SCC is favored in the case of α-brass since the shearing of the ligaments by planar slip absorbs relatively little energy whereas for pure copper the ligaments rupture less readily making propagation more difficult.

We have investigated this possibility considering two modes of step formation. The first of these envisages step formation to be a simultaneous shear of a ligament which shows that for ligament thickness, h, and yield stress, τ_y, the work to create unit length of step is approximately $\tau_y h^2$ and the energy absorption for n such steps is $n\tau_y h^2$. In practice a cleavage surface has a distribution $n(h)$ of step heights but we assume this simplified model for the purpose of an estimate. The energy for step formation is supplied by the release of potential energy which otherwise, for a brittle crack, is used to create new crack surface of energy density γ, satisfying the Griffith condition. The energy absorbed during crack advance by the shearing of 10^6 ligaments m^{-1} of crack front, each 10^{-7}m thick, under a yield stress of 10^8 Nm^{-2} is about $1Jm^{-2}$ which is comparable with γ. Step densities of this kind

are commonly found on T-SCC fracture surfaces in brasses and stainless steels.

The second estimate considers the ligament to be deforming in anti-plane strain so that the cleavage step is formed by a highly localized progressive shear which propagates along the ligament under an applied stress well below the yield stress. The tearing of the ligament can therefore be modelled by the motion of a distribution of dislocations in the manner first suggested by Bilby, Cottrell and Swinden [5]. According to this model the work done in forming unit length of cleavage step is again approximately $\tau_y h^2$. This is not surprising because, for large h, the plastic zone within which the shear takes place becomes comparable with the length of the ligament and this second model approximates to the former model of uniform shear. The dependence on h^2 means that only the larger cleavage steps have a significant effect on crack propagation and the estimates based on step heights of 0.1 μm are probably realistic.

These simple estimates demonstrate the feasibility of crack arrest by ligament formation. The crack advance distance between arrests should therefore be related to the length of the ligaments at which the restraining effect is sufficient to reduce the stress intensity at the tip of the cleavage crack to below the critical value K_{crit} for propagation. Since the maximum length attainable by a ligament must be the crack length it can be shown that the maximum restraining effect is about one-tenth of K_{crit} for a cleavage in which there are 1/10 μm steps spaced 1 μm apart. Shorter ligaments will have a smaller effect; for example, for a similar cleavage topography but ligaments extending only one-hundredth of the crack length the average restraining effect is one-hundredth of K_{crit}. This would correspond to a crack arrest distance of 10 μm for an overall crack length of 1 mm which is comparable with the observed T-SCC behavior in brass. Thus it seems possible that ligament formation can have a significant influence on brittle crack propagation, especially near the critical condition where a relatively small change in crack tip stress intensity might reduce the crack velocity to a level at which plastic blunting occurs.

REFERENCES:

1. A. J. Bursle, E. N. Pugh, "Mechanisms of Environment Sensitive Cracking of Materials," The Metals Soc. , London, p. 471, 1977.
2. M. T. Hahn, E. N. Pugh, Corrosion, Vol. 36, p. 380, 1980.
3. A. J. Forty, "Physical Metallurgy of Stress Corrosion Fracutre," Interscience, New York, p. 99, 1959.
4. J. J. Gilman, J. Appl. Phys., Vol. 27, p. 1262, 1956.
5. B. A. Bilby, A. H. Cottrell, K. H. Swinden, Proc. Roy. Soc., Vol. A272, p. 304, 1963.

TRANSGRANULAR STRESS-CORROSION CRACKING

K. SIERADZKI
Brookhaven National Laboratory, Upton, New York 11973

We discuss the phenomenon of transgranular stress-corrosion cracking. Experimental evidence is presented which indicates that during this process ductile metals such as α-brass and copper fail by the propagation of cracks whose microscopic features are consistent with the occurrence of cleavage fracture [1]. Simultaneous electrochemical and acoustic emission measurements indicate that the failure is actually the result of intermittent microcleavage events [2].

The interaction of the aqueous environment and the metal results in the formation of a thin surface film which facilitates cleavage crack nucleation. We discuss how the presence of a film surrounding a crack tip can modify the local deformation in such a way as to initiate cleavage. In this respect we are concerned with the films effectiveness in changing the balance between cleavage and dislocation emission. The important parameters determining the effectiveness of films in initiating cleavage include the film-substrate misfit, the strength of the bonding across the film-substrate interface, the film thickness and the film ductility. Suitable combinations of these parameters which can lead to microcleavage are determined by the state of coherency of the interface and the fracture toughness of the substrate. For example, if a ductile de-alloyed layer in α brass remains coherent with the substrate and has a misfit of 0.02 (equivalent to complete dealloying of a 70-30 brass), it must be ~200 monolayers thick in order to initiate a microcleavage event [3].

Experiments [3] and molecular dynamic simulations [4] indicate that under appropriate circumstances once a cleavage crack is nucleated in the film it continues on into the substrate in a brittle mode owing to dynamic effects. Once in the substrate the crack finally arrests. We shall consider various processes which may be responsible for crack arrest.

ACKNOWLEDGMENTS

This research was performed under the auspices of the U.S. Department of Energy, Division of Materials Sciences, Office of Basic Energy Sciences under Contract No. DE-AC02-76CH00016.

REFERENCES

1. K. Sieradski, R.L. Sabatini, and R.C. Newman, Metall. Trans. A 15, 1941 (1984).

2. R.C. Newman and K. Sieradzki, Scripta Metall. 17, 621 (1983).
3. K. Sieradzki and R.C. Newman, Philos. Mag. A 51, 95 (1984).
4. A. Paskin, K. Sieradzki, D.K. Som, and G.J. Dienes, Acta Metall. 31, 1253 (1983).

MECHANISMS OF LONG-LIFE FATIGUE

CAMPBELL LAIRD
Department of Materials Science and Engineering
Univeristy of Pennsylvania
3231 Walnut Street
Philadelphia, PA 19104

INTRODUCTION

Since cracks are widely, and usually correctly, believed to nucleate early in the fatigue life of most metals and structures prone to fatigue, most research effort in the last 20 years has been devoted to crack propagation. Because of the methods of linear elastic fracture mechanics, the emphasis has been on the growth of long cracks. Much progress has been made and rather secure deterministic methods have been developed for large structures. However, the great majority of fatigue critical components are not of the type in which lives can be predicted by long crack methods. Recent emphasis has therefore turned to the short crack. In this talk then, emphasis will be placed on the behavior of short cracks and its relation to cyclic deformation.

CYCLIC DEFORMATION

The conventional view is that pure metals have a two-phase structure in the range of strain amplitudes where fatigue lives are finite. These structures are "matrix structure", or dislocation loop patches separated by channels reasonably free of dislocations, and "persistent slip bands (PSB's)" consisting of the well known ladder structure. It is shown that this view of dislocation structure is oversimplistic and results on PSB nucleation are inconsistent with it. Moreover, the feeling that the average strain localized in the PSB's is constant at around 0.01 can be misleading for understanding Stage I crack propagation. The distributions of slip offsets at PSB's for copper single crystals cycled at strains in the plateau of the cyclic stress-strain curve are shown in Fig. 1. These offsets reflect the local strain and can be used to measure it precisely. Since the PSB widths also vary widely, the range of local strains is considerable. The magnitude of these strains is even larger in alloys, depending on the nature of the hardening mechanism. For much of the fatigue life, the local strains remain constant (assuming constant applied cyclic strain), but for large numbers of cycles the local strain diminishes and new PSB's are created. The reasons for this behavior and its implication for life are discussed.

STAGE I CRACK PROPAGATION

The recent results of the Basinskis' [1] and Hunsche & Neumann [2] have provided excellent data on Stage I crack growth in identifying the

locations of Stage I cracks for various types of PSB's. Extensions of their work, using the newly-developed "corner" technique for measuring the growth of Stage I cracks, have been carried out in our laboratory. A typical crack size distribution, again for a copper single crystal, is shown in Fig. 2. Note the similarity of the distribution to that in Fig. 1, showing the local strain to control the growth kinetics. The implications of these results for life behavior in pure metals and alloys are explored.

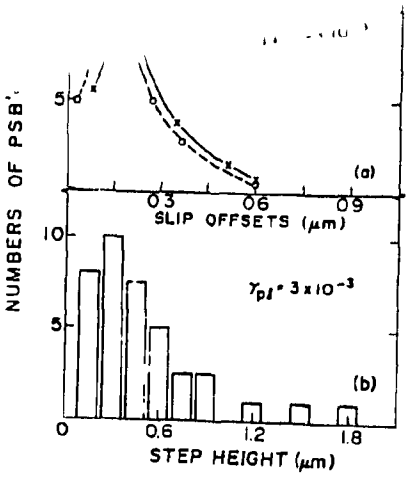

Fig. 1 Distribution curves of PSB slip offsets and step heights for copper single crystals (single slip) cycled at the indicated plastic shear strain amplitudes. Taken from [3].

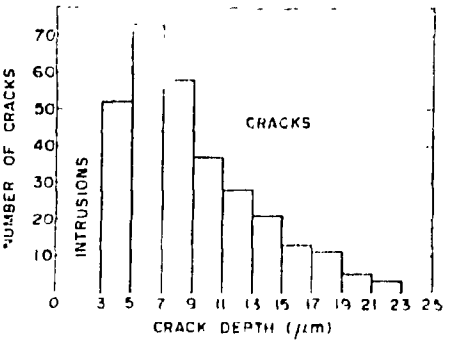

Fig. 2 Histogram of crack population in a copper single crystal cycled at $\gamma_p = 2 \times 10^{-3}$ for 30,000 cycles (~15% life). Taken from [4].

SUMMARY

Fatigue mechanisms are dominated by the occurrence of localized strain and its magnitude. New research has quantified this strain and has identified its dependence on microstructure, environment, applied amplitude and history. This information is most encouraging for understanding short crack behavior.

REFERENCES

1. Z. S. Basinski and S. J. Basinski, Scripta Met., 18, 851 (1984).
2. A. Hunsche and P. Neumann, Contribution to the Symposium on Fundamentals of Fatigue Fracture, Dallas, Tx, 1984, in press.
3. A. S. Cheng, Ph.D. Thesis, University of Pennsylvania, Philadelphia, 1981.
4. B. T. Ma and C. Laird, "On Fatigue Crack Size Distributions in Copper Single Crysals", unpublished research, 1985.

A MECHANISTIC MODEL OF FATIGUE CRACK GROWTH

J.E. SINCLAIR
AERE Harwell, Oxfordshire, U.K. OX11 ORA

As with non-cyclic fracture, fatigue cracking depends upon an interaction between mechanics on a large scale, for which some kind of elastic-plastic analysis can be used, and the microscopic processes of material separation producing crack extension. Concerning the large-scale mechanics, the chief novelty of the present approach is to allow for the formation of a wake of dislocations as crack propagation proceeds. Former models without such allowance estimated crack opening displacement and plastic zone size as if only one loading and unloading had occurred. The results for these quantities was then much the same using, for instance, the idealised co-planar yield representation of Dugdale or Bilby Cottrell & Swinden (DBCS) as with a more realistic continuum elastic-plastic model. But of course that part of the plastic zone which is not reversed at each unloading must get left behind as the crack propagates, and will need to be replenished. To allow for this, the one-dimensional DBCS model is inadequate, and the simplest related model is to use inclined bands through the tip. It can then be argued that a wake of slip-band fragments of the type illustrated below should

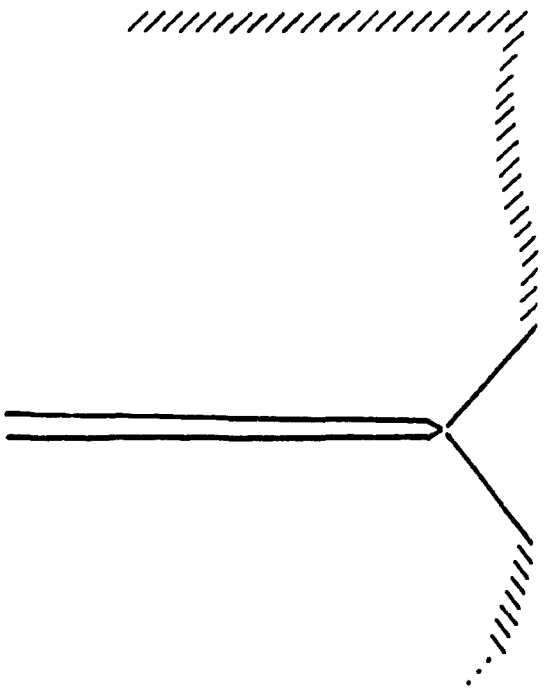

Form of the steady-state wake of dislocations generated by many cycles of load variation on a crack.

develop. In the talk I will describe solutions of the mechanics of this model when a friction stress and a crack propagation rate are given. The numbers of dislocations in the different sections of the inclined bands at high and low load relate quantitatively to the horizontal wake density and to the cyclic crack-tip plastic displacements.

To make these quantitites consistent with the propagation rate, a microscopic model is necessary. Initially, I have assumed that propagation is by plastic sliding off and re-sharpening only. This makes the crack length increment proportional to the cyclic crack-tip plastic displacement, and thus a $(\Delta K)^2$ dependence is obtained. However, it is intended to incorporate more complex propagation models. Modification of the effective ΔK by crack face closure (possibly enhanced by surface roughness) would be particularly easy to incorporate. In addition, the amount of sliding off should be reduced in accordance with the fraction of yielding which intersects the crack planes other than at the tip.

CRACK TIP SHIELDING IN FRACTURE AND FATIGUE: INTRINSIC vs. EXTRINSIC TOUGHENING

R. O. RITCHIE
Department of Materials Science and Mineral Engineering,
University of California, Berkeley, CA 94720, U.S.A.

INTRODUCTION

Crack tip shielding phenomena, whereby the "effective crack driving force" actually experienced in the near-tip region is reduced compared to the applied (far-field) value, are examined with reference to the fracture toughness and fatigue crack growth behavior in metals, ceramics and composites. Examples are taken from the extrinsic toughening of brittle materials, by mechanisms involving phase transformations, microcracking and fiber toughening, and from the crack closure and deflection of fatigue cracks, by mechanisms involving cyclic plasticity, corrosion deposits, meandering crack paths and fluids inside cracks.

FRACTURE TOUGHNESS

Extrinsic toughening of metallic alloys generally is not very important because of the high applied stresses involved in the fracture of ductile materials with their inherent toughness. Brittle materials such as ceramics and rocks, conversely, rarely can be toughened intrinsically, e.g., attempts to promote ductility in ceramics have been largely unsuccessful. As is now well known [1], extrinsic toughening utilizing crack tip shielding mechanisms, such as crack deflection, microcracking, and phase transformation, has been very successful in raising K_{Ic} values in ceramics from almost zero to above 20 MPa$\sqrt{m}$ (Fig. 1a). Similar effects are seen with deflection and fiber or ligament toughening mechanisms in composites. In all cases, the material is not inherently tougher, i.e., the local ductility or strain to failure is unchanged: simply the crack tip has been shielded from the full applied "driving force" such that the effective stress intensity actually experienced at the crack tip becomes less than the nominally applied value.

FATIGUE CRACK PROPAGATION

Extrinsic toughening can be utilized in metallic materials where applied stresses are not large, e.g., during sub-critical crack growth. The most notable example has been for fatigue crack propagation, particularly when cracks are growing at low (near-threshold) growth rates, where crack tip shielding from crack deflection and particularly crack closure can provide extremely potent mechanisms for retarding crack growth rates [2]. Whereas deflection can be promoted by such microstructural factors as coarse planar slip or the presence of a dispersed hard phase, closure is promoted by various mechanical, microstructural and environmental mechanisms (Fig. 1b).

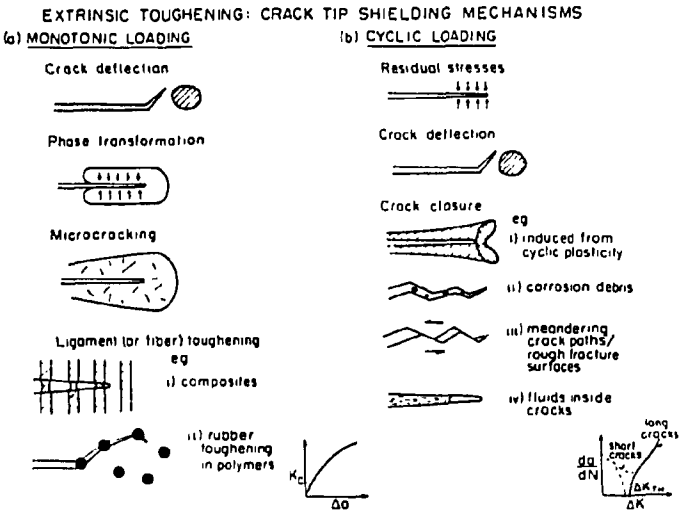

Fig. 1. Crack tip shielding mechanisms under a) monotonic and b) cyclic loading conditions.

DISCUSSION

Such extrinsic mechanisms are potentially far more potent in reducing crack extension rates than with intrinsic mechanisms which attempt to enhance the inherent resistance of the microstructure. The common phenomena here are related primarily to processes which occur in the wake of the crack tip, whether associated with an enclave of previously deformed (e.g., plastic or transformed) zones, the formation of fracture surface asperities to yield an interlocking zone behind the tip, or the presence of fluid or debris within the crack. Such processes effectively shield the crack from the full (far-field) applied loading, yet since they act on the wake of the crack, their influence must diminish with decreasing crack length and increasing applied stresses. There are specific implications of this which distinguish the intrinsic and extrinsic mechanisms, namely the existence of a resistance curve in fracture toughness measurements [3], the mean stress and "short crack" effects in fatigue [2], and in general the widely differing microstructural factors which control crack initiation as opposed to crack growth.

REFERENCES

1. A. G. Evans and K. T. Faber, J. Amer. Ceramic Soc. 67, 255-260 (1984).
2. S. Suresh and R. O. Ritchie in: Fatigue Crack Growth Threshold Concepts, D. L. Davidson and S. Suresh, eds. (TMS-AIME, Warrendale, 1984) pp. 227-261.
3. R. O. Ritchie and A. W. Thompson, Metall. Trans. A 16A, 233-248 (1985).

MECHANISMS OF FATIGUE CRACK GROWTH THROUGH ALUMINUM ALLOYS

DAVID L. DAVIDSON
Southwest Research Institute
6220 Culebra Road
San Antonio, Texas 78284

The objective of this paper will be to summarize recent observations of fatigue crack growth and measurements of crack tip mechanics, and to hypothesize a mechanism of crack growth which is consistent with the observations.

Fatigue crack growth has been observed dynamically in thick specimens through the use of a cyclic loading stage which fits into the scanning electron microscope [1]. Measurements of cyclic displacements within the near field of the crack tip were made using the stereoimaging technique [2]. Crack opening loads and displacements and strains were derived from these measurements. By combining these crack tip analyses with dynamic observations and measurements from fractography and quantitative metallography, a conceptual description of the mechanism of fatigue crack growth has emerged.

Dynamic observations of fatigue crack growth have shown that cracks do not grow on each cycle; rather, a number of cycles is required before the crack advances incrementally, with the number of cycles being dependent on the level of the crack driving force, the cyclic stress intensity factor [3,4]. These observations have been videotaped and will be shown to illustrate the process. Crack tip opening displacement and strain also follow this non-uniform but repetitive pattern.

It is a rather curious fact that Stage II fatigue crack growth rates through aluminum alloys are relatively independent of microstructure, while in the near threshold region they are not. Crack closure is often invoked to explain the near-threshold behavior. Recent, high resolution measurements of crack closure which have helped to bring some understanding to this issue will be reported.

Fractographic measurements of striations [5] have shown them to be independent of crack opening displacement for cracks grown in vacuum, but of proportional magnitude for cracks grown in moist air.

Models derived to explain fatigue crack growth must incorporate these multiple, and sometimes seemingly incompatible findings. A model has been developed which accounts for these various observations and measurements and incorporates microstructure as well [6]. An example of the crack tip slip line field produced using the model is shown in Fig. 1, where the length of the slip line is set by the microstructure and the number of slip lines is dependent on the cyclic stress intensity factor [7].

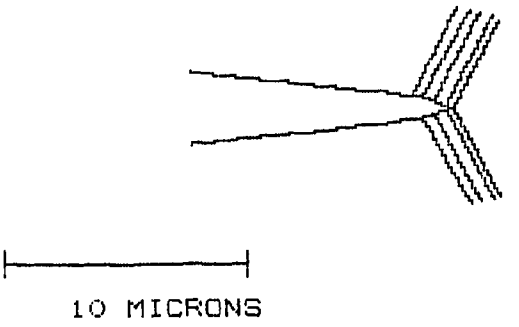

FIG. 1. Slip line field predicted by model of fatigue crack growth through 7091 aluminum alloy at ΔK = 10 and ΔK_{eff} = 6.5 MN/m$^{3/2}$.

The mechanism of crack growth envisioned is glide plane decohesion, assisted by environment when the crack is grown in moist air. Exactly how this decohesion occurs is still being investigated.

Through this process of observation and modeling, a mechanism by which cracks lengthen has been postulated. But, as with descriptions of many complex phenomena, a number of assumptions and simplifications have been made to produce a workable model, and these will be reviewed and critiqued with the purpose of determining the weaknesses in both mechanistic understanding and modeling of the fatigue crack lengthening process.

REFERENCES

1. D. L. Davidson and A. Nagy, Journal of Physics E 11, 207-210 (1978).
2. D. R. Williams, D. L. Davidson, and J. Lankford, Experimental Mechanics 20(4), 134-139 (1980).
3. D. L. Davidson, Fatigue of Engineering Materials and Structures 6(3), 287-290 (1983).
4. D. L. Davidson and J. Lankford, Fatigue of Engineering Materials and Structures 7, 29-39 (1984).
5. J. Lankford and D. L. Davidson, Acta Metallurgica 31, 1273-1284 (1983).
6. D. L. Davidson, Acta Metallurgica 32, 707-714 (1984).
7. D. L. Davidson, "The Effects of Aluminum Alloy Microstructure on Fatigue Crack Growth", Materials Science and Engineering 74 (1974) (in press).

MICROSTRUCTURE AND CLOSURE RELATED GROWTH CHARACTERISTICS OF SHORT FATIGUE CRACK GROWTH AT CONSTANT ΔK

F. H. HEUBAUM‡, M. E. FINE‡, AND R. P. GANGLOFF*
‡Dept. of Materials Science and Engineering, Northwestern University, Evanston, IL 60201; *Corporate Research Science Laboratory, Exxon Research & Engineering Company, Annandale, NJ 08801

The propagation kinetics of short fatigue cracks (<500 μm) are often substantially higher than those of long cracks (>10 mm). Proposed mechanisms for this behavior are based on excess plasticity [1], reduced crack closure [2-4], microstructural [5], or chemical environment effects [6]. Short cracks were cycled at less than 50% of the yield strength near threshold in air. Large scale plasticity effects or extraordinary environmental interactions are not expected. The experimental evidence presented suggests that the development of increasing crack closure stresses at constant ΔK is a major factor for short crack behavior in specimens in which the crack front simultaneously intersects several grains.

A537 steel (0.23C, 1.28Mn, 0.23Si) quenched and tempered at 400°C to a constant hardness and yield strength of 36 Rc and 930 MPa was investigated. The austenitizing temperature was varied to give martensite subunit cell sizes of 10, 120, and 600 μm. Single edge and corner cracked specimens with gauge dimensions 10 mm x 3 mm x 20 mm were tested in uniaxial tension under load control at a sinusoidal frequency of 5 Hz and an R ratio of 0.05. Notches nominally 100 μm in depth were prepared using electro-discharge machining. Crack depths were continuously monitored using a d.c. potential drop technique which provided constant applied ΔK control through computer interfacing and feedback. Crack closure loads were measured using an LVDT spanning the notch.

The variation of crack length with cycles is shown in Fig. 1 for a short single edge crack propagating through a 120 μm grain size specimen cycled at constant $\Delta K = 7.7$ MPa$\sqrt{m}$. The declining growth rate with increasing crack length is apparent. Approximately constant growth rate is achieved after one average grain diameter of growth. About 25 grains constitute the crack front. For this same specimen, the decrease in growth rate and the corresponding change in relative crack opening load, P_{op}/P_{max}, or equivalently K_{op}/K_{max} since ΔK is constant, are shown in Fig. 2. The decline in growth rate from 3×10^{-6} to 1.1×10^{-6} mm/cycle as crack length increases from 130 to 250 μm (10 to 130 μm plus 120 μm notch depth) is accompanied by an increase in closure stress intensity ratio from $K_{op}/K_{max} = 0.22$ to 0.35. Between 275 and 400 μm the growth rate is constant, as expected for long cracks at constant ΔK. The crack closure level is also essentially constant. When these data are analyzed in terms of $\Delta K_{eff}(K_{max} - K_{op})$ correlation exists with constant load long crack data. The 600 μm grain size specimens show comparable behavior to the above. The 10 μm grain size specimens show linear behavior from initiation to a = 1 mm. The grain size dependence for long and short crack growth rates may be understood based on surface roughness contributions to closure [3]. At 1 mm of growth at $\Delta K = 7.7$ MPa$\sqrt{m}$ the growth rates, P_{op}/P_{max} ratio, and the peak to peak fracture surface roughness as measured with a profilometer for the three grain sizes are given in Table I.

Table I. Grain size and closure data for 1 mm short crack growth at 7.7 MPa/m.

Grain Size (μm)	Growth Rate (mm/cycle)	P_{op}/P_{max}	Fracture Roughness (μm)
10	2.4×10^{-6}	0.26	2.5
120	1.1×10^{-6}	0.35	28
600	1.5×10^{-6}	0.32	>100

The 10 μm grain sized specimens showed the highest overall growth rates due to lower P_{op}/P_{max} levels resulting from lower fracture surface roughness. The 600 μm specimens showed slightly higher 1 mm growth rates than the 120 μm specimens possibly due to the larger roughness wavelength. Note the P_{op}/P_{max} values in Table I gave rise to essentially the same da/dN values as measured for the small crack in Fig. 2. Thus crack closure development provides a reasonable rationale for the short crack effect in physically small (100-500 μm) fatigue cracks extending over several grains.

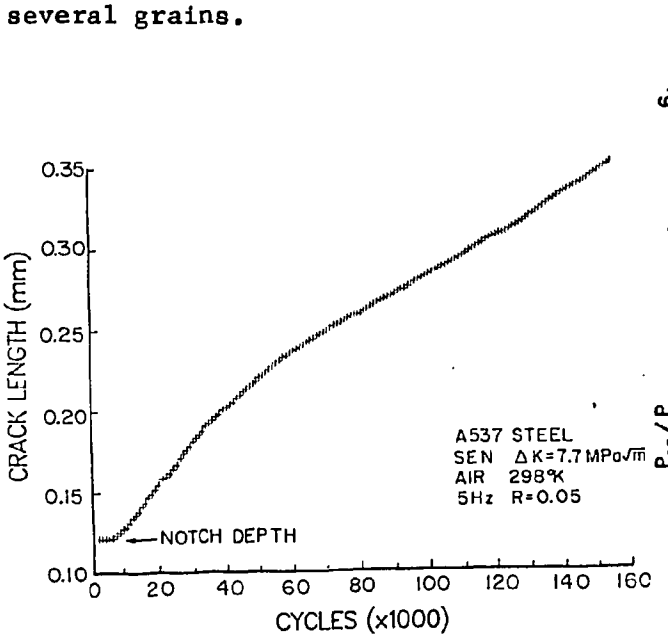

FIG. 1. Decelerating growth at constant ΔK for 120 μm grain size.

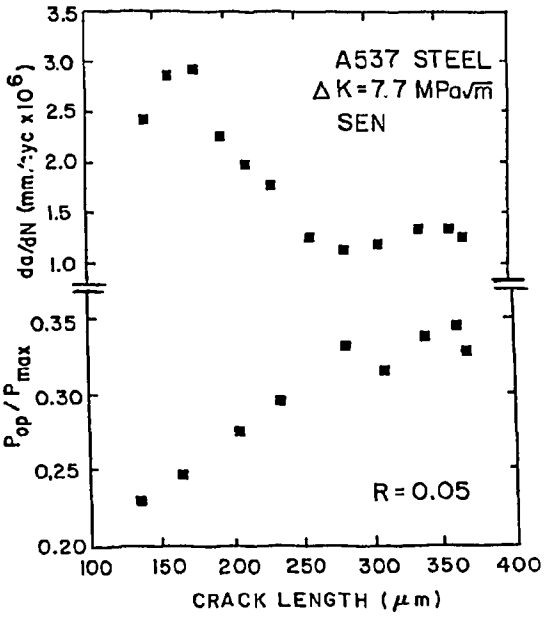

FIG. 2. Growth rate and closure variation of Fig. 1 test.

REFERENCES

1. S. Usami and S. Shida, Fat. Engr. Matl. Struc. 1, 471 (1979).
2. J. C. Newman in: Behavior of Short Cracks in Airframe Components, AGARD-CP-328 (1983).
3. S. Suresh and R. O. Ritchie, Intl. Metals Reviews 29, 445 (1984).
4. K. Tanaka and Y. Nakai, Fat. Engr. Matl. Struc. 6, 315 (1983).
5. J. Lankford, Fat. Engr. Matl. Struc. 5, 233 (1982).
6. R. P. Gangloff and R. O. Ritchie in: Fundamentals of Deformation and Fracture, Cambridge University Press, in press.

HIGH TEMPERATURE FATIGUE BEHAVIOR OF FERRITIC STAINLESS STEELS

S. KIM* AND J. R. WEERTMAN*
*Department of Materials Science & Engineering, Northwestern University, Evanston, Illinois 60201

INTRODUCTION

The relationship between high temperature fatigue behavior and microstructural changes has been investigated for several ferritic stainless steels. These steels are used in power generation and therefore they must exhibit microstructural stability over long periods of high temperature service. Much of the present work has been carried out on the alloy Fe9Cr1Mo modified by the addition of small amounts of the strong carbide formers, V and Nb. This alloy was developed as part of the Advanced Alloy Program of Oak Ridge National Laboratory. Modified Fe9Cr1Mo is used in the fully martensitic state, produced by normalizing at 1038°C 1 hour (air cool) then tempering 1 hour at 760° (air cool). The resultant microstructure consists of a highly dislocated lath structure. Carbides are present as fine MC ($V_xNb_{1-x}C$) and larger $M_{23}C_6$ particles.

EXPERIMENTAL DETAILS AND RESULTS

Specimens were tested in total strain control, in vacuum and in air, at several temperatures. For all steels tested, and for all the test conditions used, continual softening was observed throughout the specimen life. As can be seen from Fig. 1, the softening produced by aging modified Fe9Cr1Mo 5000 hours at 593°C is considerably less than the softening which takes place during some 15-20 hours of fatiguing at the same temperature (~ 70 MPa in the stress amplitude as compared to ~ 150 MPa). The aged material undergoes about the same softening during fatiguing as does the material which has been only normalized and tempered. Loss of strength with cycling was observed at all temperatures tested (Fig. 2). Note that the number of cycles to failure, N_f, is very similar throughout the temperature range 482 - 704°C. The temperature independence of N_f (for a fixed total strain range) applies only to tests run in vacuum. Fatiguing in air greatly shortens N_f, which now is a strong function of temperature. The ratio of fatigue life in vacuum to that in air depends on the strain range, becoming very large at small strain ranges, i.e., long fatigue lives. HVEM studies indicate that fatigue at high temperatures (1) drastically reduces the dislocation density; (2) changes the substructure from a lath morphology to large equiaxed subgrains; (3) changes the carbide population. The technique of small angle neutron scattering has been used to study the change in carbide populations produced by aging and by high temperature deformation. While quantitative interpretation of the results is complicated by the presence of several types of carbides it appears that the total number of carbides decreases as aging proceeds. Such a drop would contribute to the observed softening.

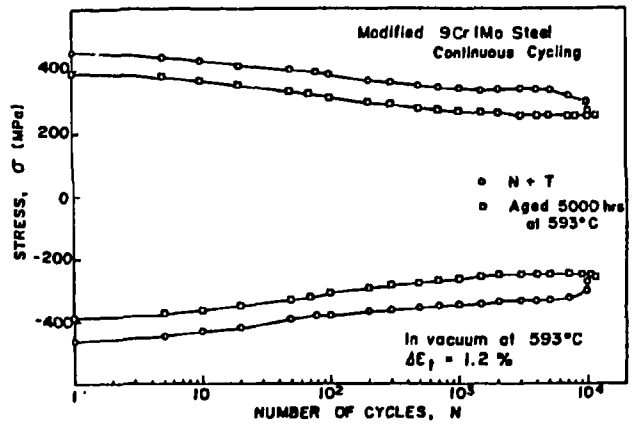

Fig. 1. Stress amplitude as a function of number of cycles for modified Fe9CrlMo fatigued in vacuum, $\dot{\epsilon} = 4x10^{-3}\ s^{-1}$, T = 593°C, total strain range = 1.2%. Curves shown for material given only normalizing and tempering treatment and for steel aged 5000 h at 593°C after normalization and tempering.

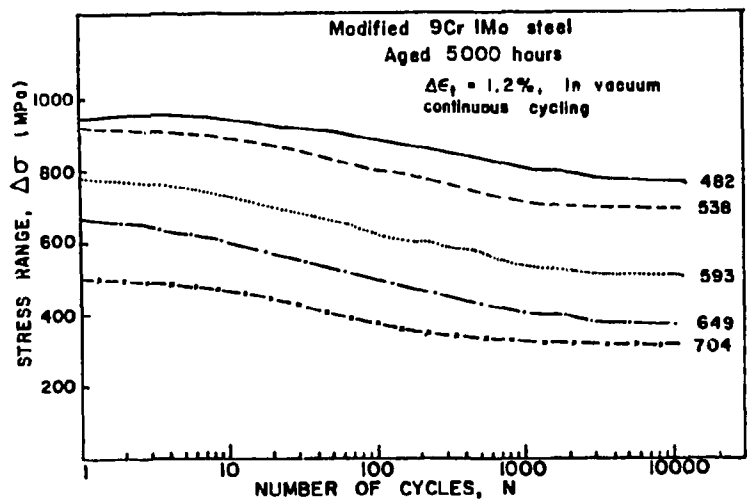

Fig. 2. Total stress range as a function of number of cycles for modified Fe9CrlMo fatigued in vacuum, $\dot{\epsilon} = 4x10^{-3}\ s^{-1}$, total strain range = 1.2%. Steel aged 5000 h at various temperatures, then tested at aging temperature.

ACKNOWLEDGEMENT

The HVEM studies were carried out at Argonne National Laboratory. This work was supported by U.S. Department of Energy, Grant Number DE-AC02-81ER10960.

LCF BEHAVIOR OF ALLOY 800H AT 800°C

B. LERCH, B. KEMPF, K. BOTHE, AND V. GEROLD
Max-Planck-Institut für Metallforschung, Institut für Werkstoffwissenschaften, Seestrasse 92, D-7000 Stuttgart 1, FRG

INTRODUCTION

In connection with a European research project the low cycle fatigue behavior of Alloy 800H was investigated with the aim of improving the insight into the damage mechanisms controlling fatigue life. During air tests at 800°C the total strain rate $\dot{\varepsilon}_t$ and the plastic strain amplitude $\Delta\varepsilon_p/2$ were kept constant. The strain rate $\dot{\varepsilon}_t$ was varied between $2\cdot10^{-5}$ and $2\cdot10^{-2}s^{-1}$ and the strain range $\Delta\varepsilon_p$ from 0.035 to 1%. In order to check the influence of the shape of the hysteresis loop asymmetrical tests (so-called slow-fast tests) with lower strain rates in the tensile than in the compressive part of the cycle were undertaken. The life time was in all cases defined as the point where the stress amplitude has decreased to 80% of the maximum amplitude. To study the influence of cycle shape and strain rate on the life time a large number of tests were performed at $\Delta\varepsilon_p$=0.3%. The broken specimens were investigated using SEM and TEM.

EXPERIMENTAL RESULTS

From all tests the relationship between the strain range $\Delta\varepsilon_p$, strain rate $\dot{\varepsilon}_t$, stress amplitude σ, cycle number to failure, N_f, and life time t_f were investigated. The tests at $\Delta\varepsilon_p$=0.3% showed a relatively small dependence of N_f on the deformation rate and cycle shape. For 13 tests N_f varied only between 650 and 4 000. The lower strain rates usually resulted in a lower value of N_f. For the slow-fast tests N_f was controlled by the tensile strain rate and was found to be slightly smaller in comparison to the corresponding symmetrical test (up to a factor 2).

The major influence of time dependent processes is clearly shown by the strong strain rate dependence of the stress response. For $\Delta\varepsilon_p$=0.3% the peak stresses vary from 90 to 170 MPa depending on the strain rate. Thus, if N_f is only discussed in terms of the controlled strain amplitude (Coffin-Manson curve), the time dependence of the failure is strongly masked by this behavior of the peak stress. A totally different picture is obtained if N_f is plotted as a function of the stress amplitude σ. In that case the data scatter widely but come closer to each other if the life time t_f is used as a variable. Only the data with high strain rates $\dot{\varepsilon}_t=2\cdot10^{-2}s^{-1}$ are an exception with smaller t_f values compared to the others. This is not surprising since the rate dependence of σ decreases considerably for strain rates above $2\cdot10^{-3}s^{-1}$. The remaining log σ-log t_f data fit quite well with life time data from creep tests on the same alloy.

Another possibility to represent life time data is to correlate the area of the hysteresis loop with the cycle number to failure. If the product $\Delta\varepsilon_p \cdot \sigma$ is plotted versus N_f the data follow a single curve for each applied tensile strain rate. The data with $\dot{\varepsilon}_t = 2 \cdot 10^{-3}$ and $2 \cdot 10^{-2} s^{-1}$ fall on the same line demonstrating that there is only a minor time dependence in this velocity range. The data for $\dot{\varepsilon}_t = 2 \cdot 10^{-4} s^{-1}$ follow a parallel line with N_f being smaller by a factor of 3. A similar shift is shown by the data for $\dot{\varepsilon}_t = 2 \cdot 10^{-5} s^{-1}$. This factor may decrease for smaller plastic strain amplitudes ($\Delta\varepsilon_p \lesssim 0.1\%$).

METALLOGRAPHIC INVESTIGATIONS

Metallographic investigations show that in all cases the damage can only be observed as cracks nucleating on the surface and propagating into the interior of the specimen. For higher strain amplitudes a high density of cracks develop with one crack leading to final failure. With decreasing strain amplitude this density decreases and finally only one crack can be observed, which indicates the increasing difficulty of crack initiation. The cracks are often initiated at grain boundaries but penetrate into the interior in a mixed mode. Heavy oxidation of the crack surface indicates a strong stress enhanced oxidation mechanism. The preference for intercrystalline crack propagation changes gradually and increases with decreasing strain rate. A similar failure mechanism is also observed in creep tests. Because of the low strain rates the creep failure can be observed as an intercrystalline crack penetrating into the interior from all sides until final overload rupture of the central part occurs.

CONCLUSIONS

In light of these results the life time for creep and LCF experiments is controlled by crack nucleation and propagation. Probably most of the life time is spent in crack propagation. The propagation rate is controlled by the applied stress in the case of creep experiments. For LCF the crack propagation per cycle depends on both the applied stress and the strain amplitude. Because crack propagation is also a time dependent process the cycle time also has an influence. Thus, as a first approximation it is suggested that cyclic life time is best described using two variables, the area of the hysteresis loop and the strain rate in tension. The first variable can be approximated by the product $\Delta\varepsilon_p \sigma$. This description may fail at lower strain amplitudes $\Delta\varepsilon \lesssim 0.1\%$ because an increasing amount of the life time is spent by crack initiation which may depend only on the loop but no longer on the cycle time.

THE GROWTH OF PERSISTENT SLIP BANDS DURING FATIGUE

W. J. BAXTER
Physics Department, General Motors Research Laboratories,
Warren, MI 48090-9055

One of the earliest manifestations of fatigue deformation is the development on the surface of so-called persistent slip bands (psb). These slip bands have long been known to play an important role in, and even becomes sites for, the initiation of fatigue cracks. Two distinctive features of psb are 1) the extrusion of thin lamella of material, and 2) the generation of dislocation structures known as ladders and cells, particularly in the near surface regions. These two features appear to be manifestations of the same process and are fundamental to the understanding of metal fatigue [1].

But despite the importance of psb, relatively little attention has been given to the kinetics of their development. One reason for this is that conventional techniques of surface examination are post-mortem in nature, so do not provide sequential information at intervals during a fatigue experiment. This paper describes the application of photoelectron microscopy to measure the early stages of the emergence of persistent slip bands in 6061-T6 aluminum. The specimens are coated with a 14 nm anodic oxide film. During fatigue cycling in the microscope this film is ruptured by emerging slip bands, which appear in the image as sources of strong electron emission known as exoelectrons [2]. These observations have revealed that:

1. The persistent slip bands in 6061-T6 aluminum appear on the surface as a linear array of individual extrusions with a periodicity of ~1-2 μm.

2. Initially a single extrusion is formed. Then the length of the slip band increases incrementally by the addition of further extrusions, while the initial ones continue to become more pronounced.

3. During the early stages of growth, the length of an individual slip band increases as the square root of the number of fatigue cycles (Fig. 1).

A model is proposed based upon a psb consisting of a periodic dislocation cell structure, the elongation of the psb being controlled by the cyclic strain (ε_c) within the cells. A comparison of the model with the experimental observations shows that under the condition of constant cyclic displacement:

1. ε_c decreases as the psb elongates, and

2. the values of ε_c are very large, encompassing a range of 10 to 100 times greater than the applied macroscopic strain.

REFERENCES

1. M. Klesnil and P. Lukas, "Fatigue of Metallic Materials," (Elsevier, Amsterdam 1980).
2. W. J. Baxter in Treatise on Materials Science and Technology 19, "Experimental Methods, Part B," (Academic Press, New York, 1983) pp. 1-66.

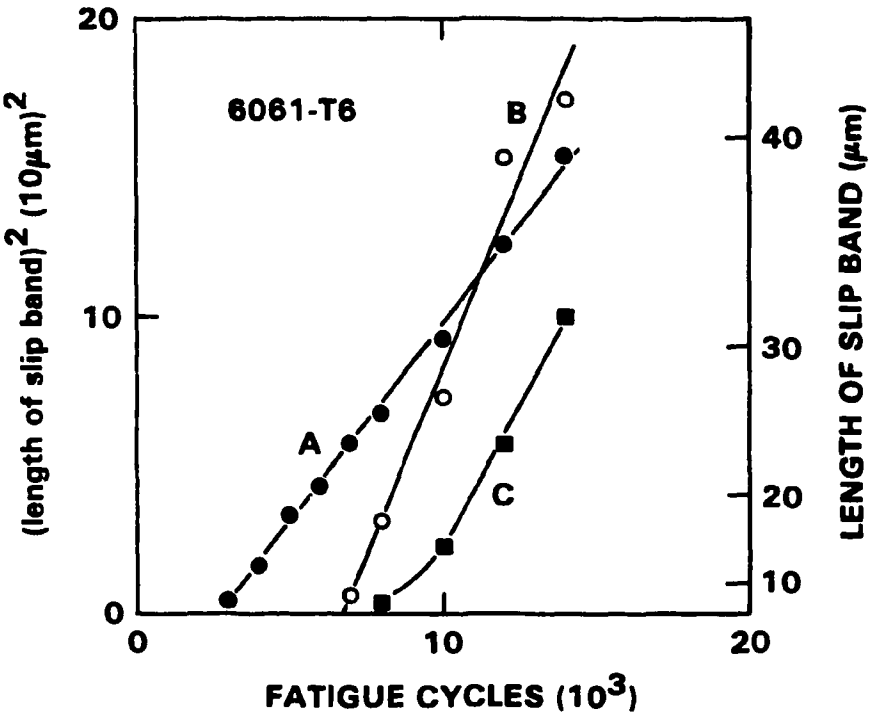

Fig. 1 Effect of fatigue cycles on the square of the length of psb.

CHEMISTRY OF FRACTURE IN GLASS

SHELDON M. WIEDERHORN
National Bureau of Standards
Gaithersburg, MD 20899

ABSTRACT

Subcritical crack growth in glass is usually attributed to a stress enhanced chemical reaction between water or other corroding species in the environment and the stressed bonds at the tips of cracks in the glass. As with most chemical reactions, the reaction rate depends on the chemical activity of the corroding species in the environment, the forces applied to the crack and the transport of the corroding species from the external environment to the crack tip. However, because of the particular geometry of the reaction site, special considerations are required to quantify the rate at crack tips compared to that obtained from normal reaction rate theory. In this paper, we discuss these considerations with regard to subcritical crack growth in several glasses, for which abundant crack growth data is available.

Because of the geometry of the crack, the reaction site is remote from the ambient environment that causes crack growth. Assuming the applicability of linear elastic fracture mechanics theory, the crack opening displacement is only 10 nm at a distance of 1 μm from the crack tip, and 0.5 nm at a distance of 0.5 nm (the approximate distance between bonds in silica glass) from the crack tip. Because of this restriction in the geometry, chemically active species traveling towards the crack tip will react with the surfaces of the crack. This reaction modifies the chemical environment so that the environment at the crack tip will differ substantially from the ambient environment. Thus, transport and chemical reaction with the crack walls are both important in establishing the composition of the environment at the crack tip in glass.

A second effect of the restricted nature of the crack geometry is the occurrence of stearic hinderance of the chemical reaction at the crack tip. Although water is the main reacting species for glasses, others such as ammonia, hydrazine and methyl alcohol can also cause crack growth. The species that are active may be identified by their chemical structure. Strong nucleophilic and electrophilic reaction sites on adjacent atoms of the reactant and a transferable hydrogen ion are needed to couple with the strained silicon-oxygen bonds of the glass at the crack tip. Although there are many such compounds, few cause crack growth because of stearic constraints. The active portion of the corroding species must be small enough to penetrate to the reaction site to promote bond breakage. Thus water and ammonia are strong crack growth agents, methanol and other normal alcohols are weaker crack growth agents, and aniline does not cause crack growth at all because it

is too large to penetrate to the crack tip. Strong adsorption of species from solution may also poison the reaction site. This is believed to happen with lithium hydroxide in highly concentrated electrolytes. Adsorption of lithium complexes at the reaction site essentially blocks the crack tip and prevents water from penetrating to the reaction site, thus slowing the reaction rate. The importance of stearic hinderance to crack growth is currently an active area of research.

The third effect of crack geometry on the reaction rate is the leverage the crack applies to any forces that arise from physical or chemical processes that occur during crack growth. Normally only the external loads are considered as driving the crack, however, other forces are also important in establishing crack growth behavior. The close proximity of the surfaces result in long range surface forces that either wedge the surfaces apart or draw them together depending on the magnitude and sign of these forces. Ion exchange near the crack tip may set up a volume of stressed material around the crack tip that also influences crack growth, and finally, if charges are created or destroyed during the bond breaking reaction, electrostriction becomes an important factor in controlling crack growth. The effect of these forces vis-a-vis crack motion are discussed with specific examples given for each of these processes. In order to estimate the effect of forces on crack growth, it is necessary to express these forces in terms of classical reaction rate theory, for which the parameter relevant to stress is the activation volume for the chemical reaction. It is shown that the activation volume for crack growth can be obtained directly from the slope of the crack growth curve.

TRANSFORMATION AND DISPERSION TOUGHENING

J. C. M. LI
Department of Mechanical Engineering, University of Rochester,
Rochester, NY 14627 U.S.A

INTRODUCTION

Transformation toughening is the increase of toughness due to a phase change induced by the crack tip stress field. It is different from dispersion toughening in which a crack propagates in a matrix distributed with existing inclusions. In the latter case, no new inclusions are formed and the existing inclusions do not disappear when the crack passes by. To understand transformation toughening by examining the effect of an inclusion on the stress intensity factor is obviously incomplete. A part of the stress intensity factor must be used for the transformation. Both toughening mechanisms are discussed here.

TRANSFORMATION TOUGHENING

As an example consider that the new phase has a dilatational expansion of the old phase. Under the mode I crack tip stress field, a volume of the material within which the hydrostatic stress exceeds a certain critical value will transform into the new phase. However as shown by McMeeking and Evans [1] and by Budiansky, et al. [2] the crack tip stress intensity factor is not affected by this transformation. Yet, like plastic flow, the transformation must relax the crack tip stresses. Also like plastic flow, the surface energy in the Giffith relation should include a term for the work of transformation. To see the relation between this effect and the stress intensity factor, Li and Sanday [3] used a dislocation model and found that the crack must enter the transformation zone before it can cause continuous transformation or maintain steady state propagation. As a result, the transformation zone does not coincide with the zone of critical hydrostatic stress. Then the stress intensity factor is given by

$$K = \sqrt{Ka^2 - \frac{2\mu}{1-\nu}\frac{\Delta w}{\Delta l}} \qquad (1)$$

where Ka is the applied stress intensity factor, μ is shear modulus, ν is Poisson ratio and $\Delta w/\Delta l$ is the work of transformation per unit length of crack extension.

DISPERSION TOUGHENING

The foregoing work of transformation is not required in dispersion toughening in which the crack propagates through the stress field of dispersed inclusions. Consider for example a square lattice of cylindrical inclusions of dilational misfit e^T (positive if the inclusion is bigger than the hole it occupies) and lattice spacing λ. Along a midplane, the tensile stress [4] is

$$\sigma = - \frac{Ee^T a^2 \pi^2}{3\lambda^2(1-2\nu)} \sum_{n=-\infty}^{\infty} \operatorname{sech}^2 \left(\frac{x}{\lambda} + n\right)\pi \qquad (2)$$

where a is the radius of the cylinder and E is Young's modulus. Eq. (2) can be appoximated by a sinusoidal function (with image stress):

$$\sigma = \sigma_o \cos (2\pi x/\lambda) \qquad (3)$$

where

$$\sigma_o = 0.35\pi \, E \, e^T V_f/3(1-2V) \qquad (4)$$

with V_f $(=\pi a^2/\lambda^2)$ being the volume fraction of inclusions.

In this midplane let a finite crack of length 2l appear at the origin, the effect on the crack tip stress intensity factor is found to be

$$\Delta K = K - K_a = 0.318 \, \sigma_o \sqrt{\pi\lambda} \cos \left(\frac{2\pi l}{\lambda} - \frac{\pi}{4} \right) . \qquad (5)$$

It is seen that the maximum ΔK is independent of crack length. It increases with the volume fraction of inclusions and also the square root of inclusion spacing. Since the effect is more important for small cracks than large cracks, dispersion toughening is more effective for crack nucleation than crack growth.

REFERENCES

1. R. M. McMeeking and A. G. Evans, J. Am. Ceram. Soc. 65, 242-246 (1982).
2. B. Budiansky, J. M. Hutchinson and J. C. Lambropoulos, Int. J. Solids Structures 19, 337-355 (1983).
3. J. C. M. Li and S. C. Sanday, Scripta Met.
4. Idem, Acta Met.

TEM STUDIES ON THE FORMATION OF MICROCRACKS IN ZIRCONIA-CONTAINING CERAMICS

M. RÜHLE
Max-Planck-Institut für Metallforschung, Institut für Werkstoffwissenschaften, Seestrasse 92, 7000 Stuttgart 1, West-Germany.

INTRODUCTION

The tetragonal (t) to monoclinic (m) martensitic transformation of confined zirconia particles (diameter $\leq 2\mu m$) embedded in a ceramic matrix can be utilized for toughening ceramics (Evans and Heuer /1/, Claussen et al. /2/). The concentration of t-ZrO_2 particles or precipitates is usually $\leq$20vol.%. The M_s temperature of bulk ZrO_2 is ~1200K, whereas M_s is substantially less for confined particles. For example, M_s is below room temperature for facetted t-ZrO_2 particles embedded in an Al_2O_3 matrix, if the diameter is $\leq 0.6\mu m$ (Heuer et al. /3/). The transformation of confined particles can be induced by the stresses in front of a crack tip ("stress-induced transformation"), and the volume and shape change connected with the t→m transformation alters the stress distribution at the crack tip; this hinders the crack from further propagation (McMeeking and Evans /4/, Budiansky et al. /5/). In this paper, we report the transformation of confined t-ZrO_2 particles during crack propagation induced by *in situ* straining experiments. Special attention will be put on microcrack formation. It is expected that microcracks form when a certain stress level is reached in the environment of transformed m-ZrO_2 inclusions. The formation of radial microcracks should also lead to an increase in toughness (Evans /6/, Evans and Cannon /7/, Hutchinson /8/).

EXPERIMENTAL DETAILS

Specimens of Al_2O_3-ZrO_2 dispersion ceramics (zirconia-toughened alumina or ZTA) were studied. The specimens contained 15 vol.% ZrO_2. The amount of t-ZrO_2 depends on the processing conditions and it varied between 23% and 86% t-ZrO_2. The sizes and size distribution of the Al_2O_3 grains as well as of the t-ZrO_2 particles were determined by standard techniques of quantitative stereology. The mean diameter of the Al_2O_3 matrix grains was $d_{mat}=0.25\mu m$ and of the t-ZrO_2 varied between $0.21\mu m$ and $0.45\mu m$, for the specimen containing 23% t-ZrO_2 and 86% t-ZrO_2, respectively. The diameter of the intercrystalline ZrO_2 inclusions ranged from 0.06 to $2\mu m$. All ZrO_2 inclusions which were larger than ~$0.6\mu m$ were monoclinic at room temperature. The m-ZrO_2 were twinned. No tangential microcracks could be observed if "domains of closure" /9/ were formed at the end of the twins.

Specimens suitable for straining experiments and with a cross-section of $3 \times 5 mm^2$ were mechanically polished carefully to a thickness of 50-$80\mu m$. The specimens were ion-thinned using a special technique so that 2 slightly elongated holes were formed. The specimen was transparent for 1 MeV electrons nearly in the entire region of the ridge between the two holes. The specimens were glued into deformation

holders which were inserted in the deformation stage and subsequently deformed in double tilting straining stage. The relative velocity of the specimen holders against one other was variable - between $1x10^{-6}$ and $1x10^{-4}$ mm/s, which results in a straining rate of $\sim 4x10^{-7}$ s^{-1} to $\sim 4x10^{-5}$ s^{-1}. Specimens were usually strained with a constant straining rate of $3x10^{-6}$ s^{-1}. The stresses applied to the specimen could not be measured. TEM specimens were also prepared out of the bulk from areas close to crack surfaces. The depth of the specimen from the crack surface could be adjusted by a special thinning procedure.

OBSERVATIONS

Micrographs of the unstrained specimens were taken of the entire transparent part of the ridge. No m-ZrO_2 particles or precipitates could be observed in either type of specimen. The beginning of elastic deformation of the specimens could be observed by the movement of bend contours in different grains. A crack started to propagate from the regions of highest stress concentrations at the thinnest area of one hole. The t-ZrO_2 particles in the specimen containing 86% t-ZrO_2 transformed in front of the crack tip, the distance of the transforming particles from the crack tip depending on the size of the particle, the depth of the particle inside the foil and on the foil thickness. The transformed m-ZrO_2 particles could easily be identified by the formation of mechanical twins inside the particles. Only few t-ZrO_2 particles transformed in front of a propagating crack in a thin foil. Also only few microcracks formed after crack propagation could be observed.

Therefore, TEM foils were prepared out of abulk specimen. The distance of the specimen from the cracked surface was either 0.5, 3 or 5μm. A high density of microcracks could be observed. The density of microcracks could be determined quantitatively.

INTERPRETATION AND DISCUSSION

The *in situ* straining experiments show that t-ZrO_2 particles or precipitates indeed transform in front of a crack tip and allow determination of the width of the transformation zone. However, caution is mandated in applying the results obtained in a thin foil to bulk ceramics. At best, a thin foil can be described by a plane stress situation, whereas the transformation zone in the bulk can best be represented by plane strain. *Microcracks* around preexisting m-ZrO_2 particles formed only if the m-ZrO_2 particles were completely confined in the surrounding Al_2O_3. The nucleation of radial microcracks requires a rather high stress level at the site of the nucleation. The critical stress level can be calculated from the experiments.

REFERENCES

1. A.G. Evans and A.H. Heuer, J. Am. Ceram. Soc. 63, 241 (1980).
2. N. Claussen, M. Rühle, and A.H. Heuer (edt.), "Proc. 2nd Int. Conf. on the Science and Technology of Zirconia", Adv. in Ceramics 11 (1984).

3. A.H. Heuer, N. Claussen, W.M. Kriven, and M. Rühle, J. Am. Ceram. Soc. 64, 642 (1982).
4. R.M. McMeeking and A.G. Evans, J. Am. Ceram. Soc. 65, 242 (1982).
5. B. Budiansky, J.M. Hutchinson, and J.C. Lambropoulos, Int. J. Solids Struct. 19, 337 (1983).
6. A.G. Evans, in /2/, p. 193.
7. A.G. Evans and R. Cannon, Acta met., in the press.
8. J.M. Hutchinson, to be published.
9. E. Bischoff and M. Rühle, J. Am. Ceram. Soc. 66, 123 (1983).

ON THE APPARENT TOUGHENING AT HIGH TEMPERATURES EXHIBITED BY CERAMICS CONTAINING AN INTERGRANULAR GLASS PHASE.

D. R. CLARKE
Thomas J. Watson Research Center, IBM, Yorktown Heights, NY 10598

INTRODUCTION.

An intriguing characteristic feature of the strength of ceramics containing an intergranular glass phase, and one not shared by their counterparts without the phase, is that at elevated temperatures there is a temperature regime in which the strength appears to increase with increasing temperature until a temperature is reached when wholescale failure occurs. This behavior has been noted in a number of experiments in the last twenty years, but without supporting microstructural evidence of what the mechanisms of fracture might be. Recent observations by the author indicate that deformation in this regime is accompanied by extensive cavitation, particularly around cracks. Using the concept of a cavitational process zone, a description in terms of materials parameters will be developed for the apparent toughening.

BACKGROUND.

At low temperatures the strength of ceramics is controlled by brittle fracture considerations and is independent of the loading rate. As the temperature of testing is increased the strength is relatively unaffected until the above mentioned regime. Whilst the macroscopic stress-strain curve remains essentially linear examination of the fracture surfaces reveals evidence for localized non-brittle behavior. The flexural strength in this regime is strain-rate dependent and also exhibits a peak in strength as a function of temperature. More recently it has been found that extensive cavitation in the intergranular glass phase occurs (fig. 1), and that the cavitation has a propensity to form in a zone around the crack itself (fig. 2). In fact, in this strain-rate temperature regime the behavior exhibits many of the features characteristic of polymer fracture in cases where crazing is important.

PRESENTATION.

After a description of the observed high temperature fracture behavior, an explanation for the apparent toughening, in terms of the formation of a constrained, cavitational process zone at the propagating crack with accompanying viscous flow of intergranular material, will be presented.

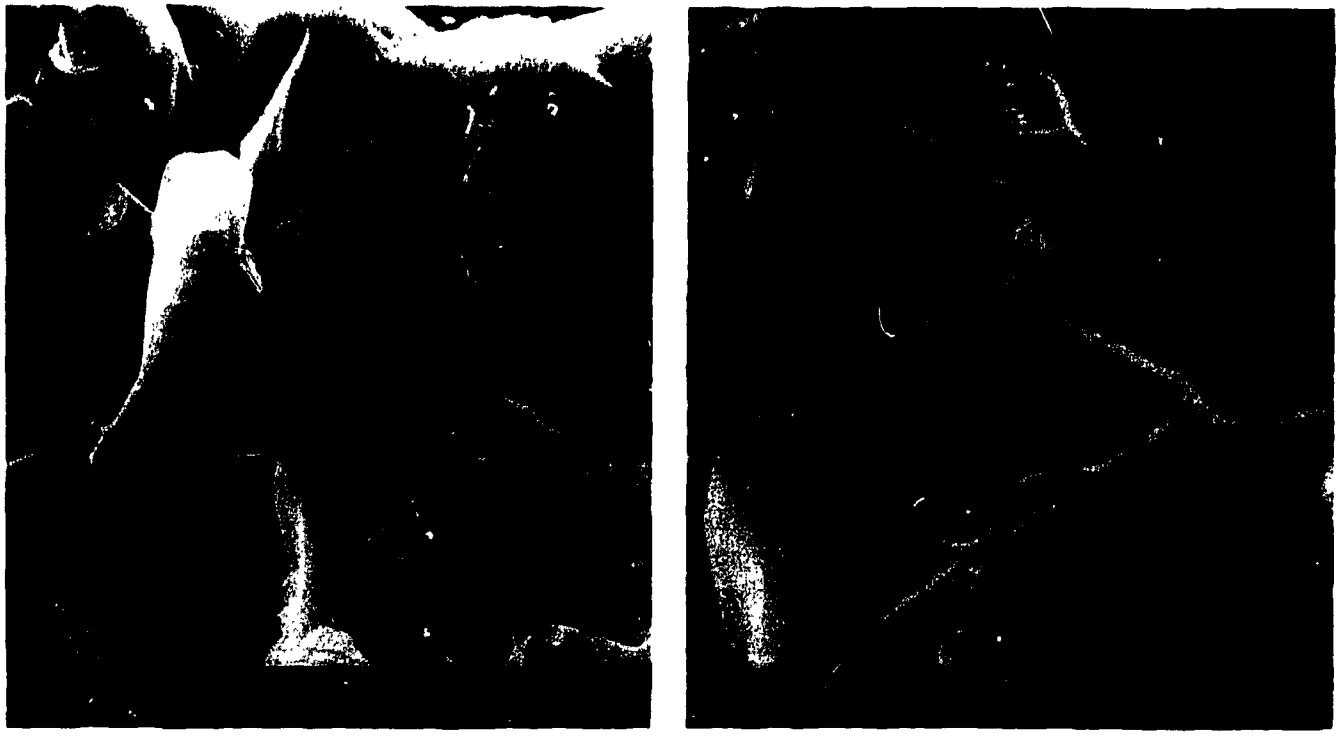

Figure 1. Part of the zone of cavities surrounding the high temperature fracture of a debased alumina.

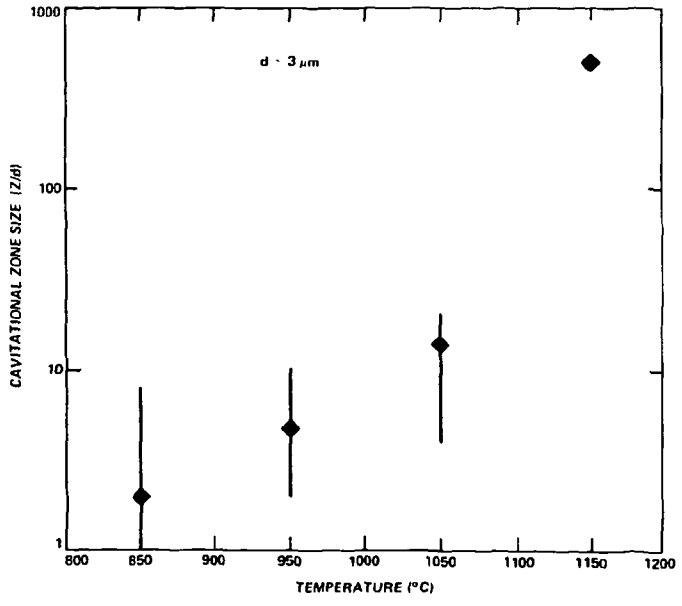

Figure 2. (Left). Size of the cavitated zone (normalized to the alumina grain size) as a function of deformation temperature for the same debased alumina.

THE ROLE OF STERIC HINDRANCE IN STRESS CORROSION FRACTURE OF VITREOUS SILICA*

T. A. MICHALSKE, B. C. BUNKER,
W. L. SMITH, and D. M. HAALAND
Sandia National Laboratories,
Albuquerque, New Mexico

A dissociative chemisorption mechanism has been postulated[1] to describe the bond rupture reactions occurring at strained crack tip bonds during stress corrosion cracking of vitreous silica. The incorporation of this chemical bond rupture model into a kink nucleation and growth model for fracture enables one to correlate experimentally measured fracture rates with the rate of dissociative chemisorption on strained siloxane bonds. To check the validity of this atomistic model for slow crack growth, a comparison has been made between the kinetics of dissociative chemisorption reactions on strained edge-shared silicate tetrahedra and the kinetics of stress corrosion of silica in the presence of chemicals such as water, methanol, and formamide. The strained edge-shared defects were produced by dehydroxylating high surface area silica powder (Cab-O-Sil S-17). The kinetics of reactions between the strained defects and chemicals such as methanol were monitored using Fourier transform infrared spectroscopy (FTIR).

The IR spectra indicate that all chemical species which cause stress corrosion in vitreous silica also participate in dissociative chemisorption reactions on strained surface defects. In addition, the rate of dissociative chemisorption on edge-shared surface defects scales

*This work performed at Sandia National Laboratories supported by the U. S. Department of Energy under contract number DE-AC04-76DP00789.

with the rate of crack propagation in vitreous silica exposed to chemical environments having similar molecular size (e.g., H_2O, NH_3). However, crack growth rates in the presence of larger molecular species (e.g., CH_3OH, CH_3NH_2) are much slower than predicted by the measured surface reaction rate. This result suggests that steric effects due to the atomistically sharp nature of the crack tip contribute strongly to the overall reaction rate by affecting the rate at which molecular species may adsorb at the strain activated crack tip bonds. Since vitreous silica is comprised of cages of linked SiO_4^- tetrahedra, we correlated crack tip steric hindrance effects with measured steric effects obtained for adsorption within zeolite cage structures. We found that zeolite adsorption data can be used to quantitatively predict the crack tip steric hindrance effects measured for environmental molecules ranging in size from water (0.15 nm) to tert-butylamine (0.43 nm).

References

1. T. A. Michalske and B. C. Bunker, J. Appl. Phys. 56(10), 2686-2693 (1984).

MICROMECHANICAL MODELING OF MICROSTRUCTURAL DAMAGE IN CREEPING ALLOYS

A.S. Argon
Massachusetts Institute of Technology, Cambridge, MA 02139

ABSTRACT

Fracture under service conditions at high temperatures in structures undergoing creep deformation is intergranular. Cavities on grain boundaries are produced on interfaces of hard particles during transient sliding of grain boundaries. The growth of grain boundary cavities by a combination of continuum creep and diffusional flow is often constrained by the creep deformation of the surrounding grain matrix. The constrained growth and linking of grain boundary cavities produces isolated cracked grain boundary facets which continue to grow by continuum creep and in the process accelerate overall creep flow. Cracked grain boundary facets are the principal form of creep damage, and their density per unit volume can be taken as the parameter characterizing creep damage. This damage parameter can be incorporated into three dimensional constitutive relations of creep deformation, and these relations can be used in large strain finite element programs to solve complex engineering problems of creeping structures.

All the microstructural mechanics that enter into the above description have been verified in a selection of key experiments on cavitation and crack growth.

NUCLEATION OF INTERGRANULAR CREEP CAVITIES†

M. H. Yoo* and H. Trinkaus**
*Metals and Ceramics Division, Oak Ridge National Laboratory, Oak Ridge, TN 37831; **Kernforschungsanlage Jülich, Institut für Festkörperforschung, D-5170 Jülich, FRG

INTRODUCTION

Creep experiments on metals and alloys at temperatures between 0.4 and 0.7 of the absolute melting point have shown that cavity formation occurs under surprisingly low applied stresses, even down to 10 MPa [1], in striking contrast to simple theoretical predictions [2]. Such a strong tendency for cavity formation under creep conditions has been attributed to (a) the effects of grain boundaries and interfaces [2], enhanced by microscale inhomogeneities and solute segregation [3,4]; and (b) the effect of microscale stress concentrations [4,5,6] on cavity formation.

In this paper, intergranular cavity nucleation under creep-induced microscale stress concentrations is discussed within the framework of a recently developed formal theory of nucleation under time-dependent supersaturation [7]. The spatial and temporal evolution of the stress concentration resulting from grain boundary sliding or slip-grain boundary interaction [8] is modelled by using a linear elasto-diffusion approach [9,10].

RESULTS

The quasi-steady-state analysis shows that significant cavity nucleation is possible only under the condition that the characteristic time for the stress evolution is large compared with the incubation time for nucleation. This condition is satisfied when the spatial range of the stress concentration is large compared with the size of the critical cavity embryo. In this case, it also ensures that, once nucleated, stable clusters will remain stably growing permanently.

The $t^{-1/6}$ type of relaxation characteristics is expected for a suddenly activated slip-interface interaction. Application of the quasi-steady-state condition to this case gives a Hall-Petch type relationship for the stress, σ_c, above which cavitation can occur

$$\sigma_c = (\mu/kT)^{1/6} F_v^{1/3} \gamma_s \ell^{-1/2} \qquad (1)$$

where ℓ is the effective slip length, γ_s is the specific surface free energy, F_v is the geometrical factor accounting for interfacial effects [2], μ is the shear modulus, and kT has the usual meaning.

†Research sponsored by the Division of Materials Sciences, U.S. Department of Energy under Contract No. DE-AC05-84OR21400 with Martin Marietta Energy Systems, Inc.

Integration of the quasi-steady-state nucleation rate over time gives the total cavity number density nucleated during a single stress pulse. If the kinetics of stress and cavity evolutions are controlled by the same diffusion process, they simply scale with each other. In this case, the cavity density yield per stress pulse is independent of the corresponding diffusivity. The average cavity nucleation rate associated with a stochastic sequence of stress pulses will, however, depend on the diffusivity controlling the frequency of the stress pulses, which is expected to increase with strain rate.

Since cavity nucleation can occur only under stress levels far above typical applied stress values, it is controlled by the extreme tail of the probability distribution of the internal stresses. Integration of the quasi-steady-state nucleation over appropriate probability distributions shows that the average nucleation rate depends much less strongly upon the average of a microscopically fluctuating (macroscopically constant) stress than on a microscopically constant stress. This result provides a possible explanation of the so-far unexpected mild stress dependence of intergranular cavitation observed in some creep experiments. If the probability of high stress concentrations is proportional to the strain rate, the overall cavity nucleation rate will appear to be strain-controlled although the individual nucleation event is actually stress-controlled.

SUMMARY

Time-dependent nucleation of intergranular creep cavities is discussed on the basis of a quasi-steady-state classical nucleation model. The critical stress for cavity nucleation is evaluated. An explanation is given for experimentally observed modest stress dependence and apparent strain dependence of cavity formation.

REFERENCES

1. J. H. Schneibel, C. L. White, and M. H. Yoo, Metall. Trans. 16A, 651–660 (1985).
2. R. Raj, Acta Metall. 26, 995–1006 (1978).
3. M. H. Yoo, C. L. White, and H. Trinkaus in: Flow and Fracture at Elevated Temperatures, R. Raj, ed. (ASM, Metals Park, OH 1985) pp. 349–382.
4. H. Trinkaus and M. H. Yoo, Scr. Metall. 18, 1165–1169 (1984).
5. T. J. Chuang, K. I. Kagawa, J. R. Rice, and L. B. Sills, Acta Metall. 27, 265–284 (1979).
6. A. S. Argon, I-W. Chen, and C. W. Lau in: Creep, Fatigue, and Environmental Interactions, R. M. N. Pelloux and N. S. Stoloff, eds. (TMS-AIME, Warrendale, PA 1980) pp. 46–85.
7. H. Trinkaus and M. H. Yoo, Phil. Mag., to be published.
8. M. H. Yoo in: Dislocations and Properties of Real Materials (The Inst. of Metals, London 1985) pp. 241–243.
9. H. Trinkaus, Phys. Stat. Sol. (b) 93, 293–303 (1979).
10. A. G. Evans, J. R. Rice, and J. P. Hirth, J. Amer. Cer. Soc. 63, 386–375 (1980).

INTERGRANULAR CAVITATION AT HIGH TEMPERATURES

HERMANN RIEDEL
Max-Planck-Institut für Eisenforschung, Max-Planck-Str. 1,
4000 Düsseldorf, FRG

When loaded for prolonged times at elevated temperatures, metallic materials often fail by cavity formation on grain boundaries. Despite the expenditure of considerable effort, the nucleation behavior of cavities can not yet be understood quantitatively on the basis of classical nucleation theory combined with local stress concentrations [1]. However, metallographic studies have lead to a useful empirical description of nucleation kinetics [2]. In many cases, the cavity nucleation rate, J^*, is found to be proportional to the strain rate:

$$J^* = \alpha \dot{\varepsilon}. \tag{1}$$

The cavity growth rate, $\dot{R}$, on the other hand, seems to be explicable by diffusive and constrained growth models [3]. This is suggested by a comparison of rupture lifetimes calculated for a constant number of cavities with measured lifetimes of pre-cavitated material (where the nucleation stage is by-passed by an appropriate pre-treatment).

Usually, however, nucleation occurs continously during creep which renders the calculation of the lifetime more complicated. The problem can be formulated in terms of the continuity equation

$$\dot{N} + \partial(N\dot{R})/\partial R = 0 \tag{2}$$

for the cavity size distribution function $N(R,t)$, where R is cavity radius and the dot denotes the time derivative. This partial differential equation is solved for special nucleation and growth kinetics. Failure occurs once the area coverage of grain boundaries with cavities, which follows from the distribution function, reaches a critical value. If diffusive cavity growth is modeled as fully creep constrained (on isolated cavitating grain facets), while nucleation is described by eq. (1), the rupture lifetime is obtained as

$$t_f = 0.52\ (d^2\alpha)^{-1/3}/\dot{\varepsilon}, \tag{3}$$

where d is grain size. The solid line in Fig. 1 represents this result in comparison with measured lifetimes [4] of a CrMo steel. Note that the theoretical curve contains no adjustable parameters. The degree of agreement shown in Fig. 1 is typical for several other materials examined.

The results are also applied to fatigue failure when cavitation is the predominant failure mode. The fatigue lifetimes of copper, nickel and an austenitic steel can then be understood, at least partly, by assuming that cavity growth occurs by unconstrained diffusion and that

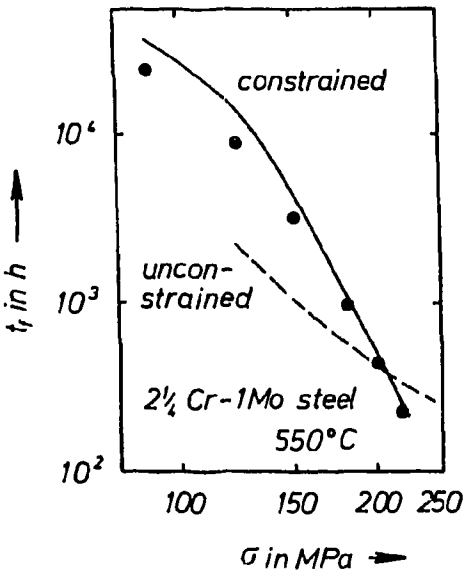

Fig. 1. Rupture lifetimes.

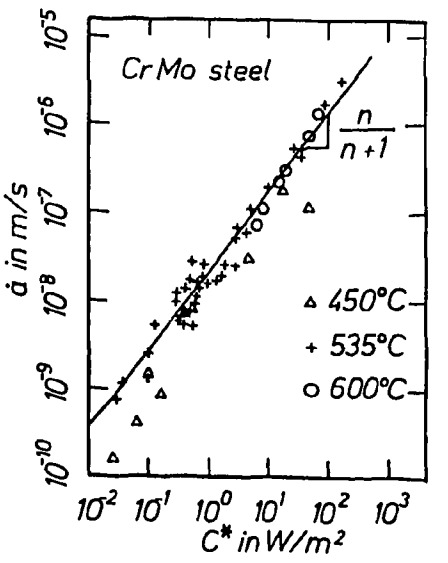

Fig. 2. Creep crack growth rates in 1Cr-1/2Mo steel as a function of the C*-integral.
Solid line: theoretical curve.

the nucleation rate obeys eq. (1).

Creep crack growth in steels generally occurs by grain boundary cavitation ahead of the main crack. By combining the stress fields of a crack with the laws for cavity nucleation and growth, creep crack growth rates can be predicted which are in good agreement with observed rates [5] as demonstrated by Fig. 2.

REFERENCES

1. H. Riedel, Acta Metall. 32 (1984) 313-321.
2. B.F. Dyson, Scripta Metall. 17 (1983) 31-37.
3. J.R. Rice, Acta Metall. 29 (1981) 675-681.
4. N.G. Needham, Report of British Steel Corporation to the Commission of European Communities, Contract No. 7210.MA/802.
5. H. Riedel, in: Flow and Fracture at Elevated Temperatures, R. Raj, Ed., American Society for Metals, Metals Park, Ohio, 1985.

CREEP FRACTURE OF POLYCRYSTALLINE CERAMICS

R. A. PAGE AND J. LANKFORD
Southwest Research Institute, Department of Materials Sciences, 6220 Culebra Road, San Antonio, TX 78284

A detailed characterization of cavity evolution during compressive creep has been accomplished using small-angle neutron scattering [1-3]. Samples of Coors AD-99 alumina (1300°C, 26 MPa, and 1150°C, 220 MPa), which contained a relatively thick continuous grain boundary phase, Lucalox alumina (1600°C, 140 MPa), which contained no continuous grain boundary phase, and Norton NC-203 silicon carbide (1600°C, 600 MPa), which contained a relatively thin continuous grain boundary phase, have been characterized. The neutron scattering measurements, which provide a means of characterizing both the nucleation rates and the growth rates of grain boundary cavities during the early stages of creep, have shown unequivocally that cavity nucleation does occur and have also identified some very significant differences in the cavity nucleation and growth phenomena of these three ceramic systems.

In both aluminas cavity nucleation occurred throughout creep. The nucleation rate in Lucalox alumina was independent of time, while the nucleation rates in AD-99 alumina were proportional to $t^{-0.69}$ and $t^{-0.81}$ at 1300°C and 1150°C, respectively. In contrast to the aluminas, cavity nucleation in the silicon carbide was limited to the very early stages of creep. In all three materials the cavities were closely spaced, with multiple cavities present on each cavitated two grain facet.

Steady-state cavity growth was not observed in any of the systems studied. Rather, transient growth with the individual cavity growth rate proportional to $t^{-0.77}$ and $t^{-0.38}$ was observed in AD-99 alumina at 1150°C and NC-203 silicon carbide at 1600°C, respectively. In AD-99 at 1300°C and Lucalox at 1600°C a zero or near zero growth rate was observed.

For the systems in which significant cavity growth occurred, the neutron scattering results, in accord with viscous hole growth models [4], indicate that nucleation strongly influences subsequent cavity growth morphology. Cavity growth in a crack-like manner occurs only when the cavities are nucleated fairly large distances apart. For more closely spaced cavities, such as observed in each of the materials of this study, a relatively equiaxed growth occurs. The formation of crack-like full facet cavities must then occur through coalescence of multiple equiaxed cavities rather than through the growth of individual cavities.

In terms of creep damage modeling, the implications of the neutron scattering results are threefold. First, cavity nucleation is a critical process; it dominates the early stage of creep in some systems (Lucalox and AD-99 at 1300°C) and it strongly influences subsequent

cavity morphology. Second, the relevance of cavity growth varies; it is of major importance in growth dominated systems, such as NC-203, it is of equal importance with nucleation in "classical" systems, such as AD-99 at 1150°C, in which nucleation and growth occur simultaneously, and it is of only minor importance in nucleation dominated systems, such as Lucalox and AD-99 at 1300°C. Third, cavity coalescence is of critical importance since it is this process, not individual cavity growth, which is responsible for the formation of full facet cavities.

REFERENCES

1. R. A. Page and J. Lankford, J. Am. Cer. Soc. 66, C-146 (1983).
2. R. A. Page, J. Lankford, and S. Spooner, J. Mat. Sci. 19, 3360 (1984).
3. R. A. Page, J. Lankford, and S. Spooner, Acta Met. 32, 1275 (1984).
4. K. S. Chan, J. Lankford, and R. A. Page, Acta Met. 32, 1907 (1984).

THE EFFECTS OF IMPURITIES ON THE HOT TENSILE DUCTILITY OF IRON

E.P. GEORGE and D.P. POPE, Department of Materials Science and Engineering, University of Pennsylvania, 3231 Walnut Street, Philadelphia, PA 19104

INTRODUCTION

Grain boundary particles are very important in the nucleation of creep cavities. Restricting ourselves to ferrous alloys we find that carbides, oxides and sulphides have been suggested as cavity nucleation sites in the past. This study uses slow strain rate (4×10^{-5}/sec), elevated temperature (500-800°C) tensile tests to evaluate the relative importance of these particles in iron and to investigate the effects of phosphorus and cerium on hot ductility.

RESULTS

1) Carbides : High purity Japanese electrolytic iron, supplied by Showa Denko K.K., (SD iron), containing only about 1 ppm S, was used to melt alloys containing carbon levels between 670 and 780 ppm. This ensured that the grain boundaries of these alloys contained carbides (but no sulphides) during the tensile test at 700°C, since the solubility limits of sulphur and carbon are ~ 35 and 200 ppm respectively at 700°C. Furthermore, because of the low level of sulphur in the SD iron, significant amounts of segregated sulphur are also absent from the grain boundaries of these alloys. Under these conditions, all the alloys fail in a completely transcrystalline manner, with ductilities approaching 100% Reduction in Area (RA). No grain boundary cavitation was detected in any of these alloys.

2) Oxides : Grain boundary oxides are evaluated in a similar manner. SD iron was used to melt alloys containing greater than 470 ppm oxygen (c.f. solubility limit of ~ 2 ppm oxygen in iron at 800°C). Again, it is seen that the alloys fail transgranularly, with no evidence of grain boundary cavitation. In slightly more impure forms of iron, containing 20-30 ppm sulphur, cerium can be used to getter the sulphur. When this is done, it is once again seen that oxides do not nucleate cavities. However, when cerium is not used to getter the sulphur in alloys containing 20-30 ppm sulphur, oxides are seen to nucleate cavities in some instances. Ductility depends on the C:S or P:S ratio of the alloys; increasing either increases ductility and decreases the amount of grain boundary fracture.

3) Sulphides : When irons containing greater than the solubility limit of sulphur (~ 35 ppm at 700°C) are tensile tested, it is seen that cavities nucleate profusely on grain boundary sulphides, resulting in com-

pletely intergranular fracture. Ductility may be improved by dissolving/ coarsening the grain boundary sulphides.

CONCLUSIONS

There appears to be a definite heirarchy of grain boundary particles with respect to the ease with which they nucleate cavities in iron. Sulphides are the worst offenders : when present in sufficient numbers on the grain boundaries of iron, cavities nucleate very easily on them. Oxides come next: by themselves they are quite harmless, but in the presence of segregated sulphur they become effective nucleants. Carbides, at least for the experimental conditions used in this study, are completely ineffective as cavity nucleation sites in iron.

INTERGRANULAR FRACTURE DUE TO IMPURITY SEGREGATION IN IRON

H. KIMURA
Research Institute for Iron, Steel and Other Metals,
Tohoku University, Sendai, Japan

INTRODUCTION

High purity iron (the residual resistivity ratio more than 3000) is not susceptible to the intergranular fracture (IGF) even at 4.2K under slow tensile test[1]. Less pure iron (the resistivity ratio less than 2000) shows IGF at 77K by tensile test[2]. IGF is caused by the segregation of impurities at grain boundaries or by the grain boundary precipitates of impurities. The present research has been planned to clarify the effects of selected solutes on IGF of iron and to discuss the mechanism of the effects.

EXPERIMENTAL

In order to reveal the effect of each solute on IGF and the effect of interaction between two kinds of solutes, high purity iron alloys with controlled addition of desired elements should be used. Only limited kinds of elements can be added to the above mentioned high purity iron (the resistivity ratio more than 3000) without contamination. A sufficient amount of alloys for toughness test is difficult to prepare from the high purity iron. Therefore, a high purity electrolytic iron was used as the base metal and high purity mother alloys were used. Alloys were melted under vacuum in a special crucible. These alloys are not as pure as the high purity iron, but considered to be pure enough to discuss the effect of an element (I) on IGF and the effect of the other element (X) on the IGF caused by I. Concentrations of other impurities are much less than those of I and M, and the effect of other impurities on IGF is considered to be constant. Here, phosphorus was chosen as I, and carbon, nickel and molybdenum as X. Charpy impact test, AES and XPS, Mossbauer spectroscopy and tensile or hardness test at low temperatures were performed.

RESULTS AND DISCUSSION

Phosphorus is known to cause IGF in iron. It has been proposed that a phosphorus atom forms a covalent-like bond with surrounding iron atoms and reduces the electron density around the iron atoms. Thus, the bond between iron atoms neighboring the phosphorus atom is weaken and so the cohesion of the grain boundary enriched with phosphorus[3]. XPS of the segregated phosphorus shows that its electronic state is similar to Fe_3P, a covalent compound[4]. Mössbauer spectroscopy shows that dissolved phosphorus atoms reduces the density of s-electrons at iron atoms neighboring the phosphorus[5].

Carbon prevents IGF caused by phosphorus and by other elements.

Carbon and phosphorus compete with each other for the sites at grain boundaries (the site competition); the degree of phosphorus segregation decreases with increasing the carbon segregation[6]. This is one mechanism of the effect of carbon preventing IGF. An experiment, however, clearly shows that the segregation of carbon itself increases the grain boundary cohesion without changing the degree of phosphorus segregation[7]. In this experiment, the aging temperature was chosen so that the degree of carbon segregation was changed but that of phosphorus remained constant. The ductile-brittle transition temperature decreased with increasing the carbon segregation. The effect of carbon preventing IGF has been found regardless the kind of the element causing IGF[8]. These results shows that the segregation of carbon increases the grain boundary cohesion in iron. The mechanism of this effect of carbon is not known as yet.

Nickel is considered to promote the temper embrittlement in low alloy steels. However, nickel does not promote IGF in Fe-P-Ni alloys quenched from the α-phase region. The degree of phosphorus segregation is not affected, and the addition of nickel reduces the tendency of IGF.[9] Nickel is known to cause the solution softening effect, which may be a mechanism of preventing IGF. Interaction between nickel and phosphorus is not very appreciable, hence it is unlikely that nickel reduces the detrimental effect of phosphorus at grain boundaries. Nickel would increase the grain boundary cohesion by itself. This point should be examined further.

Molybdenum also prevents IGF induced by phosphorus without affecting the degree of phosphorus segregation[9]. Molybdenum is known to have an attractive interaction with phosphorus[5]. Mössbauer spectroscopy shows that molybdenum increases the density of s-electrons at iron atoms surrounding it, and that the decrease in the electron density by phosphorus is recovered by the addition of molybdenum[5]. It is likely that molybdenum reduces the detrimental effect of phosphorus at grain boundaries through this interaction. Again, this point needs further investigations.

REFERENCES

1. H. Matsui, S. Moriya, S. Takaki and H. Kimura, Trans. Japan Inst. Metals 19, 163-170 (1978)
2. H. Matsui and H. Kimura, ibid 24, 539-547 (1983)
3. W. Losch, Acta Met. 27, 1885-1892 (1979)
4. S. Suzuki, K. Abiko and H. Kimura, Trans. Iron and Steel Inst. Japan 23, 746-751 (1983)
5. S. Suzuki, R. Hanada and H. Kimura, Unpublished
6. H. Erhart and H. J. Grabke, Scripta Met. 15, 531-534 (1981)
7. S. Suzuki, M. Obata, K. Abiko and H. kimura, Trans. Iron and Steel Inst. Japan 25, 62-68 (1985)
8. A. Kimura and H. Kimura, Trans. Japan Inst. Met. 25, 411-419 (1984)
9. K. Abiko, S. Suzuki, J. Kumagai, Hidetaka Kimura and H. Kimura, Unpublished

INTERFACIAL FORCES AND THE FUNDAMENTAL NATURE OF BRITTLE CRACKS

BRIAN R. LAWN AND DAVID H. ROACH
National Bureau of Standards
Institute for Materials Science and Engineering
Inorganic Materials Division
Gaithersburg, MD 20899

In addition to the covalent and ionic cohesive forces that hold brittle materials together, there are weaker (but longer-ranged) adhesive forces which come into play when new surfaces are created, particularly in the presence of interactive environments: dispersion (van der Waals), electric double layer, solvation and cation-site forces are examples. These weaker forces give rise to so-called "disjoining" pressures, which are of such great importance in colloidal chemistry. It is shown in this presentation that forces of this type are important also in fracture and strength properties of ceramics. They bear on the reversible nature of crack growth (i.e. crack healing), and hence on the existence of a "fatigue limit," i.e. an applied stress level below which propagation ceases. This interrelation between surface closure forces and crack properties is leading to a fundamentally new conception of fracture, whereby the underlying processes of bond rupture at the crack tip operate independently of the adhesive processes behind the tip. Scientifically, the decoupling of the two processes provides impetus for study on crack-tip structures at the atomic level. More importantly, it offers a possible new technique to measure surface forces using fracture. Results of recent crack opening and closing experiments on molecularly smooth mica will be presented in this context.

ATOMISTIC STUDIES OF SEGREGATION, CRACK INITIATION AND CRACK PROPAGATION

JONG K. LEE
Department of Metallurgical Engineering
Michigan Technological University
Houghton, MI 49931

We first discuss equilibrium segregation of substitutional solute atoms at both surface and grain boundaries. The emphasis is placed on the recent Monte Carlo simulations in which (100), (110) and (111) fcc surfaces and $\Sigma = 5$ (310) fcc tilt grain boundaries are studied. The atomic interactions are represented by the Johnson-type potential functions. For the Cu-Ni system, the Cu segregation predicted by the Monte Carlo method is found to be in good agreement with recent experimental data. The Cu segregation significantly decreases the surface free energy of the Cu-Ni alloy at low temperatures. While the concentration profile of the Cu segregation in a Cu-Ni alloy decreases monotonically, the Zn concentration profile in a α-brass shows an oscillatory behavior. In the second part, the embrittling effects of impurity atoms are examined with simulation results in which metal-metal bond weakening due to impurity segregation is modeled. Modeling a Cu-Sb alloy system, the preferred sites for the Sb atoms at a $\Sigma = 5$ (310) tilt grain boundary are first found through a Monte Carlo simulation. Through a bond weakening effect, the boundary atoms are rearranged to form new boundary structural units. When a tensile strain is applied in the direction perpendicular to the grain boundary plane, the weakened metal- metal bonds become the source of microcracks, thus enhancing brittle fracture along the Sb-segregated grain boundary. Lastly, crack propagation along a coherent interface in a two-dimensional bicrystal is discussed. Under a uniaxial-strain loading a crack lying in the interface is found to be stable until the applied strain reaches a critical value. Although the overall nature of the crack is brittle, dislocation nucleation introduces some degree of ductile fracture behavior. Dislocations nucleate first at the soft crystal side of the interface and glide away. As the crack grows, dislocations also nucleate in the hard crystal.

DISLOCATIONAL PILE-UP -- GRAIN BOUNDARY INTERACTION AT ELEVATED TEMPERATURE

ASHER A. RUBINSTEIN
Department of Mechanical Engineering, State University of New York at Stony Brook, Stony Brook, NY 11794-2300

INTRODUCTION

The nucleation and growth of grain boundary voids on the grain boundary facets transverse to the direction of applied load, is one of widely accepted mechanisms of damage development and material failure at high temperature. The diffusive material redistribution is driven by chemical potential gradient; the chemical potential, in turn, is related to a normal stress acting on the grain boundary. Therefore, the nucleation of voids as well as their growth process strongly depend on the stress field along the grain boundary.

The aim of this work is the analysis of certain sources of stress concentration on the grain boundary which leads to time dependent high stress gradients.

Specifically the interaction of a dislocation and dislocational pile-up with the grain boundary at high temperature are studied. Aiming analysis to a short term after load application, transient period, the problem is formulated in terms of boundary value problem for a linear elastic grain (upper half plane $y > 0$) bounded by grain boundary. So grain boundary equation

$$D\sigma''(x) + \dot{\delta}(x) = 0$$

is satisfied on $y = 0$. (Here D is diffusivity coefficient, σ is a normal stress on $y = 0$ (σ_{yy}) and $\delta = 2u_y$ is a grain boundary "thickening").

Single dislocation solution is obtained in closed form for the general case of position and orientation of dislocation. Time dependent stress field and grain boundary "thickening" along $y = 0$ demonstrate the effectiveness of the diffusive process and give quantitative data for estimation of possible grain boundary void nucleation.

The interaction of dislocational pile-up with a grain boundary is studied in order to model a variety of practically possible grain defects which can be approached on the basis of the theory of continuously distributed dislocations. Assuming the existence of the pile-up before the temperature rise, one investigates the time dependent stress field along the grain boundary, stress relaxation parameters and critical time. The diffusive absorption of the dislocations from the pile-up as well as the dislocation redistribution in the pile-up versus time are represented.

RESULTS AND CONCLUSIONS

The results demonstrate that even relatively remote from the grain boundary, dislocations can create significant diffusive material flow along the grain boundary.

The stress field due to dislocational pile-up located at the grain boundary and oriented perpendicular to it has been investigated. The analysis indicated that the grain boundary diffusion leads to partial absorption of the dislocations from the pile-up. This process is relatively fast (in terms of characteristic material time). However, as the final state (asymptotic case for $t \to \infty$) demonstrates, the significant portion of the dislocational pile-up will never be absorbed by diffusive mechanism, since the normal to grain boundary stress is decaying very fast.

As diffusional flow is progressing, the normal stress acting parallel to the grain boundary and directed against the material flux is activated. At the final state, this stress becomes singular (logarithmical singularity) at the base of the pile-up. The only visible mechanism of relaxations of this stress can be the void nucleation.

STRUCTURE-DEPENDENT INTERGRANULAR FRACTURE INDUCED BY LIQUID METAL

TADAO WATANABE
Department of Materials Science, Faculty of Engineering,
Tohoku University, Sendai, Japan

INTRODUCTION

The effects of the type and structure of grain boundaries on liquid metal-induced intergranular fracture and mechanism of the fracture have been studied in detail experimentally with use of bicrystals of zinc and aluminium, and polycrystals of beta brass. The present paper gives an overview of grain boundary structure-dependent intergranular fracture induced by liquid metal, which severely embrittles polycrystals of normally ductile metals and alloys. The electron channelling pattern (ECP) technique was applied to characterize a large number of grain boundaries contained in polycrystals.

RESULTS AND DISCUSSION

Misorientation dependence of fracture stress and strain was determined on zinc bicrystals with $<10\bar{1}0>$tilt or twist boundaries and other types of boundaries. Liquid gallium was coated at a grain boundary on specimen surface.
It was found that the fracture stress is larger for low angle boundaries and high angle boundaries of near $\Sigma 9/56.6°$ coincidence orientation than that for high angle random boundaries, as shown in Fig.1. Those boundaries which have large fracture stress showed large fracture strain.

The anisotropy of fracture was found on $<11\bar{2}0>$tilt zinc bicrystals, depending on whether liquid gallium was coated at the grain boundary on the surface perpendicular or parallel to the rotation axis of the boundary. SEM observations on fracture surfaces have revealed an important role of crystal deformation to this type of intergranular fracture.
A mechanism of liquid metal-induced intergranular fracture is proposed which considers the role of deformation ledge as penetration path of liquid metal at the grain boundary [1].

Liquid gallium-induced fracture processes in beta brass polycrystals were observed optically and by SEM. Grain boundaries contained in test specimens were characterized by ECP technique. An example of the characterization is shown in Fig.2. Low-angle boundaries are denoted by L, coincidence boundaries by Σ and numerals, and random boundaries by R.
It was found that liquid gallium-induced intergranular fracture occurs and propagates preferentially at random boundaries. Low-angle boundaries and coincidence boundaries were found to be strongly resistent to fracture. It was also found that the change in fracture mode from intergranular to trangranular fracture or vise versa occurs depending on the type of grain

boundary existing in front of a propagating crack. When random boundaries are connected to each other, a typical intergranular fracture appears to occur showing more significant embrittlement. Accordingly, high density of random boundaries are considered to lead to embrittlement, while the presence of high densities of low angle boundaries and coincidence boundaries may suppress embrittlement associated with intergranular fracture. The detailed discussion has been given elsewhere [2].

The possibility of development of strong and ductile polycrystals by grain boundary design has been pointed out by the present author [3]. It is expected that an increase in the frequency of special low energy boundaries such as low-angle boundaries and coincidence boundaries will enhance the ductility of polycrystals. Experimental supports for this have been obtained.

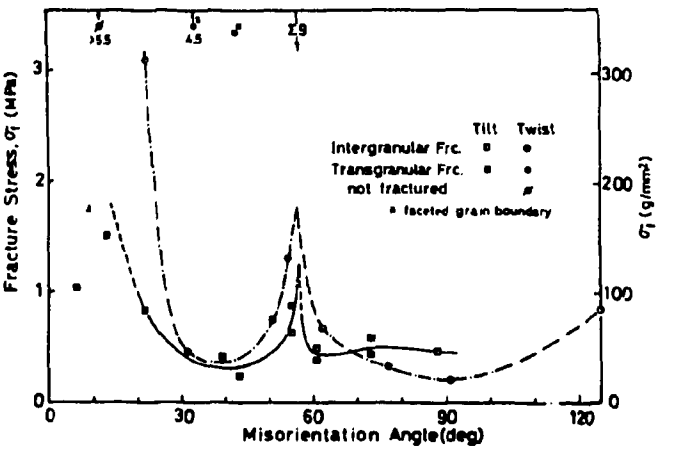

FIG.1. Misorientation dependence of fracture stress for <10$\bar{1}$0>tilt and twist boundaries in zinc bicrystals embrittled by liquid gallium.[1].

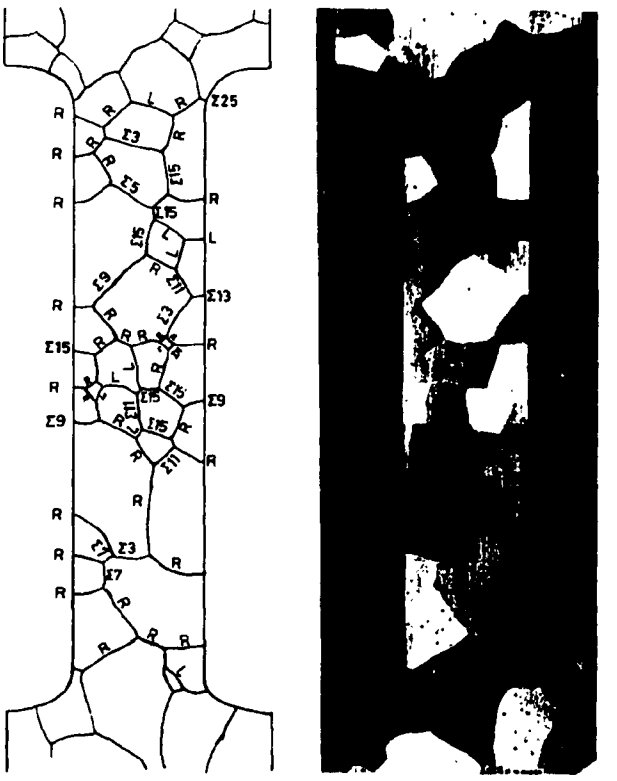

FIG.2. An example of the characterization of grain boundaries in a tensile fracture test specimen of beta brass [2].

REFERENCES

1. T.Watanabe,S.Shima and S. Karashima, Embrittlement by Liquid and Solid Metals, ed.by M.H.Kamdar,(AIME 1984) pp.161-172.
2. T.Watanabe, M.Tanaka and S Karashima, ibid,pp.183-196.
3. T.Watanabe, Res Mechanica, 11, 47-84 (1984).

BENEFICIAL VERSUS HARMFUL GRAIN BOUNDARY SEGREGANTS: BORON AND SULFUR IN Ni_3Al

C. L. White and C. T. Liu
Metals and Ceramics Division
Oak Ridge National Laboratory
Oak Ridge, TN 37831

Trace element segregation at grain boundaries has historically been associated with embrittlement of those boundaries [1]. Recent observations that certain segregating elements actually improve grain boundary cohesion have, therefore, led to speculation concerning the factors that may cause one segregant to strengthen grain boundaries and another to weaken them. Solute interactions with grain boundaries must ultimately reflect the chemical interaction of the solute with the solvent species in the host lattice, as well as in the structure of the grain boundary. These interactions may manifest themselves as modifications in the boundary structure, or as changes in the strength of interatomic bonding at the boundary, or both. There do not yet seem to be any direct observations comparing the effects of beneficial and harmful segregants on grain boundary structure, but some limited results relevant to the effects of such segregants on grain boundary strength are summarized here.

Perhaps the best characterized beneficial grain boundary segregant is boron in substoichiometric Ni_3Al. The intermetallic compound Ni_3Al normally fails intergranularly with practically zero ductility. Although the weakness of grain boundaries in Ni_3Al can be further aggravated by certain segregating impurities such as sulfur [2], removal of impurities does not ductilize Ni_3Al, and the compound appears to be intrinsically brittle. Aoki and Izumi [3], and later Liu and coworkers [4], found that small additions of boron to Ni_3Al dramatically improve its ductility [Fig. 1], and inhibits intergranular failure. Liu and coworkers found that the boron had its maximum effect when the alloy was slightly aluminum poor (24 at.% Al), and by careful control of stoichiometry and thermomechanical treatment they achieved tensile elongations greater than 50%. Auger electron spectroscopy (AES) studies of intergranular and partially intergranular fracture surfaces indicated that grain boundaries in the boron doped alloys were enriched in boron. This supported the conclusion that grain boundaries in Ni_3Al are intrinsically brittle, and that boron segregation strengthens them.

A clue to the contrasting effects of boron and sulfur was discovered when both Liu and coworkers [4] and White and coworkers [5] found that boron, unlike sulfur and many other embrittling segregants, does not segregate strongly to free surfaces. Boron's unusual segregation behavior in Ni_3Al, and its strengthening effect on grain boundaries are in substantial agreement with a thermodynamic analysis of effects of segregation on grain boundary cohesion by Rice [6]. These observations and their relevance to the general problems of grain boundary failure are discussed.

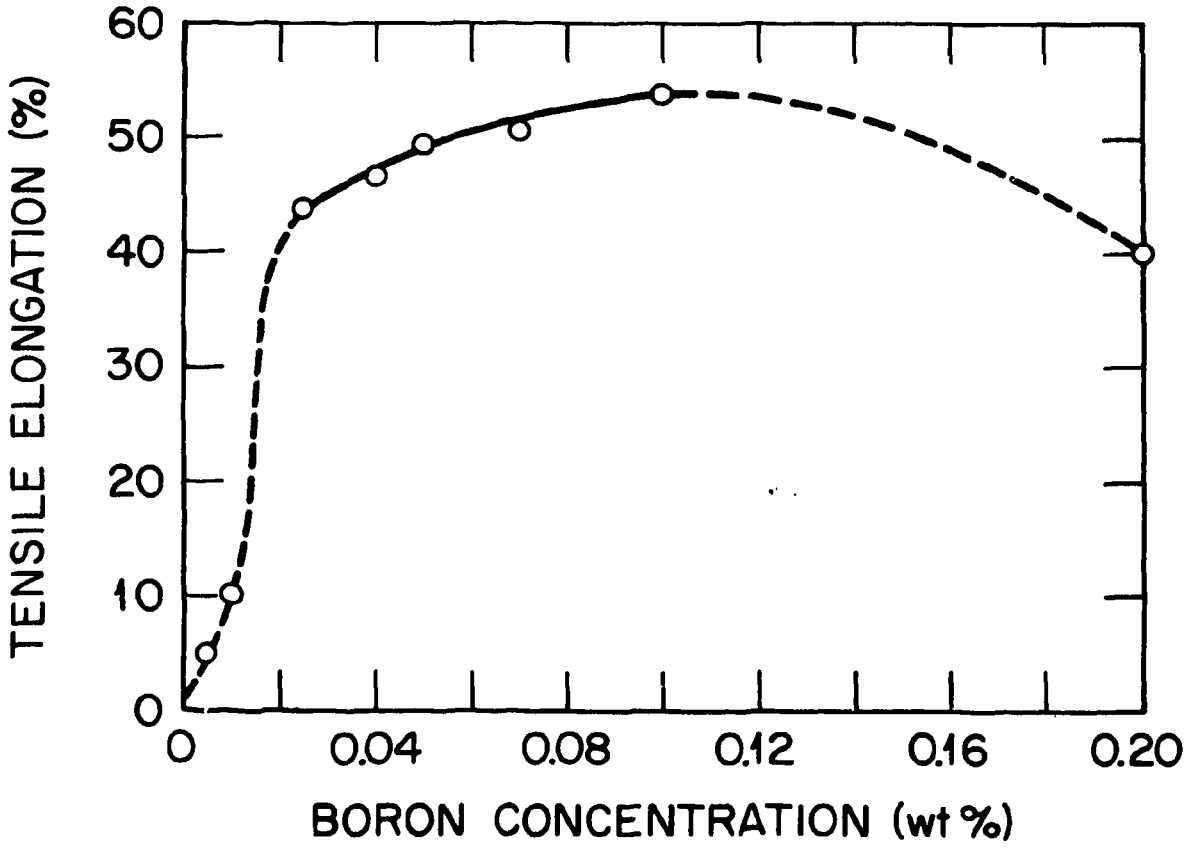

Fig. 1. Plot of tensile elongation versus boron content in Ni_3Al (24 at.% Al), after Liu et al.[4]

REFERENCES

1. E.D. Hondros and D. McLean in: Grain Boundary Structure and Properties, G.A. Chadwick and D.A. Smith, eds. (Academic Press, New York 1976) pp. 363–81.
2. C.L. White and D.F. Stein, Met. Trans., 22, 13 (1978).
3. K. Aoki and O. Izumi, Nippon Kinzoku Gakkaishi, 41, 170 (1977).
4. C.T. Liu, C.L. White, and J.A. Horton, Acta. Met., 33, 213 (1985).
5. C.L. White, R.A. Padgett, C.T. Liu, and S.M. Yalisov, Scripta Met., 18 1417 (1984).
6. J.R. Rice in: Effect of Hydrogen on Behavior of Materials, A.W. Thompson and I.M. Bernstein, eds. (AIME, New York 1976) pp. 455–66.

MACROCRACK-MICRODEFECT INTERACTION

ASHER A. RUBINSTEIN
Department of Mechanical Engineering, State University of New York at Stony Brook, Stony Brook, NY 11794-2300

ABSTRACT

Elastic interactions (in terms of the stress intensity factor variation) of the macrocrack (represented as semi-infinite crack) with microdefects such as finite size, arbitrarily positioned crack, circular hole or inclusion are considered. Solution for the problem of the interaction with dilational inclusion is given as well. The influence of the crack tip geometry on surrounding stress field is studied by analyzing the case of crack-hole coalescence.

Problems are considered in terms of complex stress potentials for linear elasticity and formulated as a singular integral equation on the semi-infinite interval. A stable numerical technique is developed for solution of such equations. In a special case, in order to evaluate the accuracy of the numerical procedure, the results are compared with analytically obtained ones and found to be in excellent agreement.

RELATIVISTIC DISLOCATION SHIELDING OF CRACKS

I.-H. Lin and R. Thomson
National Bureau of Standards
Boulder, CO and Gaithersburg, MD, USA

In other work reported at this conference,[1] we have analyzed the basic elastic theory of dislocations and cracks moving near sonic speeds. This analysis can be applied to the classic case of a modified BCS crack with shielding dislocations on the cleavage plane, but with a dislocation free zone (DFZ)[2,3,4]. For the analysis, we assume mode III, with a crack situated at the origin of a uniformly moving coordinate system with velocity v, and a set of N dislocations in a "plastic zone" distributed from position w to R relative to this same moving coordinate system. Thus, w is the size of the DFZ and R is the limit of the plastic zone. The dislocations will be assumed to be subject to a constant friction stress, $s_f(v)$, which may be velocity dependent.

Using expressions for the forces and stresses derived for the moving singularities, we obtain the basic equation for the force on a dislocation located at x

$$s_f(v) = \frac{K\sqrt{1-\beta}}{\sqrt{2\pi x}} + \sum_j{}' \frac{\mu b}{2\pi}\sqrt{\frac{x_j}{x}}\,\frac{\gamma}{x-x_j}$$

$$K(v) = K\sqrt{1-\beta} \quad ; \quad \beta=v/c \quad ; \quad \gamma=\sqrt{1-\beta^2} \qquad (1)$$

b is the Burgers vector, μ is the shear modulus, and K is the velocity independent externally applied stress intensity factor. K(v) is the velocity dependent stress intensity factor. The prime on the summation means that the sum is not taken over the reference point at x. We have neglected the image terms in this equation for reasons given in Ref. 4. With the definition of the local stress intensity given by

$$k(v) = K(v) - K_d(v)$$

$$K_d(v) = \sum_j^N \frac{\mu b\gamma}{\sqrt{2\pi x_j}}\,\frac{1}{\sqrt{1-\beta}} \qquad (2)$$

the total force on the crack-dislocation distribution is given by

$$K^2 = 2\mu A(v) \left(\sum_j^N s_f(v)\, b_j + 2\gamma_s\right)$$

$$A(v) = \sqrt{(1+\beta)/(1-\beta)} \qquad (3)$$

We have used the Griffith condition at the crack tip,

$$k_c^2(v) = 4\mu\gamma_s\gamma \qquad (4)$$

Standard methods for solving the continuum approximation of (1) give in first order in the parameter w/R[4]

$$w \simeq \frac{2\pi\mu\gamma\gamma_s}{s_f(v)(\ell n\ 8R/w)^2} \quad ; \quad R = \frac{\pi K^2(1-\beta)}{8 s_f^2(v)} \qquad (5)$$

Equations (3)-(5) can now be combined to yield toughness relations for the dynamic crack system, but to obtain useful results, the rate dependence of s_f and of N must be known. Various forms of constitutive relations will be discussed. One simple such relation is a work hardening relation connecting s_f and N,

$$s_f = s_y\, (Nb/B)^{1/m} \qquad (6)$$

Then

$$K^2 \sim \frac{2\mu AB}{s_y^m} \left[\frac{2\pi\mu\gamma\gamma_s}{w\ell n^2(8R/w)}\right]^{\frac{m+1}{2}} \qquad (7)$$

REFERENCES

1. See Dynamic Cleavage in Ductile Materials, I.-H. Lin and R. Thomson, this volume.
2. B.A. Bilby, A.H. Cottrell, and K.H. Swindon, Proc. Roy. Soc., A272, 304 (1963)
3. S. Chang and S.M. Ohr, J. Appl. Phys., 52 7174 (1981)
4. J. Weertman, I.-H. Lin and R. Thomson, Acta Met., 31 473 (1983).

THE SIZE EFFECT OF CRACK ON MODE III PLASTIC DEFORMATION

SANBOH LEE AND SHAM TSONG SHIUE
Department of Materials Science and Engineering,
National Tsing Hua University, Hsinchu, Taiwan, R.O.C.

ABSTRACT

The interaction between a finite crack and pile-up screw dislocations has been studied by computer simulation. The crack length plays an important role in determining the sizes of both the dislocation-free zone and the plastic zone. If the crack length is shorter than a critical length, there will be no equilibrium positions for emitted dislocations. A crack as large as ten times of critical crack length is large enough to be considered as a semi-infinite crack.

INTRODUCTION

The dislocation emitted from the crack tip were observed recently by in-situ electron microscopic experiments [1-5]. Some experiments [2] found the dislocation-free zone, however sometimes it was not observed [4-6]. Dai and Li [7] found that the existence of the free zone is due to the presence of a barrier at the crack tip for the emission of dislocations as well as the image forces exerted on the dislocations by the crack. They considered that the crack length is much larger than the size of the plastic zone and hence the crack size was not observed.

In the present work, the effect of crack size on the mode III plastic zone behavior is studied. The surface crack, double-tip crack and single-tip crack inside the material are included. The effects of crack size on the plastic and dislocation-free zone are also discussed.

ANALYSIS

Firstly, we consider the finite surface crack, let it be subjected to an applied stress σ (mode III) and emit n screw dislocations. The dislocations with the same Burgers vector b_s are located at X_i (i=1,2,...,n). The shear stress τ_i at the ith dislocation and stress intensity factor at the crack tip K are [8]

$$\tau_i = \sigma \frac{X_i}{\sqrt{X_i^2-L^2}} - \frac{\mu b_s}{2\pi}\left[\frac{X_i^2+L^2}{2X_i(X_i^2-L^2)} + \sum_{\substack{j=1\\ j\neq i}}^{n} \frac{\sqrt{X_j^2-L^2}}{\sqrt{X_i^2-L^2}} \frac{2X_i}{(X_j^2-X_i^2)}\right] \quad (1)$$

$$K = \sigma\sqrt{\frac{L}{2}} - \frac{\mu b_s}{2} \sum_{i=1}^{n} \frac{\sqrt{2L}}{\sqrt{X_i^2-L^2}} \quad (2)$$

In static equilibrium, K and each τ_i are equal to the barrier K_D (or stress intensity factor to generate dislocations) at the crack tip and lattice friction τ. Thus if K, τ and L are known, the (n+1) variables X_i (i = 1, 2,..., n), and σ can be solved from the (n+1) nonlinear equations by the iterative technique.

For the double-tip crack inside the material, one tip of the crack emits a positive screw dislocation and the other tip does the negative one because of the nature of geometry. This kind of problem can be solved by using the dislocation modeling [8] and the result is the same as that of surface crack. If the left-hand side tip is blunt, so that the dislocation can only be mitted from the right-hand side tip of the crack, τ_i and K become [9]

$$\tau_i = \sigma \frac{X_i}{\sqrt{X_i^2-L^2}} - \frac{\mu b_s}{2\pi} \left[\frac{X_i}{X_i^2-L^2} + \sum_{\substack{j=1 \\ j\neq i}}^{n} \frac{\sqrt{X_j^2-L^2}}{\sqrt{X_i^2-L^2}} \frac{1}{X_j-X_i} \right] \tag{3}$$

$$K = \sigma\sqrt{\frac{L}{2}} - \frac{\mu b_s}{2\pi} \sum_{i=1}^{n} \frac{\sqrt{X_i+L}}{\sqrt{2L(X_i-L)}} \tag{4}$$

RESULTS AND DISCUSSION

The relation between the space (X_n-L) and crack length L is shown in fig. 1. For each n, one finds that the crack length L exists a minimum value L_n-1. Below this value, the maximum number of dislocations pile-up in the vicinity of crack tip would reduce to n-1. It is interesting to see the curve n=1 in fig. 1. When the crack length is 1800 b_S, the distance (X_n-L) become infinity, which can be argued from eqs (2) or (4). The value 1800 is obtained from the following equation,

$$L = 2\,(K/\tau)^2 \,. \tag{5}$$

Because K and τ are constants depending on the materials, the L_0 in eq (5) is also a constant depending on the material. It is called the critical length. For the case of crack size shorter than the value L_0, the crack tip emits a dislocation if the stress intensity factor can overcome the barrier at the crack tip. But the movement of this dislocation will not stop until reaching infinity.

The region covered by pile-up dislocations is called plastic zone size. It is found that the plastic zone size increases with the barrier K at the crack tip, but decreases with increasing of frictional force τ.

The dislocation-free zone factor F is defined as the ratio of (X_1-L) to (X_2-X_1), where F is larger than one, the free zone appears in the vicinity of the crack tip, otherwise no free zone exists. The line F=1 in determining the existence of the free zone with different crack

length L is shown in fig. 2. The parameters L_d and L_s indicate the crack lengths of double-tip (or surface crack) and single-tip crack inside the material, respectively. The line goes lower when the crack length becomes longer. When the crack length is beyond the ten times of critical crack length L_0, it can be considered as a semi-infinite crack [7]. The existance of the free zone becomes more difficult with lowering of barrier K at the crack tip, increasing of frictional force τ, and shortening of the crack size.

In conclusion, the phenomena of dislocations emitted from the above three types of cracks are significantly different when the crack size is close to the critical length but show difference if crack length is long enough. When crack length is as long as ten times of critical length, thse three cases will reduce to that of the semi-infinite cack.

REFERENCES

1. S. Kobayashi and S. M. Ohr, in 37th Ann. Proc. Electron Microscopy Soc. Amer. San Antonio, Texas, 1979 (Ed. by G. W. Bailey) pp. 424-425.
2. S. Kobayashi and S. M. Ohr, Phil. Mag. A42, 763-772 (1980).
3. S. Kobayashi and S. M. Ohr, Scripta Met. 15, 343-348 (1981).
4. S. M. Ohr and J. Narayan, Phil. Mag. A41, 81-89 (1980).
5. J. Narayan and S. M. Ohr, Ninth Int. Congress on Electron Microscopy, Toronto, (1978), pp. 508-511.
6. B. S. Majumdar and S. J. Burns, Scripta Met, 14, 653-656 (1980).
7. S. H. Dai and J. C. M. Li, Scripta Met. 16, 183-188 (1982).
8. S. Lee, accepted by Engineering Fracture Mechanics.
9. N. Louat, First Inter. Conf. On Fracture, Sendi, Vol I, p. 117, (1965).

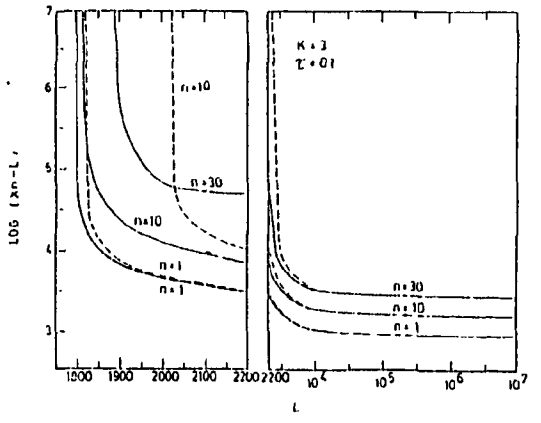

Fig. 1 The curves of (X_n-L) versus L with different n values. The units of length, K and τ are b_s, $\mu\sqrt{b_s}/2\pi$ and $\mu/2\pi$, respectively.

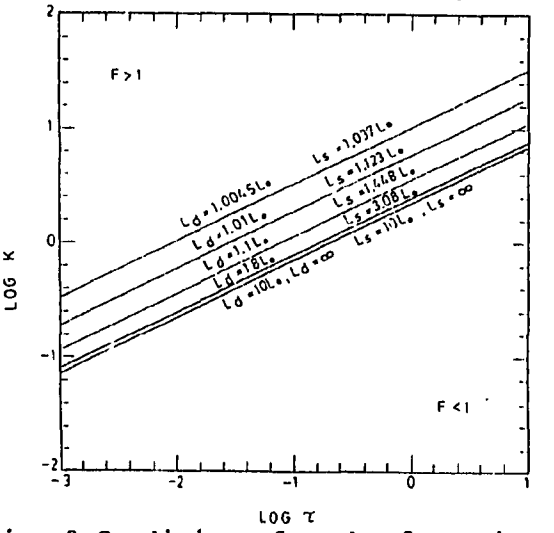

Fig. 2 Conditions for the formation of a dislocation-free zone with different L_d (L_s) value in the K,τ diagram, the units of length, K and τ are the same as fig. 1.

ELASTIC SOLUTION OF AN EDGE DISLOCATION NEAR A WEDGE CRACK

S.-J. CHANG*, S. M. OHR*, AND R. THOMSON**
*Oak Ridge National Laboratory,+ Oak Ridge, Tennessee 37831
**National Bureau of Standards, Gaithersburg, MD 20899

Dislocation pileup along an inclined direction from the tip of a sharp or wedge crack has been observed in metals during tensile deformation in an electron microscope [1]. The dislocations are primarily of edge type when mode I tensile load is applied. In the present work, we have examined the elasticity problem of an edge dislocation near a wedge crack by applying the method of complex variables. The problem of an edge dislocation near a wedge crack of an arbitrary wedge angle can be represented by an integral equation. For a semi-infinite crack, a simple analytical solution can be found.

In order to obtain a solution [2, 3], the wedge plane z is transformed to a half-plane w by

$$z = g(w)$$

where $g(w) = w^p$ $(1 < p < 2)$. Since p is in general not an integer, the analytical continuation of g(w) induces a discontinuous displacement [D] in the w-plane and its magnitude along the real axis is given by

$$2\mu [D] = \kappa[\bar{\Phi}] - \frac{g}{g'}[\Phi'] - [\Psi],$$

where Φ and Ψ are the stress functions. A fictitious distribution of dislocations f(u) is assumed along the real axis of the w-plane in order to remove the discontinuous displacement [D]. The resulting integral equation for f(u) is

$$\int_0^\infty [D_b(u, u')]\, b\, f(u')\, du' = -[D(u)].$$

In this equation, $[D_b]$ is the discontinuous displacement at u along v = 0 due to the presence of a dislocation of unit Burgers vector at u'. In order to obtain the solution for an edge dislocation near a wedge crack, this integral equation must be solved for f(u). The complete solution is then obtained by superposition.

REFERENCES

1. S. M. Ohr, J. Mater. Sci. Eng. 72, 1 (1985).
2. R. Thomson, Solid State Physics, to be published.
3. S. M. Ohr, S.-J. Chang, and R. Thomson, J. Appl. Phys. 57, 1839 (1985).

+Operated by Martin Marietta Energy Systems, Inc. under contract DE-AC05-840R21400 with the U. S. Department of Energy.

DISLOCATION-FREE ZONE MODEL OF FRACTURE UNDER CYCLIC LOADING

S.-J. CHANG AND S. M. OHR
Oak Ridge National Laboratory,* Oak Ridge, Tennessee 37831

The dislocation-free zone (DFZ) model of fracture [1, 2] has been proposed recently as an extension of the Bilby, Cottrell, and Swinden (BCS) model [3] but containing a DFZ between the crack tip and its plastic zone. It is shown that the presence of the DFZ is closely related to the condition for dislocation emission from the crack tip. In the absence of the DFZ, the crack tip is completely shielded from the applied stress and the local stress intensity factor becomes zero.

In the present work, we have examined the effect of cyclic loading on the size of the DFZ and the distribution of dislocations near the crack tip. It is shown that during reverse loading two distinct equilibrium distributions of dislocations are possible. In one of these distributions a small number of dislocations have returned to the crack tip during unloading. The distribution is very similar to the original distribution that was present before unloading and consists only of positive dislocations in the plastic zone.

The second distribution, which is also in equilibrium with the reduced applied load, is a superposition of the original distribution and a distribution of negative dislocations in the unloaded region. These two distributions give rise to distinctly different local stress intensity factors. The true distribution can be found if we assume that the local stress intensity factor is equal to the critical stress intensity factor for dislocation emission.

REFERENCES

1. S.-J. Chang and S. M. Ohr, J. Appl. Phys. 52, 7174 (1981).
2. S. M. Ohr and S.-J. Chang, J. Appl. Phys. 53, 5645 (1982).
3. B. A. Bilby, A. H. Cottrell, and K. H. Swinden, Proc. R. Soc. London, Ser. A, 272, 304 (1963).

*Operated by Martin Marietta Energy Systems, Inc. under contract DE-AC05-840R21400 with the U. S. Department of Energy.

THE STABILITY OF CRACKS FOLLOWING EXTENSIVE STABLE GROWTH

P. F. THOMASON
Department of Aeronautical and Mechanical Engineering
University of Salford, Salford, M5 4WT, England

INTRODUCTION

Many engineering structures are made from materials of such high fracture-toughness that any crack-like defect will exhibit large amounts of stable crack-growth before catastrophic fracture intervenes. Under these conditions the established methods of elastic-plastic fracture mechanics become invalid as a result of extensive non-proportional loading and elastic unloading. In an attempt to extend elastic-plastic fracture mechanics into the large stable-growth regime a new 'incremental' criterion of crack stability is developed, from the fundamental Kelvin-Dirichlet condition [1], for the case of a workhardening incremental-plastic/elastic solid.

THE CRACK-STABILITY PROBLEM FOR AN INCREMENTAL-PLASTIC/ELASTIC SOLID

In formulating the crack stability problem we consider the case where a crack has already undergone extensive sub-critical growth following the application of prescribed tractions F_i over the surface S_F and prescribed displacements u_i over the remaining surface S_u; Fig.1. We now set out to establish a sufficient condition for the <u>stability</u> of the current equilibrium state in the cracked body V, with dead loading ($dF_i=0$ on S_F) and rigid constraints ($du_i=0$ on S_u).

The current equilibrium state can be regarded as definitely <u>stable</u> if it satisfies the Kelvin-Dirichlet criterion of stability [1] for the set of virtual displacement-increment fields corresponding to the formation of <u>incipient</u> fracture damage in a fracture process zone ahead of the crack tip (Fig.1). The sufficient condition for stability has the form $\delta(I-E)>0$ for all virtual displacement - increment fields satisfying the boundary conditions; where δI is the internal energy stored or dissipated and δE is the work done by the external dead loading. Appropriate second-order expressions for δI and δE can be obtained [2] by an imaginary cutting and rewelding operation in the vicinity of the crack tip to separate the total volume V into a global volume V^G, where the incremental response will be primarily influenced by the geometry of the body, and a local volume V^L where the incremental response will be primarily influenced by the plastic flow and fracture characteristics of the material; Fig.1. The 'separate' volumes V^L and V^G are now subjected to prescribed virtual displacement-increments fields, giving the displacement-increments du_i on the common surfaces ΔS_u of the two volumes (Fig.1); thus the common surfaces remain in perfect contact when the virtual displacement-increment field is applied. Now the equilibrium stress field in V^G will change from $\sigma_{ij}{}^G$ to $(\sigma_{ij}{}^G + d\sigma_{ij}{}^G)$ and the tractions on ΔS_u from $F_i{}^G$ to $(F_i{}^G+dF_i{}^G)$; on ΔS_u of V^L the tractions will change from $F_i{}^L$ to $(F_i{}^L+dF_i{}^L)$. Hence, we can write the Kelvin-Dirichlet stability criterion ($\delta I-\delta E>0$) for the complete cracked body (V^G+V^L) in the following form [2]:-

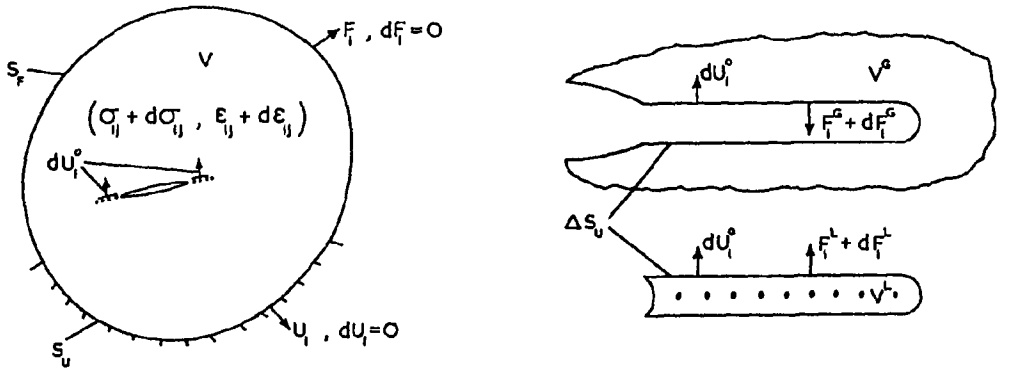

FIG.1. The imaginary cutting process ahead of a crack tip and the effect of a virtual displacement-increment field giving du_i° on ΔS_u.

$$\int_V {}^G(\overset{G}{\sigma}_{ij} + \tfrac{1}{2}d\overset{G}{\sigma}_{ij})d\overset{G}{\varepsilon}_{ij}dv + \int_V {}^L(\overset{L}{\sigma}_{ij} + \tfrac{1}{2}d\overset{L}{\sigma}_{ij})d\overset{L}{\varepsilon}_{ij}\ dv - \int_{S_F} F_i^G\ du_i^G ds > 0. \qquad (1)$$

Using the virtual work relations for the separate equilibrium stress fields in V^G and V^L the volume integrals in (1) can be transformed to give the following sufficient condition for stability of the current equilibrium state of a cracked body [2]:-

$$\tfrac{1}{2}\int_{\Delta s_u}(dF_i^L + dF_i^G)\ du_i^\circ\ ds > 0; \qquad (2)$$

where $F_i^L + F_i^G = 0$ on ΔS_u. It is important to note here that at the stability limit, where (2) just fails to be satisfied, there is no implication that $dF_i^L + dF_i^G = 0$ at all points on ΔS_u; i.e. the stability limit is not identified as an adjacent position of equilibrium.

DISCUSSION

In order to develop a method for applying the crack-stability criterion (2) in practical problems we rewrite the inequality in the form $M + S > 0$, where $M = \tfrac{1}{2}\int_{\Delta s_u} dF_i^L\ du_i^\circ\ ds$ and $S = \tfrac{1}{2}\int_{\Delta s_u} dF_i^G\ du_i^\circ\ ds$. The M integral represents a component of the total energy increment applied to ΔS_u of V^L and is related to the gradient of an effective R-curve for the material; it can therefore be regarded as an autonomous material response. On the other hand the S integral represents a component of the total energy increment applied to ΔS_u of V^G and this will be primarily dependent on the particular geometry of the cracked body, [2]. It should be noted that the M and S integrals are not path independent and the size and shape of V^L must therefore be fixed for a given problem.

The proposed 'incremental' criterion of crack-stability will of course require extensive experimental development, and a preliminary experimental procedure for measuring the M integral and evaluating the S integral in practical problems will be described in a subsequent paper [2].

REFERENCES

1. R. Hill, J. Mech. Phys. Solids 7, 209 (1959).
2. P. F. Thomason, To be published.

THE PROBABILISTIC PHYSICAL THEORY OF THERMALLY ACTIVATED FRACTURE

A.S. Krausz*, K. Krausz
Faculty of Science and Engineering
*University of Ottawa, Ottawa, Ont.

The fundamental physical processes of time dependent, thermally activated crack propagation consists of consecutive bond breaking steps and is described appropriately by the Fokker-Planck type stochastic equation [1,2].

Because the process is of random walk character the crack velocity (and the crack size) is not a deterministic quantity; the physical process always results in a crack size (and therefore, crack velocity) distribution defined by the probability density function $W(a,t)$, where a is the crack size at time t. It is shown that for the transition probability distribution of $\Psi\ (\Delta a, \Delta t)$

$$W(a,t) = \int_{-\infty}^{+\infty} W(a - \Delta a,\ t - \Delta t)\ \Psi\ (\Delta a,\ \Delta t)\ d\Delta a\ .$$

Rigorous development leads to the differential equation

$$\frac{\partial W}{\partial t} = \kappa_1 \frac{\partial^2 W}{\partial a^2} + \kappa_2 \frac{\partial W}{\partial a} \qquad (1)$$

where κ_1 and κ_2 is related to the first and second moment respectively and are expressed fully in terms of rigorously determined physical quantities (activation free energy, stress intensity factor, temperature, etc.) explicitly [3,4]. The equation is immediately recognizable as the Fokker-Planck type differential equation of stochastic processes; its relation to Brownian motion, the Langevin equation, the Liouville theorem, and transport processes is expressed in terms of crack propagation.

Applications to threshold stress intensity determination in corrosion fatigue and high temperature fracture is discussed. The deterministic theory of the atomistic, discrete concepts of the revised Griffith-theory are further developed in the probabilistic framework [5].

Previous studies have shown the significance of the behavior described by Equation (1); these were based on a derivation of an approximate character. The present paper reports the full mathematical treatment and provides the theoretically rigorous definitions of the physical conditions: it is expected that the extended abstract will make the mathematical treatment and physical meaning accessible to the expert reader.

REFERENCES

1. S. Chandrasekkar in: Noise and Stochastic Processes, N. Wax, ed., (Dover, New York, 1954) pp. 3-132.
2. A.S. Krausz, Int. J. of Fract., 12, 239 (1976).
3. A.S. Krausz, Eng. Fract. Mech., 12, 499 (1979).
4. A.S. Krausz, K. Krausz, Eng. Fract. Mech., 13, 751 (1980).
5. K. Krausz, A.S. Krausz, Proc. 2nd Int. Conf. on Fatigue Crack Propagation Rate, C.J. Beevers, J. Bachlund, P. Lukas, J. Schijve, R.O. Ritchie, eds. (Birmingham, 1984) pp. 497-510.

STRESS DRIVEN MIGRATION OF POINT DEFECTS AROUND CRACK-TIPS

J.E. SINCLAIR and C.A. HIPPSLEY
AERE Harwell, Oxfordshire, U.K. OX11 ORA

An understanding of the motion of point defects towards or away from cracks under stress is important in at least two fields: the segregation of embrittling solute species, and the effect of radiation on fracture rates and mechanisms. The analogous interaction between point defects and dislocations has been crucial to understanding radition-induced swelling and creep. Since the stress field of a loaded crack can be even more powerful than that of a dislocation, we can anticipate effects which are equally important.

Rauh and Bullough [1] recently derived an analytic solution for the drift of over- or under-sized defects in a crack-tip field, which Hippsley et al [2] have successfully used to interpret observations of sulphur segregation during high-temperature intergranular brittle fracture. The calculation ignores diffusion in comparison with stress-driven drift. This is justifiable when the stress gradients are large. More seriously, however, redistribution of stresses by plasticity and blunting were also ignored. This casts some doubt on the validity of the predictions. The question arises whether correction of any of these inadequacies in the model would help with a difficulty in the interpretation of the sulphur segregation studies, namely that the under-sized sulphur atoms drift behind the crack tip to the crack faces. If this really occurs, it is difficult to explain the chemical effect.

With varying loss of the original analytic solubility, we have tried several refinements of Rauh and Bullough's model. Firstly, with blunting but not plasticity, the stresses are everywhere finite; but the maximum tensile hydrostatic stress is still at the crack tip. With a parabolic crack profile, the drift flow in the elastic field is analytically soluble. But under-sized defects still drift towards the crack faces behind the tip.

To allow for plastic yield, we first tried a representation with inclined slip bands through the tip. Defect drift paths then had to be found by numerical integration. The slip bands introduce planes of discontinuity in both the stress field and the defect concentration. But again, because there was no allowance for tip blunting, and because of the spatially concentrated form of the plastic yield, the maximum in tensile stress is at the tip, and undersized defects are pushed behind.

Finally, we used a finite-element analyis of the stresses around a blunt notch with strain-hardening plastic deformation. In this model, a stress maximum was found about a tip radius ahead of the crack, so that sulphur migration could be predicted towards the tip surface. The total amount deposited, however, would be limited to the initial quantity

lying within about one tip radius. In this region, the assumed continuum stress-driven law is of more doubtful validity than elsewhere.

Overall, the usefulness of the original simple, analytically expressed model is confirmed for predicting defect drift on a scale larger than any crack tip blunting radius. On a small scale, microstructural details are likely to be important. Difficulties in interpreting sulphur segregation as a cause of high-temperature brittle fracture have yet to be fully resolved.

REFERENCES

[1] H. Rauh and R. Bullough, Proc. Roy. Soc. A397, 121-141 (1985).

[2] C.A. Hippsley, H. Rauh and R. Bullough, Acta Metall. 32, 1381-1394 (1984).

COMPUTER SIMULATION OF FRACTURE IN A SPATIALLY VARYING ANISOTROPIC GLASS

D.W.BERREMAN, S.MEIBOOM, J.A ZASADZINSKI AND M.J.SAMMON
AT&T Bell Laboratories
600 Mountain Ave.
Murray Hill, NJ 07974

Cholesteric liquid crystals can be quick-frozen with a jet of cold liquid propane to form a glass that retains the periodic molecular orientation of the original liquid crystal phase. These frozen samples can be fractured, and the contour of the fracture surface can be studied with electron micrographs of platinum shadow replicas.

In order to interpret these micrographs, we have developed a very simple theory of fracture in spatially varying anisotropic materials that seems to give results consistent with our observations.

We suppose that the crack progresses so slowly that inertial effects may be ignored. We set up an x, y, z coordinate system with stress in the z-direction. We suppose that the crack front is at all times parallel to the x-z plane and propagates in the y-direction. We further suppose that at each incremental advance of the crack the energy released is minimal. We use a simple Landau expansion to estimate the relative energy per unit area released, dU:

$$dU = \underline{n} \cdot \underline{\underline{R}} \cdot \underline{n}$$

where $\underline{n}$ is a unit vector that is locally normal to the crack and

$$\underline{\underline{R}} = \underline{\underline{1}} + b\underline{\underline{Q}}$$

is a symmetric, traceless tensor characterizing the liquid crystal anisotropy.[1] Approximate expressions for the spatial variation of $\underline{\underline{Q}}$ in the Grandjean texture and in the blue phases I and II of cholesteric liquid crystals have been obtained from optical diffraction[2,3] and from theory.[4] Correspondence between results of present computations and experiments will give further information about the details of the structure of these phases.

We have written a computer program that minimizes the quantity

$$\delta U = \int_0^w \frac{\underline{n} \cdot \underline{\underline{R}} \cdot \underline{n} \delta y dx}{\underline{n} \cdot \underline{e}_z}$$

for each incremental advance, δy, of the crack. The term $\underline{e}_z$ is a unit vector parallel to the stress. The factor

$$\frac{\delta y \cdot dx}{\underline{n} \cdot \underline{e}_z}$$

is the area of crack produced when the area projected on the x, y plane is $\delta y \cdot dx$. Periodic boundaries in the x-direction are optional. We arbitrarily start with a straight line at y=0. The crack generally progresses to a form that does not depend on the straight-line start after a distance approximately equal to the crack width, w.

We find that we get contours similar to those observed when b is on the order of -0.6 to -0.8, meaning that the glass breaks much more easily parallel to the long axis of the liquid crystal molecules than normal to them.

When b is zero, this theory gives a plane crack normal to the stress which minimizes the area that is represented by the constant term in R.

References:

[1] P.G.de Gennes, *Mol.Cryst.Liq.Cryst.* **12**,193(1971).

[2] S.Meiboom, M.Sammon, and D.W.Berreman *Phys.Rev.A***28**,3553(1983).

[3] D.W.Berreman, Liquid Cryst. and Ordered Fluids Vol.4, p925 (Plenum, 1984).

[4] H.Grebel, R.M.Hornreich and S.Shtrikman, *Phys.Rev.A***28**,1114(1984).

EFFECT OF SURFACE TENSION ON THE TOUGHNESS OF GLASS

TZE-JER CHUANG
Institute for Materials Science and Engineering
National Bureau of Standards
Gaithersburg, MD 20899

INTRODUCTION

The paper is concerned with fracture toughness of glass. Special attention is given to studying the effect of surface stress on the apparent toughness as observed on a typical glass specimen, for mechanical forces must exist in the fracture surfaces.

At the crack tip where surface curvature $K_{\alpha\beta}$ is highly concentrated, the residual bulk stresses σ_{ij} are generated by surface tension $\tau_{\alpha\beta}$ as $n_i\ \sigma_{ij}\ n_j = \tau_{\alpha\beta}\ K_{\alpha\beta}$ resulting from the requirements of mechanical equilibrium. These residual stresses in term alter the tip geometry leading to the following integral equation governing the crack-tip shape:

$$u(x) = \frac{4(1-\nu^2)}{E\sqrt{2\pi}}\ K_a\ \sqrt{x} + \frac{8\gamma(1-\nu^2)}{\pi E}\ \int_0^\infty m(x, x')\ u''(x')dx' \qquad (1)$$

where x is the distance away from the crack tip and $m = \log\ [\sqrt{x} + \sqrt{x'}/|\sqrt{x} - \sqrt{x'}|]$ is the kernal. First order approximation for u results in the following residual K

$$K_{res} = 4\gamma\int_0^\infty \frac{u''(x)}{\sqrt{x}}\ dx = -\ \lambda\ \gamma\ \sqrt{a}/\rho_{tip} \qquad (2)$$

where γ is surface energy, a is characteristic crack tip zone size, ρ_{tip} is the root radius of the tip and λ is of order unity.

As an example, we calculate the case of a particular crack observed in high silica glass where $\rho_{tip} \approx 1.5$ nm and $a \approx 100$ nm. The materials properties of that glass are well-determined: $E = 70$ GPa $\nu = 0.22$, $\gamma = 7\ J/m^2$ corresonding to $K_{IC} = 1\ MPa\sqrt{m}$. Using these values, the amount of toughening is computed to be $K_{res} \approx 1.5\ MPa\sqrt{m}$ from eqn. (2). This means that this crack can sustain an applied K as high as $2.7\ MPa\sqrt{m}$, a factor of 2.25 times K_{IC} resulting in geometry-induced toughening phenomenon.

SUMMARY

Mechanical stresses (i.e. surface tension) inherently exist on a general free surface because its atomic structure differ from its bulk counterpart. The effect of surface tension is amplified at a crack tip because of curvature concentration. Integral equation describing this effect on the toughness of glass is derived and first order approximations using weight function technique were made for evaluations. The qualitative results indicated that the geometry-induced toughening is linearly proportional to surface tension and crack tip curvature and to square root of crack tip zone size. An illustrative example of recently observed crack tip in SiO_2 glass is given which shows that toughness is enhanced two and quarter times the original K_{IC} value.

REFERENCES

1. R. Shuttleworth, Proc. Phys. Soc. A63, 444-57 (1950).
2. C. Herring, in: Structure and Properties of Solid Surfaces, R. Gomer and C.S. Smith, eds. (University of Chicago Press, Chicago 1953) Chapt. 1.
3. W.W. Mullins in: Metal Surfaces, W.D. Robertson and N.A. Gjostein, eds. (ASM 1963) Chapt. 2.
4. J.R. Rice and T.J. Chuang, J. Am. Ceram. Soc. 64, 43-52 (1981).
5. M. Tomozawa and Y. Oka, in: Surfaces and Interfaces in Ceramic and Ceramic-Metal Systems, Plenum, 1981, pp. 677-87.
6. C.W. Mays, J.W. Vermaak and D. Kuhlmann-Wilsdorf, Surf. Sci. 12, 134-140 (1968).
7. H. Udin, A.J. Shaler and J. Wulff, Metal Trans. 2, 186-190 (1949).
8. P.W. Tasker, Philo. Mag. 39A, 119-136 (1979).
9. R. Thomson, T.J. Chuang and I.H. Lin, submitted to Acta Metall.
10. H.F. Buecker, ZAMM 50, 529-46 (1970).
11. Y. Bando, S. Ito and M. Tomozawa, J. Am. Ceram. Soc. 67, C-36 (1984).
12. B.R. Lawn, D.B. Marshall and A.H. Heuer, J. Am. Ceram. Soc. 67, C-253 (1984).
13. S.M. Wiederhorn, J. Am. Ceram. Soc. 52, 99-105 (1969).
14. B.R. Lawn, K. Jakus and A.C. Gonzalez, J. Am. Ceram. Soc. 68, 25-34 (1985).
15. R.J. Charles and W.B. Hillig, in: Symposium on Mechanical Strength of Glass and Ways of Improving It, Charleroi 1962, pp. 511-527.

THE ROLE OF PLASTIC WORK IN THE CLEAVAGE OF BCC METALS

J. E. HACK* AND D. F. STEIN**
*Center for Materials Science, Los Alamos National Laboratory, Los Alamos, NM 87545;**Michigan Technological University, Houghton, MI 49931

Cleavage, the separation of atoms across a single atomic plane, is one of the simplest concepts in brittle fracture. However, serious gaps still remain in the reconciliation of observed behavior with theoretical predictions. One technologically important example is the persistent lack of a satisfactory predictive capability for the choice of cleavage plane in the body-centered-cubic metals. Although surface energy arguments predict (110) cleavage in most bcc systems, (100) cleavage is generally observed.

The current investigation was aimed at calculating the plastic work associated with various crack planes and directions for internally pressurized cracks in single crystals of tungsten at ambient temperature. The cracks were assumed to be moving at a velocity of 10 m/sec. The plastic work was calculated using a combination of the standard linear elastic crack tip stress field solution [2] and the Orowan equation relating strain rate to the average dislocation velocity and average [3]. For the purpose of the calculations, only the most highly stressed slip system was assumed to operate for each crack-plane - crack direction pair. Increases in dislocation density were assumed to be offset by an increase in work hardening parameter [4]. The crack system which induced the lowest combination of surface and plastic strain energy per unit crack advance was considered to be the preferred cleavage plane.

The results of the calculations are given in the table below:

Table I. Surface (γs), Plastic (γp), and Fracture (γF) energies for the various crack systems considered.

Crack Plane	Crack Direction	$2\gamma s(J/m^2)$[a]	$\gamma p(J/m^2)$	$\gamma F(Jm^2)$[b]
(001)	[100]	3.8	26.8	30.6
(013)	[100]	4.1	53.7	57.8
(103)	[30$\bar{1}$]	4.1	39.7	43.8
(012)	[100]	4.1	116.4	120.5
(102)	[20$\bar{1}$]	4.1	52.7	56.8
(023)	[100]	4.0	417.7	421.7
(203)	[30$\bar{2}$]	4.0	81.1	85.1
(011)	[100]	3.7	2274.1	2277.8
(101)	[10$\bar{1}$]	3.7	231.5	2335.2

a) Estimated

b) $\gamma F = 2\gamma s + \gamma p$

The results show several points worth noting, including: 1) The plastic work term dominates the total work to fracture; 2) The plastic and fracture energies are minimum on the (100) plane and rise to a maximum as the (110) plane is approached; 3) the absolute value of approximately 30 J/m^2 for the fracture energy of annealed tungsten at room temperature and a crack velocity of 10 m/sec agrees well with experimental data for zone refined single crystals under similar conditions [5].

REFERENCES

1. W. R. Tyson, R. A. Ayres and D. F. Stein, Acta Met., 21, 621 (1973).
2. J. R. Rice, in Fracture: An Advanced Treatise vol. 2, H. Liebowitz (ed.), Academic Press, New York, p. 191 (1968).
3. E. Orowan, Proc. Phys. Soc., 52, 8 (1940).
4. H. W. Schadler, Acta Met. 12, 861 (1964.
5. J. M. Liu and B. W. Shen, Metall. Trans. A, 15A, 1247 (1984).

THE BRITTLE-DUCTILE TRANSITION IN SILICON WITH PARTICULAR REGARD TO DOPING

Markus Brede, Peter Haasen
Institut für Metallphysik der Universität Göttingen
Hospitalstrasse 3-5, 3400 Göttingen, FRG

INTRODUCTION

An article by St. John [1] on the measurement of the brittle-ductile transition in undoped silicon reported an Arrhenius relation between crack opening velocity $\dot{d}$ and the respective transition temperature T_c, with an activation energy of 1.9 eV. With regard to conditions at the crack tip, Haasen [2] considers the possibility of thermally activated formation of a stable partial dislocation loop at the crack tip. St. John's results can be interpreted using this postulate, if crack tip blunting due to dislocation motion in the stress field of the crack tip is assumed. The motion of the dislocation is hereby described by the thermally activated formation and movement of double kinks on the partials of the dissociated dislocations. Analogous to the doping - dependence of dislocation motion, a reduction of the activation energy for the crack tip blunting is to be expected, and hence a lowering of the transition temperatures.

EXPERIMENTAL

To measure the brittle-ductile transitions, dynamic tensile tests were carried out on pre-cleaved monocrystalline samples between 800 K and 1300 K with crack opening velocities between 5 µm/min and 1000 µm/min.

RESULTS

Results are presented, which were obtained from FZ-crystals doped with phosphorus at levels of 1.6×10^{18} and 6.5×10^{18} atoms per cm^3 (FIG.1). The diagram $\ln \dot{d}$ vs. $1/T_c$ does not show the expected doping dependence of brittle-ductile transitions (see FIG.2). For the weakly doped silicon (1) open symbols) an activation energy of 1.8 eV is calculated at temperatures greater than 1000 K. Towards lower temperatures the plot shows a deviation of the Arrhenius line. In the more heavily doped material (2) closed symbols) this deviation takes place at higher temperatures and crack opening velocities. Therefore the brittle-ductile transition temperatures T_c are higher than in material 1) for small $\dot{d}$. At T>1050 K, however, the transition temperatures for a given crack opening velocity are as we have expected lower in the more heavily doped samples. If T raises above 1150 K, the curve 2) approaches an Arrhenius line with $U_{1)} > U_{2)}$. When compared with St.John's measurements [1], the brittle-ductile transitions are distinctly shifted towards lower temperatures.

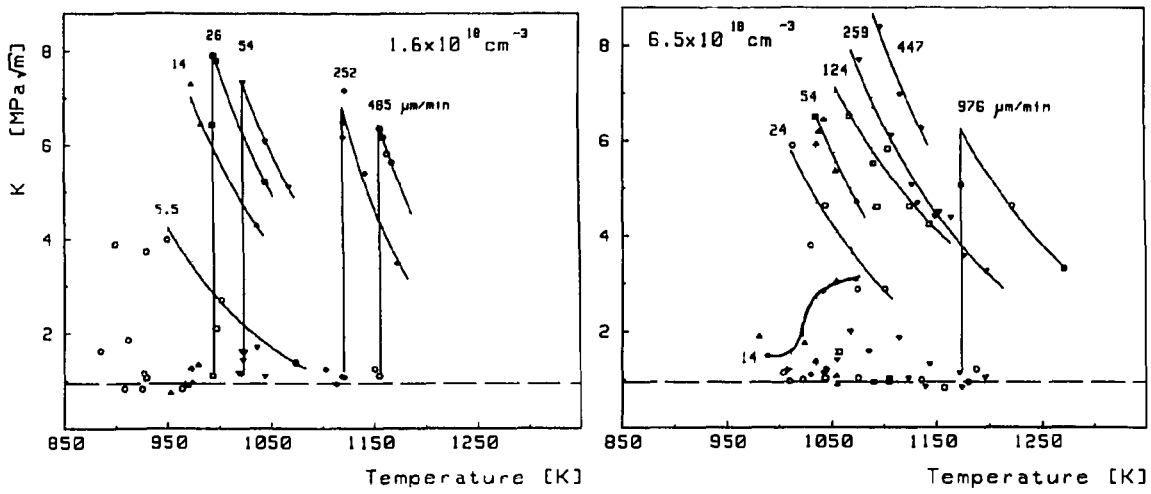

FIG.1. The brittle-ductile transitions of 1) 1.6×10^{18}, 2) 6×10^{18} doped silicon

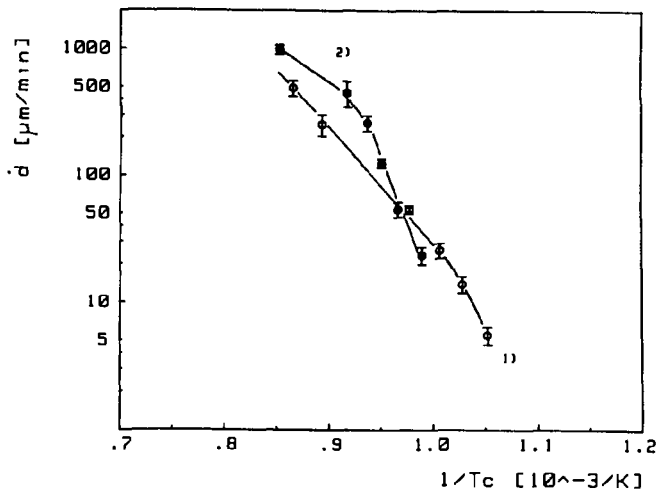

Former experiments in doped silicon have shown that the impurities bring about a deviation of dislocation velocity with stress at small velocities and low stresses[3]. The stresses might be low enough in a small distance ahead of the crack tip that the difference between the predictions and the experimental data at small crack opening velocities could be explicable by this phenomenon.

FIG.2. Crack opening velocities ḋ vs. inverse transition temperatures $1/T_c$.

REFERENCES

1. St.John, C., Phil.Mag.32, 1193 (1975)
2. Haasen, P. in: "Atomistics of fracture", (Plenum Press, New York 1983)
3. Imai, M., Sumino, K., Phil.Mag.47, 599 (1983)

MODE I CRACK TIP SHIELDING APPLIED TO WARM PRESTRESSING

B.S. MAJUMDAR AND S.J. BURNS
Materials Science Program
Department of Mechanical Engineering
University of Rochester
Rochester, New York 14627

INTRODUCTION

Some recent work [1-5] on fracture considers problems of cracking from a conceptually different viewpoint than conventional continuum plasticity theories. Individual discontinuities such as dislocations, voids or phase transforming precipitates are considered to be interacting with the crack tip, and local crack tip stress intensities are chanaged relative to externally applied stress intensities. The dislocations that become geometrically necessary for mechanical equilibrium shields [1-5] the crack tip from the external crack driving force.

The approach described above becomes especially important in the transition regime of brittle to ductile fracture, where concepts of dislocation generation and mobility are involved. Experimental results relating to shielding concepts are obtained from some in-situ straining of TEM specimens as well as bulk LiF crystals.

The present work is a continuation of shielding concepts to Mode I cleavage fracture of bulk polycrystalline 4340 steel samples. The technique of warm prestressing, whereby a precracked specimen is preloaded above the ductile to brittle transition temperature, and fractured at a low temperature (usually 77°K), allows a way to partially separate out the processes of plasticity (and attendant shielding) and cleavage cracking. Earlier work on warm prestressing [6-8], has concentrated on unloading samples at preload temperatures prior to cooling and subsequent fracture at liquid nitrogen temperature. Since some reversed plasticity may occur at the low temperature, it is desirable to unload samples only at the low temperature. This has been given special attention in the present series of experiments.

Bend bar specimens of 4340 steel have been subjected to the following two load cycles. In one case (LUCF), the specimens have been preloaded to a desired K value at a given temperature, unloaded completely, cooled to liquid nitrogen temperature, and finally fractured at 77°K. In the second case (LCUF), the cooling has been conducted with the preload held constant. For the purpose of baseline data, unpreloaded samples were fractured at 77°K, as well as at room temperature. Following fracture special fractographic features were observed in a SEM.

In an attempt to separate the effects of shielding and blunting, three approaches were taken. First, the K at fracture of LCUF specimens at 77°K were compared with corresponding values for unpreloaded machined blunt specimens. The other two approaches relied on the fact that the COD at preload at a given K varies inversely as the flow stress. Identifying COD as a parameter for blunting, it is obvious that the degree of blunting of a preloaded sample for a given K can be altered by either changing the preload temperature (since flow stress is sensitive to temperature), or by changing the microstructure. In the former approach, the temperature of

preloads has been varied between -100°C and 200°C. In the latter case, the as received rolled and annealed pearlitic strucure has been changed to a tempered martensitic structure. The tempering temperature was chosen so that at 77°K the fracture toughness of unpreloaded samples were essentially the same for both microstructures. Such a technique also allowed for the evaluation of the role of microstructure in warm prestressing effects.

Both LUCF and LCUF specimens showed increasing K at fracture with increasing preloads. However, there were two important differences. First, there was a significant scatter in the results of LUCF specimens compared to LCUF specimens. More importantly, there were marginal effects of preload for LUCF specimens (especially at higher preloads) compared to LCUF specimens. For these latter specimens, almost 90% of the effect of preload was retained at fracture. The data for LCUF specimens showed a linear increase in K of fracture with increasing preloads. Also, the plot seems to be independent of the temperature of preload or the microstructure. Considering that the flow stress for the tempered martensitic structure is almost double that of the pearlitic structure, the data clearly suggests that the effect of blunting is much smaller than that of attendant shielding. The data for blunt saw cut samples fell in the range of K values for LCUF specimens. However, considering that saw cut samples had a crack tip radius, an order of magnitude larger than LCUF specimens, the data suggests that the effect of blunting may be small.

The present results are compared with similar data from other investigations. It appears that on a normalized scale, where the stress intensity factors at preload and fracture are normalized with respect to the fracture toughness at 77°K of unpreloaded specimens, the data trend is independent of microstructure and composition within reasonable limits of preload. This seems to be an important result, and an attempt is made to understand this in terms of crack tip shielding concepts.

SEM micrographs show that cleavage fracture is essentially similar for unpreloaded, as well as LUCF and LCUF specimens. The major difference lies in the much larger frequency of secondary cracking of LCUF samples. Also for these latter specimens there are large macroscopic ridges formed on the fracture surface. Presumably, these secondary cracks and ridges are formed to dissipate the excess energy stored in LCUF specimens.

ACKNOWLEDGEMENT

Supported by the U.S. Department of Energy under grant DEFG02-84ER45051.

REFERENCES

1. B.S. Majumdar and S.J. Burns, Acta. Metall., 29, 579 (1981).
2. R. Thomson and J.E. Sinclair, Acta. Metall., 30, 1325 (1982).
3. E.W. Hart, Int. J. Sol. and Structures 16, 807 (1980).
4. S.M. Ohr and S.J. Chang, J. Appl. Phys., 53, 5645 (1982).
5. B.S. Majumdar and S.J. Burns, Int. J. Fract., 21, 229 (1983).
6. G.G. Chell, J.R. Haign and V. Vitek, Int. J. Fract. 17, 61 (1981).
7. D.A. Curry, Int. J. of Fract. 17, 335 (1981).
8. H. Nakamura, H. Kobayaski, T. Kodaira and H. Nakazawa, Proc. 5th Int. Conf. on Fracture 2, ed. D. Francois, 817 (1981).

DIRECT OBSERVATION OF CRACK TIP PROPAGATION BRITTLE MATERIALS

R. B. TAIT AND G. G. GARRETT
Department of Metallurgy, University of the Witwatersrand, 1 Jan Smuts Avenue, Johannesburg, 2001, South Africa

INTRODUCTION

In complex, multiphase, brittle materials the continuum approach to describing the mechanics of fracture, although widely used, must be interfaced with a consideration of the prevailing fracture mechanisms, particularly where there is a doubt - as there often is in such systems - of the general applicability of conventional fracture mechanics. Although scanning electron microscopy (SEM) is widely used to investigate such micromechanisms of fracture, post fracture surfaces have generally been examined and it is only relatively recently that real time "in situ" observations of slowly propagating cracks and defects have been undertaken [1,2,3]. This paper describes the details of, and typical results achieved with, a constant K double torsion (DT) loading facility operating inside the specimen chamber of a conventional SEM used in the investigation of crack tip propagation in brittle materials.

EXPERIMENTAL METHODS AND OBSERVATIONS

Small specimens (33 x 11 x 1,1 mm) of brittle materials, including cement paste, mortar, tungsten carbide-cobalt, cast iron and ceramics were readily loaded in double torsion using the facility illustrated in Fig. 1. Using a loading system comprising a micrometer screw drive, helical washer and retracting pins, pivotting of the upper loading plate resulted in application of four point loading to the DT specimen. The whole system was mounted on a goniometer stage so that the main crack region was on or close to the microscope axis thus facilitating easy following of the microcrack system.

The degree of control of crack tip advance, using the DT system, is, at close to 0,1 micron, exceptional for brittle materials, and comparable with the resolution of the microscope. Evidence of the control of such crack advance is shown in Figs. 2 (a) and (b) for cement paste, both immediately before (a) and after (b) a small increment of loading. The crack is seen to have extended by one or two microns in this pair of micrographs. In addition this in situ DT SEM testing facility enabled "process zones" of microcracking in the vicinity of the main propagating crack tip to be observed in cementitious materials but not in WC-Co or cast iron systems. Relaxation behaviour of this microcracked process zone subsequent to the passage of the main crack in cement systems was also observed. Some plastic fracture behaviour, consistent with microvoid coalescence, was also observable in the cobalt phase of the ostensibly brittle WC-Co particulate composites.

SUMMARY

An in situ double torsion SEM loading system has been used to investigate real time fracture mechanisms of brittle materials and is particularly useful because of the fine control of crack advance (at less than a micron) that can be achieved.

REFERENCES

1. R.B. Tait and H Bohm, Proc of EM Soc of SA, p 29 (Dec 1980).
2. S. Diamond, S. Mindess and J.Lovell, Cem. and Conc. Res. 13 , pp 107-113 (1983).
3. S. Kobayashi and S.M. Ohr, Philosophical Magazine A, 42 , 6, p763 (1980).

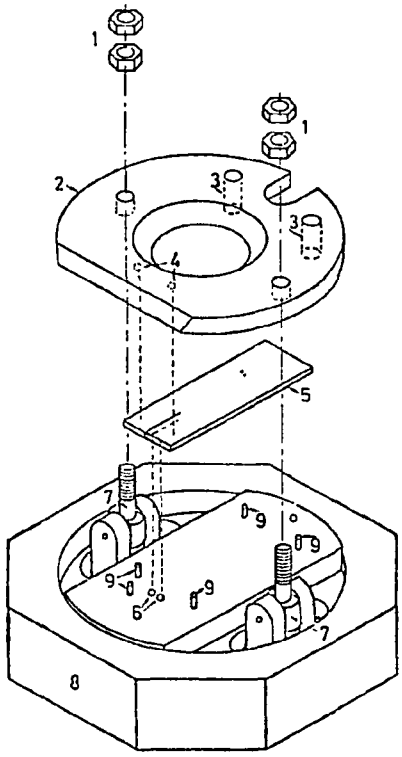

FIG. 1. Expanded view of the in situ SEM's DT loading system.

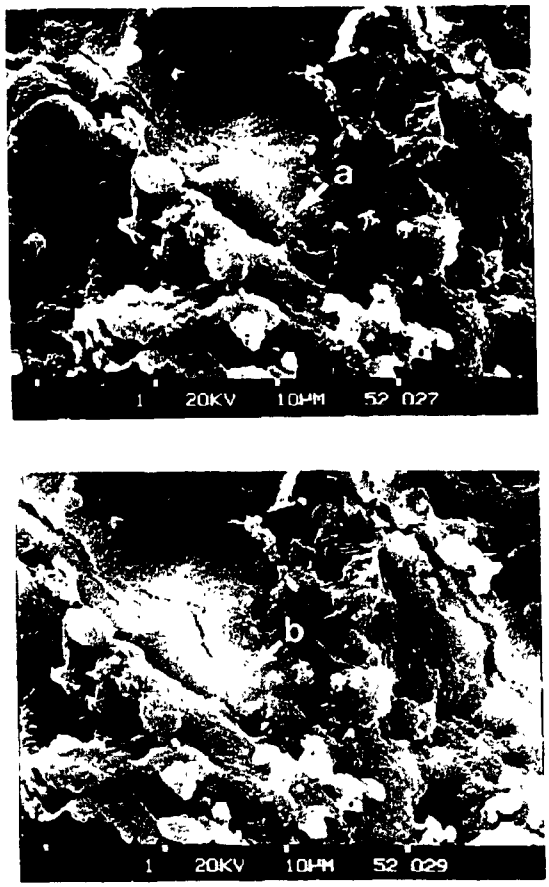

FIG. 2. Illustrating control of crack tip advance in cement paste (w/c ratio 0.38, 14 day wet cure). The crack tip (a) has advanced 1 or 2 microns in (b) following a small load increment.

DISLOCATION STRUCTURES AT CRACK TIPS*

I.M. ROBERTSON, G.M. BOND and H.K. BIRNBAUM
University of Illinois, Dept. of Metallurgy and Mining Engineering, Urbana, IL 61801

In a recent series of papers, Ohr and coworkers have presented observations on the dislocation structure at crack tips in a number of materials deformed in mode III [1-3]. They report that the plastic zone is frequently comprised of a dislocation-free zone immediately ahead of the crack tip followed by a linear array of dislocations. The dislocation array takes the form of an inverse pile-up with the dislocation spacing decreasing as the crack tip is approached. These observations tend to be limited to crack tips that are produced in the early stages of deformation or are produced by the TEM specimen preparation process.

The existence of the dislocation-free zone has been predicted by modifying the continuous dislocation plastic-zone model of Bilby et al [4] to include a barrier to dislocation emission from the crack tip. This modification removes the singularity at the crack tip. The size of the dislocation-free zone varies inversely with the number of dislocations in the array, but is still of the order of hundreds of nanometers for 100 dislocations when a value for the lattice friction stress that is characteristic of dislocations in a metal is substituted into the theoretical models [5].

The presence of the dislocation-free zone is thought to be an anomalous result since as shown in figs. 1 and 2 dislocations extend to within a few tens of nanometers of the crack tip even when the number of dislocations is small. The micrograph in fig. 1 shows a crack tip in copper with the stress released, dislocations extend to within 20 nanometers of the crack tip. Indeed, where the crack path changes direction (A on figure), a single dislocation exists within 30 nanometers of the crack tip; the theory predicts that a single dislocation should move several microns from the crack tip. The lack of dislocations within 20 nanometers of the crack tip can be attributed to the thinness of the material; the material is too thin to support dislocations because of surface image forces. Furthermore, it is difficult to keep dislocations close to the crack tip since they require only small increases in stress to induce motion and can frequently be made to move under the electron beam. The micrographs in fig. 2 were taken from an Al-7075 alloy that has been deformed in-situ in the electron microscope and held at constant stress. Immediately ahead of the crack tip in the deformation zone, an intense tangle of dislocations exists with the dislocations approaching the crack tip. The area that appears to be free of dislocations in fig. 2a can, by tilting, be shown to contain dislocations, fig. 2b.

*This work was supported by the DOE through contract DE-AC02-76ER01198.

These observations indicate that no dislocation-free zone exists at crack tips in materials with low (Cu) and high (Al-7075 alloy) values of the lattice friction stress. Similar observations have been made in a number of other materials.

REFERENCES

1. S. Kobayashi and S.M. Ohr, in 37th Ann. Proc. Electron Microscopy Soc. Amer. San Antonio, Texas 1979 (Ed. G.W. Bailey) p. 424
2. S. Kobayashi and S.M. Ohr, Phil. Mag. A42, 763-772, 1980
3. S. Kobayashi and S.M. Ohr, Scripta Met. 15, 343-348, 1981
4. B.A. Bilby, A.H. Cotrell and K.H. Swindon, Proc. Roy. Soc., A272, 304-314, 1963
5. S.H. Dai and J.C.M. Li, Scripta Met. 16, 183-188, 1982

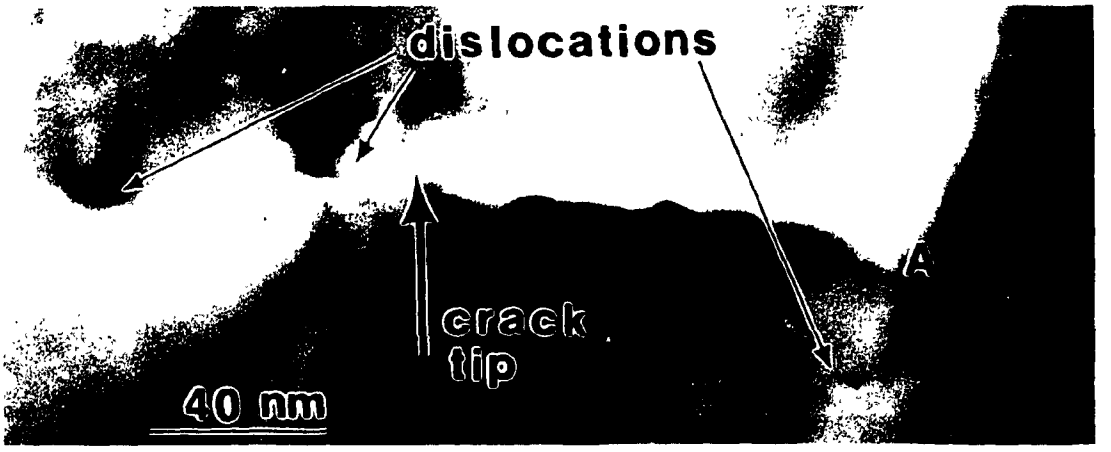

Fig. 1 Dislocation structure at a crack tip in copper.

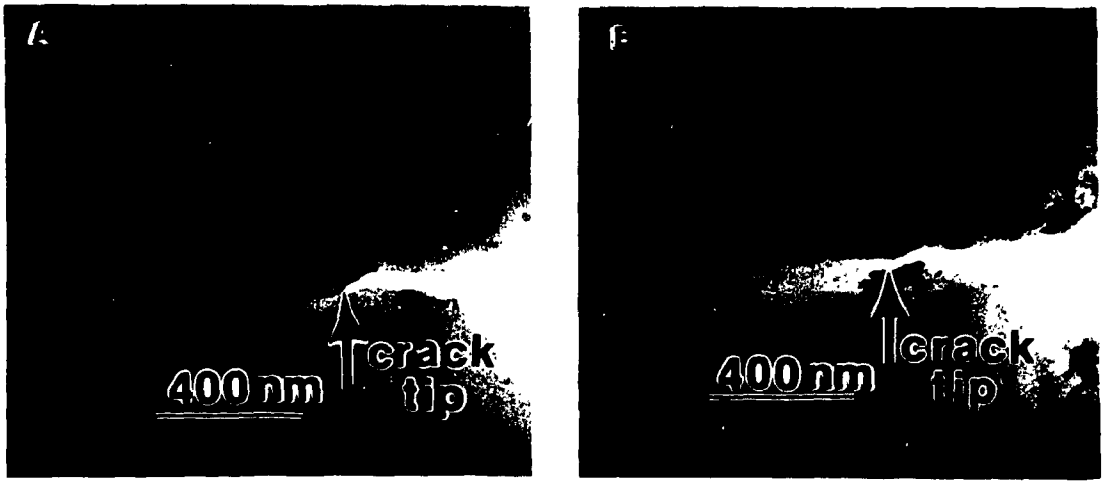

Fig. 2 Dislocation structure in an AL-7075 alloy after a significant amount of deformation. The crack tip is surrounded by a dense tangle of dislocations. The difference between (a) and (b) is in the diffraction conditions.

TEM STUDIES OF CRACK TIP DISLOCATIONS IN BCC METALS

C. G. PARK AND S. M. OHR
Solid State Division, Oak Ridge National Laboratory,*
Oak Ridge, Tennessee 37831

Crack tip deformation on a microscopic scale has been the subject of considerable interest recently because of its implication on the understanding of the fracture toughness and the overall fracture process. From a series of TEM observations [1–4] it is now well established that, when plastic deformation occurs ahead of propagating cracks, dislocations are emitted from the crack tip, rapidly driven out of the area, and piled-up in a plastic zone creating a dislocation-free zone (DFZ). The existence of the DFZ, which is a manifestation of the difficulty associated with dislocation emission from the crack tip, has contributed significantly to the understanding of the mechanism of ductile and brittle crack propagations. The relationship between the mode of crack propagation and the behavior of crack tip dislocations depends on the crack geometry and the loading conditions. However, it is not clear at present which of the material parameters are responsible in determining the geometry of crack tip deformation and its relationship to the onset of crack propagation. In the present work, we have studied the effects of unloading and hydrogen environment on the distribution of dislocations, on the DFZ, and on the crack tip slip systems during in situ TEM deformation of bcc metals.

Depending on the loading geometry, all three modes of crack tip deformation have been observed. In all of the cases studied the presence of the DFZ immediately ahead of crack tip was confirmed by imaging through 4–5 different diffraction conditions. The size of the DFZ, however, varied (1–20 μm) depending on the number of dislocations in the plastic zone, the grain size and the loading conditions, as predicted by the dislocation model of fracture [5, 6]. Figure 1 shows the variation of the size of the DFZ in two different stages of crack propagation in molybdenum. Between (a) and (b), the applied stress was increased and the crack propagated. The total number of dislocations emitted from the crack tip increased from 70 to 280 and the length of the DFZ decreased from 5.5 to 1.5 μm. During this process the grain boundary appears to have acted as a barrier to dislocation motion. More detailed examinations, however, revealed that some of the dislocations in the pile-up entered, moved along, and emerged out of the grain boundary into the same grain. When the stress was removed, some of the dislocations in the plastic zone moved backward to the crack tip and were annihilated. The dislocations left in the plastic zone redistributed themselves during the unloading. Generally, the DFZ ahead of shear cracks of mode III was shorter than DFZ's of mode I and II cracks. This indicates that the emission of screw dislocations from the crack tip is easier under the mode III loading condition.

In all of the crack tip geometries analyzed, the choice of the crack tip slip system was dictated by two factors: the dislocation emission condition from the crack tip [5] for each mode of loading and the crack tip Schmid Factor. That is, the type of crack tip deformation is determined by the ratio of the component of applied stress to the critical stress intensity factor for dislocation emission for each mode. It is found that the mode III crack tip deformation is statistically favored over modes I and II. Within each mode of deformation, the slip system possessing the maximum crack tip Schmid factor is activated from the tip of propagating cracks. The results presented here are in good agreement with the DFZ theory of fracture [5].

REFERENCES

1. S. M. Ohr and J. Narayan, Phil. Mag. A 41, 81 (1980).
2. S. Kobayashi and S. M. Ohr, Phil. Mag. A 42, 763 (1980).
3. S. M. Ohr and S. Kobayashi, J. of Met. 32, 35 (1980).
4. J. A. Horton and S. M. Ohr, J. Mat. Sci. 17, 3140 (1982).
5. S. M. Ohr, Mat. Sci. Eng. 72, 1 (1985).
6. S. Dai and J. C. M. Li, Scripta Met. 16, 183 (1982).

*Operated by Martin Marietta Energy Systems, Inc. under contract DE-AC05-840R21400 with the U. S. Department of Energy.

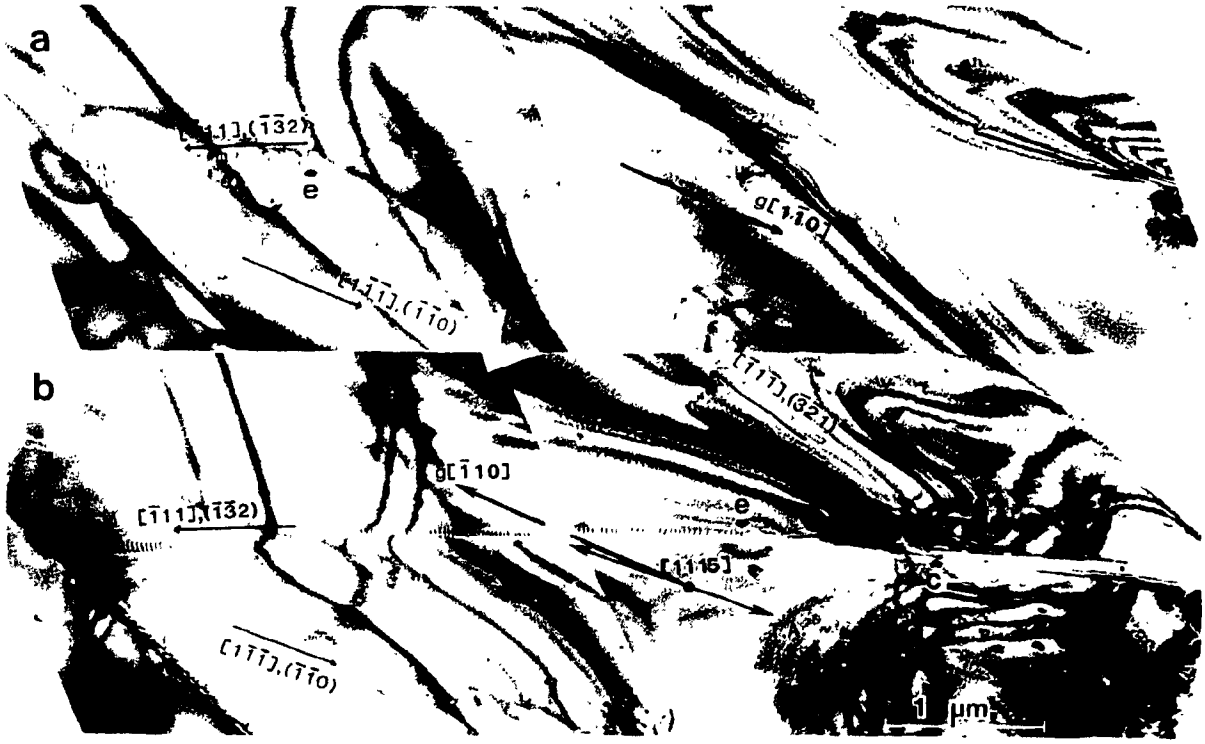

Fig. 1. Distribution of dislocations ahead of propagating cracks in molybdenum. As the applied stress increased from (a) to (b), the crack propagated and the size of the DFZ decreased.

MODELING OF CRACK GROWTH AND FRACTURE IN THIN SPECIMENS

by K. V. Jata, T. Hanamura*, and W. A. Jesser
Department of Materials Science, School of Engineering and Applied Science, University of Virginia, Charlottesville, VA 22901

INTRODUCTION

Microstructure and crack tip micro-plasticity largely affect the crack growth mode and toughness of notched components. Linear elastic fracture mechanisms, LEFM, can be conveniently employed to rationalize the crack growth behavior under small scale yielding conditions in front of the crack tip under plane-strain conditions. The maximum stress and minimum strain energy criteria can often correctly predict the crack growth direction and many existing fracture models toughness models can be used to understand the toughness behavior. However, when the component is under a plane stress condition, the large scale micro-plasticity in front of the crack tip does not permit the use of LEFM analysis with ease. In such conditions crack tip opening displacement, grain orientation and slip processes occurring in front of the crack tip would be more useful concepts to rationalize crack growth and toughness behavior. In this paper we present the models successful in bulk specimens as applied to the thin film case.

MATERIALS AND EXPERIMENTAL

Ribbons of type 304 and 316 stainless steel 12mm by 2.3mm 40μm thick were electropolished so that a thin bowl shaped region formed in the center of the specimen. The specimen was mounted in a quantitative load elongation stage of a high voltage electron microscope and pulled to failure while recording the crack propagation behavior with a video camera. From these recordings the following microscopic characteristics of the crack propagation were determined: direction with respect to grain orientation, crack tip opening displacement, deformation zone ahead of the crack tip, crack length, mode of opening and the concurrent load, elongation and elongation rate. All of these variables combine to permit a detailed analysis of the crack propagation and to model its behavior.

SUMMARY

Several models have been developed and tested against the experimental data. Fracture toughness models can account for the experimental values of toughness. Minimum strain energy release and maximum stress criteria are applied to the system in order to account for the direction of crack propagation. Only limited success was found with these two approaches. The relationship between models successful in bulk cases to those models successful in this thin film case is explored. The values of specimen thickness employed here is several micrometers, i.e. a thickness intermediate between bulk and very thin

films. This intermediate region of thickness shows behavior not seen in thin films but approaching that in bulk specimens.

*Present address: Nippon Steel Corp., Kosugi Ryo 419, Imainaka-Cho 317-2, Kawasaki, Japan 211.

INSIGHTS INTO THE FRACTURE TOUGHNESS OF MARTENSITIC STAINLESS STEELS USING STEREOSCOPIC FRACTOGRAPHIC MEASUREMENTS

D. S. GELLES
Westinghouse Hanford Company, W/A-65, P. O. Box 1970, Richland, WA

Stereoscopic fractographs of precracked compact tension and precracked miniature Charpy impact test specimens can provide critical crack opening displacement (COD) measurements (δ_c) on a microstructural scale [1]. Based on a relationship proposed by Wells [2] which compares the critical crack extension force (G_c) and critical COD (δ_c) and involves the yield strength σ_y, $G_c = n \sigma_y \delta_c$ ...(1) where n is a plastic stress intensity factor expected to vary between 1 for plane stress and 2 for plane strain, one can show $J_{1c} = m \sigma_y \delta_c$ .....(2) with m varying between 1 and 2. A technique for measuring δ_c using fractographic information can be envisioned from Figure 1 such that δ_c is the sum of $\Delta 1 + \Delta 2$. If one measures the height of a feature above the fatigue surface for a feature which can be identified on both halves of a fracture surface, then COD as a function of Δa can be determined and δ_c can be estimated. Similar techniques have been developed elsewhere [3-5].

This approach to fractographic analysis has been applied to two martensitic stainless steels, Sandvik HT-9 (Fe-12Cr-0.2C-1Mo-0.5W-0.3V-0.5Ni-0.4Si-0.6Mn) and ASTM Grade T91 (Fe-9Cr-0.1C-1Mo-0.2V-0.1Nb-0.3Si-0.5Mn). Miniature compact tension specimens were tested to provide J_{Ic} measurements [6-8], heat tinted prior to fracture of the remaining ligament and then examined by scanning electron microscopy. Examples of three such specimens are provided in Figure 2. Figure 2a shows a specimen of fully heat treated HT-9 tested at room temperature. The figure is arranged as a stereo pair to show both halves of the fracture surface with the fatigue surface at the center. Folding the stereo model along the vertical center line would allow the two surfaces to match. The fracture surface appears corregated with the axis of the corregation parallel to the original fatigue crack. Where a protrusion appears on one half of the specimen, a depression matches it on the other half. The corregation arises from the presence of delta ferrite stringers which provide crack nucleation sites. Figure 2b shows a specimen of fully heat treated T91 tested at 230°C. The fatigue surfaces, stretch zone and dimple rupture regions are more easily identified. However, several examples of dimple rupture can be found in regions close to the fatigue surface and therefore dimple rupture did occur during stretch zone formation. A third example is given in Figure 2c which shows a weld specimen of T91 which was tested at 205°C. Dimple rupture is on a much finer scale and the transition from stretch zone to dimple rupture is more clearly defined. However, even in this case examples of dimple rupture can be found on stretch zone surfaces.

Evaluation of the parameter m confirms this conclusion. "m" is found to vary from 1.7 to 2.7 with large uncertainties found in a given specimen as a result of area to area variations. It appears that crack growth is a result of non-uniform crack propagation which is averaged by bulk measurements. Therefore, Figure 1 is highly idealized. Cavity nucleation, growth and fracture of the remaining ligament can occur prior to reaching δ_c and J_{1c} or δ_c only represents a fracture energy where

failure is almost exclusively by dimple rupture failure. The concept of a blunting line is a simplification in complex martensitic steels.

REFERENCES

1. D. S. Gelles, F. H. Huang & N. F. Panayotou, Alloy Development for Irradiation Performance Progress Report, DOE/ER-0045/8, 442-459 (1982).
2. A. A. Wells, Eng. Fract. Mech., 1, 399-410 (1969).
3. T. Kobayashi, G. R. Irwin & X. J. Zhang, in Fractography of Ceramic and Metal Failures, ASTM STP 827, 234-251 (1984).
4. W. Cao and X. Lu, Int. J. Fracture, 25, 33-52 (1984).
5. O. Koledink and H. P. Stuive, Eng. Frac. Mec., 21, 145-155 (1985).
6. F. H. Huang & G. L. Wire, ibid ref. 1, DOE/ER-0045/3, 236-254 (1980).
7. F. H. Huang & G. L. Wire, ibid, DOE/ER-0045/7, 220-229 (1982).
8. F. H. Huang, ibid, DOE/ER-0045/9, 221-230 (1983).

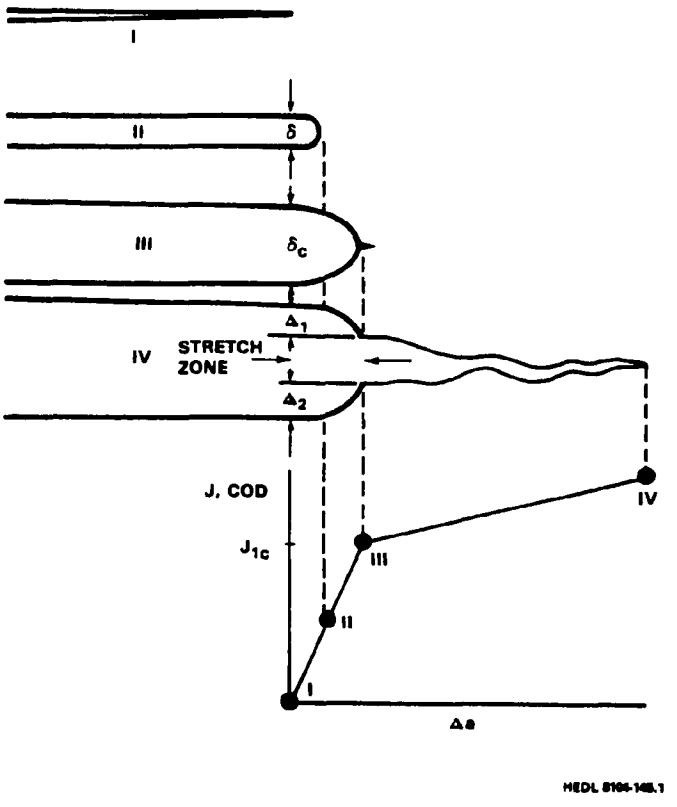

FIGURE 1. Schematic Diagram of the Sequence of Events which Occur at a Sharp Crack Tip in Comparison with Behavior on a Corresponding J-R Curve.

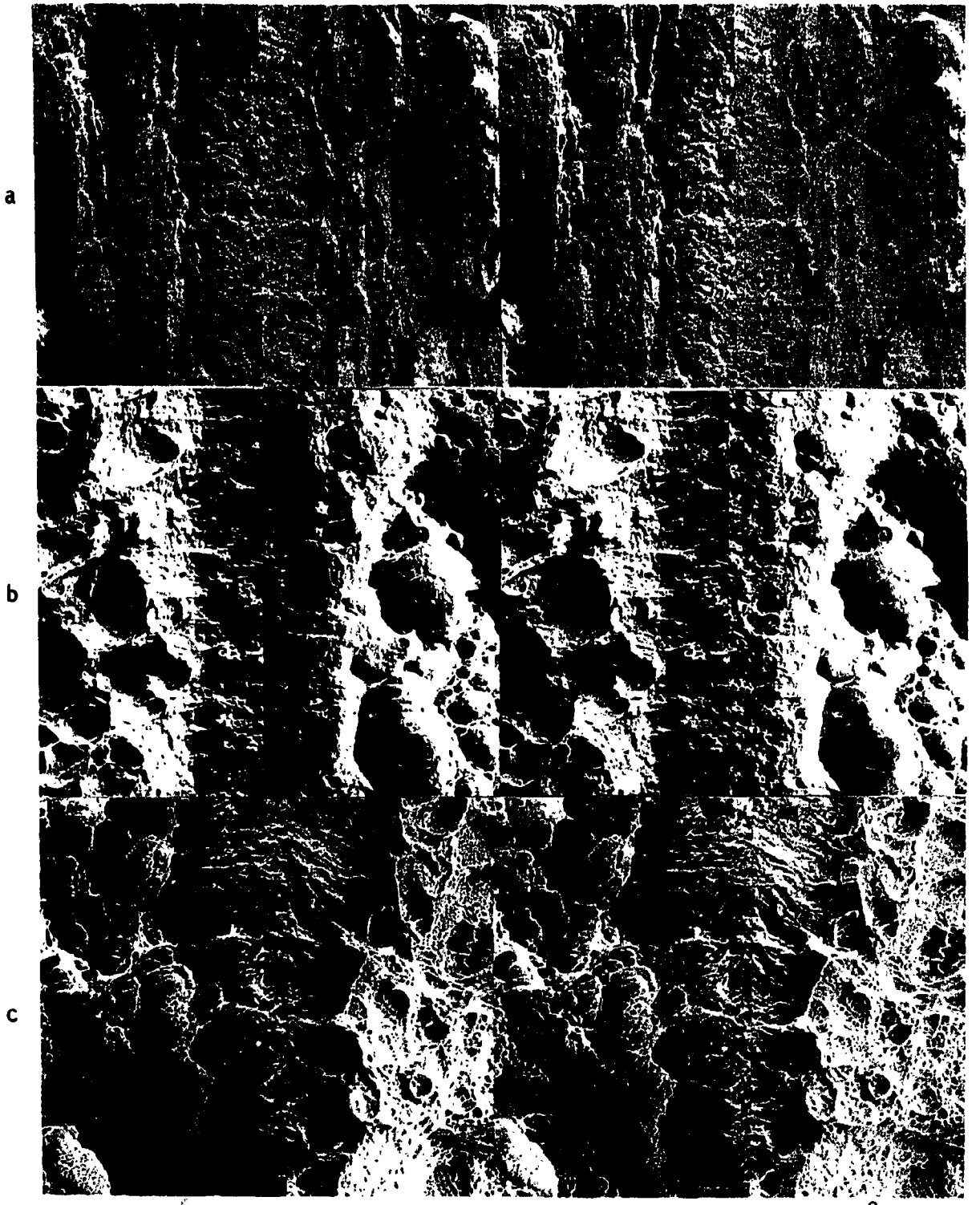

FIGURE 2. Stereo Pair Fractographs of a) HT-9 with J_{1c} = 112 KJ/m^2 and T = 121, b) T91 with J_{1c} = 72 KJ/m^2 and T = 177, and c) T91 weld metal with J_{1c} = 78 KJ/m^2 and T = 107.

THE APPLICATION OF STATISTICAL MODEL OF CLEAVAGE K_{1c} TO HOT-WORK DIE STEEL AND ITS TOUGHENING BY DOUBLE QUENCHING TREATMENT

Zheng Mingxin, Chen Baoluo and Cai Qi-gong
Department of Mechanical Engineering,
Tsinghua University, China

INTRODUCTION

In many cases, the premature brittle fracture of hot-work dies is induced by the unstable propagation of thermal fatigue cracks. However, it was found that the life of hot-work dies could be increased greatly, if the fracture toughness of die steel was improved. Using a double quenching treatment with a higher temperature of the first quenching [1] instead of the conventional one (spheroidize annealing and quenching), an increase in fracture toughness at the same level of strength had been obtained, and, consequently, it should have been beneficial to the die life.

EXPERIMENTAL

The material was available from two heats (A,B) of the same steel grade 3Cr2W8V, the composition (in wt%) of which is as follows:

heat A C-0.38, Cr-2.90, W-8.25, V-0.47, Si-0.20, Mn-0.22, P-0.027, S-0.008

heat B C-0.33, Cr-2.38, W-8.26, V-0.38, Si-0.17, Mn-0.20, P-0.005, S-0.005

Specimens of the fracture toughness (13X26X190mm) and tensile tests (Φ5mm) were cut both along the rolling direction and perpendicular, and the tests were conducted in an Instron testing machine at a cross head speed of 1mm/mm. After testing machanical properties the specimens were examined by light and scanning electron microscopes.

The heat treatment of specimens carried cut was shown by lines in Fig.1.

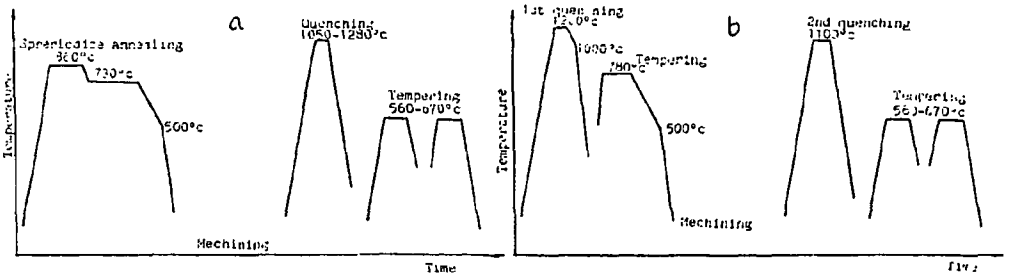

Fig.1 Heat treatment conditions for specimens
a-conventional treatment; b-double quenching treatment

RESULTS AND DISCUSSION

Results of fracture toughness testing are presented graphically in Fig.2, which indicates that K_{1C} increases with increase in quenching and tempering temperatures, while the values measured for double quenching treatment are always higher than that for the conventional one under the same temperature conditions.

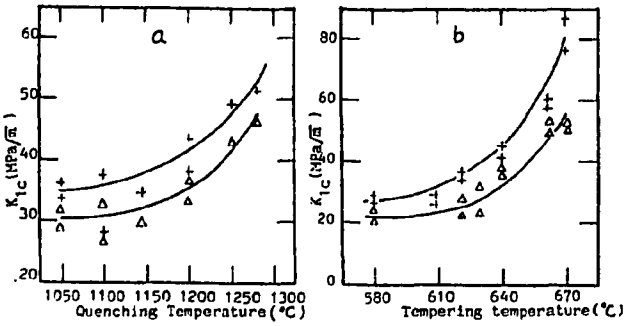

Fig.2 Variations of fracture toughness with quenching (a) and tempering temperatures (b)

SEM examinations of the fractures near the crack tip region shows that the fracture occurs by quasi-cleavage mechanism and is initiated by cracked residual carbides M_6C retained after quenching. The size distribution of residual carbide particles was determined by quantitative metallographic techniques, as shown in Fig.3. The result shows that for those largest ($2r \geqslant 2\mu m$) residual carbides that might initiate cleavage fracture, the probability density function f(r) of the particle radius (r) can be approximated by

$$f(r)=(n-1)r_0^{n-1}r^{-n}, \qquad (1)$$

where r_0 is a parameter associated with the size distribution of particles and n an experimental coefficient.

Based on the size distribution function of cracked carbides and the local Griffith fracture criterion, the cleavage fracture toughness K_{1c} can be formulated as [2]

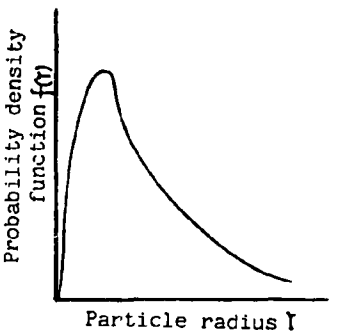

Fig.3 f(r) versus r

$$B\,\sigma_{ys}^{m}\left(\frac{K_{1c}}{\sigma_{ys}}\right)^{4}\cdot F(m,n)=\sigma_u^{m}V_u\ln\left(\frac{1}{1-p}\right) \qquad (2)$$

where V_u is the mean volume of cracks and P the probability of fracture initiated by carbide cracks under the normal stress σ_1. Or in the mean value form,

$$K_{1c} \cdot \sigma_{ys}^{\frac{m}{4}-1} = \left[\Gamma(1+\frac{1}{4})\right] \left[\sigma_u^m V_u / BF(m,n)\right]^{\frac{1}{4}} \qquad (3)$$

with $m=2(n-1)$, and $F(m,n)=\iint \left(\frac{\sigma_1(u,o)}{\sigma_{ys}}\right)^m \left(\frac{\tilde{\sigma}_1(\theta)}{\tilde{\sigma}_1(0)}\right)^m du\,d\theta$ also $\sigma_u=\left[\frac{\pi E \gamma_p}{2(1-\nu^2)r_0}\right]^{\frac{1}{2}}$.

Because carbides W_6C can form during tempering only at an elevated temperature [3,4], it may be possible to consider that the size and distribution of the large residual carbide particles are not substantially changed at tempering in the range used. And, at this time the matrix of the steel must have got a structure with an approximately definite dislocation density, and hence the effective surface energy of cleavage fracture must also abtain an approximately definite value. Based on these, it can be made an assumption that in the tempering range of 560~670°C the characteristic $\sigma_u^m V_u$ of the Weibull statistical model keeps a relatively constant value. Therefore, under the condition of quasi-cleavage fracture the relationship given by equation (3), can be approximately written in the following form:

$$\bar{K}_{1c} \cdot \sigma_{ys}^{\frac{m}{4}-1} = \text{const} \qquad (4)$$

Testing results (Tab.1) indicate that the assumption can be considered valid, and the agreement between experimental results and predicted values is satisfactory with a scatter band of cleavage K_{1c} expressed by

Tab.1 Testing results

Heat treatment	$\bar{K}_{1c}$-$\sigma_{0.2}$ relationship	Corelation coefficient	m
Conventional treatment (quenched from 1100°C)	$\bar{K}_{1c}\cdot\sigma_{0.2}^{1.66}=10^{6.72}$ (MPa$^{2.66}\sqrt{m}$)	0.95	10.64
Double quenching treatment (quenched from 1100°C)	$\bar{K}_{1c}\cdot\sigma_{0.2}^{1.96}=10^{7.72}$ (MPa$^{2.96}\sqrt{m}$)	0.98	11.84

$$K_{1c} = \frac{\left[\ln(\frac{1}{1-p})\right]^{\frac{1}{4}}}{\Gamma(1+\frac{1}{4})} \bar{K}_{1c} \quad , \qquad (5)$$

from which the $\bar{K}_{1c} - \sigma_{0.2}$ curves are obtained, shown in Fig.4. Obviously, the scatter band lies entirely in the range of probabilities from p = 0.1 to p = 0.9.
Besides, the effective surface energy γ_p of cleavage fracture

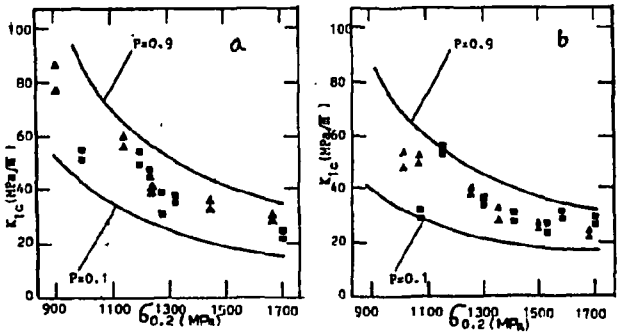

Fig.4 $\overline{K}_{1c}$ - $\sigma_{0.2}$ curves

▲ Axial
■ Perpendicular

a-heat A for double quenching treatment; b-heat A for conventional treatment

propagation was calculated by using the measured cleavage stress σ_f^*, some values of which are given in Tab.2.

Tab.2 Some values of cleavage stress σ_f^*

Heat treatment conditions (°C)	Yield stress σ_{ys} (MPa)		Cleavage stress σ_f^* (MPa)	
Quenched from 1100 Tempered at 610	1660	3776	3460	3847
Quenched from 1100 Tempered at 580	1750	3591	3847	3796

According to the size distribution of carbides M_6C in the steel (Fig.3) tempered at 580°C, the largest residual carbides that might initiate cleavage fracture are as follows:
the size of carbide particle with a probability density higher than 10%, or $(2r)_{30\%}$ = 1.40mm; the size of carbide particle with a probability density high than 20%, or $(2r)_{80\%}$ = 1.12mm. Substituting these data into $\gamma_p=(1-\nu^2)d\sigma_f^2/\pi E$, we have γ_p=24.6, 19.7 J/m for (2r)=d=1.40, 1.12mm, respectively.
Similarly, for the steel tempered at 610°C γ_p=25.8, 20.6 J/m. Therefore, the effective surface energy of cleavage fracture propagation in steel 3Cr2W8V γ_p=20~25 J/m. This value is somewhat higher than that of the ferrite matrix and it may be explained by the higher dislocation density in the tempered martensite matrix of the die steel. It is obvious, as can be seen in Fig.5, that the mean distance between carbide particles gradually increases with increasing quenching temperature, and the law of variation is similar to that of fracture toughness of the steel tempered at temperatures near and higher than the secondary hardening peak. The analysis of our quantitative metallographic determination reveals that this variation is associated with the dissolution of carbides in matrix in appreciable quantities. The same type of relationship and similar consideration had also been presented by V.F.Zackay[5].

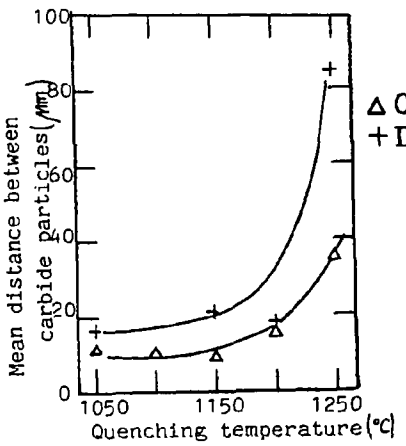

Fig.5 Mean distance between carbide particles versus quenching temperature (heat B)

CONCLUSIONS

1. When the hot-work die steel 3Cr2W8V is tempered at temperatures higher than the secondary hardening peak, its yield strength increases and the fracture toughness decreases. Under the same quenching temperature conditions, there is an approximate relationship between yield strength and fracture toughness, as described by

$$\overline{K}_{1c} \cdot \sigma_{0.2}^{\frac{m}{4}-1} = \text{const} \quad ,$$

which well adapts for the Weibull statistical model of quasi-cleavage fracture toughness.

2. When the steel is tempered near the secondary hardening peak temperature, its fracture toughness increases with increasing quenching temperature, and as the temperature approaches to 1250°C, the fracture toughness may get a much higher value.

3. The replacement of the conventional heat treatment by the double quenching one with higher temperature of the first quenching must be beneficial to improving the hot-work die life.

REFERENCES

1 Cao Wei-Di et al, Heat Treatment of Metals, 10, 30(1981).
2 A.Pineau, ICF5, 2, 553(1981).
3 K.J.Kuo, J.Iron and Steel Inst. 174, 223 (1953)
4 T.Sato, T.Nishizawa and K.Murai,Tetsuto-Hagane, 44, 1378(1958).
5 V.F.Zackay, E.R.Parker, R.D.Gools by and W.E.Wood, Nature Phys. Sci., 236, 108(1972).

DELAYED FRACTURE UNDER MODE II LOADING

Tong-Yi Zhang, Wu-Yang Chu, Ying Li and Chi-Mei Hsiao
Dept. of Metal Physics, Beijing University of Iron and Steel Technology
CHINA

Hydrogen induced cracking (HIC) and stress corrosion cracking (SCC) of a high-strength steel $34CrNi_3Mo$ (T.S.=1700MPa) under Mode II loading were investigated with notched specimens. The stress field around the notch tip was analysed by means of finite element method. The origin of coordinate system (xoy) is selected in the interior of the notch and at distance $\rho/2$ from the notch tip, where ρ is curvature radius of the notch tip. The site of each point on the notch surface and the direction of stress components at the points are denoted by angle θ and α, respectively, as shown in Fig.1. The maximum shear stress on the whole notch surface τ_{max} is located at $\theta=80^{\circ}$, i.e. the point A in Fig.1, and its direction is $\alpha=5^{\circ}$. The maximum hydrostatic stress σ_{hmax} and the maximum principal stress σ_{1max} on whole notch surface is located at $\theta=-110^{\circ}$, i.e. the point B in Fig.1. The directions of σ_{1max} and τ^* are $\alpha=10^{\circ}$ and $\alpha=-35^{\circ}$, respectively, as shown in Fig.1, where τ^* denotes the maximum shear stress at the point B, i.e. at $\theta=-110^{\circ}$.

The initiation and propogation of HIC under Mode II loading were traced with a metallograph. The specimen would be unloaded as soon as the initiation of HIC was found. Therefore, the site and the direction of HIC during initiation could be determined certainly. A typical photograph of HIC initiation is illustrated in Fig.2. The cracking initiated at site B in the back of notch tip, i.e. $\theta=-110^{\circ}$, where the hydrostatic stress had the maximum value. The HIC was along the maximum shear stress τ^* at site B, i.e. $\alpha=-35^{\circ}$, not normal to the direction of σ_{1max} at the same site. The average measured value of α and θ for 7 specimens were -38° and -107°, respectively, which were basely consitent with the calculation values $\alpha=-35^{\circ}$ and $\theta=-110^{\circ}$. It can be concluded that HIC initiates at the maximum hydrostatic stress site and is along the maximum shear stress direction at that site. The initiation of SCC in 3.5% NaCl solution under Mode II loading is the same as SIC.

On the contrary, if the specimens are loaded to fracture in air under Mode II loading the cracking is in the maximum shear stress site around the notch tip and the cracking direction coincides with the direction coincides with the direction of the maximum shear stress, as shown in Fig.3. Above facts indicate that hydrogen induced delayed plastic deformation is a necessary condition for HIC and the nature of SCC for high-strength steel in 3.5% NaCl solution is HIC.

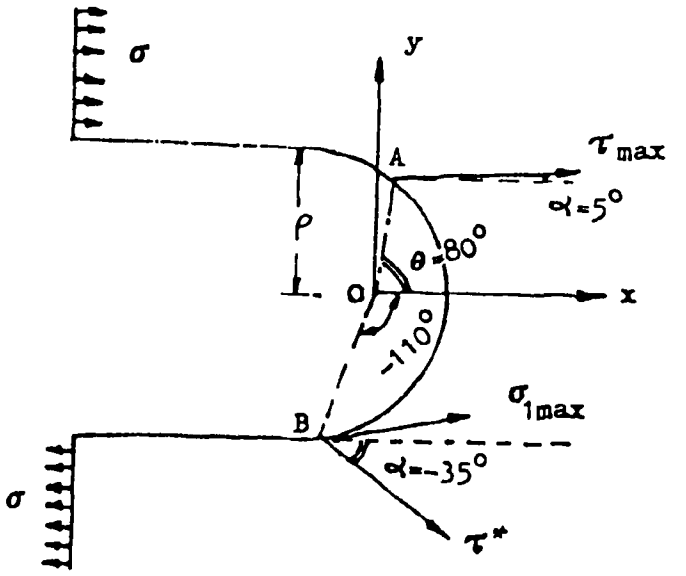

Fig.1. The sites and directions of the maximum hydrostatic stress σ_{hmax}, maximum principal stress σ_{1max}, maximum shear stress τ_{max} on the whole notch surface.

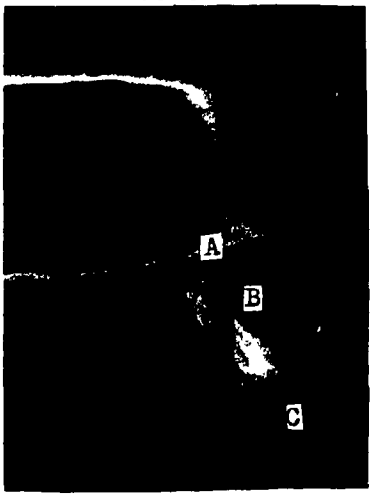

Fig.2. The site and direction of HIC under Mode II loading. A B for crack, B C for plastic zone. (dark field x160)

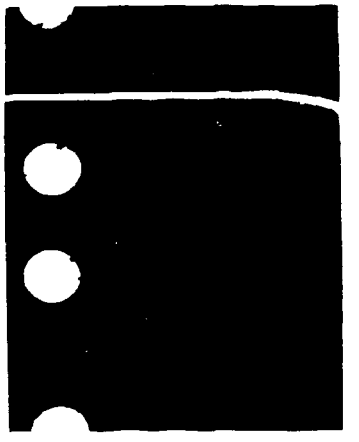

Fig.3. Mode II specimens overloaded in air.

FRACTO-EMISSION: PARTICLES FROM THE FRACTURE OF SOLIDS*

J. THOMAS DICKINSON, LES C. JENSEN, AND M. RANDY MCKAY
Department of Physics, Washington State University, Pullman, WA 99164

INTRODUCTION

We have been investigating the emission of particles due to deformation and fracture of materials [1-3 and references therein]. We observe the emission of electrons, ions, neutral species, photons (triboluminesence), as well as long wavelength electromagnetic radiation; collectively we refer to these emissions as **fracto-emission (FE)**. The goals of our research are to characterize the properties of FE, determine the mechanisms for each emission component, and relate the FE behavior to the physics and chemistry of deformation and fracture of interesting materials and systems. The properties of the emission we measure include identification of the emitted species, total intensities, time distributions relative to crack growth, energies, and correlations in time between various FE components. The dependence of these characteristics on the material properties, locus of fracture, crack velocity, and temperature have also been investigated. The emission effects can be observed over a wide range of materials. We have made a number of FE measurements on inorganic single crystals, ceramics, organic molecular cyrstals, polymers, composites, and interfaces. As we continue to gain understanding of the mechanisms of FE, we hope to provide detailed information about crack propagation and failure mechanisms. In this presentation, we show recent results on specific FE components accompanying the fracture of inorganic single crystals, in particular, neutral species.

RESULTS ON NEUTRAL EMISSION FROM INORGANIC SINGLE CRYSTALS.

We have been investigating the emission of neutral species from oriented single crystals of pure alkali halides, and metal oxides. A quadrupole mass spectrometer is used to mass select ions created by electron impact. Fracture was produced by three point bend. For the first time we have observed the emission of atomic species accompanying the fracture of such materials. Figures 1 and 2 show the mass 23 (Na) and 35 (Cl) signals from two different specimens of NaCl. No significant

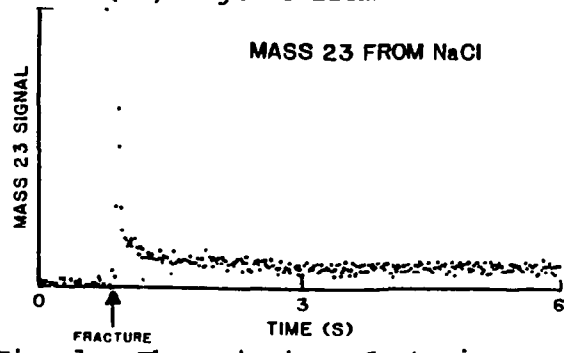

Fig. 1. The emission of atomic sodium from fracture of NaCl.

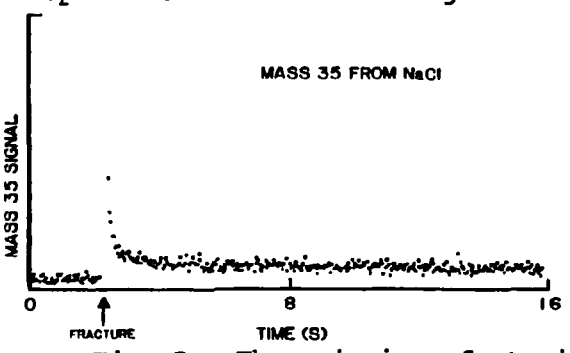

Fig. 2. The emission of atomic clorine from fracture of NaCl.

mass 58 (and 60) from molecular NaCl is observed; thus, these signals are from the emission of atoms. An additional intense mass peak from NaCl is mass 36 (HCl). Similarly, from LiF we observe Li, F, and HF from LiF. We have evidence that the HF and HCl observed are a result of fracturing LiF and NaCl crystals that contain dissociated water molecules. Fracture drives a chemical reaction that favors HX evolution over H_2O (gas) formation.

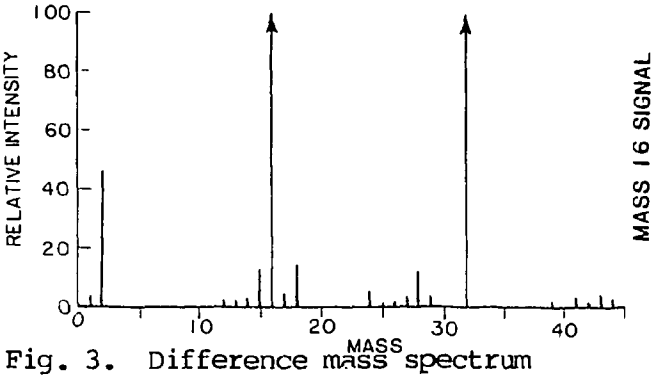

Fig. 3. Difference mass spectrum of neutral emission from MgO.

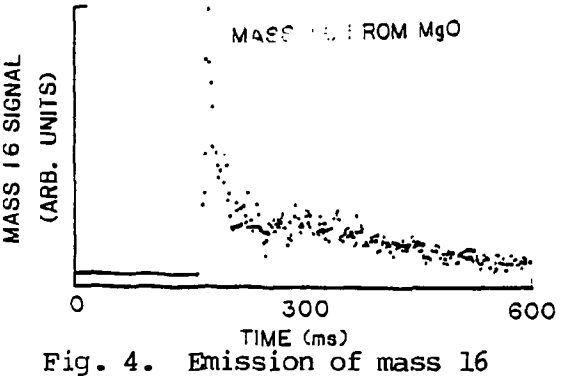

Fig. 4. Emission of mass 16 from fracture of MgO.

Fig. 3 shows a difference curve between two mass scans taken immediately before and after fracture of single crystal MgO (total time/scan = 80 ms). Frequently observed emission peaks were masses 44, 32, 28, 24, 16, 15, and 2. Figure 4 shows the mass 16 emission from MgO vs time. Tentative assignment to the parent species released are CO_2, O_2, CO, atomic Mg, CH_4 and H_2. Other hydrocarbons were frequently detected. Mass 16 is due to contributions from O_2, CH_4, and perhaps some atomic O. MgO contains a wealth of impurities which contribute to these emissions. The carbon containing compounds observed are due to chemical reactions accompanying and following fracture with bulk (impurity) carbon with O type defects (e.g., O^-, a positive hole) and dissolved hydrogen. It is important to note that these compounds do not exist in the crystal prior to fracture. The fracture surface is acting as a catalyst for recombination reactions of the reactive species in the crystal. The atomic Mg is more likely a product inherent to bond breaking of the crystalline MgO itself.

REFERENCES

1. J. T. Dickinson, L. C. Jensen, and A. Jahan-Latibari, J. Vac. Sci. Technol.A 2, 1112 (1984).

2. J. T. Dickinson, W. D. Williams, and L. C. Jensen, J. Am. Ceramics Soc. 68 235 (1985).

3. L. A. K'Singam, J. T. Dickinson, and L. C. Jensen, "Electron and Photon Emission Accompanying Failure of Metal/Glass Interfaces," to appear in J. Am. Ceramics Soc.

*Work supported by National Science Foundation (DMR 8210406) and Office of Naval Research (Contract N00014-80-C-0213, NR 659-803).

THE INFLUENCE OF HYDROGEN ON DEFORMATION AND FRACTURE PROCESSES IN HIGH-STRENGTH ALUMINUM ALLOYS*

G.M. BOND, I.M. ROBERTSON AND H.K. BIRNBAUM
University of Illinois, Dept. of Metallurgy and Mining Engineering and the Materials Research Laboratory, Urbana, IL 61801

The effects that hydrogen in solid solution and in the environment has on the dislocation mobility and fracture of age-hardened 7050 and 7075 Al-Zn-Mg alloys have been investigated by the in-situ TEM deformation technique. The in-situ environmental cell studies were performed in the HVEM environmental cell facility at Argonne National Laboratory. Both peak-aged and over-aged materials were examined, some samples being cathodically charged prior to testing.

The large silicon- and iron-rich constituent precipitates influenced crack initiation and propagation in charged samples from both alloys in both tempers. Microcracks initiated at these precipitates, Figure 1, and the path of propagating cracks deviated towards the precipitates. Cracks tended to pass through the matrix near the precipitates rather than cutting through them or causing decohesion along the matrix-precipitate interface. This type of interaction between the crack and precipitate was only observed when hydrogen was present. A simliar association between cracks and coarse precipitates was found by Pickens et al. [1] for stress-corrosion cracks in Al-7075. They attributed this association to greater hydrogen penetration of the oxide at surface precipitates. This mechanism may account for a high hydrogen intake into the sample but cannot account for the present observations since the particles observed by TEM were not near the surface during charging.

The distribution of hydrogen in the sample was investigated by examination of deuterium-charged samples in the SIMS. A step-scan profile of the deuterium distribution in an Al-7050 sample is shown in Figure 2. From the figure, it can be seen that the deuterium concentration is significantly higher in the vicinity of iron- and silicon-containing particles. The profile also shows that the deuterium distribution follows closely that of carbon, even in the matrix; this can be attributed to the association of deuterium with interstitial carbon. These observations suggest that hydrogen accumulates around the precipitates. The initiation of microcracks and the deviation of propagating cracks can then be explained in terms of hydrogen causing a local softening around the precipitates.

The introduction of either dry or water-saturated hydrogen atmospheres during in-situ HVEM deformation experiments increased the dislocation mobility and crack propagation rate in both alloys; similar

*Work supported by DOE, Division of Materials Science through contract DE AC02 76ER01198.

results were obtained in pure aluminum samples [2]. (The effectiveness of dry hydrogen results from the increased fugacity caused by the dissociation of molecular hydrogen in the electron beam). Irrespective of the crack path (intergranular or transgranular), the presence of hydrogen reduced the stress required to cause crack propagation and tended to localize the deformation ahead of the crack; this is similar to the effect of hydrogen on other materials (Ni [3], Fe [4]). There was no evidence that the presence of hydrogen caused decohesion. When intergranular fracture occurred, the crack propagated in the vicinity of the boundary rather than along the boundary interface, as has been observed previously in nickel [3].

FIG. 1. Microcracks and plastic thinning near coarse precipitates in hydrogen-charged Al-7075 under tension.

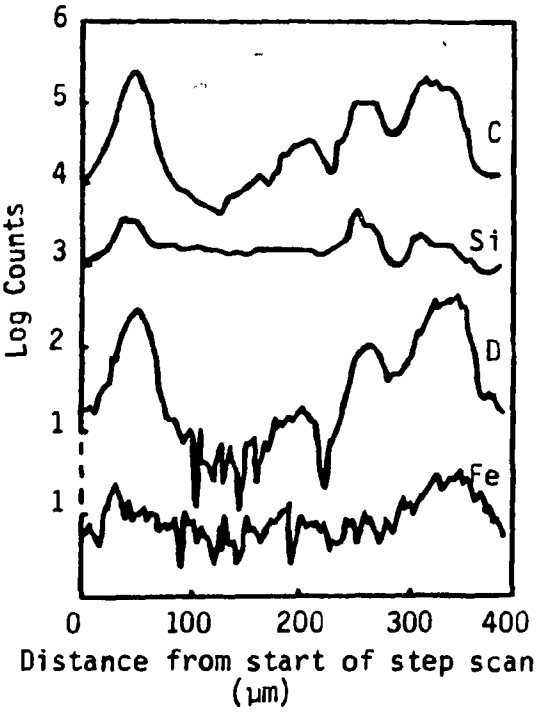

FIG. 2. SIMS step-scan profile along line of coarse precipitates in deuterium-charged Al-7050.

REFERENCES

1. J.R. Pickens, J.R. Gordon, and L. Christodoulou, Proc. Symp. on High-Strength Powder Metallurgy Aluminum Alloys, Ed. M.J. Koczak and G.J. Hildeman, AIME, 177-192 (1982).
2. G.M. Bond, I.M. Robertson, and H.K. Birnbaum, unpublished work.
3. I.M. Robertson and H.K. Birnbaum, to be published in Acta Met. (1985).
4. T. Tabata and H.K. Birnbaum, Scripta Met. 18, 231-236 (1984).

MECHANISM OF HYDROGEN INDUCED SOFTENING

Tong-Yi Zhang, Wu-Yang Chu, Chi-Mei Hsiao
Department of Metal Physics, Beijing University of Iron and Steel Technology, Beijing, CHINA

The calculation based Boltzmann distribution shows that the strain field of hydrogen in α-Fe is of intensive tetragonal symmetry, e.g., $\varepsilon_{11}=0.1772$, $\varepsilon_{22}=\varepsilon_{33}=0.0026$. Therefore, there is an elastic interaction between hydrogen and a screw dislocation and the minimum of the interaction energy is about 28KJ/mol.

The equilibrium hydrogen concentrations around the screw dislocation under Boltzmann distribution and Fermi-Dirac distribution can be represented as follows, respectively:

$$C_i=C_o \exp(-u_i/kT), \quad C_i^*=C_o \exp(-u_i/kT)/(1+C_o \exp(-u_i/kT)) \qquad (1)$$

where i=1,2,3 stands for that the largest strain component ε_{11} is along [100], [010] and [001] direction respectively. The C_i or C_i^* has the trigonal symmetry around the screw dislocation. When an external stress σ is applied along the [001] direction, the active slip system will be [111] $(\bar{1}\bar{1}2)$, i.e., the direction of the external force acting on the screw dislocation should be the [$\bar{1}$10].

The interaction energies between the stress σ along the [001] direction and the strain field of hydrogen with ε_{11} in the [100], [010] and [001] directions are as follows, respectively:

$$E_1=E_2=-a^3\varepsilon_{22}\sigma, \quad E_3=-a^3\varepsilon_{11}\sigma \qquad (2)$$

Then, the interaction energy u_i' between hydrogen and the resultant stress field, which equals to the external stress plus the stress field of the screw dislocation, is given by $u_i'=u_i+E_i$. E_i does not have the trigonal symmetry around the screw dislocation, so does u_i'. Under the resultant stress field, the hydrogen atoms in the atmosphere have to be rearranged, because the rate of hydrogen diffusion is faster than the motion speed of dislocation, only if the temperature is not very low.

The equilibrium hydrogen concentrations under the resultant stress field for the Boltzmann and Fermi-Dirac distribution are, respectively:

$$C_i'=C_o \exp(-u_i'/kT) \qquad C_i^{*'}=C_o \exp(-u_i'/kT)/(1+C_o\exp(-u_i'/kT)) \qquad (3)$$

Both of C_i' and $C_i^{*'}$ are not of the trigonal symmetry around the screw dislocation. Therefore, where the interaction energy u_i' has the minimum value there is the maximum concentration of hydrogen, and then the screw dislocation will move towards the direction in order to reduce the energy of the system. As a result, the asymmetrical atmosphere can produce an additional stress F_H on the screw dislocation.

If the resistant force, i.e. the yield strength τ_s, to the motion of dislocation is not effected by the hydrogen atoms, the screw dislocations in the samples containing hydrogen can multiply and move on a large scale and lead to macroscopical deformation when the resultant force of the external force and the additional force is equal to τ_s.

The τ_c/τ_s under various temperatures and initial concentrations of hydrogen has been calculated using the Fermi-Dirac distribution, as shown in Table 1.

Table 1. τ_c/τ_s under various conditions

T(K)	300	250	200
C_o	10^{-5}	10^{-7}	10^{-8}
τ_c/τ_s	0.37	0.53	0.21

Table 1 shows that the apparent yield stress τ_c is less than half of τ_s at room temperature and $C_o=10^{-5}$ (about 0.18 wppm). Thus, hydrogen induced plastic deformation may occur under a very low external stress. If there exists a stress gradient, e.g. ahead of a crack or notch, the C_o should be the local concentration of hydorgen, which has a higher value.

According to this model, the relationship between apparent yield stress and various factors of temperature, strain rate, initial hydrogen content was quantitatively analyzed. Besides this model predicts the change of slip plane in a charged specimen. All of the theoretical results are consistent with the experimental observation.

HYDROGEN AND IMPURITY SEGREGATION INDUCED SUBCRITICAL CRACK GROWTH OF FE AND NI*

R. H. JONES
Pacific Northwest Laboratory, P. O. Box 999
Richland, Washington 99352

INTRODUCTION

Differences in crystal structure, dislocation dynamics and hydrogen permeation would be expected to cause the fracture properties Fe and Ni to respond differently to impurity segregation and hydrogen. However, this is not the case as intergranular fracture of Fe and Ni has been induced separately by H [1,2] and S segregation [3,4] as well by combinations of S+H [4,5]. For the combined S+H case, the following processes could account for this similarity: 1) equal grain boundary permeation along S enriched grain boundaries, 2) equal bulk H transport due to dislocation transport of H in Ni and lattice diffusion in Fe, and 3) local (a few atom distances where bulk diffusion processes are not in effect) crack tip interaction between S and H.

RESULTS

Intergranular subcritical crack growth rate measurements have been made on Fe and Ni samples at cathodic potentials in 1N H_2SO_4 at 25°C. Samples with thicknesses of 2.5 mm, 5 mm and 10 mm were tested. Grain boundary sulfur concentrations as measured by Auger Electron Spectroscopy were about 0.2 monolayers in both. Plastic zone sizes were determined by electron channeling pattern analysis and microhardness, Fig. 1. Subcritical intergranular crack growth measurements at cathodic potentials showed that Fe and Ni have similar values of K_{TH} and comparable stage I and II crack growth rates, Fig. 2, while the K_{TH} for Fe decreased with increasing thickness and the K_{TH} for Ni was independent of thickness up to 10 mm, Fig. 3. Based on calculations, the plastic zone of both materials develops at a stress intensity equal to or less than the K_{TH}. This suggests that crack tip dislocations may be important in the crack growth process of both Fe and Ni.

SUMMARY

The subcritical crack growth behavior of Fe and Ni at cathodic potentials has been shown to be very similar. This similarity is thought to result from an equal H permeation rate along S enriched grain boundaries in Fe and Ni.

*Research sponsored by the Division of Materials Sciences of U.S. Department of Energy, under Contract DE-AC06-76RLO 1830 with Battelle Memorial Institute.

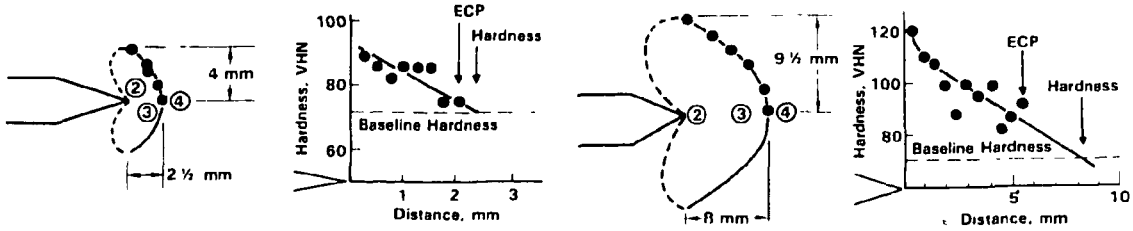

(a) (b)

FIG. 1 Microhardness profile of the plastic zone size for 10mm thick (a) Fe loaded to 30 MPa √m (elastic) and (b) Ni loaded to 60 MPa √m (elastic-plastic).

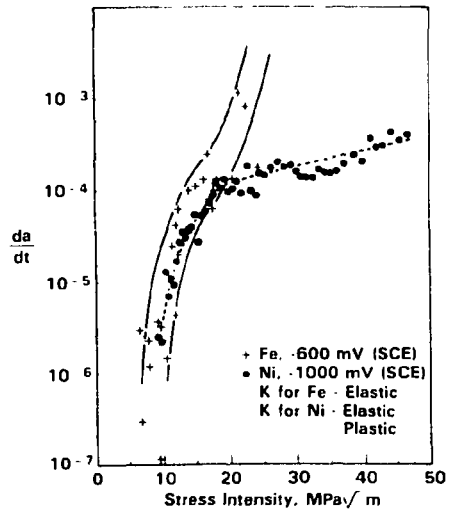

FIG. 2 Subcritical crack growth of Fe and Ni.

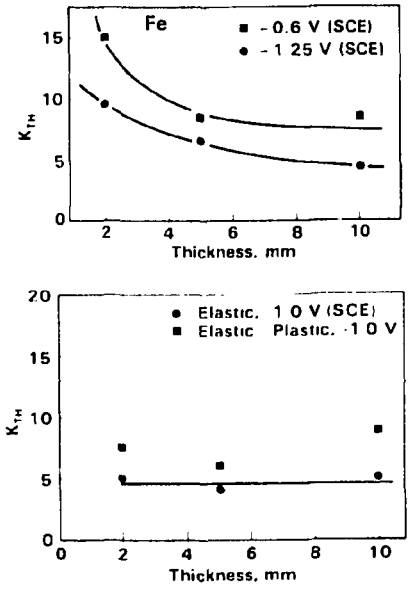

FIG. 3 K_{TH} versus thickness for Fe and Ni.

REFERENCES

1. S. Talbot-Besnard, in Atomistics of Fracture, R.M. Latanision and J.R. Pickens, eds., NATO Conference Series IV, (Plenum Press, NY, 1983) pp. 889-893.
2. J. Eastman, T. Matsumoto, N. Narita, F. Heubaum, and H.K. Birnbaum, in Hydrogen Effects in Metals, I.M. Bernstein and A.W. Thompson, eds., (TMS-AIME), Warrendale, PA, 1980) pp. 397-409.
3. K.S. Shin and M. Meshii, Acta Metall. 31, 1559-1566 (1983).
4. R.H. Jones, S.M. Bruemmer, M.T. Thomas, and D.R. Baer, Metall. Trans. 14A, 1729-1736 (1983).
5. S.M. Bruemmer, R.H. Jones, M.T. Thomas, and D.R. Baer, Scripta Met., 14A, 1729-1736 (1983).

STRESS CORROSION CRACKING OF AN ALUMINUM ALLOY UNDER COMPRESSIVE STRESS

Wu-Yang Chu,* Chi-Mei Hsiao* and Jun-Wen Wang*
*Dept. of Metal Physics, Beijing Univ. of Iron and Steel Technology, China.

Previous work showed that macroscopic compressive stress was able to induce stress corrosion cracking (SCC) of Type 304 stainless steel in a boiling 42 wt.% $MgCl_2$ solution (1). The incubation period of the SCC under compressive stress, however, was one to two orders of magnitude longer than that under tensile stress (1). Further work indicated that SCC of mild steels in a boiling nitrate solution under compressive stress could occur and the incubation period of SCC under compressive stress was also ten to hundred times longer than that under tensile stress (2).

A thinned WOL notched specimen of 7075 aluminum alloy is used. Thickness of the specimen is 2.5 mm but the loading part is thickened to 20 mm. The notch angle and the radius of the notch root are 60° and about 0.1mm, respectively. If the specimen is loaded with a bolt and a spacer, the notch open displacement V is positive and there is tensile stress at the notch tip. If the specimen is loaded in the opposite direction by the bolt through a half of the specimen, the displacement V is negative and there is compressive stress at the notch tip. This is confirmed qualitatively by the needle-compression method of photoelastic experiment and quantitatively via the finite-element computation.

A set of specimens with various K_I under compressive stress were tested in 3.5% NaCl aqueous solution and the times initiating SCC with 0.1 to 0.2 mm length, designated t_i, were recorded. The K_I vs t_i curve and then the threshold value nucleating stress corrosion cracking from the notch under compressive stress can be obtained, i.e., K_{ISCC}=27.6MPam$^{\frac{1}{2}}$. The corresponding threshold value under tensile stress is K_{ISCC}=8.3 MPam$^{\frac{1}{2}}$ and K_{IC} is 43.2 MPam$^{\frac{1}{2}}$, which corresponded to the opening displacement V=0.57 mm.

Experiment showed that the incubation period for SCC under the compressive stress was one order of magnitude longer than that under the tensile stress in the same K_I and the threshold value for SCC under the compressive stress was more than four times that under the tensile stress. In addition, if the unloading displacements after SCC under compressive stress are larger than 0.57 mm which corresponds to K_I=43.2MPam$^{\frac{1}{2}}$, the mechanical cracking would occur in these specimen during unloading since the K_I during unloading was larger than K_{IC}=43.2 MPam$^{\frac{1}{2}}$. This again proves that there exists compressive stress close to the notch tip in the compressive specimens throughout the SCC.

Experiment indicated that a typical intergranular fracture was obtained for stress corrosion cracking caused by tensile stress. The fracture surfaces of SCC under the compressive stress, however, were quite

different from those under the tensile stress. They were quasi-cleavage and parallel striation pattern was often observed on the fracture surface

1. W.Y.Chu, Y.Jao, and C.M.Hsiao, Corrosion 40, 302-306(1984).
2. W.Y.Chu, R.T.Ma, and C.M.Hsiao, scri. Metall. 18 579-582(1984).

OBSERVATIONS OF CREEP CAVITATION IN TYPE 304 STAINLESS STEEL

T.-S. Liu*, Y.-W. Wu*, R.J. Fields**, D.G. Harlow*, and T.J. Delph*
*Dept. of Mech. Eng. & Mechanics, Lehigh Univ., Bethlehem, PA 18015;
**Fracture & Deformation Div., N.B.S., Washington, D.C. 20234

Reported herein are some recent measurements of creep cavities in type 304 stainless steel. The data were obtained through the use of an automatic image analyzing computer, a device which is capable of making individual measurements of large numbers of creep cavities. The techniques used, as well as some preliminary results, are described in greater detail in [1].

The test program utilized flat, plane stress tensile specimens fabricated from strip stock of a commercial heat of AISI type 304 stainless steel. All specimens were tested in air at 600°C under constant load creep conditions. Two series of tests were conducted. The first was a set of replicate tests in which four groups of three specimens were tested under conditions identical for each group. The second involved a group of specimens tested at various loads and test durations, analyzed, retested at the same load for an additional period of time, and then reanalyzed. In all cases the central 3-4 cm. of the specimen test section was carefully polished prior to analyzis on the image analyzing computer. With the magnification used in the present study (406x), this device is capable of measuring cavity areas down to 1.7 μm^2. A sufficient number of fields were examined so that at least 1000 cavities were measured per specimen. The results were corrected for the presence of inclusions by measuring the inclusion size distribution on an uncavitated specimen, and subtracting this distribution from the measured cross-sectional area distribution.

Figure 1 is a histogram showing the measured distribution of cavity cross-sectional areas on a typical specimen. A well-defined peak in the distribution may be seen in the neighborhood of 15 μm^2. Figure 2 shows the same distribution plotted on Weibull probability paper. It can be seen that the probability distribution function for the measured cavity cross-sectional area is reasonably well represented by a Weibull cumulative distribution function over most of the range. Of interest is the fact that the slope of the distribution flattens towards the upper end of the curve, indicating a substantially greater degree of scatter in the size variations of the largest cavities.

The results indicate that the mean measured cavity area varies with time and applied stress according to the relation $A = Ct\sigma^{\alpha}$, where C and α are constants. The mean cavity areas obtained from the replicate tests are plotted according to this relation in Figure 3. The error bars indicate the standard deviation of the measured values within each group of tests. The correlation coefficient for the fit is greater than 0.99.

REFERENCES

1. T.-S. Liu et al Scripta Metall. 19, 299 (1985).

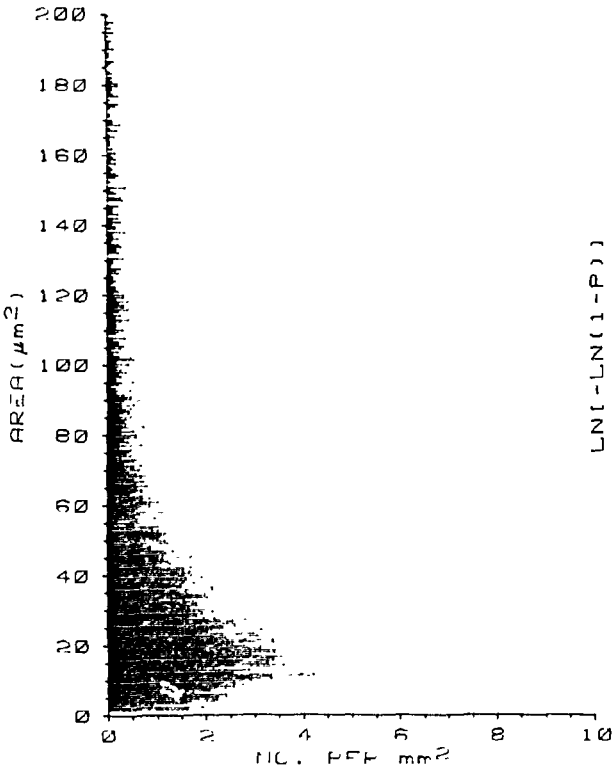

Fig. 1. Cavity area histogram

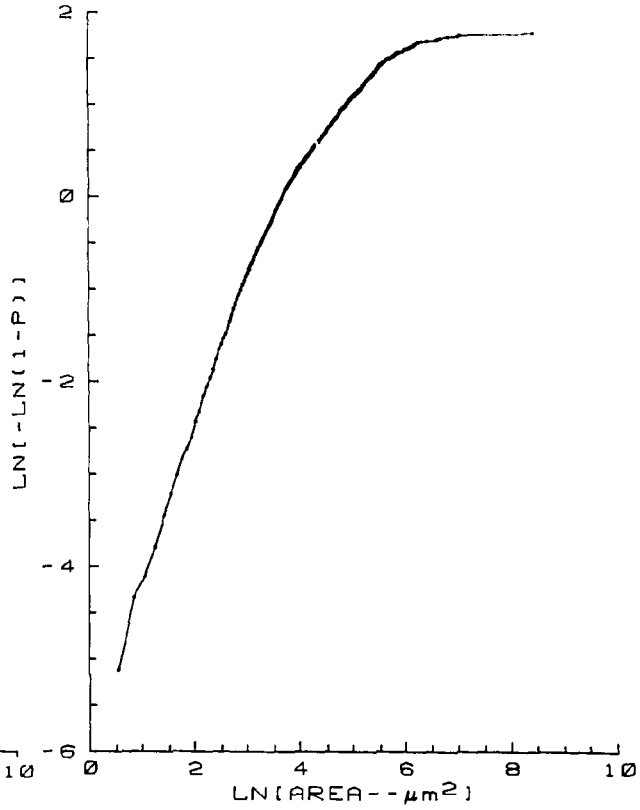

Fig. 2. Weibull plot of cavity area distribution

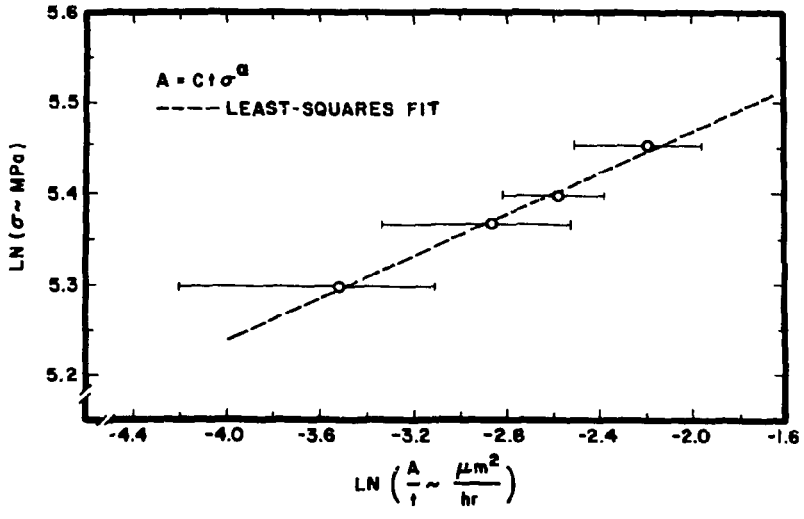

Fig. 3. Fit of mean cavity area for replicate tests

THE EFFECT OF SULPHUR SEGREGATION AND ALN PRECIPITATION ON THE HOT FRACTURE OF ULTRA HIGH PURITY IRON BASE ALLOYS.

M. TACIKOWSKI, G.A. OSINKOLU and A. KOBYLANSKI
Ecole Nationale Supérieure des Mines, Département Matériaux,
158 cours Fauriel, 42023 Saint-Etienne Cédex 2, France.

Low alloy carbon steel can exhibit a loss of hot workability. To understand this phenomenon alloys of ultra high purity iron containing only selected additions of trace elements were prepared. Three kinds of alloys were used : iron-sulphur (0 to 100 ppm) ; iron-aluminium (150 to 1000 ppm) -nitrogen (100 ppm), and iron with aluminium, nitrogen and sulphur. Hot ductility was examined by tensil test in the temperature range 800 to 1200°C at a strain rate $\dot{\varepsilon} = 2 \times 10^{-3}\ s^{-1}$.

In the iron-sulphur alloys (F[illegible] sulphur contents greater than 50 ppm were necessary to pr[illegible] f[illegible] intergranular brittleness at high temperatures (fig. 1). In the high sulph[illegible]r alloys, failure occured at the grain boundaries (G.B.) in [illegible]e of the onset of dynamic recrystallisation (D.R.). At lower S conc[illegible] (S < 50 ppm) the fracture was ductile and the voids which formed at austenitic G.B. did not propagate rapidly. The D.R. process ensured good d[illegible]tility before final failure.

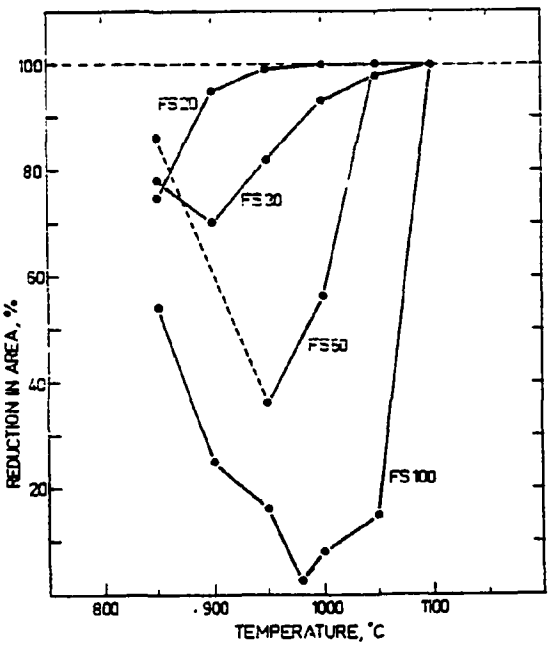

Fig. 1 : Evolution of hot ductility with increasing S content.

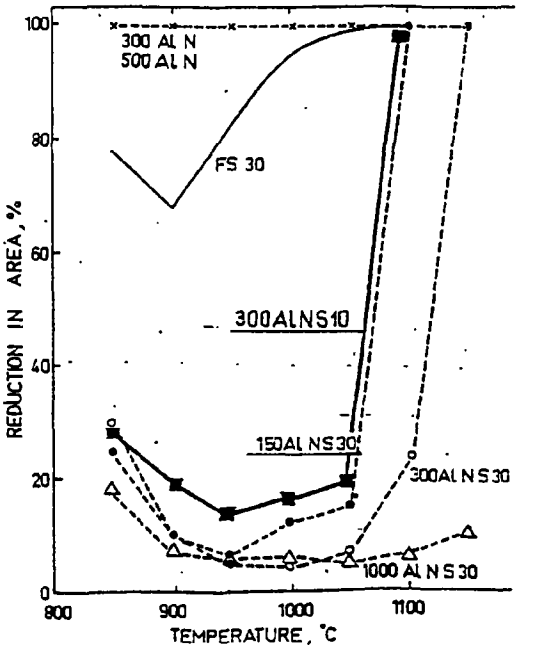

Fig. 2 : Evolution of hot ductility with increasing AlN and S content.

No lack of hot ductility was found in high purity Fe-Al-N alloys. This is contrary to previous observations. In contrast, when AlN and S were both present, a pronounced loss of hot ductility was observed for S content as low as 10 ppm when combined with AlN contents (Al from 150 to 1000 ppm, fig. 2). These results can be understood as a combined effect of strengthenning by AlN precipitation and of weakenning of the G.B. by S segregations. The presence of AlN precipitates was confirmed by electron microscopy. The presence of S segregation was confirmed metallographically and by autoradiography of quenched samples.

The fracture mechanism can be explained on the basis of a shear stress τ_{GB}, required to iniciale G.B. cracking. Its value depends mainly on the intergranular concentration of S. The role of S will be to reduce the cohesion strength across the G.B., while the role of AlN is to increase the resistance to deformation which results in greater stress concentration at the austenitic grain boundary.

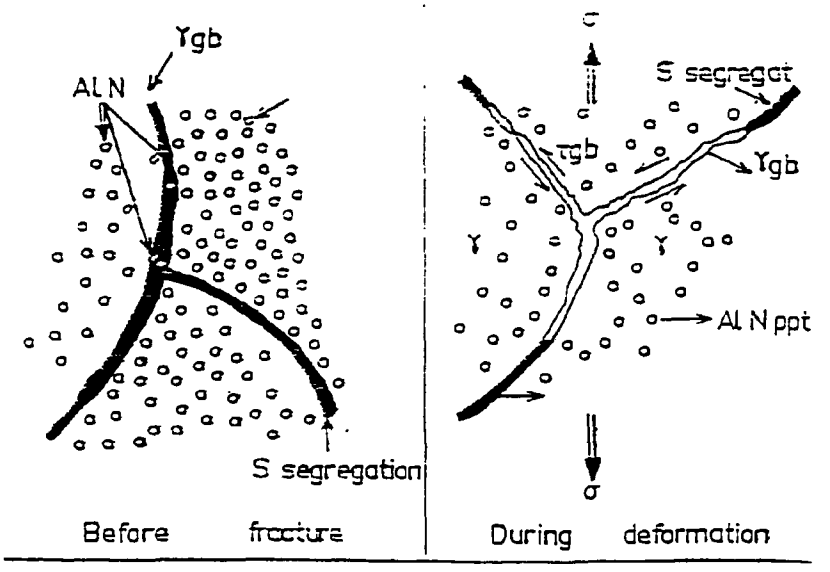

Fig. 3 : Hot fracture mechanism.

References :

1. P. Heritier, A. Fourdeux and A. Kobylanski, Scr. Metal., 15, 753-755, (1981).
2. G.A. Osinkolu, M. Tacikowski and A. Kobylanski, Mat. Science and Technology, 1, 520-525, (1985).
3. M. Tacikowski, G.A. Osinkolu and A. Kobylanski, to be publis. in Materials Science and Technology.

RARE EARTH EFFECTS IN INTERGRANULAR FRACTURE

Frederic Cosandey
Department of Mechanics and Materials Science
Rutgers University, P. O. Box 909, Piscataway, NJ 08854

The high temperature deformation and fracture behavior of polycrystalline alloys is greatly influenced by the presence of trace elements. In nickel alloys minor concentrations of O and S promote high temperature intergranular cracking with drastic reductions in ductility [1,2]. Such embrittlement effects may be counteracted by additions of rare earth elements, such as La and Ce, even at the ppm level [1,3]. In this paper tensile results of Ni-Cr-Ce alloys and mechanisms by which rare earth effects may be accounted for are presented.

Tensile tests as a function of strain-rate and temperature have been performed on three Ni-Cr alloys containing respectively 0, 66 and 180 ppm Ce. Results indicate [4] that Ce additions have little effects on either yield or ultimate tensile strength. The maximum variations have been observed for the ductilities as shown in Fig. 1 for a nominal test strain rate of $4.6 \times 10^{-4} s^{-1}$. The elongations of all three alloys remain the same for test temperatures of up to $500^{o}C$, after which variations are observed. Alloys with Ce additions show an increase in ductility with a maximum at around $800^{o}C$ while the one without Ce experiences a drastic ductility loss. These variations are accompanied by changes in fracture mode from transgranular to intergranular as shown in Fig. 2. In addition, optical observations on transverse sections reveal extensive cavitation and secondary cracks for specimens without Ce while very few cavities and pronounced grain deformation are observed for Ce containing alloys. These variations are the most pronounced for the slowest strain and for temperature between 700 to $850^{o}C$. These results indicate that Ce additions prevent intergranular fracture with a resulting increase in ductility.

The beneficial effects of Ce additions on cavitation and fracture may be the result of three basic processes. First, refining of grain boundary embrittlement elements such as O and S during melting procedure as a result of the low energy of formation of rare earth oxides and sulfides [5]. Second, prevention of environmental attacks as a result of the reduced oxidation rate for rare earth containing alloys [6]. Third, modification of intrinsic grain boundary properties such as an increase in interfacial energy or a reduction in diffusivity resulting in a decrease in cavity formation and growth. These intrinsic variations caused either directly by Ce additions or from the reduction in O and S content have indeed been observed [7], where a 20% increase in grain-boundary energy have been measured for alloys containing 500 ppm rare earth.

ACKNOWLEDGEMENTS

We thank the National Science Foundation for supporting this research under Grant NSF-DMR-84-06605. We are also grateful to the Rutgers Research Council for partial support.

REFERENCES

1. R. T. Holt and W. Wallace, Int. Met. Rev., 21, 1 (1976).
2. R. H. Bricknell and D. A. Woodford, Met. Trans., 12A, 425 (1981).
3. J. Kandra and F. Cosandey, Scripta Met., 19, 397 (1985).
4. F. Cosandey and J. Kandra, Met. Trans., to be published.
5. F. Cosandey, D. Li, F. Sczerzenie and J. K. Tien, Met. Trans. 14A, 611 (1983).
6. G. Ecer and G. Meier, Oxidation of Metals, 13, 159 (1979).
7. A. D. Koval and V. E. Olshanetski, Akad. Nauk. Izv. Met., 1, 124 (1972).

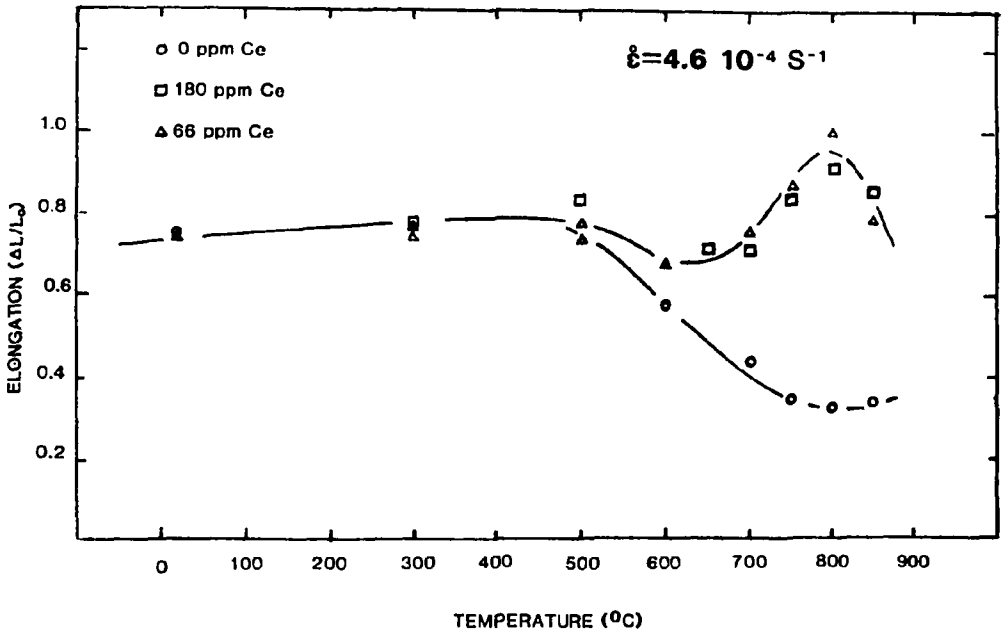

Fig. 1 Fracture elongation (ΔL/Lo) of Ni-20 Cr alloys as a function of temperature for three Ce concentrations; 0, 66 and 180 ppm.

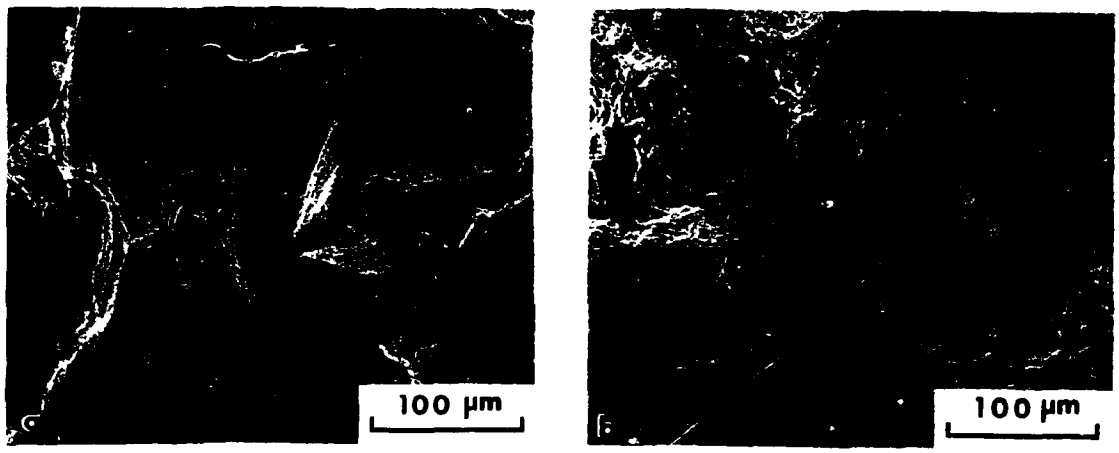

Fig. 2 Fracture surfaces of Ni-20 Cr alloys containing a) 0 ppm, and b) 66 ppm Ce. Test temperature T = 700°C.

INTERGRANULAR CRACKING IN HYDROGENATED ALLOY STEELS

JUN KAMEDA*
*Ames Laboratory, Iowa State University, Ames IA 50011

In this study, by means of fracture mechanics analyses, acoustic emission (AE) techniques, and fracture surface analyses by scanning Auger microscopy (SAM) and x-rays, it has been determined how segregated phosphorus (P), yield strength and grain size affect the equilibrium and growth characteristics of hydrogen-induced intergranular cracking (HIIC) in high strength steels. This work will be reported in detail elsewhere [1]. The results are briefly presented and discussed along with a recently developed microscopic model for equilibrium [2] and steady state [3] growth for HIIC.

The materials used in this study were P-doped and undoped I and II alloy (3.5Ni-1.7Cr) steels with various austenite grain sizes. Pre-cracked compact tension specimens of these steels were hydrogenated at 300°C for 0.5 hr using 1 atm of high purity hydrogen, water quenched and then loaded. Hydrogenated specimens of the P-doped and undoped I steels, and the undoped II steel showed yield strength of 1275 and 1450 MPa, respectively. The relationships between the average crack growth rate, da/dt, the average AE count rate $\dot{N}$, and the applied stress intensity, K, were established by means of compliance and AE measurements.

The SAM analysis has indicated clear evidence of intergranular P segregation in the P-doped steel and its negligible presence in the high purity steels. The dependences of the threshold stress intensity, K_{th}, and da/dt at K = 25 MPa$\sqrt{m}$ on grain size in the three types of steel are shown in Fig. 1(a) and (b), respectively. The effect of yield strength on K_{th} was found to be greater than those of P segregation and grain size. The intergranular P segregation greatly accelerated da/dt while the effect of yield strength on da/dt was not observed in the high purity steels. Changing grain size substantially affected da/dt; da/dt increased in the P-doped steel and decreased in the high purity steels with increasing grain size.

The relationship between $\dot{N}$ and da/dt obtained from all the tests is shown in Fig. 2 in order to demonstrate two different modes of the microscopic growth of HICC: mode (i) associated with a large amount of AE and mode (ii) accompanied by only occasional AE. It is clear that increasing P segregation strongly affects the growth mode transition of HIIC. Fracture surface analyses by scanning electron microscopy and x-ray have indicated more featureless intergranular fracture facets and higher levels of residual strain in the lattice adjacent to the fracture surface in the P-doped steel than in the high purity steels. These results are consistent with those obtained from the microscopic model for equilibrium crack growth for HIIC [2]; while in steels with segregated impurities the microcrack tends to grow by discretely rapid for-

mation of intergranular microcracking (mode (i)) which gives rise to dislocation emissions at the growing crack tip, in high purity steels slow growth of intergranular microcracking (mode (ii)) proceeds which is not accompanied by the generation of dislocations at the crack tip.

Conflicting effects of grain size on da/dt between the tests on the P-doped and high purity steels appear to be closely related to the two microscopic growth modes (i) and (ii) of HIIC. It is unequivocal that mode (i) can proceed more favorably with increasing grain size because of increasing growth unit size of microcracking. On the other hand, mode (ii) controlled by the hydrogen flux presumably along grain boundaries can be facilitated by decreasing grain size because a higher amount of the hydrogen flux can be maintained at the steadily moving crack tip region in the fine-grained steel than in the coarse-grained steel [3].

This work was performed for the U.S. Department of Energy, by Iowa State University, under contract no. W-7405-Eng-82.

REFERENCES

1. J. Kameda, submitted to Acta Metall. for publication.
2. J. Kameda, Acta Metall., in press.
3. J. Kameda, Acta Metall., in press.

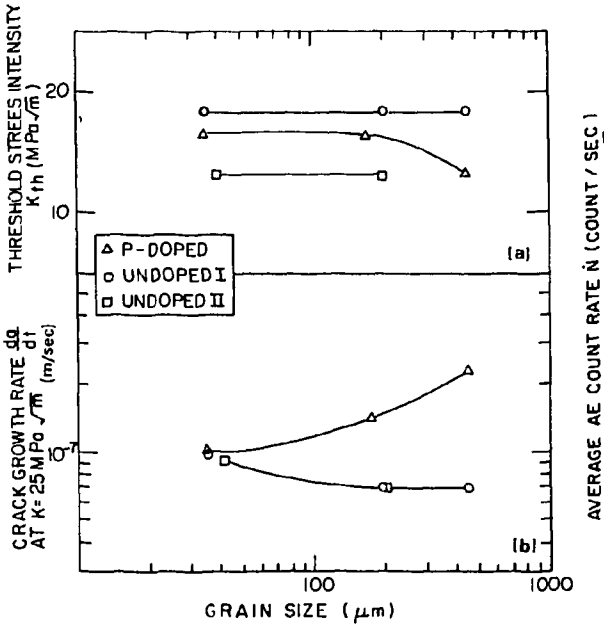

Fig. 1. Dependences of (a) K_{th} and (b) da/dt at K = 25 MPa$\sqrt{m}$ on grain size.

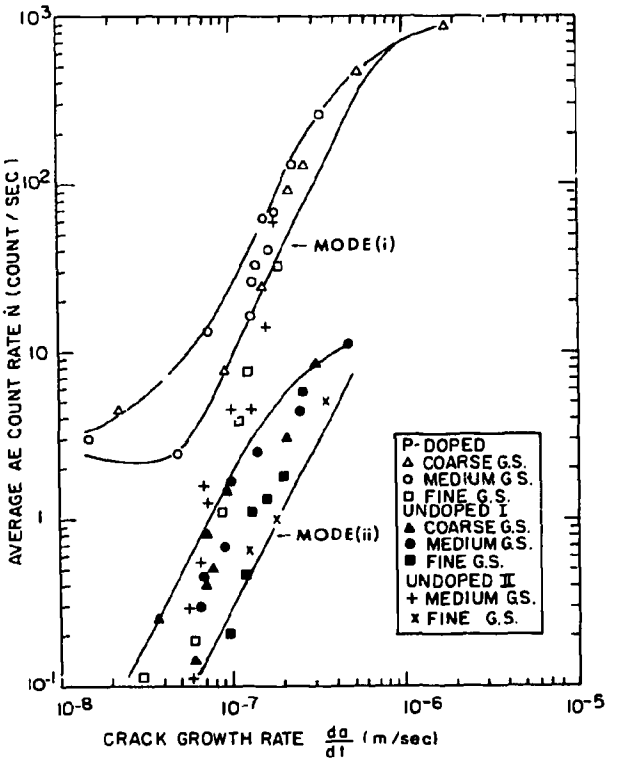

Fig. 2. Relationship of $\dot{N}$ to da/dt.

TEMPERATURE VARIATIONS AROUND THE CRACK TIP DURING A FRACTURE TEST

M.G.BEGHI,* C.E.BOTTANI,*+ AND G.CAGLIOTI*+

*Istituto di Ingegneria Nucleare, CESNEF, Politecnico di Milano, via Ponzio 34/3, I 20133 Milano, Italy;
+Gruppo Nazionale di Struttura della Materia, CNR, Unita' di Ricerca 7, Milano

INTRODUCTION

The objective of this contribution is to offer indications on the possibility of obtaining relevant information on the fracture process from temperature variations measured on the sample surface during mechanical tests. Theoretical analysis and experimental knowledge accumulated on tensile specimens are exploited to interpret the temperature behaviour of a compact tension specimen during a fracture test.

THERMODYNAMICS OF STRAINED METALS AND FRACTURE TESTS

Elastic deformations of metals generate temperature variations, which are negative when the relative volume variation is positive (thermoelastic effect). The associated equivalent heat source is proportional, via the Grüneisen parameter, to the rate of the elastic volume change [1].

Plastic deformations are always accompanied by significant heat generation, due to mechanical energy degradation, via e.g. dislocation creation and motion. A plastically deformed metal absorbs irreversibly a mechanical power W; a fraction f of this power is at once converted into heat, resulting in an equivalent positive heat source of strength fW ("thermal emission")[2]. f is a function of the microstructure, the stress, the strain rate and the temperature [3].

The above effects are evident in tensile tests (Fig.1 reports results from an AISI 316 steel sample tested at constant stress rate). The elastic deformation is accompanied by a continuos cooling; at the onset of plastic flow the temperature exhibits a sudden rise. The temperature kink can be used to pinpoint the 'physical' yield point, or thermoelastic-plastic instability [2].

Preliminary results are reported (Fig.2) of measurements performed on a fatigue pre-cracked compact tension specimen of AISI 316, loaded at constant cross-head speed [4]. The temperature variations in the regions surrounding the crack tip are sensed by three point-like thermistors.

At the thermoelastic-plastic instability the load vs. time characteristic exhibits a barely perceptible kink. Conversely, the initial thermoelastic cooling is followed by a sudden temperature rise near the crack tip while at greater distances, instead, the cooling rate increases. A smoother

temperature rise is eventually reached everywhere.

CONCLUSIONS

In metals under stress, sites where cooling occurs are dilated elastically, while sites where thermal emission is produced are plastically flowing. Thus the experimental procedure presented above allows to identify with precision the nucleation of the plastic zone and, in principle, to map the evolution of its dimensions and shape.

1. L.D.Landau and E.M.Lifshitz, Theory of Elasticity (Pergamon Press, 1960).
2. C.E.Bottani and G.Caglioti, Mechanical Instabilities of Metals, Europhys. News 14, (12) 10 (1983), and references therein.
3. M.G.Beghi, C.E.Bottani and G.Caglioti, to be published in Res Mechanica (1985).
4. M.G.Beghi, C.E.Bottani and G.Caglioti, Metallurg. Sc. and Tecnol., 2, 102 (1984)

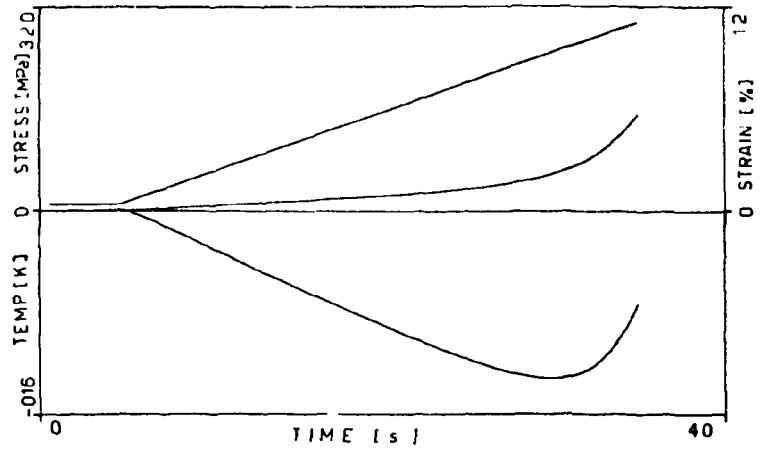

Fig. 1

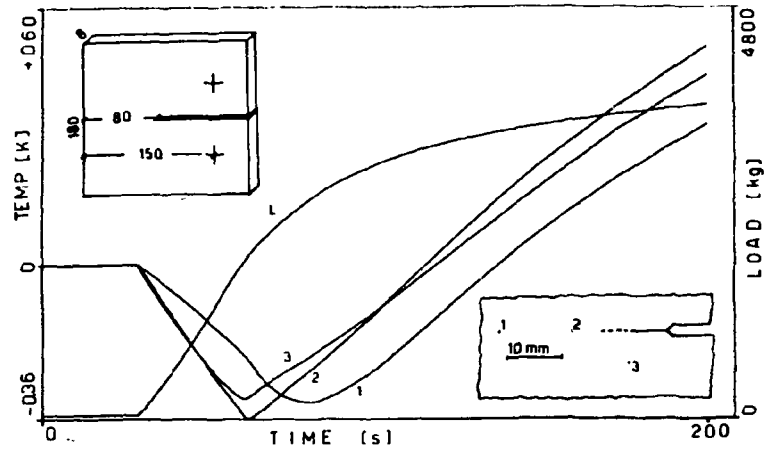

Fig. 2

AUTHORS' INDEX

K

L

M

N

O

P

Q

R

S

T

V

W

X

Y

Z